

**Super-resolution light microscopy
studies of the organisation and
architecture of the hepatitis C virus
RNA replication complex**

Christopher Paul Bartlett

Submitted in accordance with the requirements for the degree of
Doctor of Philosophy

The University of Leeds
Astbury Centre for Structural Biology
School of Molecular and Cellular Biology

September 2016

The candidate confirms that the work submitted is his own, except where work which has formed part of jointly-authored publications has been included. The contribution of the candidate and the other authors to this work has been explicitly indicated below. The candidate confirms that appropriate credit has been given within the thesis where reference has been made to the work of others.

Chapter 4 within this thesis has been based on work from a jointly-authored publication:

Mohl, B.-P., Bartlett, C., Mankouri, J., Harris, M. (2016). Early events in the generation of autophagosomes are required for the formation of membrane structures involved in hepatitis C virus genome replication. *Journal of General Virology*. DOI: 10.1099/jgv.0.000387.

- Dr B.-P. Mohl performed experiments for figures 1, 2, 3, 4a, 6 and 7 and co-authored the paper.
- C. Bartlett performed experiments for figures 4b-c, 5 and 8 and co-authored the paper.
- Dr J. Mankouri provided supervision and co-authored the paper.
- Prof. M. Harris provided supervision and co-authored the paper.

This copy has been supplied on the understanding that it is copyright material and that no quotation from the thesis may be published without proper acknowledgement.

© 2016 The University of Leeds Christopher Paul Bartlett

The right of Christopher Paul Bartlett to be identified as Author of this work has been asserted by him in accordance with the Copyright, Designs and Patents Act 1988.

Acknowledgements

I would like to firstly thank my supervisors Prof. Mark Harris and Prof. Michelle Peckham for their continued expertise, advice, enthusiasm and support throughout the last four years.

Secondly, to all members past and present of the Harris and Peckham research groups who have always provided helpful discussion as well as a lively and enjoyable workplace. In particular, thanks to Jamel Mankouri, Douglas Ross-Thriepland and Joe Lattimer for thought provoking ideas and taking my mind off science from time to time.

A special thanks to Alistair Curd and Dmitry Ushakov who managed to teach a biologist some physics.

I would also like to thanks all my friends and family for their continued support, especially during the more frustrating times, A special mention to Anne-Marie for her constant enthusiasm and the continued supply of cups of tea!

Finally, I would like to thank the Wellcome Trust for funding, without which this project would never have developed.

Abstract

Hepatitis C virus causes a chronic infection in ~3% of the world's population and is a leading cause of liver diseases such as cirrhosis and hepatocellular carcinoma. It is a positive-sense single-stranded RNA virus that persists in ~85% of infections. Viral genome replication occurs within a specialised membranous compartment, termed replication factories. This provides an environment suitable for the production of infectious virus, and correct formation and maintenance is critical for virus replication. The process is coordinated by the non-structural proteins in a macromolecular protein assembly, but the precise mechanisms of biogenesis and protein organisation within replication factories are unknown.

New super-resolution light microscopy approaches allow resolutions of tens of nanometres, 10-fold higher than standard wide-field or confocal microscopy. The goal of this research was to use these techniques to determine the organisation and architecture of proteins within replication factories.

Super-resolution imaging revealed clusters of viral proteins that were equivalent to the diffraction limited puncta observed by wide-field microscopy. A detailed analysis of protein clusters identified significant differences in size and organisation between the non-structural proteins NS3 and NS5A with a defined minimum distance to the cluster centroid. Additional investigations into the functions of NS5A revealed altered cluster phenotypes with both pharmacological inhibition and mutants defective in phosphorylation. A number of strategies were also explored to facilitate fluorescence labelling of viral components in replication factories.

In parallel, investigations into the biogenesis of replication factories were explored by characterising interactions between hepatitis C virus and autophagy. This study identified a requirement of HCV replication for early steps in the formation of autophagosomes.

The findings from this research are the first descriptions using super-resolution microscopy to understand the hepatitis C virus replication complex and provide insight into the organisation and architecture of the non-structural proteins during infection.

Table of Contents

Chapter 1 - Introduction	1
1.1 Hepatitis C virus	3
1.1.1 Identification and classification.....	3
1.1.2 Epidemiology and transmission	5
1.1.3 Pathology	6
1.1.4 HCV therapies	9
1.2 Molecular biology	13
1.2.1 Genome organisation	13
1.2.2 Virion architecture.....	14
1.2.3 HCV entry.....	16
1.2.4 Polyprotein translation	19
1.2.5 Genome replication.....	20
1.2.6 Assembly and release	21
1.3 Individual HCV proteins.....	24
1.3.1 Core – nucleocapsid protein	24
1.3.2 E1 and E2 – envelope glycoproteins.....	24
1.3.3 p7 – viroporin.....	25
1.3.4 NS2 – autoprotease.....	25
1.3.5 NS3/4A – protease/helicase	25
1.3.6 NS4B – transmembrane protein.....	26
1.3.7 NS5A – multifunctional phosphoprotein	26
1.3.7.1 Structure of NS5A	26
1.3.7.2 Roles of NS5A during HCV infection	27
1.3.7.3 Interaction partners	30
1.3.7.4 Phosphorylation of NS5A	33
1.3.7.5 NS5A as a target for direct acting antivirals.....	34
1.3.8 NS5B – RNA-dependent RNA polymerase	35
1.4 HCV replication complex	36
1.4.1 HCV membrane rearrangements	36
1.4.2 Formation of double membrane vesicles	38
1.4.3 HCV replication factory composition	39

1.5 Light microscopy.....	42
1.5.1 History of light microscopy	42
1.5.2 Diffraction in light microscopy.....	42
1.5.3 Extending the optical image resolution	44
1.5.4 Breaking the diffraction limit	45
1.5.4.1 Localisation microscopy.....	47
1.5.4.1.1 Principle	47
1.5.4.1.2 Multi-colour and three dimensional super-resolution imaging ...	48
1.5.4.1.3 Resolution in SMLM	50
1.6 Aims and objectives.....	55
Chapter 3 - Materials and Methods	57
3.1 General materials	59
3.1.1 Bacterial strains	59
3.1.2 Mammalian cell lines.....	59
3.1.3 Antibodies – Primary	60
3.1.4 Secondary antibodies and fluorescent reagents.....	61
3.1.5 SGR and virus constructs.....	61
3.1.6 Expression constructs	61
3.2 General Methods.....	62
3.2.1 Nucleic acid manipulation.....	62
3.2.1.1 Transformation of Z-competent bacteria	62
3.2.1.2 Preparation of plasmid DNA from bacterial cultures.....	62
3.2.1.3 Polymerase chain reaction	62
3.2.1.4 Site-directed mutagenesis	63
3.2.1.5 Restriction digestion	63
3.2.1.6 Agarose gel electrophoresis	63
3.2.1.7 DNA fragment extraction from agarose gels	63
3.2.1.8 DNA/RNA quantification	63
3.2.1.9 Ligation.....	64
3.2.1.10 Construct verification	64
3.2.1.11 Preparation of linear DNA.....	64
3.2.1.12 In vitro transcription of RNA	65
3.2.1.13 Denaturing RNA electrophoresis	65
3.3 Protein biochemistry	66
3.3.1 SDS-PAGE electrophoresis	66

3.3.2	Coomassie blue staining.....	66
3.3.3	Western blot analysis.....	66
3.3.4	Protein quantification	67
3.4	<i>In vitro</i> methods.....	67
3.4.1	Protein expression	67
3.4.2	NS5B Δ C21 expression	67
3.4.3	RNA-dependent RNA polymerase <i>in vitro</i> activity assay	68
3.4.4	Generation of Adhirons	68
3.4.5	Phage ELISA	69
3.4.6	Adhiron purification	69
3.4.7	Adhiron labelling	70
3.4.8	NS5B dot blot	70
3.5	Tissue culture.....	70
3.5.1	Passaging of cells.....	70
3.5.2	RNA electroporation of mammalian cells	70
3.5.3	Stable cell selection	71
3.5.4	Transient luciferase assays	71
3.5.5	DNA transfection.....	71
3.5.6	Infectious virus propagation	71
3.5.7	Virus titration.....	72
3.6	Fluorescence microscopy.....	72
3.6.1	Sample preparation	72
3.6.2	Click Chemistry.....	72
3.6.3	Wide-field Microscopy.....	72
3.6.4	Primary antibody labelling.....	73
3.6.5	PALM/dSTORM sample preparation.....	73
3.6.6	PALM/dSTORM microscopy	73
3.6.7	Computational methods.....	74
Chapter 4 - Super-resolution microscopy studies of the HCV replication		
	complex	77
4.1	Introduction	79
4.2	Localisation microscopy methods.....	85
4.2.1	Workflow for localisation microscopy	85
4.2.1.1	SMLM image acquisition	85
4.2.1.2	SMLM image processing.....	87
4.2.1.3	SMLM image reconstruction.....	87

4.2.1.4 Analysis of protein clusters	88
4.2.2 NS5A-mEos3.2 cloning strategy	90
4.3 Results	93
4.3.1 Characterisation of NS5A-mEos3.2 fusion protein.....	93
4.3.2 Visualising NS5A-mEos3.2 by 3D-PALM	93
4.3.3 Super-resolution imaging of untagged NS5A by dSTORM	97
4.3.4 Comparison of NS5A protein clusters from different genotypes	102
4.3.5 dSTORM of HCV infection	106
4.3.6 Internal cluster organisation of NS5A	109
4.3.7 NS5A clusters around lipid droplets.....	109
4.3.8 NS3 clusters during HCV infection differ from NS5A	113
4.3.9 Effect of daclatasvir treatment.....	117
4.3.10 NS5A phosphorylation mutants	121
4.4 Discussion	127
4.4.1 DBSCAN analysis of clusters	127
4.4.2 The internal architecture of HCV replication complexes	130
4.4.3 Association of protein clusters with lipid droplets.....	132
4.4.4 HCV replication complexes are organised differently between genotypes	136
4.4.5 Effect of daclatasvir treatment.....	137
4.4.6 Roles of phosphorylation during HCV infection	138
4.4.7 Model of HCV replication complexes.....	139
Chapter 5 - The PI3P binding protein DFPC1 is required for HCV replication complex formation.....	141
5.1 Aims and Objectives	143
5.2 Introduction.....	145
5.4 Results	149
5.4.1 Validation of an mCherry-DFCP1 expression construct.....	149
5.4.2 HCV replication complexes do not stably associate with DFCP1 during infection	151
5.4.3 Incomplete colocalisation is observed between DFCP1 with NS5A or NS4B expression constructs	154
5.4.4 Expression of WIPI2b, another PI3P effector protein in autophagosome formation.....	154
5.5 Discussion	159

Chapter 6 - Developing fluorescence microscopy tools to study HCV infection	163
6.1 Aims and Objectives.....	165
6.3 Part I – Detection of HCV non-structural proteins	167
6.3.1 Fusion proteins as reporters on protein localisation	167
6.3.2 Non-antibody binding reagents	170
6.4 Part I – Cloning strategies	175
6.4.1 Tetracycline tag cloning into NS3 and NS5B	175
6.4.2 NS5B Δ C21 expression construct.....	177
6.4.3 Cloning of Adhiron expression constructs.....	177
6.5 Part I – Results.....	179
6.5.1 Replicative fitness of TC-tagged SGRs.....	179
6.5.2 Expression and purification of NS5B Δ C21	179
6.5.3 Purified NS5B Δ C21 exhibits polymerase activity	182
6.5.4 Five Adhiron were identified from NS5B Δ C21 screening.....	184
6.5.5 Expression and purification of Adhiron	186
6.5.6 Adhiron were labelled with Alexa Fluor 647.....	189
6.5.7 Purified Adhiron do not bind native NS5B	189
6.6 Part I – Discussion	193
6.6.1 Characterisation of TC-tagged NS3 and NS5B proteins	193
6.6.2 Selection of Adhiron targeted towards NS5B	194
6.7 Part II – Metabolically labelling HCV RNA	197
6.7.1 Visualising RNA transcription within cells.....	197
6.8 Part II – Results.....	199
6.8.1 HCV replication is unaffected by actinomycin D or 5-ethynyl uridine treatment of cells	199
6.8.2 5-ethynyl uridine is incorporated into cellular RNA transcripts... ..	199
6.8.3 5EU was not incorporated into HCV RNA	202
6.9 Part II – Discussion	207
Chapter 7 - Conclusions and future perspectives	209
Chapter 8 - References	215
Chapter 9 - Appendix	257

Table of Figures

Figure 1.1: Phylogenetic analysis of the <i>Flaviviridae</i> family and HCV genotypes.....	4
Figure 1.2: Global distribution and prevalence of HCV.....	6
Figure 1.3: Disease progression of HCV infection.	8
Figure 1.4: Organisation of the HCV genome and virion architecture.	15
Figure 1.5: Entry of HCV into the cell.	18
Figure 1.6: Membrane topologies and major functions of HCV proteins.....	20
Figure 1.7: HCV assembly.....	23
Figure 1.8: Structure of NS5A.	29
Figure 1.9: Organisation of NS5A with interaction partners.....	32
Figure 1.10: Vesicle structures produced during HCV infection.....	37
Figure 1.11: Diagram of autophagosome biogenesis.....	41
Figure 1.12: Diagram illustrating structured illumination microscopy.	45
Figure 1.13: Diagram illustrating stimulated emission depletion microscopy.....	46
Figure 1.14: Diagram illustrating localisation microscopy image collection.	49
Figure 1.15: Determination of axial coordinates in 3D-STORM using astigmatism.....	51
Figure 3.1: Ray diagram and PALM/STORM microscope layout.	75
Figure 4.1: Correlative light-electron micrographs of cells harbouring a GFP-tagged SGR.....	80
Figure 4.2: STORM microscopy of clathrin coated pits and HCV structural proteins.	82
Figure 4.3: Flowchart of localisation microscopy image acquisition and processing.....	86
Figure 4.4: Schematic illustrating DBSCAN clustering of localisations.	89
Figure 4.5: Illustration of NS5A-mEos3.2 cloning strategy.....	91
Figure 4.6: Characterisation of SGR-Feo-JFH1 [NS5A-mEos3.2].	94
Figure 4.7: 3D-PALM imaging of SGR-Feo-JFH1 [NS5A-mEos3.2].....	95
Figure 4.8: DBSCAN analysis of SGR-Feo-JFH1 [NS5A-mEos3.2] protein clusters.....	96
Figure 4.9: Optimisation of different permeabilisation conditions for antibody labelling of NS5A.....	98

Figure 4.10: 3D-dSTORM imaging of antibody labelled NS5A.	99
Figure 4.11: DBSCAN analysis of SGR-Neo-JFH1 antibody labelled NS5A protein clusters.	100
Figure 4.12: Comparison of cluster characteristics between PALM and dSTORM imaging.....	101
Figure 4.13: 3D-dSTORM image reconstruction of NS5A from genotype 1b.....	103
Figure 4.14: 3D-dSTORM image reconstruction of NS5A from genotype 3a.....	104
Figure 4.15: Comparison of NS5A protein clusters between genotypes.....	105
Figure 4.16: 3D-dSTORM imaging of NS5A in HuH7 cells infected with JFHcc.	107
Figure 4.17: Comparison of NS5A protein clusters between SGR and virus replication.....	108
Figure 4.18: Distance of localisations in clusters from cluster centroid position.	110
Figure 4.19: Architecture of individual protein clusters.	111
Figure 4.20: Association of NS5A protein clusters with lipid droplets.....	112
Figure 4.21: 3D-dSTORM imaging of NS3 in HuH7 cells infected with JFHcc.	114
Figure 4.22: Comparison of NS3 and NS5A protein clusters 24 h.p.i. of HuH7 cells with JFHcc.	115
Figure 4.23: Distance of localisations in NS3 protein clusters from centroid position.	116
Figure 4.24: Alterations in NS5A distribution during daclatasvir treatment.....	118
Figure 4.25: 3D-dSTORM imaging of NS5A in JFHcc infected cells treated with DCV.....	119
Figure 4.26: Comparison of NS5A protein clusters after treatment with DCV.....	120
Figure 4.27: 3D-dSTORM imaging of SGR-Neo-JFH1 with S146A phosphorylation mutation.	122
Figure 4.28: 3D-dSTORM imaging of SGR-Neo-JFH1 with S146D phosphorylation mutation.	123
Figure 4.29: 3D-dSTORM imaging of SGR-Neo-JFH1 with S225A phosphorylation mutation.	124
Figure 4.30: 3D-dSTORM imaging of SGR-Neo-JFH1 with S225D phosphorylation mutation.	125
Figure 4.31: Comparison of NS5A phosphorylation mutation.	126
Figure 4.32: Diagrams illustrating different clustering algorithms.....	129

Figure 4.33: Susceptibility of NS proteins to proteinase K digestion. Digitonin permeabilised cells were incubated with proteinase K at varying concentrations (0 µg/ml lane 1, 1 µg/ml lane 2, 5 µg/ml lane 3, 10 µg/ml lane 4, 50 µg/ml lane 5 and 100 µg/ml lane 6). Asterisk denotes the position of calnexin NH ₂ -terminal segment located in the ER lumen. BiP/Grp78 which is located in the ER lumen was used as a negative control for proteinase K digestion. Reproduced from (Miyanari et al., 2003).	133
Figure 4.34: Revised model of HCV replication complex formation.....	135
Figure 4.35: Model of HCV replication.....	140
Figure 5.1: Validation of an mCherry-DFCP1 construct as a marker for autophagosome formation.	150
Figure 5.2: Colocalisation analysis from mCherry-DFCP1 expression plasmid validation.....	151
Figure 5.3: HCV replication complexes do not stably colocalise with mCherry-DFCP1.	153
Figure 5.4: Incomplete colocalisation between NS5A or NS4B with DFCEP1, either expressed alone or in the context of NS3–5B.....	156
Figure 5.5: Colocalisation analysis of DFCEP1 and non-structural protein expression constructs.....	157
Figure 5.6: Transient expression of GFP-WIPI2b.....	158
Figure 5.7: Model of HCV replication complex formation using the autophagosome biogenesis pathway.....	162
Figure 6.1: Tetracysteine tag cloning sites identified from transposon mutagenesis studies.....	169
Figure 6.2: Size comparison between protein binding molecules.....	171
Figure 6.3: Adhiron scaffold and phage display procedure.....	173
Figure 6.4: NS3 and NS5B tetracysteine tag cloning strategies.....	177
Figure 6.5: Adhiron cloning strategy.....	178
Figure 6.6: Replication of TC-tagged SGR constructs.....	180
Figure 6.7: NS5B ΔC21 protein purification.....	181
Figure 6.8: Purified NS5B ΔC21 is correctly folded and functional.....	183
Figure 6.9: Adhiron identified from phage display screening against NS5B ΔC21.	185
Figure 6.10: Expression of Adhiron from pET11b in BL21(DE3) cells.....	187
Figure 6.11: Adhiron purification fractions analysed by Coomassie stain of SDS-PAGE.....	188
Figure 6.12: Alexa Fluor 647 labelling of Adhiron cysteines.	190
Figure 6.13: Validation of Adhiron as non-antibody binding proteins for fluorescence microscopy detection of NS5B.....	191

Figure 6.14: <i>In vitro</i> binding of 647-labelled Adhirons to purified NS5B ΔC21.....	192
Figure 6.15: SGR-Feo-JFH1 replication in the presence of actinomycin D or 5EU.....	200
Figure 6.16: Localisation of 5EU incorporated into cellular transcripts.....	201
Figure 6.17: 5EU labelling of HCV RNA in cells stably harbouring SGRs.	203
Figure 6.18: 5EU incorporation into transiently replicating SGR-Feo-JFH1 RNA.....	204
Figure 6.19: 5EU incorporation into HCV genomes during virus infection.	205

Table of Tables

Table 1.1: Current FDA approved therapies for HCV as of 29/09/2016 from www.fda.gov.....	12
Table 6.1: Properties of Adhiron as computed by the ExPASy ProtParam bioinformatics tool. Extinction coefficients presented are for Adhiron with reduced cysteines.	187

Table of Equations

Equation 1: Abbe diffraction limit.....	43
Equation 2: Localisation precision.....	47
Equation 3: Nyquist criterion.....	52

Abbreviations

5EU	5-ethynyl uridine
AD	actinomycin D
AH	amphipathic helix
apoB	apolipoprotein B
apoE	apolipoprotein E
ATP	adenosine triphosphate
BrUTP	5-bromouridine 5'-triphosphate
BSA	bovine serum albumin
CKI	casein kinase I
cLD	cytosolic lipid droplet
CLDN1	claudin 1
CRE	<i>cis</i> -acting replication element
CsA	cyclosporin A
CTP	cytidine triphosphate
CypA	cyclophilin A
D1	domain I
D2	domain II
D3	domain III
DAA	direct acting antiviral
DAPI	4'6-diamino-2-phenylindole
DBSCAN	density based spatial clustering of applications with noise
DCV	daclatasvir
DEPC	diethylpyrocarbonate
DFCP1	double FYVE-domain containing protein 1
dH ₂ O	de-ionised water
DMEM	Dulbecco's modified Eagle's medium
DMSO	dimethyl sulfoxide
DMV	double membrane vesicle
DNA	deoxyribonucleic acid
dNTP	deoxynucleotide triphosphate
dsRNA	double stranded RNA
dSTORM	direct STORM

DTT	dithiothreitol
E1	envelope protein 1
E2	envelope protein 2
EBSS	Earle's balanced salt solution
EDTA	ethylenediaminetetraacetic acid
EGFR	epidermal growth factor receptor
ELISA	enzyme-linked immunosorbent assay
EM	electron microscopy
EMCCD	electron multiplying charged-coupled device
ER	endoplasmic reticulum
FBS	foetal bovine serum
FDA	Food and Drug Administration
FP	fluorescent protein
fPALM	fluorescence activated localisation microscopy
FRC	Fourier ring correlation
GAG	glycosaminoglycans
GFP	green fluorescent protein
GTP	guanosine triphosphate
HAV	hepatitis A virus
HBV	hepatitis B virus
HCC	hepatocellular carcinoma
HCV	hepatitis C virus
HDL	high-density lipoprotein
HEPES	4-(2-hydroxyethyl)-1-piperazineethanesulfonic acid
HIV	human immunodeficiency virus
h.p.i	hours post infection
HSPG	heparin sulphate proteoglycans
HVR1	hypervariable region 1
IF	immunofluorescence
IPTG	isopropyl β -D-1-thiogalactopyranoside
IRES	internal ribosome entry site
JFH1	Japanese fulminant hepatitis 1
kDa	kilo Daltons
LB	lysogeny broth
LC3	light chain 3
LCS I	low complexity sequence 1
LCS II	low complexity sequence 2

LD	lipid droplet
LDL	low-density lipoprotein
LDLR	low-density lipoprotein receptor
LVP	lipoviral particle
MAM	mitochondrial-associated ER membranes
MEA	2-mercaptoethylamine
MMV	multi-membrane vesicle
NA	numerical aperture
NANBH	non-A non-B hepatitis
NPC1L1	Niemann-Pick C1-like-1
NPHV	non-primate hepacivirus
ns	not statistically significant
NS	non-structural
NS2	non-structural 2
NS3	non-structural 3
NS4A	non-structural 4A
NS4B	non-structural 4B
NS5A	non-structural 5A
NS5B	non-structural 5B
NTP	nucleotide triphosphate
OCLN	occludin 1
ORF	open reading frame
OSBP	oxysterol-binding protein
PALM	photoactivated localisation microscopy
PBS	phosphate buffered saline
PCR	polymerase chain reaction
PCF	pair correlation function
PE	phosphatidylethanolamine
Peg-IFN α	pegylated-interferon α
PFA	paraformaldehyde
PI3K	phosphatidylinositol 3-kinase
PI3P	phosphatidylinositol 3-phosphate
PI4KIII α	phosphatidylinositol 4-kinase III α
PI4P	phosphatidylinositol 4-phosphate
PKA	cAMP-dependent protein kinase
Plk	Polo-like kinase
PPIase	peptidyl-prolyl isomerase

PSF	point spread function
PVDF	polyvinylidene fluoride
RAV	resistance-associated variant
RBV	ribavirin
RC	replication complex
RdRp	RNA-dependent RNA polymerase
RESOLFT	reversible saturable optical linear fluorescence transitions
RNA	ribonucleic acid
RT	room temperature
SELEX	systemic evolution of ligands by exponential enrichment
SD	standard deviation
SDS-PAGE	sodium dodecyl polyacrylamide gel electrophoresis
SEM	standard error of the mean
SGR	sub-genomic replicon
SH3	Src-homology 3
SIM	structured illumination microscopy
siRNA	small interfering RNA
SMLM	single molecule localisation microscopy
SNP	single nucleotide polymorphisms
SOC	standard of care
SOE	splice overlap extension
SRB1	scavenger receptor class B member 1
STED	stimulated emission depletion
STORM	stochastic optical reconstruction microscopy
SVR	sustained virological response
TBS	Tris-buffered saline
TC	tetracysteine
TCEP	tris(2-carboxyethyl)phosphine
TEMED	N,N,N',N'-tetramethylethylenediamine
TGN	<i>trans</i> -Golgi network
UPR	unfolded protein response
UTP	uridine triphosphate
UTR	untranslated region
VLDL	very-low-density lipoprotein
WB	Western blot
WIPI	WD-repeat PI3P effector protein

Chapter 1 - Introduction

1.1 Hepatitis C virus

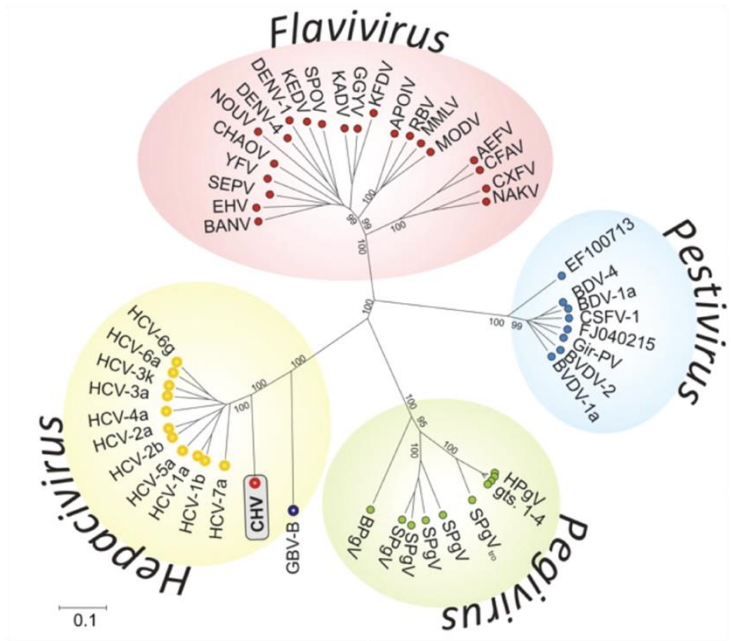
1.1.1 Identification and classification

Hepatitis is a term used to describe inflammation of the liver and is predominantly caused by viral infection from one of the human hepatitis A–E viruses. Prior to the identification of hepatitis C virus (HCV), most cases of viral hepatitis were attributed to hepatitis A virus (HAV) or hepatitis B virus (HBV) infection. The identification of a novel pathogen came after the majority of post-transfusion hepatitis cases were unreactive in HAV or HBV diagnostic tests (Feinstone et al., 1975). A small enveloped virus was attributed to non-A non-B hepatitis (NANBH) after transmission of infectious plasma to chimpanzees through intravenous injection (Bradley et al., 1985, 1983). Isolation of a cDNA clone derived from NANBH identified an RNA molecule which encoded an antigen associated specifically with NANBH infections (Choo et al., 1989). Termed hepatitis C virus, this single infectious agent was later attributed to the majority of post-transfusion NANBH (Choo et al., 1990).

Significant sequence homology with members of the *Flavivirus* genus classified HCV into the *Flaviviridae* family (Figure 1.1). HCV is most closely related to the genera *Pestivirus* and *Pegivirus* and became the prototype member of the *Hepacivirus* genus. The origin of HCV has long been a mystery with George-Barker virus B, which causes hepatitis in tamarins (Stapleton et al., 2011), the only other *Hepacivirus* member. Recently the most closely related virus to HCV was identified, termed non-primate hepacivirus (NPHV). Originally isolated from domestic dogs (Kapoor et al., 2011), NPHV has subsequently only been identified in horses (Burbelo et al., 2012; Lyons et al., 2012). Following the discovery of NPHV, deep sequencing has identified a wide range of highly divergent hepaciviruses and pegiviruses in rodent and bat species (Kapoor et al., 2013; Quan et al., 2013).

Following the identification of HCV in 1989, the substantial diversity of isolates from different individuals and countries became apparent. A unified nomenclature (Simmonds et al., 2005) originally classified HCV into 6 different genotypes, further divided into subtypes (a, b, c, etc.). This has subsequently been expanded to 7 genotypes and 67 subtypes (Smith et al., 2014). The genotypes of HCV differ by 30–35% in nucleotide sequence across the genome with <15% variation between each subtype (Smith et al., 2014).

A



B

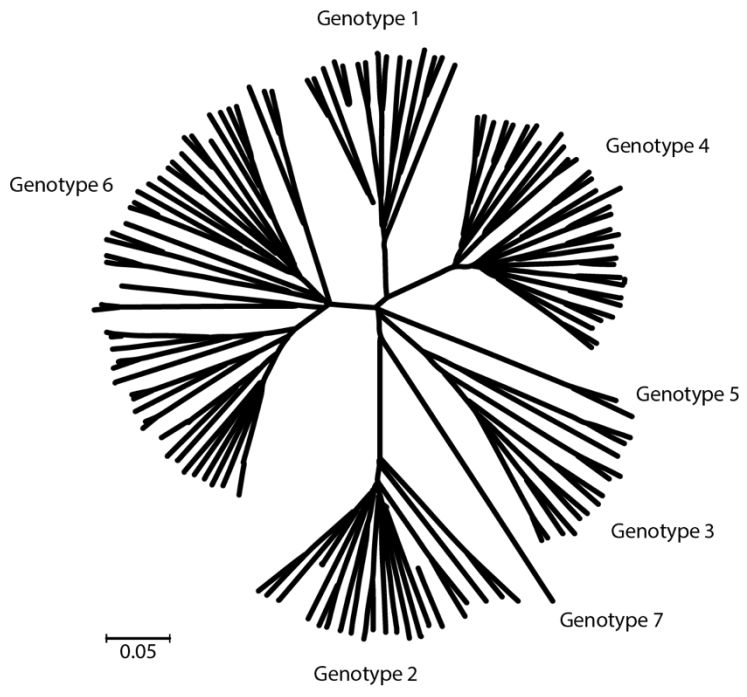


Figure 1.1: Phylogenetic analysis of the *Flaviviridae* family and HCV genotypes.

A: Phylogenetic tree of conserved regions in the RNA-dependent RNA polymerase within the *Flaviviridae* family, reproduced from (Kapoor et al., 2011).

B: Phylogenetic tree from 129 complete HCV coding sequences, adapted from (Smith et al., 2014).

1.1.2 Epidemiology and transmission

Current estimates indicate that ~2.8% of the world's population are seropositive for HCV, corresponding to >185 million infected individuals (Mohd Hanafiah et al., 2013). The distribution of HCV genotypes varies globally, along with prevalence within the population (Figure 1.2) (Messina et al., 2015). Genotype 1 and 3 infections account for the majority of infections worldwide with approximately 46% and 30% seroprevalence respectively. Genotype 1 infections are mostly attributed to subtypes 1a and 1b and are widely distributed globally, whereas genotype 3 dominates in south Asia (Messina et al., 2015). The other five genotypes account for the remaining ~25% of infections and are more geographically constrained.

Hepatitis C virus is a blood borne pathogen and transmission requires contact with contaminated blood products. Medical blood transfusion was the leading cause of HCV transmission until the introduction of screening for liver disease, increased serum alanine aminotransferase (ALT) levels and HCV antibodies, which dramatically reduced the incidence rate (Donahue et al., 1992; Schreiber et al., 1996). However, this still remains a route of transmission in most developing countries due to the continued use of unsafe healthcare practises. Currently the most common cause of transmission is through intravenous drug use which is estimated to account for around 80% of new infections in the developed world (Sy and Jamal, 2006). Other routes of transmission include sexual contact and perinatal transmission, however these are much less common, typically <10%.

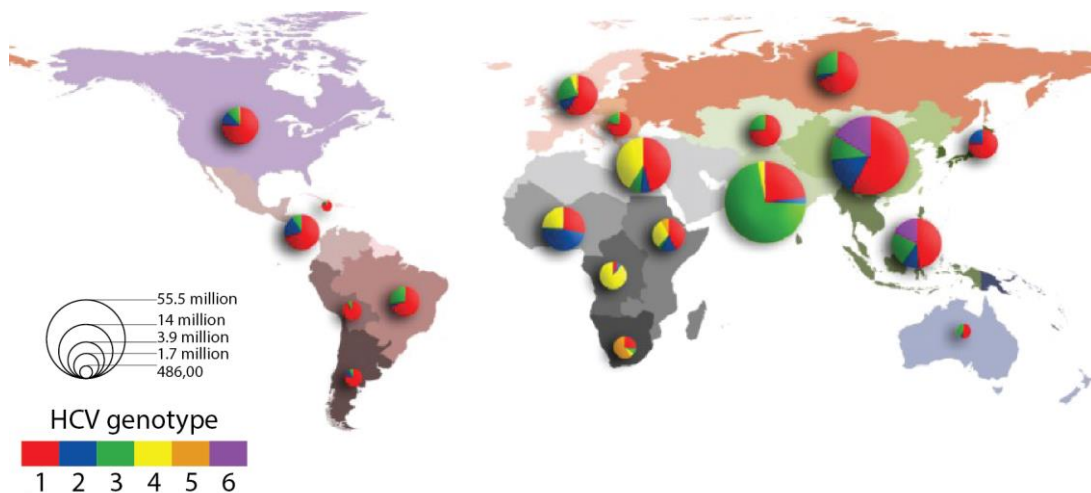


Figure 1.2: Global distribution and prevalence of HCV.

Size of pie chart proportional to the number of seroprevalent cases, adapted from (Messina et al., 2015).

1.1.3 Pathology

Acute infection with HCV is often undiagnosed because around 70–80% of cases are asymptomatic (McCaughan et al., 1992). Symptoms that do present occur within 3–12 weeks after exposure and include malaise, nausea and jaundice (Alter and Seeff, 2000; Thimme et al., 2001). The levels of HCV RNA increase rapidly within the first few weeks, peaking at 10^5 – 10^7 IU/ml, which coincides with the peak of serum ALT levels and onset of symptoms (Chen and Morgan, 2006). Acute infection can be severe, but fulminant liver failure is rare (Farci et al., 1996; Younis et al., 2015; Yu et al., 2005).

However, in the majority of cases (75–85%), acute hepatitis is not resolved and patients develop a chronic infection (Figure 1.3). This is defined by the presence of HCV RNA within the blood after 6 months. Risk factors associated with the development of chronic infection include genotype, age, gender, race, presence of symptoms during acute infection and immunosuppression or human immunodeficiency virus (HIV) coinfection (Chen and Morgan, 2006; Núñez and Soriano, 2005).

Persistent infection with HCV causes progressive damage of the liver resulting in liver fibrosis, developing to cirrhosis in 10–20% of cases. This is typically an asymptomatic process and diagnosis with HCV usually occurs when patients present with the complications of end-stage liver disease and failure (Chen and

Morgan, 2006). Following diagnosis of cirrhosis there is an additional risk, 1–4% per year, of developing hepatocellular carcinoma (HCC).

The risk factors associated with disease progression are varied and include age at time of infection, gender, coinfection with HIV or HBV, and excessive consumption of alcohol (Chen and Morgan, 2006). Additionally, differences in disease progression exist between genotypes. Patients infected with genotype 4 are more likely to develop chronic infection, whereas genotype 3 infections are often cleared during acute infection but have a faster progression to liver fibrosis and steatosis in chronic infections (Lehmann et al., 2004; Núñez and Soriano, 2005). Liver failure and HCC caused by HCV infection is a leading cause of liver transplantation in many countries, with the added complication of graft re-infection in most cases (Rubín et al., 2011).

Regular screening is therefore important for monitoring the development of liver fibrosis to cirrhosis and HCC. These tests typically include liver biopsies and histological staining to score the extent of fibrosis and hepatocyte death (Theise, 2007). Advances in techniques for grading liver fibrosis using biochemical markers, ultrasound and magnetic resonance now provide more suitable methods for regular screening and monitoring of disease progression which are less invasive (Faria et al., 2009; Huwart and van Beers, 2008). However, these approaches do not reach sufficient diagnostic accuracy to replace the gold standard of liver biopsies (Papastergiou et al., 2012).

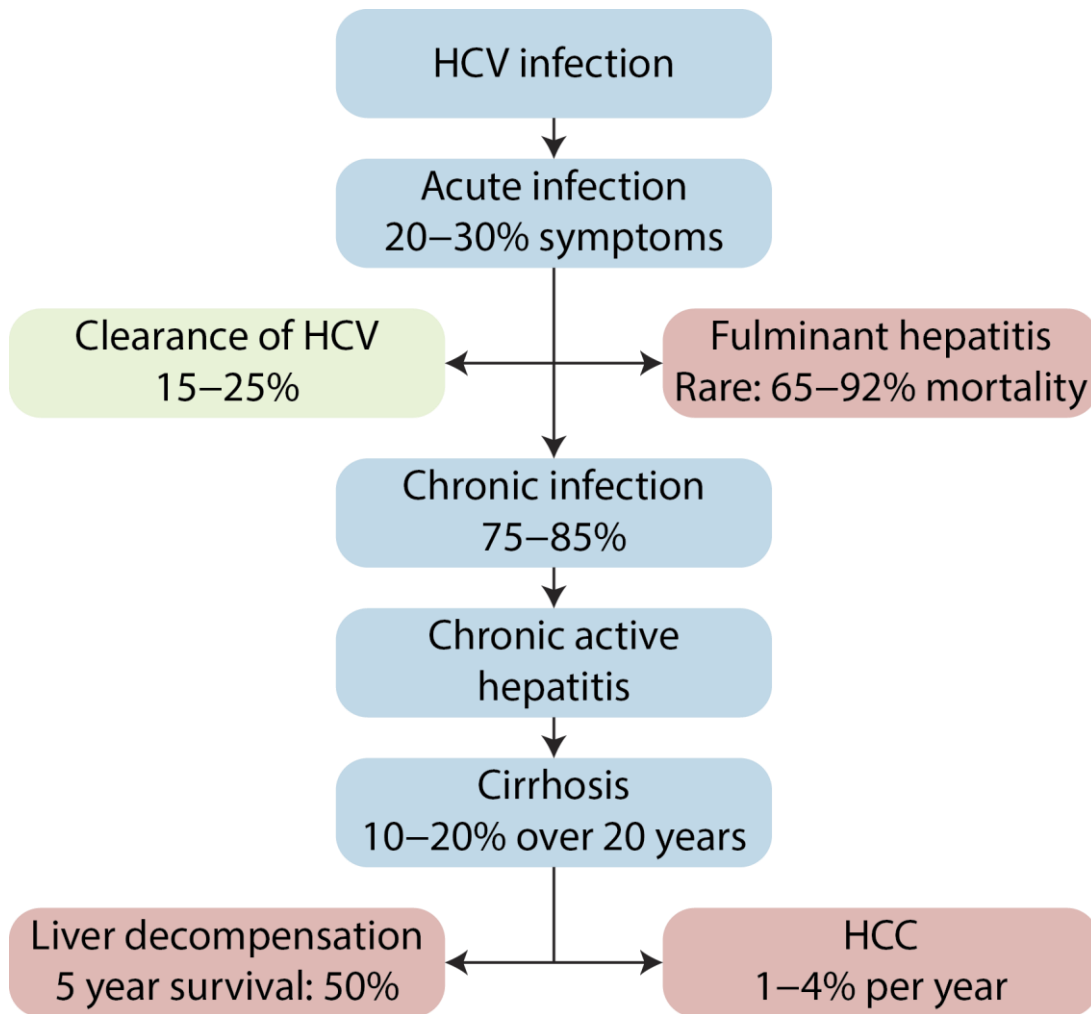


Figure 1.3: Disease progression of HCV infection.

The natural progression of HCV infection in the absence of therapeutic treatment.

Adapted from (Chen and Morgan, 2006).

1.1.4 HCV therapies

A cure for HCV is classified by a sustained virological response (SVR), defined as undetectable HCV RNA 12–24 weeks following cessation of treatment. Historically, the standard of care (SOC) for chronic HCV infection was pegylated-interferon alpha (Peg-IFN α) and ribavirin (RBV) therapy which achieved SVR in 54–63% of cases depending of virus genotype (Hadziyannis et al., 2004; Manns et al., 2001). A 90% chance of resolving infection could be achieved with Peg-IFN α monotherapy for 24 weeks if HCV infection was identified early in symptomatic acute infections (Jaeckel et al., 2001; Santantonio et al., 2005; Wiegand et al., 2006).

However, major drawbacks to these therapies are the side effects which manifest as headaches, myalgia, nausea and flu-like symptoms. The severity of side effects during a 24–48 week therapy reduce the adherence of patients to the treatment regimen and therefore its success (Manns et al., 2001). Other than patients withdrawing from treatment a proportion are non-responders, those who do not achieve viral clearance at the end of therapy, or relapsers, who initially achieve SVR but HCV RNA levels are then detectable at a later date (Pearlman and Traub, 2011). There are also patients with a partial response who achieve a 1–2log₁₀ drop in HCV RNA levels.

Predicting the patient response to therapy is therefore a major consideration in the clinical setting. Along with HCV genotype, a number of host genetic variants have recently been identified which strongly correlate with therapy response and spontaneous clearance of HCV, reviewed in (Rau et al., 2012). Interferon- λ 3 (previously interleukin 28B) is the best understood with multiple single nucleotide polymorphisms (SNP) reported across the IL28B locus. Genotyping of both HCV and the patient have become mandatory in the clinical setting for determining the best treatment regimen.

Recently a number of direct acting antivirals (DAA) have been approved for use by the Food and Drug Administration (FDA). These have considerably improved the clinical outcomes for HCV infected patients (Table 1.1). The DAAs described to date are targeted towards the HCV non-structural proteins NS3/4A, NS5A or NS5B. The first two DAAs licenced by the FDA were the NS3/4A protease inhibitors boceprevir and telaprevir in combination with RBV and Peg-IFN α . Both of which are linear peptidomimetic structures that reversibly form a covalent bond with the catalytic serine of NS3/4A (Hazuda et al., 2013; Kwong et al., 2011). The addition of a single DAA into the RBV and Peg-IFN α treatment regimen improved SVR rates for genotype 1 infected patients from 46% to 70% (Manns and von Hahn, 2013).

Despite these improvements in SVR both boceprevir and telaprevir have a number of limitations including a narrow genotype specificity, low barrier to resistance and adverse side effects. The resistance-associated variant (RAV) Arg155 in NS3 reduces the binding properties of these drugs with minimal effect on the natural substrate (Romano et al., 2012, 2010). Additional first generation NS3/4A inhibitors were trialled with improved tolerability and similar antiviral efficacy profiles, but from a number of candidates only simeprevir was approved in combination therapy with Peg-IFN α and RBV (Zeuzem et al., 2014). Since their original licencing in 2011, Merck and Vertex have voluntarily discontinued production of boceprevir and telaprevir due to the rapid developments of second generation NS3/4A inhibitors and pan-genotypic therapies. The second generation NS3/4A protease inhibitor grazoprevir retains NS3/4A binding properties in the context of the R155K mutation and was recently licensed in a combination therapy with the NS5A inhibitor elbasvir (Romano et al., 2012; Summa et al., 2012).

The viral polymerase NS5B is another key target for DAA therapy with drugs classed as either nucleotide or non-nucleotide inhibitors (Sofia et al., 2012). Non-nucleotide inhibitors bind NS5B and inhibit the polymerase through an allosteric mechanism before or at the point of initiation, inhibiting the transition to elongation. Beclabuvir (Rigat et al., 2014) and dasabuvir (Kati et al., 2015) are examples of non-nucleotide inhibitors. However, due to their low barrier to resistance, only dasabuvir is licenced in the multi DAA therapy Viekira Pak.

Nucleotide inhibitors on the other hand are metabolically activated from prodrugs and compete with the incoming nucleotide triphosphates (Sofia et al., 2012). They typically show pan-genotypic activity with a high barrier to resistance making them attractive candidates. Resistance-associated variants that do occur are typically less fit and exhibit catalytic deficiency (Dutartre et al., 2006; Svarovskaia et al., 2014; Tong et al., 2014). The major limitation in their development to the clinic are toxic side effects (Feld, 2014). The nucleotide inhibitor sofosbuvir was the first DAA licenced without the need for co-administration with Peg-IFN α as part of the Sovaldi treatment and has since become a common part of Peg-IFN α free therapies alongside NS5A inhibitors.

The most potent HCV inhibitors target the NS5A protein and are active at pM concentrations (Belema et al., 2014). The absence of an enzymatic activity for NS5A has raised additional questions as to the mechanism of action of these inhibitors and is discussed further in Section 1.3.7.5. Daclatasvir, ledipasvir and ombitasvir are all currently licenced and when in combination with sofosbuvir can

achieve SVR rates >90% with no benefit from RBV addition (Afdhal et al., 2014; Kowdley et al., 2014). The biggest challenge for NS5A inhibitors is the emergence of RAVs which are generally fit and persist within the patient (Krishnan et al., 2015), a challenge currently being addressed with second generation NS5A inhibitors with pan-genotypic properties. The Epclusa formation, composed of second generation velpatasvir with sofosbuvir, was recently licenced and is the first therapy effective against genotypes 1 through 6 (Feld et al., 2015). The effectiveness of NS5A inhibitors in combination with the nucleotide inhibitor sofosbuvir indicate that this combination will become common components of many if not all therapies in the future.

The development of DAAs has dramatically changed the landscape of HCV treatment with improved tolerability and SVR rates. However the high price associated has so far limited their use to patients with advanced liver disease (Trooskin et al., 2015). This approach will not tackle the ongoing transmission and development of advanced liver disease and HCC in those patients not yet at end-stage liver failure (Nuys et al., 2015). Despite the price of DAA therapies, their cost of cure is comparable to Peg-IFN α and ribavirin therapy due to the improved SVR rates (Rosenthal and Graham, 2016). However, the cost of treatment has limited access of new therapies and become a major stalling point for the treatment of HCV.

Brand Name (Company)	DAA (target)	Combination therapy	Genotype	Approval date
Victrelis ¹ (Merck)	Boceprevir (NS3/4A protease)	RBV & Peg-IFN α	1	13/05/2011
Incivek ¹ (Janssen – Vertex)	Telaprevir (NS3/4A protease)	RBV & Peg-IFN α	1	23/05/2011
Olysio (Medvir – Janssen)	Simeprevir (NS3/4A protease)	RBV & Peg-IFN α	1 or 4	22/11/2013
Sovaldi (Gilead)	Sofosbuvir (NS5B polymerase)	RBV ²	1, 2, 3 or 4	06/12/2013
Harvoni (Gilead)	Ledipasvir (NS5A) Sofosbuvir (NS5B polymerase)	³	1, 4, 5 or 6	10/10/2014
Viekira Pak (AbbVie)	Paritaprevir (NS3/4A protease) Ombitasvir (NS5A) Dasabuvir (NS5B polymerase) Ritonavir (Cytochrome P450-3A4)	⁴	1	19/12/2014
Technivie (AbbVie)	Paritaprevir (NS3/4A protease) Ombitasvir (NS5A) Ritonavir (Cytochrome P450-3A4)	RBV	4	24/07/2015
Daklinza (Bristol Myers Squibb – Gilead)	Daclatasvir (NS5A) Sofosbuvir (NS5B polymerase)	n/a	1 or 3	24/07/2015
Zepatier (Merck Sharp Dohme)	Grazoprevir (NS3/4A protease) Elbasvir (NS5A)	⁵	1 or 4	28/01/2016
Epclusa (Gilead)	Velpatasvir (NS5A) Sofosbuvir (NS5B polymerase)	⁶	1, 2, 3, 4, 5 or 6	28/06/2016

¹ discontinued voluntarily due to scientific advancement and improved tolerability of other therapies

² with Peg-IFN — for patients with genotype 1 or 4

³ with ribavirin — dependent on genotype, amount of liver damage and prior treatment history

⁴ with ribavirin — for genotype 1a, or genotype 1b with cirrhosis

⁵ with ribavirin — dependent on baseline NS5A polymorphisms and prior treatment history

⁶ with ribavirin — for patients with decompensated cirrhosis

Table 1.1: Current FDA approved therapies for HCV as of 29/09/2016 from www.fda.gov.

1.2 Molecular biology

1.2.1 Genome organisation

HCV is a single stranded RNA virus of positive polarity. The genome of around 9.6 kb contains a number of complex RNA structures and encodes for a single open reading frame (ORF) flanked by untranslated regions (UTR) (Figure 1.4A) (Davis et al., 2008; Mauger et al., 2015; Simmonds, 2004).

The 5' UTR can be divided into four domains (I–IV) which share more than 90% sequence identity among HCV genotypes (Figure 1.4A inset) (Brown et al., 1992; Honda et al., 1999, 1996; Smith et al., 2014). Domains II–IV constitute a type III internal ribosome entry site (IRES) which drives translation of the ~3000 amino acid HCV polyprotein via a cap-independent mechanism (Brown et al., 1992). The first 40 nucleotides of the 5' UTR constitute domain I which is not essential for translation and is involved in replication (Friebe et al., 2001; Luo et al., 2003). Domains II and III contain a number of complex RNA structures including hairpin loops (Klinck et al., 2000), a novel tetraloop fold (Lukavsky et al., 2000), and a pseudoknot (Wang et al., 1995), all of which are critical for IRES activity. The initiation codon AUG is located in a single stranded loop region of a small stem loop in domain IV (Honda et al., 1996).

Within the 5'UTR are two microRNA-122 (miRNA-122) binding sites, a highly abundant and liver-specific miRNA (Jopling et al., 2005). In comparison to the usual mechanisms of miRNAs in negative regulation, miRNA-122 functions to enhance HCV RNA replication and IRES translation, and protects the viral RNA from degradation (Niepmann, 2013). Additional RNA regulatory elements within the core and NS5B coding regions are involved in long range RNA-RNA interactions that modulate different stages of the HCV life cycle (Tuplin et al., 2004; You et al., 2004). In particular the *cis*-acting replication element (CRE) at the 3' end of the ORF exerts an inhibitory effect on IRES function (Romero-López et al., 2012).

The last 200–235 nucleotides of HCV constitute the 3' UTR which stimulates HCV IRES translation and facilitates HCV encapsidation (Figure 1.4A inset) (Shi et al., 2016; Song et al., 2006). This can be subdivided into three distinct domains, a variable region, a poly(U/UC) tract and a 98 nucleotide X region (Blight and Rice, 1997; Kolykhalov et al., 1996; Tanaka et al., 1996, 1995; Yamada et al., 1996). Highly conserved within genotypes, the variable domain immediately follows the termination codon and ranges in length from 27 to 70 nucleotides (Kolykhalov et al., 1996; Yanagi et al., 1998). The variable domain is required with the other domains

in the 3' UTR for the 3'UTR-40S ribosomal subunit interactions (Bai et al., 2013). The length of the poly(U/UC) tract region is variable between genotypes and correlates with replication capability (Friebe and Bartenschlager, 2002; Kolykhalov et al., 1996; Tanaka et al., 1996; Yanagi et al., 1998; Yi and Lemon, 2003). The X region contains three stem loops and is involved in translation, functioning much like the poly(A) sequence of mRNAs (Wood et al., 2001).

1.2.2 Virion architecture

The architecture and composition of the HCV particle has long remained enigmatic. Filtration and electron microscopy (EM) studies have identified predominately spherical particles with a heterogenous diameter of 40–80 nm (Bradley et al., 1985; Catanese et al., 2013; Gastaminza et al., 2010; Merz et al., 2011).

Negative stain and cryoelectron microscopy studies have identified the HCV virion is membrane enveloped with a smooth surface and displays the two glycoproteins, E1 and E2, which direct cell receptor binding (Figure 1.4B and C). The core protein forms a nucleocapsid which surrounds a single copy of the virus genome. This nucleocapsid is discernible in cryoelectron micrographs (Figure 1.4B) and exhibits a similar size to non-enveloped particles which co-purify with membrane enveloped particles (Gastaminza et al., 2010).

Serum- and cell culture-derived HCV particles are associated with lipoprotein components such as apolipoprotein A-I (apoA-I), apoB-48, apoB-100, apoC-I and apoE (Figure 1.4C) (Catanese et al., 2013; Diaz et al., 2006; Felmler et al., 2010; Gastaminza et al., 2010; Kono et al., 2003; Merz et al., 2011; Thomssen et al., 1992), and their lipid composition is similar to serum lipoproteins (Merz et al., 2011). Due to the interactions with lipoproteins, infectious HCV particles have an unusually low and heterogenous buoyant density for an enveloped virus (Hijikata et al., 1993; Lindenbach et al., 2005). It is therefore proposed that HCV particles form hybrid lipoviral particles (LVP), either through transient interactions with serum lipoproteins in the two-particle model, or by directly sharing an envelope with a low-density lipoprotein (LDL) in the single particle model (Figure 1.4D) (Lindenbach and Rice, 2013).

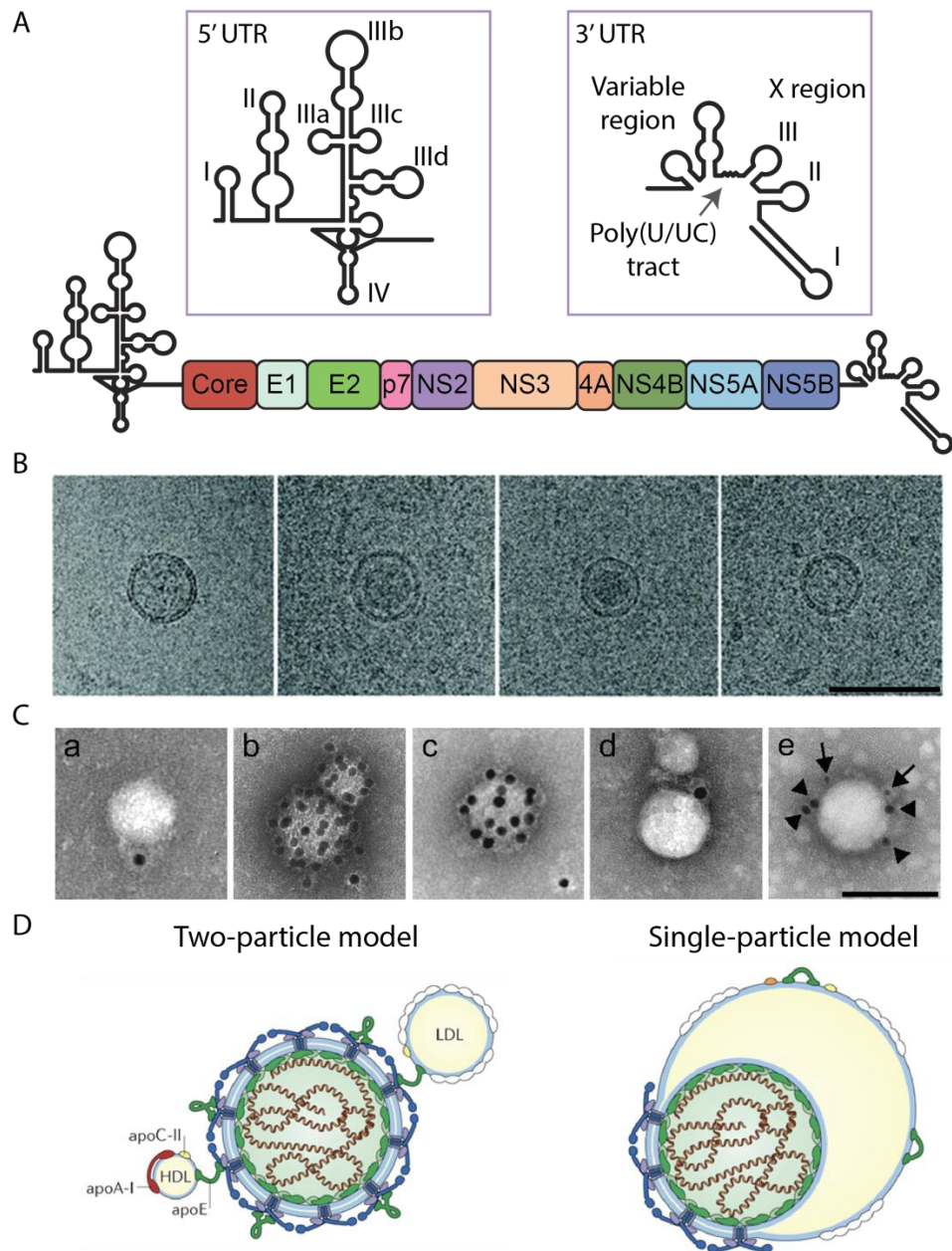


Figure 1.4: Organisation of the HCV genome and virion architecture.

A: Genome organisation of HCV with 5' and 3' UTRs (insets). Protein organisation within the polyprotein is indicated. B: Electron cryomicrographs of purified virus. Scale bar 100 nm. Adapted from (Gastaminza et al., 2010). C: Immunogold labelling of purified HCV particles (a) E2, (b) apoE, (c) apoA-I, (d) apoB, (e) E2 (arrows, 8 nm gold) and apoE (arrowheads, 18 nm gold). Scale bar 100 nm. Adapted from (Catanese et al., 2013). D: Models of HCV virion architecture; two-particle model with transient interaction between serum lipoproteins (high-density lipoprotein [HDL] and low-density lipoprotein [LDL]) and HCV particles. Single particle model with membrane sharing between HCV and low-density lipoprotein. Adapted from (Lindenbach and Rice, 2013).

1.2.3 HCV entry

Hepatocytes are the cellular target of HCV and account for 60–70% of the liver cell mass (Lee and Luk, 2010). They adopt a polarised architecture and are infected by HCV from the blood at the basolateral surface (Lindenbach and Rice, 2013). HCV particles bind receptors on the cell surface of hepatocytes and are internalised by clathrin-mediated endocytosis (Blanchard et al., 2006). Unlike other viruses, HCV requires binding and attachment to a number of receptors on the cell surface in a receptor binding cascade (Figure 1.5).

Initial receptor binding occurs via the virion-associated apoE onto low-density-lipoprotein receptor (LDLR) and glycosaminoglycans (GAGs) present on heparin sulphate proteoglycans (Agnello et al., 1999; Germi et al., 2002; Monazahian et al., 1999). The presentation of apoE on the surface of HCV is important for facilitating HCV entry into cells. Polymorphisms in the apoE gene, specifically the $\epsilon 3$ allele, are associated with increased risk of developing persistent infection (Price et al., 2006). Stabilisation of receptor binding by scavenger receptor class B member 1 (SRB1) to virus-associated lipoproteins and subsequent lipid transfer activity, in a post-binding event, are then required for productive HCV entry (Dao Thi et al., 2012; Zahid et al., 2013). SRB1 then interacts with the hypervariable region 1 (HVR1) of E2, altering its conformation, to facilitate E2 binding to CD81 (Bankwitz et al., 2010; Dao Thi et al., 2012; Scarselli et al., 2002). Binding of CD81 to E2, is thought to prime HCV for pH-dependent fusion (Sharma et al., 2011), and this interaction requires the tight junction protein claudin 1 (CLDN1) (Harris et al., 2010).

Tight junctions are a critical component in liver architecture which maintain tissue integrity, cellular interactions and cell-cell communications (Lee and Luk, 2010). Both CLDN1 and occludin are multiple transmembrane spanning proteins at the tight junction which mediate HCV internalisation in a post binding step (Evans et al., 2007; Harris et al., 2010; Ploss et al., 2009; Sourisseau et al., 2013). Although CLDN1 does not bind HCV directly, interaction with CD81 mediates HCV internalisation (Evans et al., 2007; Harris et al., 2010). Additional receptors such as transferrin receptor 1 and Niemann-Pick C1-like 1 are also important for HCV entry, although their roles in HCV entry remain to be elucidated (Sainz et al., 2012).

Following receptor binding a number of intracellular signal transduction pathways are activated which facilitate HCV entry. Binding of E2 to CD81 facilitates the lateral movement of HCV on the cell surface to the tight junction (Brazzoli et al., 2008). This is through modification of cortical actin filaments after activation of

Rho-GTPases by CD81 (Brazzoli et al., 2008; Farquhar et al., 2012). Further interactions with epidermal growth factor receptor (EGFR) promote the CD81-CLDN1 interaction (Lupberger et al., 2011) and mediate the step between receptor engagement and clathrin-mediated endocytosis (Diao et al., 2012).

After clathrin-mediated endocytosis, HCV particles are trafficked to endosomal compartments (Coller et al., 2009; Farquhar et al., 2012), where fusion of endosomal membranes with the HCV envelope releases the genome into the cytoplasm. This requires acidification of endosomal compartments (Tscherne et al., 2006) which is thought to induce rearrangements in the glycoproteins to mediate membrane fusion at pH 5.0 (Haid et al., 2009; Lavillette et al., 2006). Although the precise mechanism is yet to be fully elucidated, the E1 glycoprotein harbours a putative fusion peptide (Drummer et al., 2007). Support for this fusion peptide was reported recently with the discovery of resistance mutations within E1 to a compound that inhibits HCV membrane fusion (Perin et al., 2016).

HCV can also be directly transmitted through cell to cell contact which is dependent on the tight junction proteins CLDN1 and occludin, and SRB1 and CD81 (Brimacombe et al., 2011; Timpe et al., 2008). Originally thought to be independent of CD81, this process does require CD81 along with the full complement of HCV proteins including E1 and E2 (Brimacombe et al., 2011; Timpe et al., 2008; Witteveldt et al., 2009).

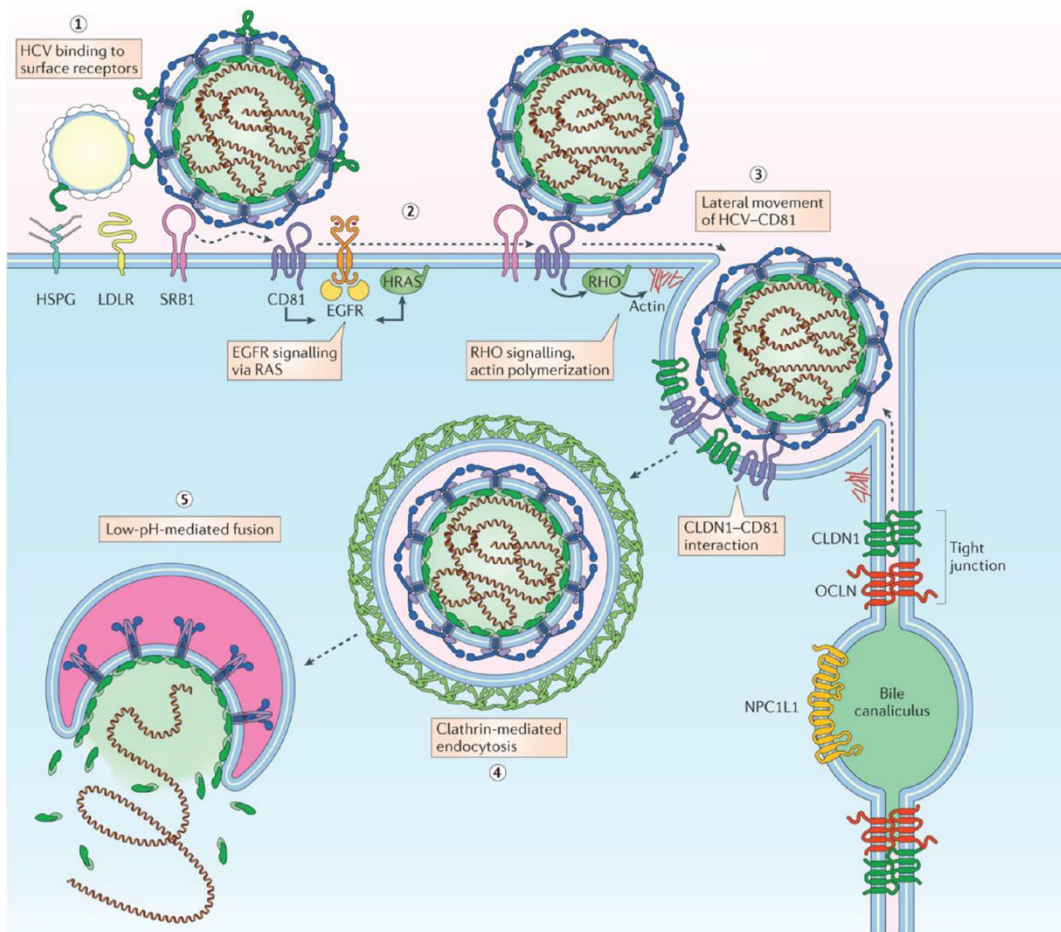


Figure 1.5: Entry of HCV into the cell.

Step 1: HCV lipoviral particles associate with the cell surface by interactions with heparin sulphate proteoglycans (HSPG), low-density-lipoprotein receptor (LDLR) and scavenger receptor class B member 1 (SRB1) before interaction with CD81. Step 2: Interaction of E2 with CD81 mediates epidermal growth factor receptor (EGFR) signalling through Rho GTPases. Step 3: Lateral movement of HCV to sites of cell-to-cell contact. Step 4: Interaction of CD81 with claudin 1 (CLDN1) initiates HCV internalisation by clathrin-mediated endocytosis. Step 5: The low pH of the endosomal compartment induces HCV membrane fusion and genome release. Niemann-Pick C1-like 1 (NPC1L1), occludin (OCLN). Reproduced from (Lindenbach and Rice, 2013).

1.2.4 Polyprotein translation

Most eukaryotic mRNA translation is initiated by binding of the 5'-m₇G cap-structure to the cap-binding complex and subsequent recruitment of the 40S ribosomal subunit and associated eukaryotic initiation factors (eIF) (Jackson et al., 2010; Sonenberg and Hinnebusch, 2009). This pre-initiation complex then scans along the mRNA until an initiation AUG codon is encountered.

HCV bypasses this process by recruiting the 40S ribosomal subunit directly via interactions with the IRES in the 5' UTR (Fukushi et al., 1997; Honda et al., 1996; Pestova et al., 1998; Rijnbrand et al., 1995; Rijnbrand and Lemon, 2000). Since the discovery of this mechanism for virus translation several cellular IRES have been identified and studied (Komar and Hatzoglou, 2011). For HCV, this process only requires eIF3 and eIF2, which bring the initiator methionyl-tRNA to the 40S ribosomal unit, and is mediated by domain III of the IRES (Figure 1.4A inset) (Ji et al., 2004; Otto and Puglisi, 2004; Pestova et al., 1998; Rijnbrand et al., 1995). The basal portion of domain III forms the core interaction with the 40S subunit and involves a conserved GGG motif within III_d, while the apical portion (III_b) interacts with eIF3 (Kieft et al., 2001; Kolupaeva et al., 2000; Lytle et al., 2002, 2001).

Binding of the HCV IRES to the 40S ribosomal subunit induces rotation of the head domain and opening of the mRNA binding channel (Spahn et al., 2001). Subsequent recruitment of the 60S ribosomal subunit forms an active 80S ribosome positioned directly on the HCV initiation AUG codon (Reynolds et al., 1996, 1995). Correct positioning of the ribosome on the start codon requires both sequence and structural stability of domain IV (Honda et al., 1996).

Translation of the HCV open reading frame produces a polyprotein of approximately 3000 amino acids which is later cleaved into the individual proteins (Figure 1.6). The signal peptide sequence at the core-E1 boundary stalls polyprotein translation and directs the ribosome to the endoplasmic reticulum through the signal recognition particle (Hüssy et al., 1996; McLauchlan, 2000; McLauchlan et al., 2002; Reid and Nicchitta, 2015; Santolini et al., 1994). Signal peptidase cleavage of the core-E1 junction, and a series of further signal sequences at the E1-E2, E2-p7 and p7-NS2 boundaries, liberate the structural proteins and p7 (Griffin et al., 2005; Hijikata et al., 1993). Autocatalysis by NS2 at the NS2-3 boundary frees NS2 from the polyprotein (Grakoui et al., 1993; Hijikata et al., 1993), before the remaining HCV proteins are released by NS3 (Bartenschlager et al., 1994). The cofactor NS4A is required to complete the NS3 protease domain and anchor the protein to the ER (Bartenschlager et al., 1995). All HCV proteins are membrane associated

and this is required for their function (Figure 1.6) (Brass et al., 2008; Elazar et al., 2004; Gosert et al., 2005; Moradpour et al., 2003; Schmidt-Mende et al., 2001).

1.2.5 Genome replication

Positive strand RNA viruses replicate in close association with cytoplasmic host cell membranes (Paul and Bartenschlager, 2015). These virally-induced structures are specialised sites for genome replication termed viral replication factories. HCV infection induces the production of single, double and multi-membrane vesicles in the cytoplasm, termed the “membranous web”, which give infected hepatocytes a “sponge-like” appearance by EM (Egger et al., 2002; Gosert et al., 2003). The formation and architecture of these membranous structures are a major focus of this study and are discussed in further detail in (Section 1.4).

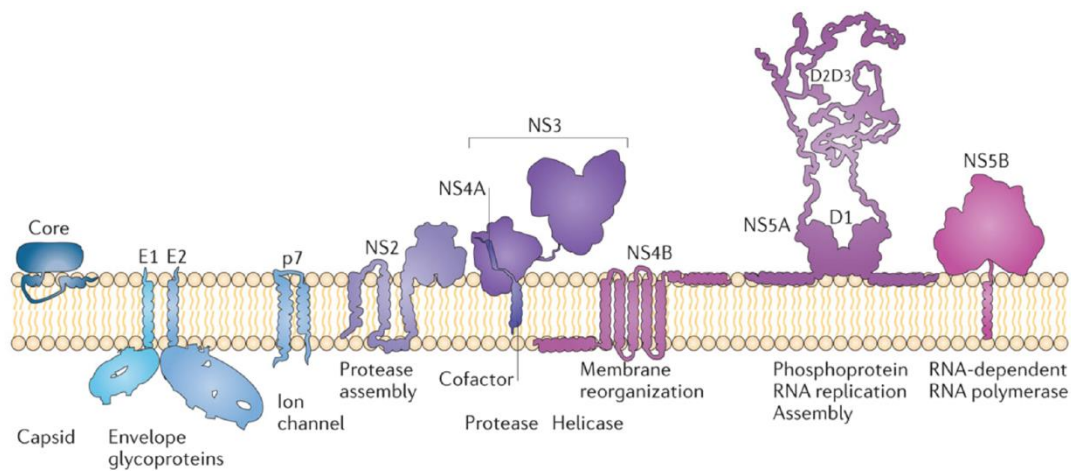


Figure 1.6: Membrane topologies and major functions of HCV proteins.

Each protein is membrane bound by one or several transmembrane helices, except core and NS5A which use amphipathic helices. Only NS5A is represented as a dimer, although most, if not all form homo- heterodimers or oligomeric complexes. Adapted from (Bartenschlager et al., 2013).

Genome replication and polyprotein translation are two inter-linked processes controlled by HCV RNA regulatory elements and cellular proteins (Isken et al., 2007; Romero-López et al., 2014; Romero-López and Berzal-Herranz, 2009). HCV genome replication is mediated by the virally encoded RNA-dependent RNA polymerase NS5B (Appleby et al., 2015). The synthesis of negative strand RNA appears to be rate-limiting for HCV replication as positive strand copies are generated in 5–10-fold excess (Quinkert et al., 2005). The control between genome replication and translation is postulated to be instigated by genome circularisation (Isken et al., 2007). This prevents conflict between translating ribosomes travelling 5'–3' versus the 3'–5' movement of NS5B in negative strand synthesis.

Another feature of HCV genomes are their genetic variability. HCV circulates as a quasispecies of closely related genomes (Martell et al., 1992). This is due to the low fidelity of NS5B with an error rate, *in vivo*, of $\sim 2.5 \times 10^{-5}$ mutations per nucleotide per genome replication (Ribeiro et al., 2012). A consequence of this is the high genetic diversity of HCV genotypes and the rapid occurrence of resistance mutations to the recently licensed DAAs.

1.2.6 Assembly and release

The assembly and release of HCV particles crucially depends on an association of core protein with cytosolic lipid droplets (cLDs) following synthesis and maturation on the ER (Figure 1.7) (Boulant et al., 2006; Miyanari et al., 2007). Cytosolic lipid droplets are a lipid storage organelle containing a hydrophobic core with a phospholipid monolayer that is derived from the outer leaflet of the ER membrane (Gross and Silver, 2014). The complete processing of core by signal peptide peptidase is important for this association with cLDs, as disruption of processing reduces HCV titres (Okamoto et al., 2008; Targett-Adams et al., 2008b).

Multiple interactions between the HCV proteins facilitate the assembly and egress of virus particles. NS5A contains three domains (I, II and III) and is a key player in this process (Miyanari et al., 2007). The regulation of the switch between NS5A involvement in replication and assembly is thought to occur by phosphorylation (Masaki et al., 2008; Tellinghuisen et al., 2008a). Two distinct regions in domain III, comprising a cluster of basic amino acids and a separate cluster of serine's, are involved in recruitment of replication complexes to core, and transfer of HCV RNA to core respectively (Zayas et al., 2016).

Another two non-structural proteins, p7 and NS2 are required for the correct organisation and recruitment of non-structural proteins and core-containing cLDs to

the assembly complex (Gentsch et al., 2013; Jirasko et al., 2010; C. T. Jones et al., 2007; Popescu et al., 2011). Although not involved in replication, p7 deletions in HCV do not produce infectious particles (C. T. Jones et al., 2007; Lohmann et al., 1999; Steinmann et al., 2007).

The NS2 requirement for virus production does not depend on its catalytic activity as this is dispensable in the assembly process (Jirasko et al., 2010). Instead, the NS2 transmembrane domains are required which recruit the E1/E2 and NS3/4A complexes to sites of core associated cLDs (Counihan et al., 2011; Phan et al., 2009).

The recruitment of NS3/4A may be required for helicase-dependent packaging of HCV genomes. Accordingly, the NS3 helicase domain has been shown to be required for HCV particle production at a step after the association of core and NS5A but before the assembly of progeny virions (Ma et al., 2008; Yi et al., 2007).

Progeny virions then bud from the assembly complex using the ESCRT (endosomal sorting complex required for transport) pathway which involves ubiquitination of NS2 to facilitate direct interactions with the ESCRT machinery (Ariumi et al., 2011; Barouch-Bentov et al., 2016; Corless et al., 2010; Tamai et al., 2012). The process of RNA packaging and budding is most likely a coordinated process comparable to other enveloped viruses (Welsch et al., 2009) as no preformed capsids are identified within cells.

After assembly, virions travel through the *trans*-Golgi network (TGN) and endosome pathways in a process of maturation where the E1/E2 envelope proteins are glycosylated (Gastaminza et al., 2008; Mankouri et al., 2016; Vieyres et al., 2010). This process disrupts the TGN architecture in an NS2-dependent manner, resulting in TGN redistribution to regions containing HCV core on lipid droplets (Mankouri et al., 2016).

After glycosylation of the E1/E2 proteins in the Golgi, HCV virions are released at the plasma membrane by trafficking through the endosome network in a VAMP-1-dependent manner (Coller et al., 2012). The endosome pathway appears to be important for multiple stages of the HCV lifecycle as the early endosome protein Rab5 is required for HCV genome replication (Manna et al., 2010; Stone et al., 2007).

Serum-derived HCV particles are associated with lipoprotein components and share a similar lipid composition (Section 1.2.2). However, there is conflicting data whether HCV virions associate with serum lipoproteins during egress. Assembly

has been reported to depend on the apolipoprotein apoE due to a specific interaction with NS5A (Benga et al., 2010; Counihan et al., 2011; Jiang and Luo, 2009). However, more recent studies indicate that HCV release may be independent of the very-low-density lipoprotein (VLDL) pathway (Mankouri et al., 2016). Accordingly, the VLDL pathway requirements apoB and microsomal triglyceride transfer protein are dispensable for HCV particle assembly (Benga et al., 2010; Jiang and Luo, 2009).

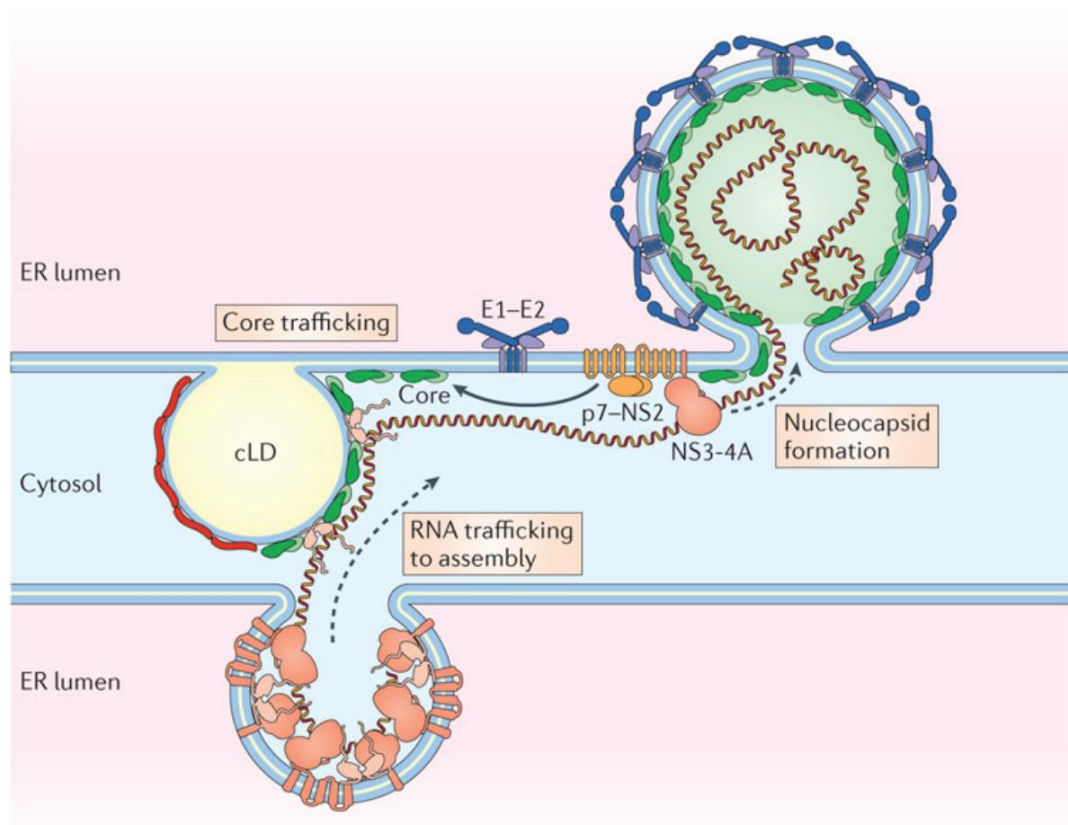


Figure 1.7: HCV assembly.

Viral RNA is transferred from replication complexes to core on cytosolic lipid droplets, the site of virus assembly. The transfer of viral RNA is proposed to be mediated by NS5A. The non-structural proteins p7 and NS2 are critical for the recruitment of core, E1/E2 and NS proteins at the site of assembly. Virus particles assemble by recruitment of E1/E2 complexes and budding into the ER. Reproduced from (Lindenbach and Rice, 2013).

1.3 Individual HCV proteins

1.3.1 Core – nucleocapsid protein

The mature core protein is a 21 kDa RNA binding protein which binds the genomic RNA and forms the HCV nucleocapsid (Gawlik and Gallay, 2014). The protein is divided into two domains, DI and DII which have different hydrophobicity profiles (Boulant et al., 2006, 2005). The N-terminal domain is hydrophilic and rich in basic amino acid residues, whereas the C-terminus is hydrophobic. The DI domain is mostly involved in RNA binding and oligomerization which are required for particle formation (Ivanyi-Nagy et al., 2006; Majeau et al., 2004). The amino acids 1–82 of DI are intrinsically disordered (Duvignaud et al., 2009) and this property is thought to be vital for genomic RNA packaging into the virus particle (Cristofari et al., 2004). The DII domain contains two amphipathic α -helices which coordinate core localisation to the ER and lipid droplet (LD) membranes (Boulant et al., 2006). The association of core with lipid droplets is critical for protein function and may be regulated by palmitoylation of Cys-172 (Majeau et al., 2009).

1.3.2 E1 and E2 – envelope glycoproteins

The E1 and E2 envelope glycoproteins are present on the surface of HCV virions and mediate receptor binding at the cell surface. Both E1 and E2 are type I transmembrane proteins with an ectodomain facing the ER lumen and a C-terminal transmembrane domain (Cocquerel et al., 2002). They are synthesised on the ER where they form non-covalent heterodimers (Dubuisson et al., 1994; Rouillé et al., 2006), an interaction mediated by their transmembrane domains and ectodomains (Albecka et al., 2011; Ciczora et al., 2007). The N-glycosylation of both E1 and E2 control their protein folding and heterodimerisation (Goffard et al., 2005; Meunier et al., 1999) with complex glycans added during trafficking through the Golgi during virion maturation (Mankouri et al., 2016; Vieyres et al., 2010).

Structures for the E1 amino-terminal portion and E2 core domain were solved by X-ray crystallography in recent years (El Omari et al., 2014; A. G. Khan et al., 2014; Kong et al., 2013). The E2 core is formed of a compact immunoglobulin-like fold and an additional novel domain comprising a central β -sheet surrounded by loops, short helices and two β strands (A. G. Khan et al., 2014; Kong et al., 2013). Like E2, the E1 amino-terminal portion also adopts a novel architecture composed of β strands with a single long α -helix sandwiched between two and three antiparallel β strands (El Omari et al., 2014). Other members of the *Flaviviridae* family encode class II fusion proteins which mediate virion envelope fusion with the

host cell membrane (Kielian, 2006). The structural data of E1 and E2 contradict the prediction that they are also class II fusion proteins and indicate that HCV membrane fusion might proceed by another mechanism which is currently not understood (El Omari et al., 2014; A. G. Khan et al., 2014; Khan et al., 2015; Kong et al., 2013).

1.3.3 p7 – viroporin

The p7 protein of HCV is a viroporin of only 63 amino acids. It is a transmembrane protein that crosses the membrane twice and displays its N- and C-termini towards the cytoplasm (Lin et al., 1994). p7 is localised predominately at ER membranes with some association on mitochondria or lipid droplets, and is mostly colocalised with E2 (Vieyres et al., 2013). Oligomerisation of p7 into hexameric or heptameric cation-selective ion channels facilitate proton conductance across membranes (Griffin et al., 2003; Premkumar et al., 2004). This reduces the acidic conditions in the virion egress and release pathway which would otherwise damage maturing virions (Gentzsch et al., 2013; Wozniak et al., 2010). In contrast to the M2 protein of influenza virus that forms a proton channel in the viral envelope (Pielak and Chou, 2011), p7 is not incorporated into HCV virions (Vieyres et al., 2013).

1.3.4 NS2 – autoprotease

The NS2 protein is 23 kDa and contains an N-terminal transmembrane domain and a C-terminal cytoplasmic domain. The C-terminal domain is a cysteine protease which processes the NS2–3 boundary of the HCV polyprotein by autoprotease activity (Grakoui et al., 1993; Hijikata et al., 1993). The establishment of sub-genomic replicons (SGR) demonstrated that NS2 is not required for genome replication (Lohmann et al., 1999). However, the C terminal catalytic domain was shown to be required for virus assembly (C. T. Jones et al., 2007). Additionally, NS2 has been implicated in host cell modulation with involvements in ER stress and apoptosis (von dem Bussche et al., 2010; Welbourn and Pause, 2006).

1.3.5 NS3/4A – protease/helicase

The 70 kDa NS3 is a two domain protein that encodes two enzymatic activities. The N-terminal and C-terminal domains encode for a serine protease and NTPase-dependent RNA helicase, respectively (Lin, 2006).

The N-terminal protease domain is involved in polyprotein processing and maturation of the remaining non-structural proteins. Efficient protease processing of NS3 requires the NS4A cofactor which both contributes to the protease fold of NS3

and anchors the NS3/4A protein to membranes (Bartenschlager et al., 1995, 1994). After polyprotein processing, the NS3/4A protease is involved in virus host interactions such as innate immunity interference (Li et al., 2005). NS3/4A efficiently cleaves and inactivates MAVS, an essential component in the RIG-I cytosolic sensory pathway (Foy et al., 2003), and the adaptor protein TRIF in the TLR3 pathway (Li et al., 2005).

The C-terminal helicase domain is a member of the DExH helicase superfamily-2 and exhibits polynucleotide-stimulated NTPase activity (Suzich et al., 1993) which drives unwinding of RNA in a 3'–5' direction (Kim et al., 1995; Tai et al., 1996). Crystallographic structures of three conformations during helicase activity identified a “ratchet” mechanism for the unidirectional translocation along RNA with a step size of one base per nucleotide hydrolysis (Gu and Rice, 2010).

The purpose of linking two enzymatic activities onto a single protein remains elusive. Recent studies hypothesise that the helicase helps evade the immune response by binding pathogen associated molecular patterns, bringing the protease near immune receptors for cleavage (Corby et al., 2016).

1.3.6 NS4B – transmembrane protein

The 27 kDa hydrophobic protein NS4B is ER associated and contains 4 transmembrane domains and 2 helices at its N- and C-terminus (Gouttenoire et al., 2010). Within the middle of the protein on the cytosolic side is a nucleotide binding domain (Gouttenoire et al., 2010) which has been implicated in GTP and ATP binding and hydrolysis (Einav et al., 2004). The expression of NS4B alone in cells has been shown to induce formation of the membranous web and is thought to occur through oligomerisation (Egger et al., 2002; Paul et al., 2013). Therefore it plays a key role in replication complex formation and is involved in interactions with other viral proteins (Aligo et al., 2009; David et al., 2015), RNA (Einav et al., 2004) and the production of virus (Han et al., 2013).

1.3.7 NS5A – multifunctional phosphoprotein

1.3.7.1 *Structure of NS5A*

NS5A is a 49 kDa protein, however 56 and 58 kDa forms, termed basal- and hyper-phosphorylated respectively, are resolvable by SDS-PAGE analysis (Neddermann et al., 1999). It is composed of three domains (I, II and III) separated by loop regions, termed low complexity sequences (LCS) (Tellinghuisen et al., 2004) (Figure 1.8).

At its N-terminus is a short (33 amino acid) amphipathic helix which is required for HCV replication and directs NS5A membrane association (Penin et al., 2004). This is followed by domain I which is the only domain with a crystal structure (Lambert et al., 2014; Love et al., 2009; Tellinghuisen et al., 2005). The structures revealed that domain I coordinates a zinc atom within a tetracysteine motif, has a disulphide bond at the C terminus, and the presence of a basic RNA-binding groove between the NS5A dimer interface.

Although dimeric in the crystal structure, limited evidence exists to support a dimeric structure *in vivo* (Lim et al., 2012). Models for NS5A dimer associated with the membrane have been proposed, however these lack experimental evidence (Ross-Thriepland and Harris, 2015). Both the tetracysteine motif and disulphide bond are required for maintaining the structure of domain I.

The second two domains of NS5A are intrinsically disordered (Hanouille et al., 2010, 2009b; Liang et al., 2007, 2006; Verdegem et al., 2011). Nuclear magnetic resonance studies have identified α -helical structures within domain II (Feuerstein et al., 2012). NS5A is a multifunctional protein known to interact with a large number of cellular interaction partners (Tripathi et al., 2013). This promiscuity is proposed to derive from the ability of domains II and III to adopt a multitude of different conformations (Ross-Thriepland and Harris, 2015). Consistent with an unstructured and disordered peptide sequence, domains II and III are able to tolerate gene insertions at a number of discrete positions (Arumugaswami et al., 2008; Remenyi et al., 2014). These have been exploited for insertions of protein tags (e.g. GFP) to monitor NS5A trafficking within cells (D. M. Jones et al., 2007; Moradpour et al., 2004; Schaller et al., 2007).

Recently, a number of HCV related hepaciviruses have been identified which share a high degree of sequence homology with domain I but not domains II and III (Burbelo et al., 2012; Kapoor et al., 2013, 2011; Lauck et al., 2013). Secondary structure prediction programs indicate that the organisation of NS5A into three domains separated by LCS are shared among the hepaciviruses (Lauck et al., 2013).

1.3.7.2 Roles of NS5A during HCV infection

NS5A is involved in stages of genome replication and virus assembly, the separation of which is controlled by different domains. Domains I and II are required for genome replication (Ross-Thriepland et al., 2013; Tellinghuisen et al., 2004). In comparison, although domain III contributes to genome replication it is dispensable

(Tellinghuisen et al., 2008b) and is instead required for HCV assembly (Hughes et al., 2009b; Zayas et al., 2016).

The separation of these two functions are spatiotemporally regulated and fluorescence microscopy studies have revealed multiple populations of NS5A (Shulla and Randall, 2015). Live cell imaging studies with GFP-tagged NS5A have identified large immobile structures and smaller faster moving structures (D. M. Jones et al., 2007; Wölk et al., 2008), the movement of which is dependent on dynein (Eyre et al., 2014).

Disruption of the protein fold in the N-terminus of domain I by mutation of the tetracysteine motif inhibits HCV replication (Tellinghuisen et al., 2004). This region also contains an important PTPPL sequence which associates NS5A to lipid droplets and is required for release of infectious HCV (Miyanari et al., 2007). In line with its involvement in genome replication, domain I is responsible for double membrane vesicle formation (Romero-Brey et al., 2015). However, a comprehensive description of domain I functions are not yet reported despite the detailed structural information.

Domain II has been more extensively studied and is known to interact with host and viral proteins (Evans et al., 2004; Goh et al., 2001; Shirota et al., 2002). Studies with different genotypes have identified that deletions of 15–35 amino acids in the C-terminus abrogate replication, of which 23 were found to be essential (Appel et al., 2008; Tellinghuisen et al., 2008b). Conversely, deletion in the N-terminus has no effect on replication.

NS5A domain III is mostly involved in virus assembly, in particular the C-terminal 38 amino acids are required (Appel et al., 2008). Genotype 2 isolates contain an additional 18 amino acids within this C-terminal region that, conversely, is dispensable for assembly, with deletion only modestly effecting genome replication (Hughes et al., 2009b). A cluster of serines within the last 15 residues of domain III are phosphorylated and required for the interaction with core (Masaki et al., 2008). NS5A is reported to localise to core containing lipid droplets (Miyanari et al., 2007), and this localisation is mediated by the interaction and activity of diacylglycerol acyltransferase, a cellular enzyme involved in triglyceride synthesis in hepatocytes (Camus et al., 2013; Yen et al., 2008).

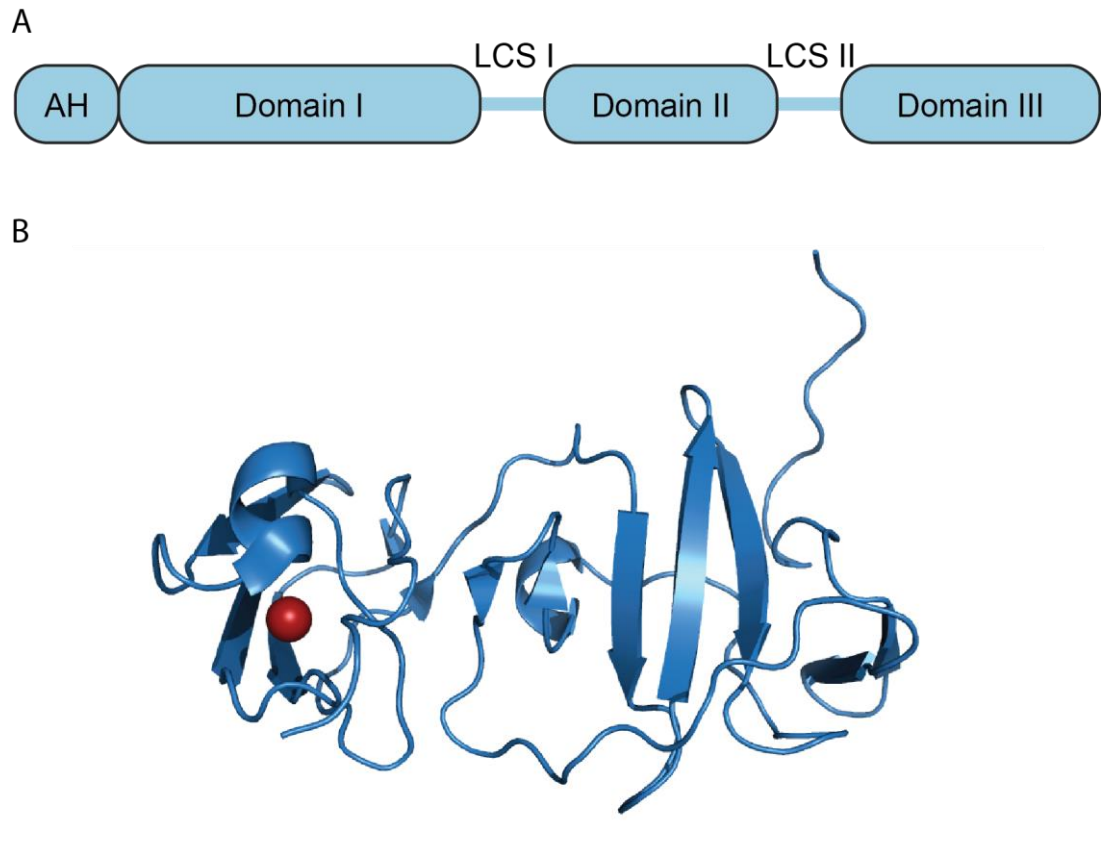


Figure 1.8: Structure of NS5A.

A: Schematic of NS5A protein organisation. NS5A is composed of three domains separated by low complexity sequences (LCS) with an N-terminal amphipathic helix (AH). B: Crystal structure of genotype 1b NS5A domain I. The zinc atom coordinated by the tetracysteine motif is shown in red. (PDB ID No. 1ZH1).

1.3.7.3 Interaction partners

Proteomic approaches with NS5A have identified over 130 cellular interaction partners (Tripathi et al., 2013), of which 60 have a reported functional consequence (Figure 1.9) (Ross-Thriepland and Harris, 2015). These interactions are likely spatially and temporally separated with only a subset occurring at any one time (Shulla and Randall, 2015). The ability of NS5A to interact with numerous partners likely stems from domains II and III which are intrinsically disordered and may adopt multiple conformations (Feuerstein et al., 2012).

HCV replication is intrinsically linked to lipid metabolism in hepatocytes. Inhibition of phosphatidylinositol 4-phosphate (PI4P), cholesterol and fatty acid biosynthesis all disrupt HCV replication (Kapadia and Chisari, 2005; Reiss et al., 2011). NS5A directly interacts and activates the phosphatidylinositol 4-kinase (PI4K) III α which increases the quantity of PI4P (Reiss et al., 2011), and is required to maintain the membranous web (Section 1.4.1). A short seven amino acid region in domain I of NS5A is responsible for this interaction, and negative regulation of NS5A hyperphosphorylation was also reported (Reiss et al., 2011).

Cyclophilins play an important role in the replication of HCV as inhibition of their activity abrogates HCV replication (Nakagawa et al., 2005, 2004; Watashi et al., 2003). This is mediated through a direct interaction of cyclophilin A (CypA) with the C-terminus of domain II (Chatterji et al., 2010; Coelmont et al., 2010; Hanouille et al., 2009a) and domain III (Verdegem et al., 2011). Cyclophilins are a family of peptidyl-prolyl isomerases (PPIase) that catalyse the *cis-trans* isomerisation of the peptide bond preceding a proline residue and are the target of the immunosuppressive drug cyclosporin A (CsA) (Handschumacher et al., 1984). Mutations that confer resistance to CsA are reported in both domain II and III, although these mutations do not prevent binding of either CsA or CypA to NS5A (Coelmont et al., 2010). The precise role of CypA isomerisation of NS5A is not known, although the multifunctional nature of NS5A suggests that this may provide another mechanism for switching the functions of domains II and III. Accordingly, a binding site for CypA on domain II of NS5A is shared with the HCV polymerase, NS5B (Rosnoblet et al., 2012).

A number of cellular proteins contain Src homology 3 (SH3) domains which mediate protein-protein interactions (Mayer, 2001). These are bound by NS5A through the polyproline motif (PxxPxxR) within LCSII of NS5A which is completely conserved across all HCV genotypes (Macdonald et al., 2004; Tan et al., 1999). Mutation of this motif does not affect replication or virus production in cell culture (Hughes et al.,

2009a), but is required to establish infection in the chimpanzee model (Nanda et al., 2006). NS5A protein interactions utilising the polyproline motif include the regulation of apoptosis (Mankouri et al., 2009) through the SH3-domain-containing kinase mixed lineage kinase 3 (Amako et al., 2013) and amphiphysin II (Zech et al., 2003), and trafficking of epidermal growth factor receptor (Mankouri et al., 2008) through the Cas ligand with multiple SH3 domains (Igloi et al., 2015).

Other than cellular interaction partners, NS5A also binds HCV RNA (Foster et al., 2010; Huang et al., 2005; Hwang et al., 2010). These studies identified that NS5A preferentially binds short (5–6 nucleotide) uracil-rich RNAs (Hwang et al., 2010) and exhibits a higher affinity for the poly(U/UC) tract in the 3' UTR than the X region (Foster et al., 2010). The regulation of NS5A RNA binding may coordinate different stages of the HCV life cycle such as the switch from replication to assembly. Although no evidence to support or dispute this hypothesis is reported, domain II RNA-binding is stimulated by CypA *in vitro* (Foster et al., 2010) and CypA inhibition reduces NS5A RNA binding in HCV infected cells (Nag et al., 2012).

Lipid droplet binding
100–104

PI4KIII α binding
202–210

DCV resistance
28, 31, 93

Cyclophilin A binding
311–318

Tetracysteine
39, 57, 59
and 80

SH3 binding
343–356

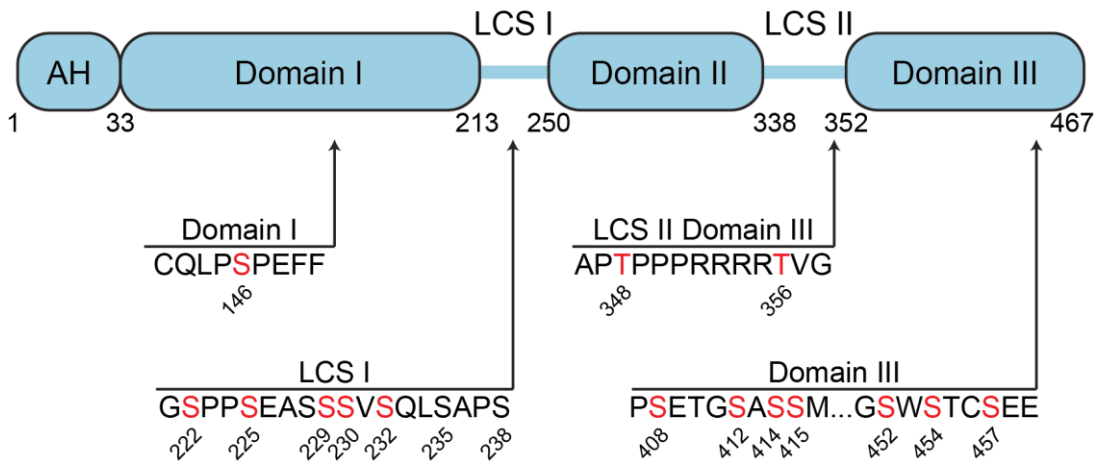


Figure 1.9: Organisation of NS5A with interaction partners.

Amphipathic helix (AH), tetracysteine coordinated zinc (Tellinghuisen et al., 2005), daclatasvir resistance mutants (Fridell et al., 2010), lipid droplet binding motif (Miyanari et al., 2007), PI4KIII α -binding motif (Reiss et al., 2011), cyclophilin A binding site (Hanouille et al., 2009a; Coelmont et al., 2010), and P2 polyproline SH3-binding motif (Hughes et al., 2009a) are indicated. Known phosphorylation sites are highlighted (red). Sequence presented is genotype 2a (JFH1). Adapted from (Ross-Thriepland and Harris, 2015).

1.3.7.4 Phosphorylation of NS5A

Phosphorylation is a posttranslational modification that regulates an estimated 30% of proteins in mammalian cells (Cohen, 2000). Serine, threonine and tyrosine phosphorylation are the mostly widely studied but phosphorylation of histidine, lysine, arginine, aspartate, glutamate and cysteine also occur (Cieřla et al., 2011).

NS5A is a highly phosphorylated protein existing as both basal and hyperphosphorylated species within infected cells (Neddermann et al., 1999). Mass spectrometry studies have identified multiple phosphorylation sites within the NS5A LCS and indicate a complex regulation of NS5A functions (Lemay et al., 2013; Masaki et al., 2014; Ross-Thriepland and Harris, 2014). Mutation of serines in LCS (S225, S232 and S235) to alanine all impair replication, whereas no effect was observed with mutation to aspartate, a phosphomimetic residue (Ross-Thriepland and Harris, 2014). Additionally, the first serine within LCS, S222, was identified in all three studies and is a hallmark of the hyperphosphorylated species as the final phosphorylated residue in the phosphorylation cascade of LCS (Ross-Thriepland and Harris, 2014).

The precise regulatory roles of NS5A phosphorylation remain elusive despite recent findings. Opposite effects are observed with mutation of the same serines between genotype 1b (Con1) compared to 2a (JFH1) (Appel et al., 2005; Ross-Thriepland and Harris, 2014). In genotype 1b, the role of hyperphosphorylation negatively effects replication (Evans et al., 2004), and the culture adaptive mutation S2204I (corresponding to S232 in genotype 1b) abrogates hyperphosphorylation and confers a 20,000-fold increase in replication efficiency (Blight et al., 2000). This particular mutation is adaptive in genotypes 3a, 4a, 5a and 6a (Kim et al., 2014; Kinge et al., 2014; Saeed et al., 2012; M. Yu et al., 2014), but not 2a or the recently described 1a cell culture adapted virus TNcc (Li et al., 2012).

Interestingly, S146 in genotype 2a appears to negatively regulate hyperphosphorylation with a reduction of hyperphosphorylation observed in S146D mutant replicons (Ross-Thriepland and Harris, 2014). The consequence of this particular residue is unclear as in all other genotypes, except 1a, S146 is an alanine. In contrast, mutation of S225 to alanine resulted in deficient HCV replication (Ross-Thriepland and Harris, 2014) which correlated with an altered cellular distribution (Ross-Thriepland et al., 2015). Again, the mechanism underlying this is unclear.

A number of kinases are reported to phosphorylate NS5A including casein kinase I (CKI) and CKII, Polo-like kinase (Plk), and cAMP-dependent protein kinase (PKA)

(Chen et al., 2010; Cordek et al., 2014; Quintavalle et al., 2007). CKI- α was shown to phosphorylate S232 dependent on S229 phosphorylation (Quintavalle et al., 2007). Inhibition and siRNA silencing studies have confirmed the activity of CKI- α on NS5A *in vivo* (Masaki et al., 2014; Quintavalle et al., 2007). Plk phosphorylates NS5A *in vitro* to both the 56 and 58 kDa forms, although specific residues were not identified (Chen et al., 2010). Lastly, T356 within domain III of NS5A is phosphorylated by PKA (Cordek et al., 2014). Inhibition of PKA reduces the infectivity of secreted virus particles with no effect on replication or the formation of intracellular infectious particles (Farquhar et al., 2008).

1.3.7.5 NS5A as a target for direct acting antivirals

The most potent direct acting antivirals target NS5A, which has no intrinsic enzymatic activity. Daclatasvir (DCV), developed by Bristol-Myers Squibb, was identified from cell based screening assays for compounds that inhibited SGR activity (Gao et al., 2010). It exhibits extraordinary potency, specificity and pan genotypic activity. The half maximal effective concentration (EC_{50}) is <100 pM but >10 μ M for other viruses (Gao et al., 2004). Additionally, the half maximum cytotoxic concentration (CC_{50}) is >50 μ M, providing a therapeutic index >100,000.

NS5A was confirmed as the target after no effect of DCV on NS3 or NS5B activities and the development of resistance mutations specifically within the amphipathic helix and domain I of NS5A (Gao et al., 2010). Resistance mutations typically occur at positions 28, 30, 31 or 93 and can provide up to 10,000-fold increase in EC_{50} values (Fridell et al., 2010). Since its first description alternative first generation molecules ledipasvir and ombitasvir have been described. Although each first generation NS5A inhibitor exhibits a low barrier to resistance, they have proven effective in the clinic in combination with either NS3/4A or NS5B inhibitors (Pawlotsky, 2014). Second generation elbasvir and velpatasvir have since been described with comparable potency and specificity to the first generation inhibitors but with an improved resistance barrier profile (Nakamoto et al., 2014). The FDA has approved all five of these NS5A inhibitors in various combination therapies (Table 1.1).

Although these drugs have reached the clinic, the precise mode of action against NS5A remains obscure. Based on the EC_{50} value of DCV it is estimated that 1 molecule can inhibit ~10,000 molecules of NS5A (Belda and Targett-Adams, 2012). The drug molecules are large (>700 Da) dimeric molecules and therefore are proposed to interact with the dimeric form of NS5A in a number of models (Barakat et al., 2015; Kazmierski et al., 2014; Lambert et al., 2014; Nettles et al., 2014;

O'Boyle et al., 2013). Direct binding of DCV to NS5A has been observed in cells using a biotin-tagged derivative (Berger et al., 2014; Gao et al., 2010), supported by *in vitro* evidence demonstrating a loss of binding with the Y93H resistance mutation and a reduction in RNA binding by domain I (Ascher et al., 2014).

Global effects on NS5A have also been observed with DCV, including relocalisation, altered fractionation patterns and reductions in hyperphosphorylation (Fridell et al., 2011; Lee et al., 2011; Qiu et al., 2011). Other studies have identified abrogation of the HCV induced membrane rearrangements independent of RNA replication and NS5A redistribution (Berger et al., 2014). Furthermore, treatment of cells established with HCV infection show no effect on pre-formed replication complexes but rapidly block virion assembly and release (McGivern et al., 2014).

The effects of DCV treatment agree with the model of NS5A as a multifunctional protein with distinct populations in the cell involved in different stages of the HCV life cycle. These populations may be differentially accessible to DCV and explain the observed temporal difference in DCV inhibition. For example cytosolic exposed NS5A involved in virion assembly and membrane enclosed involved in replication. Although these observations have provided initial insight into the mode of action of this family of compounds, further investigations are required to fully elucidate their mechanism.

1.3.8 NS5B – RNA-dependent RNA polymerase

NS5B is the virally encoded RNA-dependent RNA polymerase (RdRp) of 62 kDa which is anchored into membranes by a C-terminal transmembrane domain (Lee et al., 2004). *De novo* priming by NS5B for negative strand synthesis occurs at the 3' UTR and requires two nucleotide binding sites within the enzyme to synthesise a dinucleotide primer (Ferrari et al., 2008). High concentrations of GTP have been shown to stimulate *de novo* initiation by binding to an allosteric site (Bressanelli et al., 2002). Structural studies have identified significant conformational changes in NS5B after binding GTP which open the catalytic pocket and allow double stranded RNA (dsRNA) binding (Mosley et al., 2012; Scrima et al., 2012). This appears to encourage transition from primer-dinucleotide formation to elongation and productive RNA synthesis (Ranjith-Kumar and Kao, 2006). This model is supported by the X-ray crystallography structure of NS5B from the highly replication competent HCV isolate JFH1 in which the polymerase finger and thumb domains are connected, producing a "closed" conformation which facilitates efficient *de novo* initiation (Simister et al., 2009).

1.4 HCV replication complex

1.4.1 HCV membrane rearrangements

A common phenotype of all positive strand RNA virus infections is the rearrangement of intracellular membranes in the cytoplasm, creating an environment suitable for replication (Figure 1.10) (Romero-Brey and Bartenschlager, 2014). These structures are commonly referred to as replication factories and serve several functions.

First, they spatially separate the different steps of the virus lifecycle, namely RNA translation, replication and packaging into new virions. Second, the membranous compartments serve to sequester the viral non-structural proteins and required cellular proteins and metabolites, facilitating efficient RNA replication. Finally, they act to protect or shield the HCV components, for example double stranded RNA intermediates, from cellular immune surveillance and degradation, reviewed in (Romero-Brey and Bartenschlager, 2014).

Electron microscopy studies have revealed that HCV infection results in the accumulation of membrane vesicles, mostly double membrane vesicles (DMV), embedded in a compact membrane network (Figure 1.10) (Egger et al., 2002; Ferraris et al., 2012, 2010; Romero-Brey et al., 2012). More recently, soft X-ray microscopy has supported EM studies and provided a detailed description of HCV induced membrane structures in whole intact cells (Pérez-Berná et al., 2016). The production of DMV increases during infection and correlates with the kinetics of HCV replication (Romero-Brey et al., 2012). Therefore, they are suggested to play an important role in viral RNA replication. Accordingly, purified DMV contain active polymerase and the presence of both NS5A and double stranded RNA (Ferraris et al., 2010; Paul et al., 2013). As infection progresses, larger and more complex structures of multi-membrane vesicles (MMV) are observed (Figure 1.10D), although whether MMV play a role during infection is not clear (Ferraris et al., 2012; Romero-Brey et al., 2012). Treatment of infected cells with the antiviral drug Silibinin inhibits HCV in a genotypic specific manner and is associated with an increased number of MMV (Esser-Nobis et al., 2013).

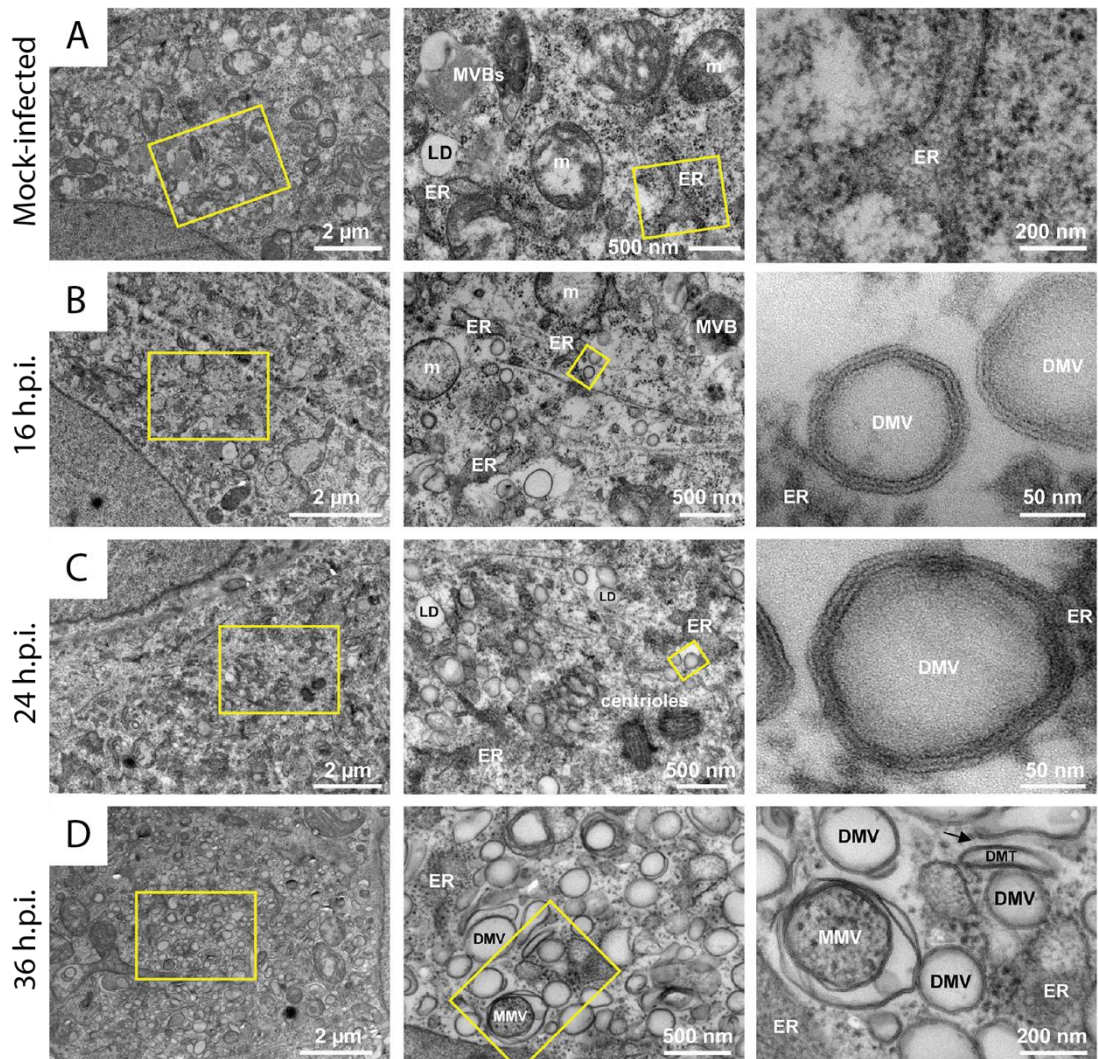


Figure 1.10: Vesicle structures produced during HCV infection.

Electron micrographs from high-pressure-frozen and freeze-substituted naïve and HCV infected cells depicting the membranous rearrangements induced by HCV. Yellow squares indicate the areas shown in higher magnification on the right of each subpanel. ER, endoplasmic reticulum; m, mitochondria; MWB, multi-vesicular bodies; LD, lipid droplet; DMV, double membrane vesicle; DMT; double membrane tubule (labelled with black arrow). Adapted from (Romero-Brey et al., 2012).

The average diameter of DMVs measured by electron microscopy is approximately 200 nm, although structures vary from ~100–1000 nm (Ferraris et al., 2012; Romero-Brey et al., 2012). DMV are typically associated with the ER and around 10% were observed with an opening or pore into the cytoplasm (Romero-Brey et al., 2012). Additionally, the accumulation of DMV were observed around cytoplasmic lipid droplets (Romero-Brey et al., 2012), an important cellular organelle for HCV which is associated with both core and NS5A (Miyanari et al., 2007).

1.4.2 Formation of double membrane vesicles

The double membrane nature of HCV induced structures are morphologically similar to the cellular structures produced by autophagy. During times of nutrient starvation or stress, the engulfment of cytoplasmic contents from the expansion of ER membranes results in the production of double membrane vesicles, termed autophagosomes (Figure 1.11) (Tanida, 2011). Fusion of autophagosomes with lysosomes results in bulk degradation and recycling of the vesicle contents (Tanida, 2011). This process is dynamic and involves multiple protein complex interactions in a sequential pathway.

Initiation of autophagy starts with ER localisation of the ULK complex, composed of ULK1, ULK2, Atg13, FIP200 and Atg101 (Hosokawa et al., 2009; Jung et al., 2009). Subsequent recruitment of the class III phosphatidylinositol 3-kinase (PI3K) complex (Atg14-Vps34-Beclin1) (Wirth et al., 2013) produces a local pool of phosphatidylinositol 3-phosphate (PI3P). Increased local concentration of PI3P recruits PI3P effector proteins such as double FYVE-domain containing protein 1 (DFCP1) and the WIPI family of proteins which form an ER derived structure termed the omegasome (Axe et al., 2008; Karanasios et al., 2013; Koyama-Honda et al., 2013; Polson et al., 2010). PI3P effector proteins in turn recruit the Atg12-Atg5-Atg16 complex and Atg3-LC3 conjugate (Dooley et al., 2014). Assembly of these complexes results in conjugation of LC3 onto phosphatidylethanolamine, converting LC3-I to LC3-II (Fujita et al., 2008). Progressive accumulation of LC3-II results in membrane engulfment of cytoplasmic contents and autophagosome formation (Mizushima, 2010). Finally, fusion of the autophagosome outer membrane with lysosomes forms the autolysosome and degradation of autophagosomal contents (Gutierrez et al., 2004; Jäger et al., 2004).

The induction of autophagy is well documented during HCV infection and is proposed to provide the membrane structures for the formation of HCV replication factories (Chan and Egan, 2005; Ke and Chen, 2011; Mohl et al., 2012; Shinohara

et al., 2013). Accordingly, pharmacological inhibition and downregulation of autophagy proteins inhibit HCV replication (Dreux et al., 2009; Mizui et al., 2010; Mohl et al., 2016; Sir et al., 2008). Although autophagy is induced by HCV, the process is manipulated by direct interactions with viral proteins (Aweya et al., 2013; Guévin et al., 2010; Su et al., 2011) which alter the maturation of autophagosomes and prevent fusion with lysosomes (Sir et al., 2008).

The morphological similarities between HCV DMV and autophagosomes indicate they may arise from a common biogenesis pathway. Recently, the autophagy elongation complex (Atg5-12-19L1) was shown to be critical for the formation of the membranous web, and the presence of Atg5-12 and Atg16L1 were identified in purified HCV membranes with the non-structural proteins (Fahmy and Labonté, 2017). Interestingly, LC3 recruitment and the formation of LC3-II was not required, demonstrating a key subversion to the conventional cellular pathway (Fahmy and Labonté, 2017)

1.4.3 HCV replication factory composition

The formation of *bona fide* HCV replication factories requires additional modifications to the DMV scaffold such as modification of its lipid profile to expand the size, increase positive membrane curvature and recruit additional accessory factors (Paul and Bartenschlager, 2015). The local alteration of membrane environments, for example the production of PI3P during autophagosome formation, are critical modifications to biological membranes involved in recruitment of factors and cellular signalling (van Meer et al., 2008).

The alteration of lipid metabolism during the HCV lifecycle is well documented and reported to account for the pathology associated with chronic infection (Popescu et al., 2014). High-throughput lipidomic profiling of HCV infected cells have revealed significant alterations to lipid compositions (Diamond et al., 2010). The phosphatidylinositol 4-kinase III α (PI4KIII α) and its product phosphatidylinositol 4-phosphate (PI4P) was shown in multiple studies to be important for functionality and integrity of HCV membrane structures (Berger et al., 2009; Borawski et al., 2009; Q. Li et al., 2009; Reiss et al., 2011; Tai et al., 2009; Trotard et al., 2009). Colocalisation of PI4P with NS5A indicated activation of PI4KIII α at sites of HCV replication and direct interactions between PI4KIII α , NS5A and NS5B were observed in coimmunoprecipitation experiments (Reiss et al., 2011). PI4P addition to membranes is known to alter membrane curvature (Furse et al., 2012) and disruption of PI4KIII α by pharmacological inhibition or knockdown of expression during HCV infection reduces DMV diameter (Reiss et al., 2011).

Addition of PI4P to membranes also functions to recruit lipid transfer proteins for the addition of other lipids such as cholesterol and sphingolipids (Holthuis and Menon, 2014). The modification of DMV with a number of lipids is consistent with the reported association of replication complexes with intracellular detergent-resistant lipid-raft-like assemblies (Shi et al., 2003, p. 2–). HCV replication factories are ~9-fold enriched in cholesterol over ER membranes and removal from DMV reduces their size and HCV genome stability (Paul et al., 2013). Additionally, oxidation of cholesterol by the cholesterol 25-hydroxylase abrogates HCV replication (Chen et al., 2014). The cholesterol transport protein oxysterol-binding protein (OSBP) and glycosphingolipid transporter four-phosphate adaptor protein 2 are both required for HCV replication (I. Khan et al., 2014; Wang et al., 2014). This is mediated by the adaptor proteins VAP-A and VAP-B which are also required for HCV replication and interact directly with NS5A and OSBP (Hamamoto et al., 2005; Tu et al., 1999). Although the precise details of sphingolipids in HCV replication are unknown, their upregulation in infected cells stimulates NS5B activity (Hirata et al., 2012; Weng et al., 2010).

Other than lipid composition, the introduction of amphipathic α -helices and oligomerisation of integral membrane proteins asymmetrically into membranes can alter local membrane curvature (Kozlov et al., 2014; McMahan and Gallop, 2005). The recruitment of proline-serine-threonine phosphatase interacting protein 2 by NS4B and NS5A is crucial for replication (Chao et al., 2012). Dimerization of this protein yields a concave-shaped structure which induces positive membrane curvature and is involved in endocytosis and intracellular trafficking (Qualmann et al., 2011; Rao and Haucke, 2011).

However, the major components of HCV replication factories are the non-structural proteins which are all membrane associated (Moradpour et al., 2003). The expression of NS3–5B alone is sufficient to induce DMV structure indistinguishable from those produced during infection (Romero-Brey et al., 2012). NS4B was proposed as the major determinant for induced DMV formation (Egger et al., 2002), although recent evidence suggest that NS5A alone produces DMV (Romero-Brey et al., 2012). The insertion of amphipathic helices into the membrane from both NS4B and NS5A likely contribute to membrane curvature (Palomares-Jerez et al., 2012, 2013, 2010). Expression of NS3/4A or NS5B alone resulted in altered vesicle architectures, suggesting a less critical role in DMV formation (Romero-Brey et al., 2012).

The membrane structure and architecture of HCV induced DMV are well characterised, however a detailed understanding of the associated protein organisation is lacking. Using light microscopy, antibody labelling for NS3 and NS5A result in diffraction limited dot-like structures in the cytoplasm (El-Hage and Luo, 2003; Gosert et al., 2003; Mottola et al., 2002; Shi et al., 2003). Although immunolabelling and NS5B polymerase activity confirmed the presence of active replication complexes within nuclease and protease protected DMV, the low labelling efficiency of immunogold labelling precluded a detailed description of protein organisation (Ferraris et al., 2010; Paul et al., 2013; Romero-Brey et al., 2012).

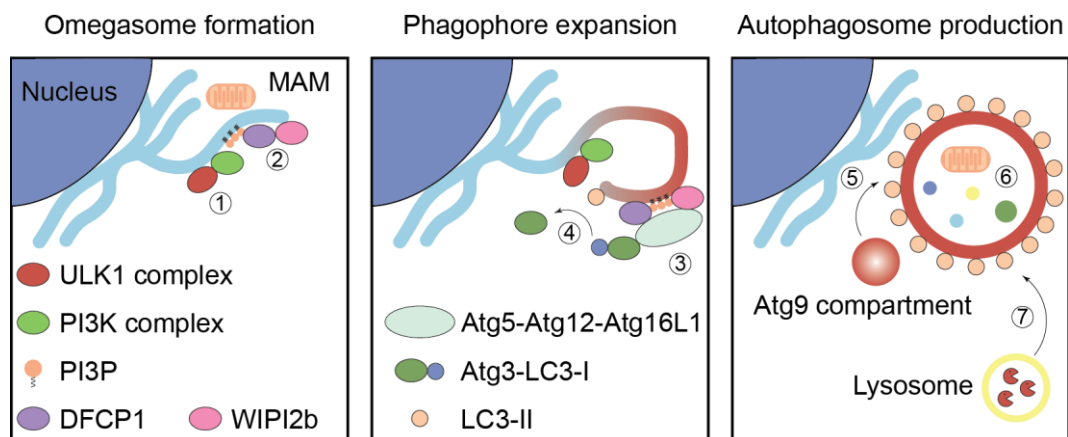


Figure 1.11: Diagram of autophagosome biogenesis.

1: ULK1 and PI3K complexes recruited to curved mitochondrial-associated ER membranes (MAM). 2: DFCP1 and WIPI2b recruitment to PI3P-rich membrane. 3: Recruitment of Atg5-Atg12-Atg16L1 complex and Atg3-LC3-I. 4: Lipidation of LC3-I onto phosphatidylethanolamine producing LC3-II. 5: Phagophore membrane expansion from Atg9 containing vesicles. 6: Engulfment of cytoplasmic contents and autophagosome closure. 7: Fusion of autophagosomes with lysosomes for degradation.

1.5 Light microscopy

1.5.1 History of light microscopy

A great deal of knowledge about biological processes derives from the ability to observe them at the cellular and sub-cellular level. Microscopes use a lens system to provide magnified images of objects which are too small to see with the naked eye. The first description of microscopes in the study of biological structures dates to the 17th century with Antonie Van Leeuwenhoek and Robert Hooke (Hooke, 1667; Leewenhoek, 1677). Using simple illumination techniques, Robert Hooke coined the word cell after observing plant cell walls in cork (Hooke, 1667). Although detailed illustrations of animals such as the flea and gnat were recorded by Hooke, the contrast from these bright-field images is low and comes from absorbance of the transmitted light with dense regions of the sample. To improve the contrast of bright-field microscopy a number of techniques were developed such as phase contrast and dark field (Murphy, 2002). However, these techniques are limited in their applications as no specific labelling of cellular structures is achieved.

The application of fluorescence probes conjugated to a designated target revolutionised light microscopy and allowed the direct visualisation of cellular processes within cells (Giepmans et al., 2006). The number of techniques for labelling targets of interest have developed over the years and the analysis of protein trafficking within live cells are routine laboratory experiments (Giepmans et al., 2006). Using different strategies such as antibody labelling and genetic tag incorporation, targets of interest can be specifically visualised using fluorescent dyes, quantum dots and fluorescent proteins (Giepmans et al., 2006).

1.5.2 Diffraction in light microscopy

Although microscopy techniques have increased the understanding of a number of biological processes, image magnification does not translate to an increase in the resolution of small details. An ideal lens focuses light rays from each point on the object to the image plane. However, the properties of light as a wave mean it is subject to diffraction, caused by interaction of the wave with an obstacle or slit (Born and Wolf, 2000). Diffraction prevents perfect convergence of light rays from the sample at the image plane and causes the image of point objects to blur into a finite-sized spot (Born and Wolf, 2000). In a microscope system, light from a point object travels through a lens with a circular aperture, producing the Airy pattern in the image (Airy, 1835). For a point object, this three dimensional intensity distribution is called the point spread function (PSF).

The size of the PSF determines the resolution, level of detail, that can be obtained from an image and is related to the wavelength of light and the numerical aperture (NA) of the objective (Abbe, 1873). Commonly referred to as the Abbe diffraction limit, this is defined as:

$$\Delta_{xy} \approx \frac{0.61\lambda}{NA}$$

Equation 1: Abbe diffraction limit

where λ is the wavelength of light, and NA is the numerical aperture of the objective; defined as $NA = n \cdot \sin\alpha$ with n the refractive index of the medium and α the half-opening angle of the objective. The axial width of the PSF is around 2–3 times larger than the lateral width.

Resolution is defined as the smallest separation distance between the diffraction images of two point sources in which they can still be distinguished from each other. Using the Rayleigh criterion, this minimum distance is equal to the principal diffraction maximum of one PSF coinciding with the minimum of the other (Rayleigh, 1896). For light microscopy with visible light ($\lambda \approx 550$ nm) and a high oil immersion objective with an $NA = 1.4$, the PSF is ~ 240 nm in the lateral dimension and ~ 500 nm axially. This diffraction limit is significantly larger than many subcellular structures which are on the order of tens of nanometers, and thus precludes a detailed investigation of their arrangement.

Resolution is directly related to the wavelength of the illumination source, therefore a shorter wavelength can achieve a higher resolution. Electron and X-ray microscopy use illumination sources with wavelengths much shorter than light and therefore provide much higher resolutions (Milne et al., 2013; Sakdinawat and Attwood, 2010).

1.5.3 Extending the optical image resolution

Other than using a different illumination source a number of imaging methods have been developed to extend the resolution of optical microscopy. Combining a focused laser beam and a pinhole in confocal microscopy can in principle achieve a $\sqrt{2}$ improvement in image resolution (Pawley, 2012). Contraction of the pinhole to much smaller than the image of a point emitter directly minimises the size of the scanned focal point (Pawley, 2012). However, this reduces the quantity of light detected and the resolution improvement afforded is often outweighed by the low signal to noise ratio (Pawley, 2012).

An alternative technique takes advantage of two-photon absorption to reduce the effective size of the excitation PSF (Zipfel et al., 2003). However, this decrease in PSF size is counteracted by the increased wavelength of light required for excitation (Zipfel et al., 2003). The advantages of both techniques over wide-field illumination are the reduction of out-of-focus fluorescence, therefore a greater sectioning and axial resolution is achieved.

Structured illumination microscopy (SIM) increases the spatial resolution of light microscopy by using a patterned illumination field (Figure 1.12) (Gustafsson, 2000; Gustafsson et al., 2008). Combining the spatial frequency components from the illumination pattern and the sample from multiple orientations, higher frequency information can be collected resulting in ~ 100 nm lateral and ~ 300 nm axial image resolution (Gustafsson, 2000). Other techniques using constructive interference of light fields include 4Pi and I⁵M microscopy (Gustafsson et al., 1999; Hell and Stelzer, 1992).

A separate SIM approach was described more recently and takes advantage of a multifocal excitation pattern that is scanned across the image with contracted pinholes either computationally or using optical hardware (York et al., 2013, 2012). In this set-up, each pixel of the detector is considered a tightly closed confocal pinhole with a degree of transverse misalignment (York et al., 2012). This misalignment shifts the image and decreases signal but does not change the shape of the measured feature or degrade the transverse resolution (Sheppard, 1988). Processing by correcting the image displacement and summing the images produces the $\sqrt{2}$ improvement in resolution of a tightly closed pinhole without the loss of signal (York et al., 2012). A major advantage of the multifocal approaches over original SIM methods are the rapid image acquisition rates (~ 100 frames per second) which facilitate live cell imaging with ~ 100 nm resolution (York et al., 2013).

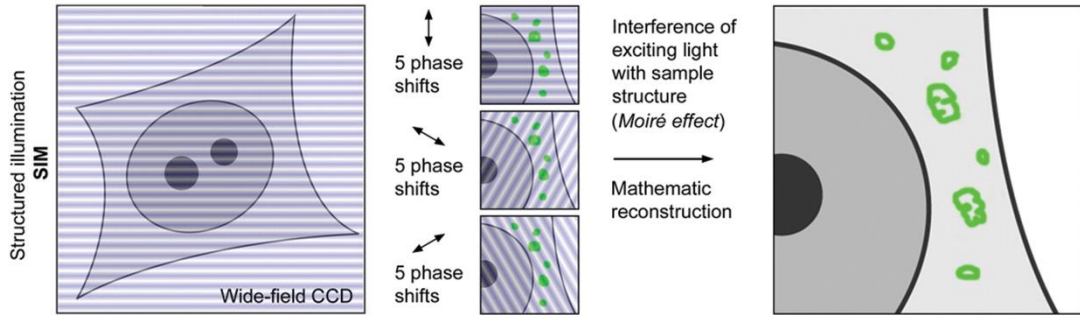


Figure 1.12: Diagram illustrating structured illumination microscopy.

The sample is illuminated with multiple stripe-shaped sinusoidal interference patterns derived from laser light passing through optical grating. This nonuniform wide-field illumination combines with sample information below the diffraction limit producing moiré fringes. This places high spatial frequency information into the lower spatial frequency band of the microscope. Mathematical reconstruction produces an image with ~ 2 -fold improvement in resolution. Adapted from (Schemmelleh et al., 2010).

Despite these approaches extending the image resolution, the best achievable resolution improvement equates to ~ 100 nm in all three dimensions, as demonstrated for I5S microscopy (Shao et al., 2008). This stems from each of these methods remaining fundamentally limited by the diffraction of light.

1.5.4 Breaking the diffraction limit

Recently a number of techniques have been described which break the diffraction barrier by exploiting photophysics and photochemistry; they are collectively termed super-resolution microscopy (Huang et al., 2010).

Stimulated emission depletion microscopy (STED) was first demonstrated in 1999 and uses a second laser, with an intensity of zero at its centre, to suppress fluorescence around the centre of excitation (Figure 1.13) (Klar et al., 2000). This suppression is achieved through stimulated emission, where photons of the same energy as an excited fluorophore cause it to be brought back to the ground state. The result is a smaller effective PSF controlled by the size of the zero intensity in the STED laser (Klar et al., 2000). Super-resolution imaging is conducted by scanning this effective PSF over the sample, and has achieved resolutions in the x-y plane of ~ 30 nm (Harke et al., 2008). By performing STED in a 4Pi geometry, axial resolution of ~ 50 nm has also been reported (Dyba et al., 2003). The depletion of fluorescence can also be accomplished by using fluorophores which switch

between fluorescent on and off states, termed RESOLFT (reversible saturable optical linear fluorescence transitions), which has the advantage of a much lower depletion laser power (A. Schwentker et al., 2007).

Additional developments in SIM (described in Section 1.5.3) can further increase the resolution by exploiting the non-linear dependence of the fluorescence emission rate on the illumination intensity (Gustafsson, 2005). In saturated SIM, the sample is illuminated with a sinusoidal excitation pattern of high intensity which produces an emission pattern that contains higher spatial frequency information than the illumination pattern (Gustafsson, 2005). Super-resolution images are then reconstructed analogous to SIM and have achieved a 2 dimensional resolution of ~50 nm (Gustafsson, 2005)

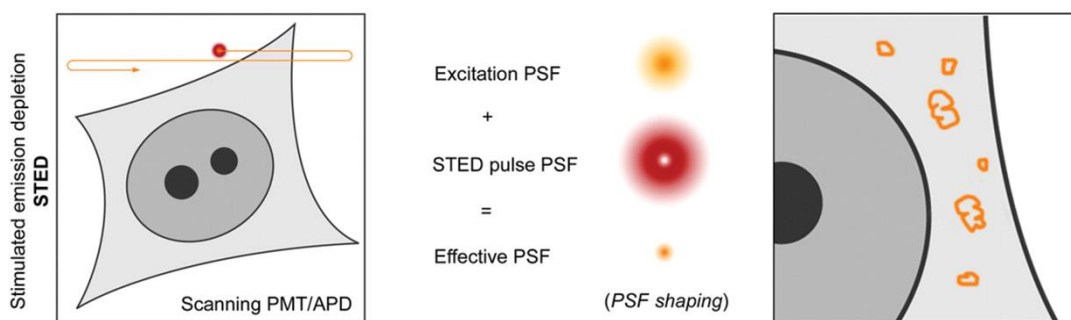


Figure 1.13: Diagram illustrating stimulated emission depletion microscopy.

The sample is scanned with two overlapping laser beams. Depletion of fluorescence excited with the first laser by a doughnut-shaped laser drives excited fluorophores back to the ground state by stimulated emission. The volume through which emitted light is detected is smaller than the diffraction limit, producing a smaller effective PSF. Adapted from (Schermelleh et al., 2010).

1.5.4.1 Localisation microscopy

1.5.4.1.1 Principle

An alternative super-resolution approach involves determining the precise localisation of individual fluorescent events for each probe position on a labelled sample (Huang et al., 2010). These techniques were independently developed by three labs as STORM (stochastic optical reconstruction microscopy) (Rust et al., 2006), PALM (photoactivated localisation microscopy) (Betzig et al., 2006), and FPALM (fluorescence photoactivation localisation microscopy) (Hess et al., 2006), which are collectively called single molecule localisation microscopy (SMLM). STORM was described with dual fluorophore labelled targets in an activator-reporter combination whereas PALM and FPALM utilised photoactivated fluorescent proteins (FP).

Each of these methods rely on determining the origin of the PSF from a single fluorescent event, the precision of which is significantly higher than the diffraction limit (Thompson et al., 2002). Determining the true position of the fluorophore depends on the size of the PSF and the number of photons emitted and is called the localisation precision (Thompson et al., 2002). This can be approximated by:

$$\Delta_{loc} \approx \frac{\Delta}{\sqrt{N}}$$

Equation 2: Localisation precision

where Δ_{loc} is the localisation precision, Δ the size of the PSF and N the number of photons.

The localisation precision directly scales with the photon number and with bright fluorescent particles precisions as high as $\sim 1 \text{ \AA}$ have been achieved (Abbondanzieri et al., 2005). However, localisation becomes inaccurate when multiple molecules are within close proximity as the fluorophore images overlap (Thompson et al., 2002).

Biological samples typically contain thousands of fluorophores at high density; therefore significant overlap prevents accurate localisation of fluorophore positions. In order to visualise individual fluorophores their activation to a fluorescent state is separated in time to allow a subset of spatially distinct fluorophores to be localised (Betzig et al., 2006; Hess et al., 2006; Rust et al., 2006) (Figure 1.14). Cycles of different fluorophore activation, localisation and deactivation to a dark state allow

precise localisation of multiple fluorophores within a diffraction limited volume. Conducted over a wide-field imaging system the coordinates of all localised fluorophores can then be plotted to reconstruct a super-resolution image.

For each of the original methods, target molecules were imaged using photoswitchable fluorescent dyes or proteins which are activated with a spectrally distinct wavelength from the imaging light that excites fluorescence and deactivates fluorophores (Betzig et al., 2006; Hess et al., 2006; Rust et al., 2006). Variations of these techniques have subsequently been reported such as spectral precision distance microscopy (Lemmer et al., 2009), ground state depletion and single molecule return (Fölling et al., 2008) and direct STORM (dSTORM) (Heilemann et al., 2008). dSTORM uses reducing buffer conditions to induce the reversible photoswitching of fluorescent dyes to a long-lived dark state (triplet state), thereby allowing some conventional fluorescent dyes to be used.

1.5.4.1.2 Multi-colour and three dimensional super-resolution imaging

First described in two dimensions, a number of challenges had to be overcome for three dimensional imaging to distinguish separate channels. Fluorophores could be identified based on the emission colour, however, this requires either spectral demixing of the emission channels (Lampe et al., 2012), post-acquisition correction of chromatic aberrations (Erdelyi et al., 2013), or splitting the channels and using geometrically fixed filter sets (Zhao et al., 2015). Chromatic aberrations arise from imperfections in the optical imaging setup which leads to asymmetries and coordinate-dependent variations in the optical transfer function of the microscope (Stallinga and Rieger, 2010). These distortions are dependent on the wavelength and can result in offsets of 50–150 nm between different channels (Bock et al., 2007; van de Linde et al., 2009). This impedes analysis of colocalisation in SMLM studies which routinely achieve localisation precisions of ~20 nm.

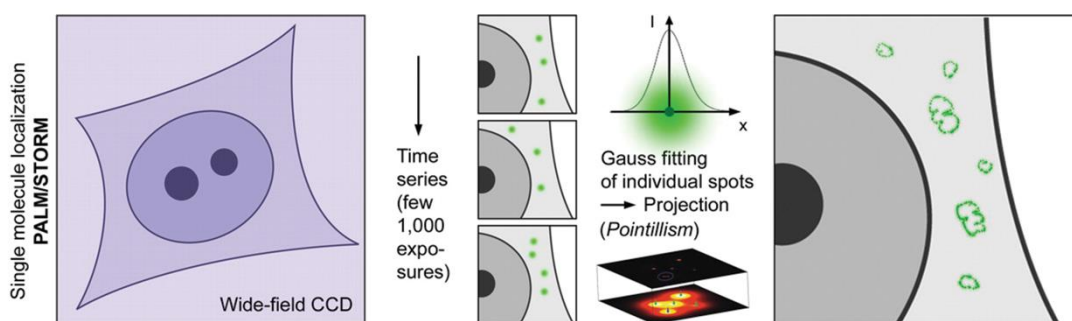


Figure 1.14: Diagram illustrating localisation microscopy image collection.

Activation of spatially distinct fluorophores with wide-field illumination allows observation of single molecule fluorescent events. Mathematical fitting of single emitters allows precise determination of the fluorescent event origin. Cycles of activation, fitting and deactivation allow reconstruction of super-resolution images from the coordinates of multiple single molecule emitters. Adapted from (Schemmelleh et al., 2010).

Despite these limitations, multi-colour methodologies have been implemented, facilitating the analysis of protein-protein interactions at 10-fold improvements in image resolution compared to wide-field (Bates et al., 2007; Lampe et al., 2012). In the STORM methodologies, altering the activator fluorophore allows differentially labelled samples to be distinguished from the activation wavelength (Bates et al., 2007). Three colour imaging of DNA, mitochondria and microtubules have all been demonstrated by this approach (Bates et al., 2007; Huang et al., 2008b).

For PALM and FPALM, the implementation of two colour imaging was initially complicated by the overlap of red-emitting FP preactivation emission wavelengths with postactivation fluorescence of green-emitting FP, for example the green fluorescence of mEos derivatives before activation to red fluorescence (McKinney et al., 2009; Zhang et al., 2012). This has been overcome by the developments of FP with shifted emission profiles such as bsDronpa (Andresen et al., 2008), or FP which are activated from a dark state such as photoactivated-mCherry (Subach et al., 2009). However, the poor photon yield from these short-wavelength FP compromises localisation precision and therefore image resolution.

Additional, developments have extended methodologies to resolve cellular structures in sub-diffraction-limited resolution in all three dimensions (Huang et al., 2008b). First implemented by inserting a cylindrical lens into the light path which

distorts the PSF of single emitters to an elliptical shape in x and y dependent on the axial position (Figure 1.15) (Huang et al., 2008b). The centroid of the PSF provides the lateral positions and the ellipticity the axial position. Localisation precisions of ~ 20 nm and ~ 50 nm have been reported for the lateral and axial position, respectively (Huang et al., 2008b).

A separate implementation of 3 dimensional super-resolution imaging used two-focal-plane imaging (Jüette et al., 2008). This method achieved an axial resolution of ~ 75 nm by splitting the emitted light onto two regions of the camera with different path lengths. This allowed simultaneous detection of fluorescence from two different focal planes (Jüette et al., 2008). The defocused shape of individual images were fitted to a 3D PSF derived from a fluorescent bead to determine the x , y and z coordinate positions over several microns (Jüette et al., 2008).

1.5.4.1.3 Resolution in SMLM

Resolution in wide-field microscopy is defined by the size of the PSF (Equation 1), whereas the resolution in SMLM is limited by a number of factors including localisation precision (Equation 2), labelling density and fluorescent probe size.

The precision of determining the position of a localised molecule describes the uncertainty around the fluorophore origin, and is therefore a principal measure of resolution (Hendrik Deschout et al., 2014). This defines the physical limit of the smallest structure it can resolve. Accordingly the localisation precision should be smaller than the desired resolution. A robust approach for measuring the localisation precision is from the standard deviation of localisations from the same emitter from multiple imaging frames (Hendrik Deschout et al., 2014).

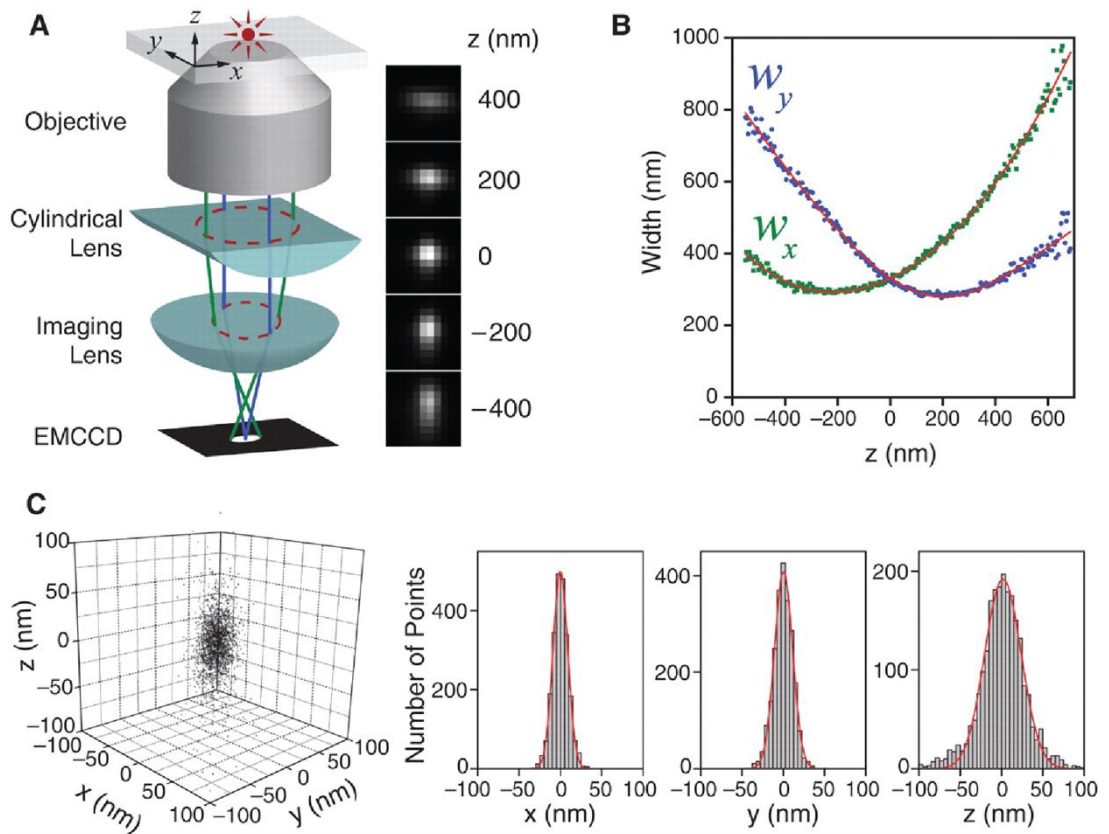


Figure 1.15: Determination of axial coordinates in 3D-STORM using astigmatism.

A: Simplified optical diagram illustrating z coordinate determination of fluorescent object from ellipticity of image by cylindrical lens in imaging path. B: calibration curve of the image widths in W_x and W_y as a function of z . Data were fit to a defocusing curve (red). C: Three dimensional localisation distributions of single molecules. Histogram distributions were fit to a Gaussian function with standard deviation of 9 nm in x , 11 nm in y , and 22 nm in z . Reproduced from (Huang et al., 2008b).

The labelling density of biological samples is an additional consideration when considering image resolution. Because SMLM images are constructed from thousands of fluorophore coordinates, insufficient labelling produces artefacts such as the observation of gaps in continuous structures. Labelling density can be quantified by the Nyquist criterion which states that the distance between two neighbouring emitters must be smaller than half of the sample feature that can be resolved (Shannon, 1949). Thus the smallest resolvable feature follows:

$$\Delta_{Nyquist} = \frac{2}{N^{1/D}}$$

Equation 3: Nyquist criterion

where N is the density of labelling and D is the dimension of the structure to be imaged.

From this formula, to achieve 20 nm resolution in 2D, a labelling density of 10^4 randomly distributed localisations per μm^2 are required. However, in practice lower labelling densities are sufficient as heterogeneous biological structures often occupy smaller regions than the total observed space. Therefore, regions of high local density can resolve structures despite low overall density.

The last consideration for image resolution is the displacement of detected fluorescent probes from the target. The conventional labelling methodology of antibodies can displace the fluorophore by around 10–15 nm (Huang et al., 2008a). In comparison, Fab fragments and FPs position fluorophores ~6 nm and ~4 nm away respectively. Therefore the choice of target detection is a compromise, between genetically encoded but less than ideal photophysical FPs, and displacement of bright and well localised fluorescent dyes on antibodies. Approaches to combine the benefits of both involve coupling organic dyes directly onto proteins with genetic tags, for example the tetracysteine tag (Griffin et al., 1998) or enzymatic reactions (Chen et al., 2005; Fernández-Suárez et al., 2007; Popp et al., 2007).

Measuring image resolution therefore depends on both localisation precision and labelling density. However, it was shown recently that the Nyquist criterion can overestimate the increase of resolution with label density (Fitzgerald et al., 2012). In continuing efforts to define the image resolution in SMLM imaging, methods to directly measure the resolution from reconstructed images have been explored

using Fourier ring correlation (FRC) (Banterle et al., 2013; Nieuwenhuizen et al., 2013), which is commonly used to assess the resolution in single-particle reconstructions in cryoelectron microscopy (Saxton and Baumeister, 1982; Unser et al., 1987). This was demonstrated for both line-like (microtubules) and ring-like (nuclear pore) structures (Banterle et al., 2013; Nieuwenhuizen et al., 2013). However, simulated datasets reconstructed with the same localisation precision and label density but different spatial frequencies, identified that the FRC curve decays quicker as the image contains structures with lower spatial frequencies (Legant et al., 2016). Therefore the application of FRC should be interpreted with caution when comparing between samples with different labels or structures.

1.6 Aims and objectives

There remain a number of questions regarding the architecture of the HCV replication complex, in particular the organisation of the non-structural proteins and how DMVs are formed. The NS5A protein is critical during the virus lifecycle with a number of known functions, one of which is the hypothesised link between HCV replication and assembly. This study aimed to address the current lack of knowledge in these areas.

In chapter 3, advances in light microscopy were used to observe the protein organisation of non-structural proteins below the diffraction limit. In particular, the study was aimed at determining the organisation of non-structural proteins associated with DMVs. In parallel, the localisation of NS5A in cells was investigated when targeted using direct acting antivirals, or by mutation of key phosphorylation residues.

In chapter 4, the interactions of HCV replication complexes with the autophagosome biogenesis machinery were investigated. A cellular protein involved in the early stages of omegasome formation was targeted, and interactions with the HCV replication complex analysed.

Lastly, in chapter 5, a number of fluorescence labelling strategies were explored to visualise HCV replication complex components for super-resolution imaging. These included the insertion of genetic tags into non-structural proteins, identifying non-antibody binding proteins to the HCV polymerase, and incorporating a nucleotide analogue into actively replicating HCV RNA.

Chapter 3 - Materials and Methods

3.1 General materials

3.1.1 Bacterial strains

Escherichia coli (*E. coli*) DH5 α : Genotype; F⁻ Φ 80lacZ Δ M15 Δ (lacZYA-argF) U169 recA1 endA1 hsdR17 (rk⁻, mk⁻) phoA supE44 λ ⁻ thi⁻1 gyrA96 relA1 used for cloning were purchased from Life Technologies.

E. coli BL21 (DE3): Genotype; F⁻ ompT hsdS_B(r_B⁻ m_B⁻) gal dcm λ (DE3 [lacI lacUV5-t7 gene 1 ind1 sam7 nin5]) used for protein expression were purchased from Life Technologies.

Chemically competent bacteria were produced using the Z-competent kit (Zymo Research).

3.1.2 Mammalian cell lines

HuH7 cells are a human hepatoma carcinoma cell line (Nakabayashi et al., 1982) capable of supporting replication of HCV sub-genomic replicons (Lohmann et al., 1999). HuH7.5 cells are a sub-population of cells derived by clearing SGRs from HuH7 cells, using IFN α , which support greater levels of HCV infection (Blight et al., 2002). This cell line was a kind gift from Charles Rice, The Rockefeller University, New York.

A polyclonal population of cells stably expressing SGR-Feo-JFH1 (Genotype 2a; (Wyles et al., 2009)) or SGR-Feo-Con1 (Genotype1b; (Lohmann et al., 1999)) were produced in HuH7.5 cells by Yutaka Amako at the University of Leeds.

Stable cell lines expressing SGR-Neo-JFH1 with or without NS5A phosphorylation mutations were produced in HuH7 cells as a polyclonal population by Niluka Goonawardane at the University of Leeds.

SGR-Feo-S52 (Genotype 3a All variant; (Saeed et al., 2012)) stably expressing cells were produced in HuH7.5 cells as a polyclonal population by Lorna Kelly at the University of Leeds.

3.1.3 Antibodies – Primary

Target	Species	Source	Comments	Concentration
αNS5A	Sheep	(Macdonald et al., 2003)	Polyclonal serum	WB: 1:4,000 IF: 1:2,000
	Mouse	(Lindenbach et al., 2005)	Monoclonal (9E10)	0.2 µg/ml
αNS3	Mouse	Thomas Pietschmann	Monoclonal (HZT)	2 µg/ml
αNS5B	Sheep	In house	Polyclonal serum	1:500
αCore	Mouse	ThermoFisher Scientific	Monoclonal (C7-50)	2 µg/ml
αE2	Mouse	(Owsianka et al., 2005) (via Genentech)	Monoclonal (AP33)	5.6 µg/ml
αGAPDH	Mouse	Abcam (ab8245)	Monoclonal (6C5)	0.2 µg/ml
αHis ₆	Mouse	Sigma	Monoclonal, ascites fluid (HIS-1)	1:1,000
αLC3B	Rabbit	Abcam (ab51520)	Polyclonal	1 µg/ml
αHistone H3	Rabbit	Cell Signalling Technology (#4499)	Monoclonal	20 ng/ml
αFibrillarlin	Rabbit	Cell Signalling Technology (#2639)	Monoclonal (C13C3)	30 ng/ml

3.1.4 Secondary antibodies and fluorescent reagents

Species/Name	Target	Source	Comments	Concentration
Donkey	α Sheep	Life Technologies	Fluorescence various	2 μ g/ml
Chicken	α Mouse	Life Technologies	Fluorescence various	2 μ g/ml
Chicken	α Rabbit	Life Technologies	Fluorescence various	2 μ g/ml
Goat	α Mouse	LI-COR	Fluorescence 700 nm	0.1 μ g/ml
Donkey	α Goat/Sheep	LI-COR	Fluorescence 800 nm	0.1 μ g/ml
LipidTOX™	Lipid droplets	ThermoFisher Scientific	Fluorescence 647 nm	1:1,000
Alexa Fluor® 488 azide	5-ethynyl uridine	Thermofisher Scientific	Fluorescence 488 nm	5 μ M

3.1.5 SGR and virus constructs

HCV sequences were obtained from the EU HCV database with the Genbank accession numbers AB047639 (JFH1), AJ238799 (Con1) and GU814264 (S52). DNA constructs pJFH1 (Wakita et al., 2005) and pSGR-Feo-JFH1 (Wyles et al., 2009) were used as reported. A sub-clone of JFH1 (mSUB: Mair Hughes Leeds Thesis) using the NsiI/HindIII fragment was generated in pLitmus28i (NEB).

3.1.6 Expression constructs

pNS5B Δ C21 from JFH1 (Simister et al., 2009) was a kind gift from Volker Lohmann, University Heidelberg. pCMV NS3–5B was provided by Dan Jones at the University of Glasgow (D. M. Jones et al., 2007).

3.2 General Methods

3.2.1 Nucleic acid manipulation

3.2.1.1 *Transformation of Z-competent bacteria*

Plasmid DNA was incubated with Z-competent DH5 α cells at a volume ratio of 1:10 on ice for 5 min before incubation at 37 °C in lysogeny broth (10 g/L tryptone, 10 g/L NaCl, 5 g/L yeast extract [LB]) for 60 min. After incubation transformed cells were pelleted at 3,000 x g for 5 min. Pelleted cells were re-suspended in LB, plated onto agar containing appropriate antibiotic and incubated until colony formation. Ampicillin and kanamycin were used at 100 μ g/ml and 50 μ g/ml respectively. Transformed bacteria were grown at 37 °C, or 30 °C if plasmid DNA contained the NS5A protein sequence.

3.2.1.2 *Preparation of plasmid DNA from bacterial cultures*

Single colonies from 3.2.1.1 were picked and grown for 16 h in LB in a rotary shaking incubator at 200 rpm in the presence of antibiotic before centrifugation at 4,000 x g for 15 min at 4 °C. Plasmid DNA was purified by alkaline lysis using GeneJET Plasmid Miniprep/Midiprep kit (Thermo Scientific) using the manufacturers protocol. For long term storage of plasmids, glycerol stocks of bacterial cultures were prepared from 1 ml cultures re-suspended in 30% (v/v) glycerol : 70% (v/v) LB and frozen at -80 °C.

3.2.1.3 *Polymerase chain reaction*

Polymerase chain reaction (PCR) was used to amplify sequences for cloning. Oligonucleotide primers (Appendix 1) purchased from Integrated DNA Technologies were re-suspended in de-ionised water (dH₂O) to a final concentration of 100 μ M and stored at -20 °C. 50 μ l PCR reactions used Vent® DNA polymerase (New England Biolabs: NEB) with 50 ng plasmid DNA, 0.1 μ M forward and reverse primers and 0.2 μ M of each deoxynucleotide triphosphate (dNTP). In the event of a poor PCR yield the addition of 3% (v/v) dimethyl sulfoxide (DMSO) was included in subsequent reactions to disrupt DNA secondary structures and facilitate annealing of primers (Jensen et al., 2010). PCR reactions were incubated for an initial denaturation step of 95 °C for 5 min before 30 cycles of 30 sec denaturation, 60 sec annealing and 60 sec/kilobase (kb) extension at 72 °C. Annealing temperatures were determined for each primer set based on the calculated T_m (Appendix 1). A final extension of 72 °C for 5 min was undertaken before reactions were stored at 4 °C.

3.2.1.4 *Site-directed mutagenesis*

Complementary site-directed mutagenesis primers were designed with the mutant sequence encoded within the centre of primer sequences (Appendix 1). 50 µl PCR reactions used PfuUltra II Fusion HS DNA polymerase (Agilent Technologies) and contained 0.2 µM forward and reverse primers, 0.2 µM each dNTP, 3% (v/v) DMSO and 1% (v/v) glycerol. Reactions were incubated at 95 °C for 5 min before 5 cycles of 30 sec at 95 °C, 60 sec at 55 °C and 2 min/kb at 68 °C. A second round of PCR was conducted using 30 cycles of 30 sec at 95 °C, 60 sec at primer pair annealing temperature and 5 min plus 2 min/kb at 68 °C. A final 5 min extension at 68 °C was carried out before storage at 4 °C. Input PCR template was then degraded with 1 µl *DpnI* (NEB) for 60 min at 37 °C prior to transformation of Z-competent bacteria with 10 µl PCR reaction as described (Section 3.2.1.1).

3.2.1.5 *Restriction digestion*

Restriction digestion enzymes were supplied by NEB. Reactions were carried out in 20 µl with the recommended buffers at the suggested temperature. Reactions were incubated for a minimum of 1 hour with at least 1 Unit of enzyme per µg of DNA.

3.2.1.6 *Agarose gel electrophoresis*

DNA gels of 1% (w/v) agarose in TAE buffer (40 mM Tris-HCl, 0.11% (v/v) acetic acid, 1 mM ethylenediaminetetraacetic acid [EDTA]) with 1:10,000 SYBR® Safe DNA Gel Stain (Invitrogen) were used to separate DNA fragments. DNA samples were loaded onto agarose gels in DNA loading buffer (1% (w/v) sucrose, 0.0125% (w/v) bromophenol blue in ddH₂O) and run in TAE buffer at 8 V/cm. DNA fragments were compared to Hyperladder I markers (Bioline).

3.2.1.7 *DNA fragment extraction from agarose gels*

DNA fragment bands were imaged under blue light illumination with an orange filter and those of interest excised. Gel pieces containing DNA were purified using QIAquick Gel Extraction kit (QIAGEN).

3.2.1.8 *DNA/RNA quantification*

DNA and RNA was quantified using the absorbance at 260 nm on a NanoDrop 1000 by the following equation, using the relationship that A_{260} of 1.0 = 50 µg.ml⁻¹ pure dsDNA:

$$\text{Concentration } \mu\text{g. ml}^{-1} = (A_{260} - A_{320}) \times 50 \mu\text{g. ml}^{-1}$$

The purity of DNA and RNA from contaminating protein was determined by the 260/280 nm absorbance ratio.

3.2.1.9 *Ligation*

DNA fragments were mixed in a vector : insert ratio of 1 : 3 for “sticky” end cloning, and 1 : 10 for “blunt”, on ice for 10 min. Reactions were made up to 20 µl and DNA fragments ligated using 10,000 Units of T4 DNA ligase (NEB) in a room temperature (RT) water bath cooled to 4 °C overnight in a cold room. 5 µl of the resultant reaction was transformed into Z-competent DH5α as described previously.

3.2.1.10 *Construct verification*

For single restriction site cloning, colonies were screened using colony PCR to determine insert orientation. Colonies were picked and re-suspended in ddH₂O with 0.2 µM forward and reverse primers and 0.2 µM dNTPs. PCR reactions were run for 30 cycles with 30 sec denaturation at 95 °C, 60 sec annealing at 55 °C and 60 sec/1 kb at 72 °C with an initial denaturation of 95 °C for 5 min and a final extension of 72 °C for 5 min using Vent® DNA polymerase. The resultant PCR products were analysed by agarose gel electrophoresis as described (Section 3.2.1.6). Bacteria re-suspended in ddH₂O from colony PCR, or picked from colonies, were inoculated into LB containing antibiotic and grown at the appropriate temperature for 16 h at 200 rpm. Plasmid DNA was prepared (Section 3.2.1.2) for each construct and sequenced to confirm correct sequence identity at Beckman Coulter Genomics.

3.2.1.11 *Preparation of linear DNA*

For the generation of virus and SGR RNA, 10 µg of plasmid DNA was linearised with *Xba*I at 37 °C overnight. Denaturation of *Xba*I at 65 °C for 20 min was conducted before degradation of 5' overhangs using Mung Bean Nuclease (NEB) for 45 min at 30 °C and purification using phenol/chloroform extraction and ethanol precipitation. Linear DNA was mixed in an equal volume of phenol : chloroform : isoamylalcohol (25 : 24 : 1 [pH8.0]), vortexed for 10 sec and centrifuged at 17,000 x g for 5 min. The upper aqueous phase was extracted, mixed in a 1 : 1 ratio with chloroform, vortexed for 10 sec and centrifuged at 17,000 x g for 5 min. The second upper aqueous phase was extracted and the purified DNA precipitated in 3 sample volumes of 100% (v/v) ethanol with 75 mM sodium acetate at -20 °C for at least 1 hour. DNA was pelleted at 20,000 x g for 30 min, washed in 70% (v/v) ethanol and centrifuged at 20,000 x g for 5 min. The resultant DNA pellet was air dried before re-suspension in ddH₂O.

3.2.1.12 *In vitro transcription of RNA*

All solutions used for RNA preparation were firstly treated to remove RNases by incubation with 1:1000 diethylpyrocarbonate (DEPC) at 37 °C for 16 h. Excess DEPC was subsequently removed by autoclaving. RNA was generated using the T7 RiboMAX™ Large Scale RNA Production System (Promega) using 1 µg of linear DNA generated from Section 3.2.1.11 as a template. Reactions were incubated at 37 °C for 60 min before degradation of template DNA using 1 Unit of DNase for 15 min at 37 °C. In vitro transcribed RNA was subsequently purified by phenol/chloroform extraction [pH 6.0] and isopropanol precipitation. Phenol/chloroform extraction was conducted as described for DNA. Purified RNA was pelleted using 3 sample volumes of isopropanol and 75 mM sodium acetate at 17,000 x g for 20 min. Pellets were washed in 70% (v/v) ethanol, centrifuged at 17,000 x g for 5 min and air dried. Pelleted RNA was subsequently re-suspended in DEPC treated ddH₂O, quantified, and stored in aliquots at -80 °C.

3.2.1.13 *Denaturing RNA electrophoresis*

In vitro transcribed RNA was analysed by denaturing agarose gel electrophoresis (1% (w/v) agarose, 1X MOPS (40 mM 3-(*N*-morpholino)-propanesulfonic acid [pH 7.0], 10 mM sodium acetate, 1 mM EDTA), 4.7% (v/v) formaldehyde) at 70 V for 1 h in 1X MOPS running buffer. RNA samples were loaded onto gels after denaturation at 65 °C for 10 min in RNA loading buffer (47.5% (v/v) formamide, 9 mM EDTA, 0.0125% (w/v) SDS, xylene cyanol and bromophenol blue). RNA was visualised under blue light illumination and compared to ssRNA ladder (NEB).

3.3 Protein biochemistry

3.3.1 SDS-PAGE electrophoresis

Protein samples were analysed by separation using Tris-Glycine polyacrylamide gel electrophoresis (12–15% [resolving] or 6% [stacking] (v/v) acrylamide, 0.1% (w/v) SDS, 0.1% (w/v) ammonium persulphate (APS), 0.01% (v/v) N,N,N',N'-tetramethylethylenediamine (TEMED), in 375 mM Tris-HCl [pH 8.8] or 126 mM Tris-HCl [pH 6.8] for resolving and stacking respectively. Protein samples were loaded onto gels after boiling at 95 °C for 5 min in Laemmli buffer (17.5 mM Tris-HCl [pH 6.8], 9% (v/v) glycerol, 1% (w/v) SDS, 2.5% (v/v) β -mercaptoethanol, 0.05% (w/v) bromophenol blue) and run in SDS-PAGE running buffer (25 mM Tris-HCl, 192 mM glycine, 0.1% (w/v) SDS) at 180 V for 50–60 min. Protein size was compared to ColorPlus Prestained Protein Marker, Broad Range (7–175 kDa) (NEB).

3.3.2 Coomassie blue staining

Protein bands were visualised using Coomassie Brilliant Blue R-250 stain (41% (v/v) methanol, 18% (v/v) acetic acid, 0.2% (w/v) Coomassie Brilliant Blue R-250) for at least 1 hour. Gels were de-stained using 50% (v/v) methanol, 10% (v/v) acetic acid.

3.3.3 Western blot analysis

Proteins resolved by SDS-PAGE were transferred to polyvinylidene fluoride (PVDF) Immobilon®-FL Transfer Membrane (Immobilon) using a dry transfer unit at 40 mA/membrane for 1 hour. PVDF membranes were first activated in methanol before being soaked in transfer buffer (25 mM Tris-HCl, 193 mM glycine, 20% (v/v) methanol). Transferred membranes were subsequently blocked in 50% (v/v) Odyssey® Blocking buffer (LI-COR) in TBS (50 mM Tris-HCl, 150 mM NaCl) for 15–30 min. Primary and secondary antibodies were incubated in 25% (v/v) Odyssey® Blocking buffer for at least 1 h at RT or 4 °C overnight at the appropriate dilution. After each antibody incubation transfer membranes were washed 3–5 times in TBS to remove unbound antibody. Blots were allowed to dry before imaging using an Odyssey Imager (LI-COR).

3.3.4 Protein quantification

Mixed protein samples were quantified using Bradford's reagent (8.5% (v/v) H₃PO₄, 5% methanol, 0.005% Coomassie Brilliant Blue G-250) (Bradford, 1976). Absorbance at 570 nm was measured and protein concentration calculated from a standard curve of bovine serum albumin (BSA).

Pure protein samples were quantified by absorbance at 280 nm with the corresponding molar extinction coefficients and molecular weight (ExpASy Bioinformatics Resource Portal) on a NanoDrop 1000.

3.4 *In vitro* methods

3.4.1 Protein expression

Single colonies of BL21 (DE3) cells carrying the desired expression plasmid were grown in 10 mL of LB with antibiotic for 16 h at 37 °C. Overnight cultures were pelleted at 4000 x g for 15 min, re-suspended in 10 ml of LB and inoculated 1:1000 into LB containing antibiotic. Bacterial cultures were grown to an OD₆₀₀ of 0.6–0.8 before induction of protein expression using 0.1 mM isopropyl β-D-1-thiogalactopyranoside (IPTG) at 25 °C for 4 h. Final cultures were centrifuged at 4000 x g for 15 min and stored at -20 °C.

3.4.2 NS5B ΔC21 expression

Pelleted cultures from Section 3.4.1 were lysed in NS5B lysis buffer I (100 mM Tris-HCl [pH 8.0], 100 mM NaCl, 1 mM MgCl₂, 2% (v/v) Triton X-100, 2 mg/ml lysozyme [Alfa Aesar], 1 Unit/ml Benzonase [Sigma]) (5B-LB-I) for 30 min on ice and centrifuged at 20,000 x g at 4 °C for 15 min. The resultant pellet was re-suspended in NS5B lysis buffer II (20 mM sodium phosphate [pH 7.5], 500 mM NaCl, 0.1% (v/v) β-octylglucopyranoside, 20 mM imidazole, 50% (v/v) glycerol) (5B-LB-II). The suspension was sonicated on ice 10 times with 20 sec on/off pulses using a Sanyo Soniprep 150 sonicator with amplitude of 6 microns and a microtip. The sonicated suspension was centrifuged at 20,000 x g for 20 min at 4 °C and the resultant supernatant mixed with Ni²⁺-chelated Sepharose™ Fast Flow (Ni-resin; GE Healthcare) for 1–2 h at 4 °C with end-over-end rotation. Ni-resin was centrifuged at 1,000 x g for 2 min, washed at least 5 times in 5B-LB-II containing 50 mM imidazole before protein elution in 5B-LB-II containing 250 mM imidazole. Eluted protein was quantified using Bradford's reagent and stored at -80 °C. An

NS5B Δ C21 [GND] expression plasmid was expressed and purified in parallel as described above.

3.4.3 RNA-dependent RNA polymerase *in vitro* activity assay

150 nM purified NS5B Δ C21 or NS5B Δ C21 [GND] was incubated in RNA dependent RNA polymerase (RdRp) reaction buffer (20 mM Tris-HCl [pH 7.6], 5 mM MgCl₂, 1 mM dithiothreitol (DTT), 25 mM KCl, 1 mM EDTA, 20 Units RNasin (Promega) with 0.5 μ g *in vitro* transcribed full length JFH1 [GND] RNA for 30 min at 25 °C. *In vitro* transcribed RNA was re-folded before addition to RdRp reaction buffer by denaturation at 95 °C for 3 min, cooling on ice for 2 min and incubation in refolding buffer (100 mM 4-(2-hydroxyethyl)-1-piperazineethanesulfonic acid (HEPES) [pH 8.0], 100 mM NaCl, 6.6 mM MgCl₂) for 20 min at 37 °C. RdRp reactions were initiated by the addition of NTP mix (10 μ Ci [α -³²P]-CTP [Perkin Elmer], 10 μ M cold CTP, 1 mM ATP, 1 mM UTP, 5 mM GTP) and incubated for 1 h at 25 °C. Products from transcription reactions were purified using RNeasy Mini Kit (QIAGEN) and diluted into Emulsifier-Safe™ liquid scintillation cocktail (Perkin Elmer) and read on a Tri-Card® 2100 TR liquid scintillation counter.

3.4.4 Generation of Adhiron

Purified NS5B Δ C21, 12.4 μ M, was surface biotinylated by incubation with 20-fold Molar excess EZ-Link NHS-SS-biotin (Pierce) for 1 h at room temperature before removal of excess biotin using Zeba spin 7K MWCO Desalting column (Thermo Fisher Scientific) by centrifugation at 1500 x g for 2 min. Biotinylated protein was provided to the Leeds Adhiron BioScreening group for the generation of adhiron specific to the HCV polymerase (Tiede et al., 2014). In summary, biotinylated NS5B Δ C21 was bound to streptavidin-coated wells (Pierce) for 1 h before 10¹² colony forming units of phage were added for 2.5 h with shaking. Phage were initially pre-screened against biotinylated BL21 DE3 cell lysate from NS5B Δ C21 plasmid naïve cells. Naïve bacterial cell lysate from 5B-LB-II supernatant was biotinylated as described for NS5B. Panning wells containing phage were washed 10 times before elution of bound phage with 50 mM glycine-HCl [pH 2.2] and neutralisation with 1 M Tris-HCl [pH 9.1], followed by an additional elution with 100 mM trimethylamine for 6 min and neutralisation with 1 M Tris-HCl [pH 7.0]. ER2738 cells were infected with eluted phage by incubation for 1 h at 37 °C and 90 rpm before plating on agar with 100 μ g/ml carbenicillin and culturing overnight at 37 °C. Single colonies were picked, grown in 30 mL LB containing 100 μ g/ml carbenicillin and infected with 1 x 10⁹ M13K07 helper phage. After 1 h at 90 rpm, kanamycin was

added to 25 µg/ml and incubated at 25 °C for 16 h at 170 rpm. Phage were precipitated using 4% (w/v) polyethylene glycol 8000, 0.3 M NaCl and re-suspended in 1 ml TE buffer (10 mL Tris [pH 8.0], 1 mM EDTA). For the second round of selection, 2 µl of phage suspension was incubated for 1 h with NS5B labelled streptavidin beads (Invitrogen). Beads were then washed five times and phage eluted and amplified as above. A third panning round used neutravidin high binding capacity plates (Pierce) as described for panning round 1 with phage eluted using 100 µl of 100 mM DTT.

3.4.5 Phage ELISA

Individual colonies of ER2738 cells (Section 3.4.4) were grown in 100 µl of LB with 100 µg/ml carbenicillin in a 96 well plate at 37 °C for 6 h at 900 rpm. A 25 µl aliquot of culture was inoculated into 200 µl of LB with carbenicillin and grown at 37 °C for 1 h at 900 rpm. 10 µl of 10¹¹/ml helper phage were added with 25 µg/ml kanamycin and incubated overnight at 25 °C (450 rpm). Streptavidin-coated plates (Pierce) were blocked with 2X casein blocking buffer (Sigma) overnight at 37 °C followed by incubation with biotinylated NS5B ΔC21 or biotinylated plasmid-deficient BL21 (DE3) cell lysate for 1 h. 45 µl of overnight growth medium containing phage were then added and incubated for 1 h. After washing, phage were detected using horseradish peroxidase-conjugated anti-phage antibody (1:1000; Seramun) for 1 h and visualised with 3,3',5,5'-tetramethylbenzidine (Seramun) at 610 nm.

3.4.6 Adhiron purification

Plasmids coding for adhiron were grown in BL21 (DE3) cells (Section 3.4.1) and lysed in Adhiron lysis buffer (50 mM sodium phosphate, 300 mM NaCl, 20 mM imidazole, 10% (v/v) glycerol, BugBuster® [Novagen], Halt Protease Inhibitor cocktail – EDTA free [ThermoFisher Scientific], 10 Units/ml Benzonase [Sigma]) (Ad-LB) supplemented with 1 mM DTT for 20 min with end-over-end rotation. Lysis and subsequent buffers were pH 7.4 for adhiron, 21 and 28; pH 8.4 for adhiron 10 and 16. Bacterial lysate was centrifuged at 5,000 x g for 20 min before incubation with Ni-resin for 1–2 h with end-over-end rotation. Ni-resin was centrifuged at 1,000 x g for 2 min, washed at least 5 times in Ad-LB containing 100 mM imidazole before elution in Ad-LB containing 300 mM imidazole. Pure protein was quantified using 280 nm absorbance and frozen at -80 °C for long term storage.

3.4.7 Adhiron labelling

Purified Adhiron, 18.75 µg, was incubated with tris(2-carboxyethyl)phosphine (TCEP) resin (ThermoScientific) pre-equilibrated in phosphate buffered saline (137 mM NaCl, 2.7 mM KCl, 10 mM Na₂HPO₄, 1.8 mM KH₂PO₄ [pH 7.4]) (PBS) containing 1 mM EDTA for 1 h with end-over-end rotation. Reduced Adhiron was recovered from TCEP resin by centrifugation at 1,000 x g for 60 sec and immediately incubated with 80 µM Alexa Fluor® 647 C₂ Maleimide (Life Technologies) for 16 h at RT whilst protected from light. Excess Alexa Fluor label was removed from labelled Adhiron using Zeba spin 7K MWCO Desalting Column by centrifugation at 1500 x g for 2 min. 647-labelled Adhiron was mixed with an equal volume of 80% (v/v) glycerol and stored at -20 °C.

3.4.8 NS5B dot blot

Purified NS5B ΔC21 was dotted onto methanol activated PVDF transfer membranes for 1 h before blocking in 50% (v/v) Odyssey® Blocking buffer for 15 min. Adhiron or antibodies were incubated with transfer membranes at 4 °C overnight or 1 h at RT in 25% Odyssey® Blocking buffer. Membranes were washed 3 times in PBS to remove excess Adhiron/antibodies before drying and imaging on either an FLA-5000 fluorescent (Fujifilm) or Odyssey (LI-COR) imager.

3.5 Tissue culture

3.5.1 Passaging of cells

Mammalian cells were cultured in Dulbecco's modified Eagle's medium (DMEM; Sigma) supplemented with 10% (v/v) foetal bovine serum (FBS), 100 IU/ml penicillin, 100 µg/ml streptomycin and 1% (v/v) non-essential amino acids (Lonza) in a humidified incubator at 37 °C with 5% CO₂. Cells were passaged at 80–90% confluence by washing in PBS prior to incubation with 0.5 mg/ml trypsin-EDTA (Sigma) to detach cells. Once detached, trypsin was inactivated by addition of excess complete media and cells seeded into culture flasks or plates for further passage or experimentation.

3.5.2 RNA electroporation of mammalian cells

Trypsinised cells were counted after dilution 1 : 1 into HyClone® Trypan Blue solution (Fisher Scientific) to identify live cells. Cells were pelleted at 700 x g for 5 min then washed twice in ice cold DEPC-treated PBS. Pelleted cells were re-suspended in RNase free PBS to a final concentration of 1 x 10⁷ cells/ml for SGR

assays and 2×10^7 for infectious virus. RNA, 5 μg for SGR and 10 μg for virus, was mixed with 0.4 ml of cell suspension in a chilled electroporation cuvette (Geneflow) before electroporation at 950 μF , 260 V for 25 msec (BioRad Gene Pulser). Cells were immediately recovered in complete media and seeded into culture plates. Media was replaced with fresh complete media at 4 h post electroporation (h.p.e.) to remove cell debris.

3.5.3 Stable cell selection

Cells electroporated with SGRs were cultured in complete media containing 500 $\mu\text{g}/\text{ml}$ G418 (Sigma) at 24 h.p.e. Cell death was monitored daily with media replacement as required but at least every 2–3 days. Polyclonal populations of G418 resistant cell colonies were propagated and maintained in the presence of 500 $\mu\text{g}/\text{ml}$ G418.

3.5.4 Transient luciferase assays

Six well plates seeded with 1×10^5 cells from SGR electroporations were harvested for luciferase activity at 4, 24, 48 and 72 h.p.e. by washing in PBS and lysis in 0.2 ml Passive Lysis Buffer (PLB; Promega). Samples were stored at $-20\text{ }^\circ\text{C}$ until analysis by the addition of 30 μl Luciferase Assay Reagent (Promega) to 20 μl of cell lysate. Light emission was monitored on a BMG plate reader.

3.5.5 DNA transfection

Cells were seeded the day before DNA transfection into 24 well culture plates with glass coverslips and media exchanged for Opti-MEM (Life Technologies) 30 min prior to transfection. 250 ng DNA was diluted into 0.1 ml Opti-MEM before addition of 0.5 μl FuGENE6 transfection reagent (Promega) and incubation at RT for 15–30 min. Transfection complex was subsequently added to cells dropwise and incubated in a humidified incubator for 8 h before complex-media replacement with fresh complete DMEM.

3.5.6 Infectious virus propagation

Cells electroporated with infectious HCV RNA were transferred to BSL3 containment 4 h.p.e. and media replaced with complete media supplemented with 25 mM HEPES (Lonza). Cell culture supernatant was collected and replaced every 24 h and stored at $4\text{ }^\circ\text{C}$ or $-80\text{ }^\circ\text{C}$. Naïve cells were infected with virus by incubation with supernatant derived from electroporations for the indicated time points between 0.1–1 multiplicity of infection (m.o.i.).

3.5.7 Virus titration

Virus preparations were titred against HuH7 cells as described in (Stewart et al., 2015). Briefly, 8×10^3 cells were seeded 8 h before titration. Either a 1 in 2 or 1 in 10 dilution series of virus was prepared in complete media and incubated with cells for 48 h. Infected cells were washed in PBS and fixed in 4% (w/v) paraformaldehyde (PFA) in PBS for 20 min. Cells were then washed in PBS and permeabilised in 0.2% (v/v) Triton X-100 in PBS for 15 min before incubation with α NS5A primary and 594-fluorescent secondary antibodies sequentially in PBS for 2 h at RT. Cells were washed in PBS between each antibody incubation. Red fluorescent positive cells were imaged using an IncuCyte® ZOOM and virus concentration determined as infectious units/ml (IU/ml). Alternatively, labelled plates of titrated virus were imaged by eye and titre recorded as focus forming units/ml (f.f.u/ml).

3.6 Fluorescence microscopy

3.6.1 Sample preparation

Cells seeded onto glass coverslips were manipulated for experimentation as required before fixation in 4% (w/v) PFA in PBS or 2% (w/v) PFA in complete media, at RT for 10 min. Samples were washed in PBS three times before permeabilisation in 0.2% (v/v) Triton X-100 in PBS for 10 min. Primary and secondary antibodies against targets were incubated sequentially in PBS at RT for one hour with PBS washes after each incubation. Coverslips were mounted in ProLong Gold or Diamond (Life Technologies), after 5 min incubation with 300 nM 4',6-diamidino-2-phenylindole (DAPI) in PBS, and cured overnight in the dark.

3.6.2 Click Chemistry

Cells were labelled with 5-ethynyl uridine (5EU) by addition of 1 mM 5EU to complete DMEM under normal growth conditions for the indicated times. Samples were then fixed and permeabilised as described in Section 3.6.1. Prior to antibody labelling, 5EU was detected using the Click-iT RNA labelling kit (Life Technologies) with 5 μ M Alexa Fluor® 488 azide for 30 min at RT.

3.6.3 Wide-field Microscopy

Cured coverslips from Section 3.6.1 were imaged on a DeltaVision Deconvolution microscope; a wide-field Olympus IX70 inverted microscope with either an Olympus PlanApo 60X or 100X 1.4 NA oil immersion objective. Images were captured on a

CoolSNAP HQ CCD camera (Photometrics) with 1X gain at -30 °C. Typically camera binning was 1 x 1 or 2 x 2 with an image size of 512 x 512. To prevent light reaching the camera, filters for DAPI, fluorescein, tetramethylrhodamine, or Cyanine 5 (Cy5) were used prior to the CCD camera. Image acquisition and deconvolution were controlled by softWoRx® software.

3.6.4 Primary antibody labelling

Primary antibodies for super-resolution microscopy were labelled directly. For dSTORM an ~1:1 ratio of fluorescent dye per antibody molecule was routinely achieved. Alexa Fluor® 647 NHS ester (Life Technologies) and Cy3B NHS ester (GE Healthcare) were lyophilised from DMSO into 20 µg aliquots and stored at -20 °C in the dark. Fluorescent dyes were re-suspended in DMSO fresh for labelling reactions. For single fluorescent dye labelling, 0.1 µg Alexa Fluor® 647 and 1 µg Cy3B were incubated with 3 µl of primary antibody (1 mg/ml) and 125 mM NaHCO₃ in PBS for 30 min in the dark. Labelled antibodies were then purified from excess unreacted fluorescent dye using 40K MWCO Zeba Spin Desalting columns (Thermo Fisher Scientific). Labelled antibodies were stored at 4 °C in the dark for up to three days.

3.6.5 PALM/dSTORM sample preparation

25 mm diameter high tolerance, #1.5 thickness (0.17 ± 0.01 mm), round glass coverslips (Cat #: 64-0735 [Model #: CS-25R17]; Warner Instruments) were cleaned with a 1:1:5 solution of ammonium hydroxide : hydrogen peroxide : ddH₂O at 80 °C for 16 h in the fume hood. Coverslips were then washed in copious amounts of ddH₂O before dipping in methanol and, under sterile conditions, air-dried and stored in tissue culture plates. Cells were seeded onto sterile 25 mm coverslips and fixed in 4% (w/v) PFA in PBS or 2% (w/v) PFA in complete media. For dSTORM, cells were permeabilised in 0.2% (v/v) Triton X-100 in PBS for 10 min and blocked in 1% (v/v) normal donkey serum (Sigma) in PBS for one hour. Samples were washed in PBS three times before labelling with the freshly prepared directly labelled primary antibody (Section 3.6.4) at RT for one hour. Labelled αNS5A and αNS3 were used at dilutions of 1:2,000 and 1:1,000 respectively. Excess, unbound antibody was removed with three PBS washes. Once labelled, samples were imaged within three days.

3.6.6 PALM/dSTORM microscopy

Super-resolution imaging was performed on a custom built microscope (Figure 3.1) comprising a wide-field Olympus IX81 inverted microscope using a water immersion

Olympus UPlanSApo 60X 1.2 NA objective. Prior to image capture on an Andor iXon Ultra EMCCD camera two additional magnifiers of 1.6x and 1.2x were used before a cylindrical lens with a focal length of 150 mm. Laser wavelengths of 405, 488, 561 and 647 nm were supplied by an Omicron Laserage Light Hub. To prevent light reaching the camera a filter cube (Chroma) was used prior to the EMCCD camera. Samples were mounted in an ASI MS-2000 (XYZ) stage with drift mitigation using stage position control by a C-focus (Mad City Labs Inc.).

Before imaging, samples were incubated in 0.01% (v/v) poly-L-Lysine (Sigma) for 10 min before addition of fiducial markers, either 100 nm or 150 nm gold nanoparticles (Cat #: 742031 or 743058; Sigma) diluted in PBS. A calibration file of z positions were acquired from the PSF of fiducials from 50 nm steps in the z axis. Calibration files were acquired for each wavelength used in PALM or dSTORM imaging. PBS or dSTORM imaging buffer (glucose oxidase (10 Units), catalase (50 Units), 12.5 mg/ml glucose, 1 mM 2-mercaptoethylamine (MEA) in PBS [pH 8.0]) was then added to samples for PALM and dSTORM imaging, respectively. dSTORM imaging buffer was replaced with freshly prepared buffer every hour at the end of image acquisitions.

Images were acquired under wide-field illumination with 561 nm at 30–50 mW for PALM and 642 nm at 50 mW for dSTORM. 0–1.6 μ W 405 nm illumination was used to encourage photo-switching of fluorescence molecules. Multiple data sets of 11,000 frames were acquired at a frame rate of 20 Hz with an EMCCD camera gain of 100. Typically this was 50 repetitions of 200 frames followed by 20 frames of the fiducial position.

3.6.7 Computational methods

To reconstruct super-resolution images, individual fluorescent event localisation and sample drift correction were conducted using the palm3d software (York et al., 2011). The same software was then used to generate histogram representations of the microscopy data. Additional processing, image analysis and visualisation was subsequently conducted in either R (R Core Team, 2013), python (Oliphant, 2007) or ImageJ (NIH) (Schindelin et al., 2015; Schneider et al., 2012). A more detailed description of the methods are provided in Chapter 4 Section 4.2.1) with the processing scripts provided in Appendix 3-5. Colocalisation analysis of fluorescence images were conducted in ImageJ with the JACoP plugin (Bolte and Cordelieres, 2006). Graphical representations and statistical tests were conducted in GraphPad Prism.

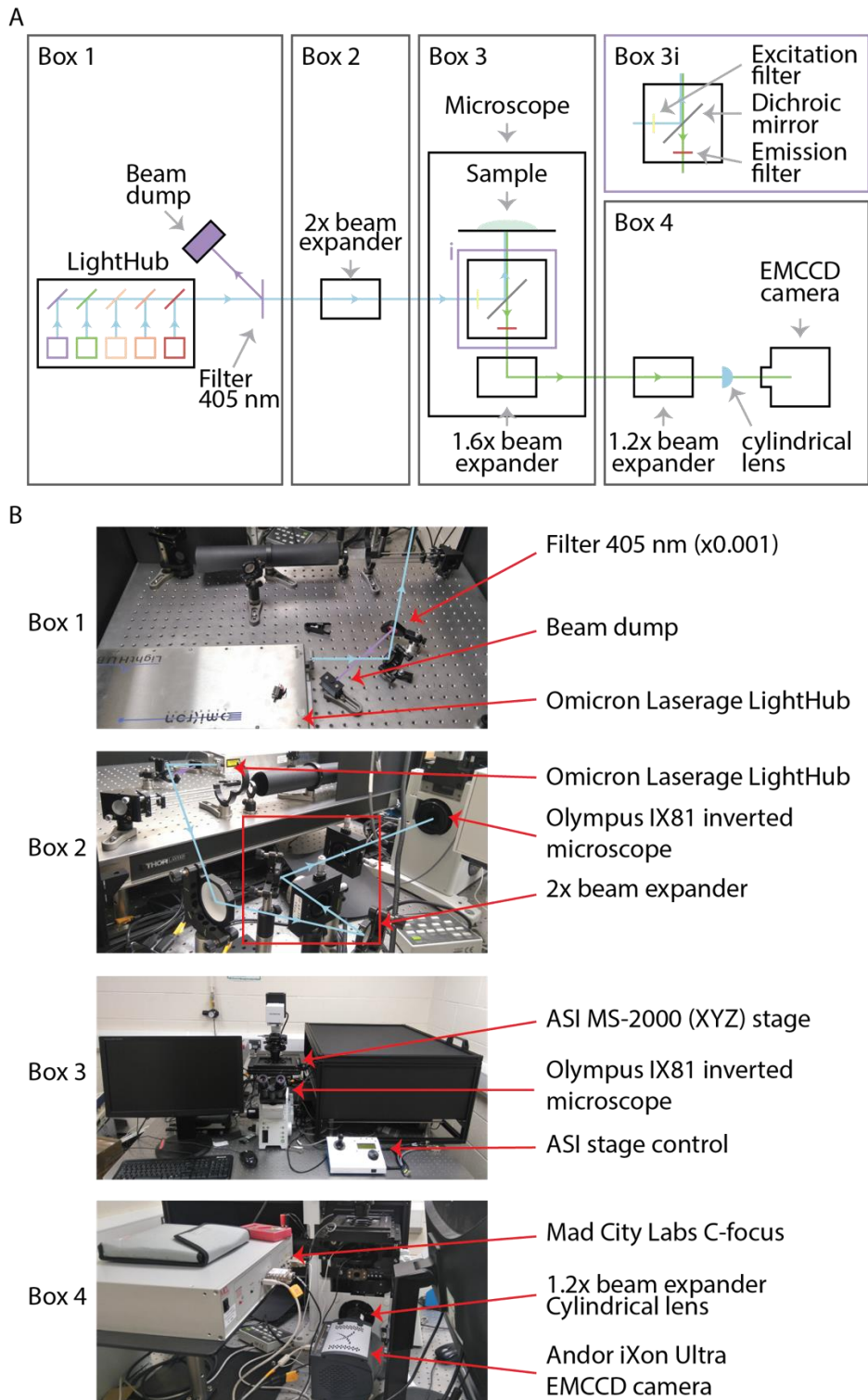


Figure 3.1: Ray diagram and PALM/STORM microscope layout.

A: Ray diagram of the PALM/STORM microscope. Individual components are labelled with grey arrows. B: Images of the PALM/STORM microscope corresponding to labelled boxes in A. Individual components are labelled with red arrows. Blue, purple and green arrows indicate the direction of light through the system.

Chapter 4 - Super-resolution microscopy studies of the HCV replication complex

4.1 Introduction

The HCV replication complex (RC), like other positive strand RNA viruses, is closely associated with cellular membranes (Romero-Brey and Bartenschlager, 2014). For HCV, these membrane rearrangements are termed replication factories and consist of vesicles compacted into a membranous matrix (Egger et al., 2002). These structures are derived from the ER and autophagy pathways (see Chapter 5) and provide a specialised environment for productive infection (Paul and Bartenschlager, 2015).

The current ultrastructural knowledge of HCV RCs derive from electron microscopy (EM) and soft X-ray microscopy studies of the membranous rearrangements during HCV infection (Figure 4.1) (Ferraris et al., 2010; Pérez-Berná et al., 2016; Romero-Brey et al., 2012). The production of double membrane vesicles (DMV) correlated with the kinetics of HCV RNA replication, and were typically between 100–1000 nm in diameter (Ferraris et al., 2010; Romero-Brey et al., 2012).

DMV were identified as sites of HCV replication by immunogold labelling with antibodies to the non-structural proteins and dsRNA (Ferraris et al., 2010; Gosert et al., 2003). Additionally, purified DMV contain active viral replicases capable of *de novo* synthesis of HCV RNA (Paul et al., 2013). However, a major limitation of the immunogold staining was the inefficient labelling of HCV RC components. Although these studies identified the presence of HCV proteins on DMV, a detailed description of their organisation about HCV-induced membrane structures was not revealed.

Correlative light and electron microscopy studies have aimed to address this deficit in knowledge by characterising NS5A fluorescent puncta at the ultrastructural level using EM (Figure 4.1) (Romero-Brey et al., 2012). These studies identified NS5A-GFP fluorescence signal corresponded to accumulations of DMV in close proximity to LDs and the ER. However, light microscopy is fundamentally limited to ~200 nm resolution in the visible light range by the diffraction of light (Section 1.5.2, Equation 1) (Abbe, 1873; Rayleigh, 1896). Consequently, at the light microscopy level NS3 and NS5A staining appears as diffraction limited spots by conventional light microscopy (El-Hage and Luo, 2003; Gosert et al., 2003; Mottola et al., 2002; Shi et al., 2003). Therefore, the precise organisation of HCV components within these membranous structures remains elusive.

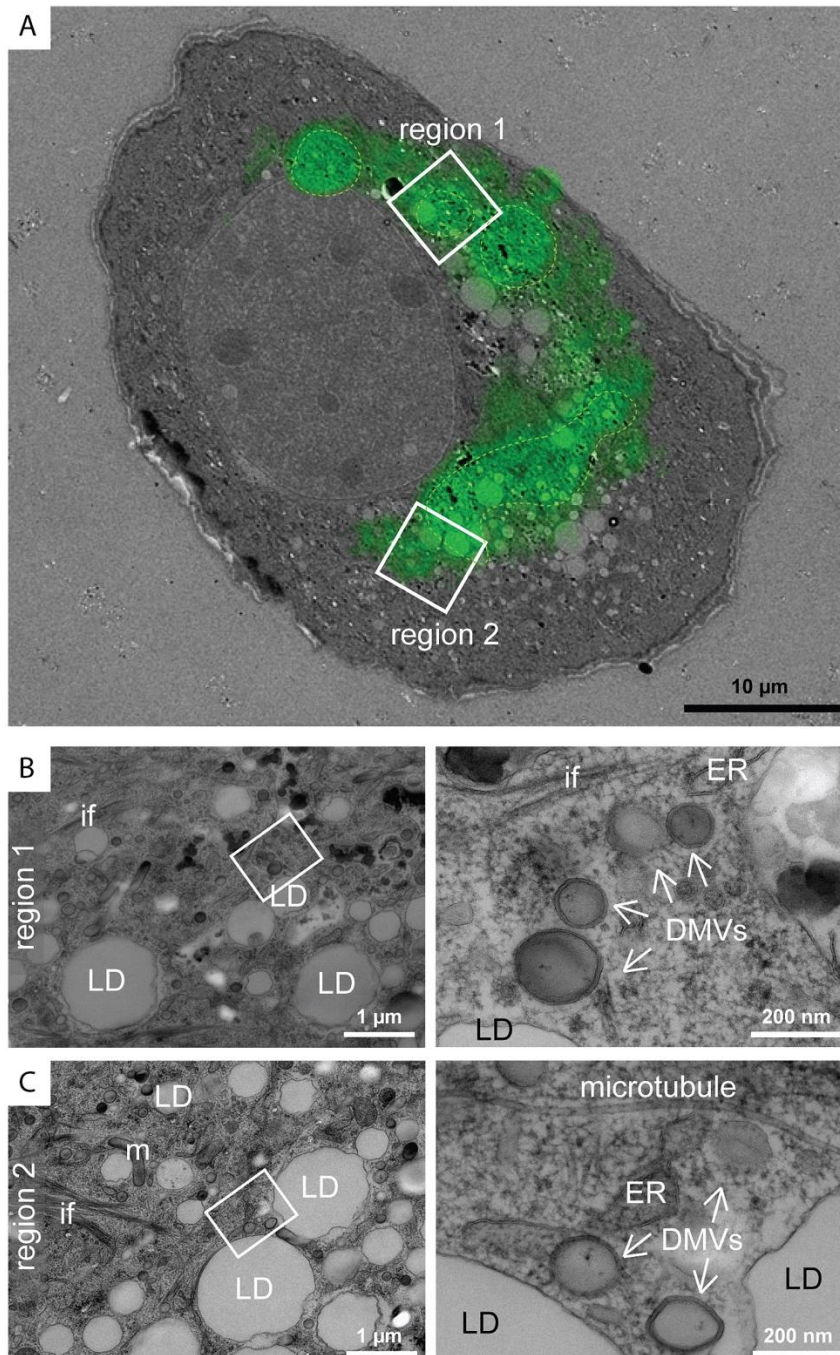


Figure 4.1: Correlative light-electron micrographs of cells harbouring a GFP-tagged SGR.

A: Overlay of whole cell fluorescence and 60 nm ultrathin electron micrograph from correlative light and electron microscopy of NS5A-GFP replicon harbouring cells. Areas marked with green dotted line indicate regions of intense fluorescence. B and C: Higher magnification of regions 1 and 2 respectively. Areas marked in white boxes are magnified in corresponding right panels. LD, lipid droplet; ER, endoplasmic reticulum; DMV, double membrane vesicle; m, mitochondrion; if, intermediate filaments. Adapted from (Romero-Brey et al., 2012).

Recent developments in light microscopy now allow observations of structures below the diffraction limit revealing previously unknown protein organisations (Schermelleh et al., 2010). Single molecule localisation microscopy (SMLM) using both fluorescent proteins (Betzig et al., 2006; Hess et al., 2006), and antibodies (Rust et al., 2006), has achieved image resolutions of 10–20 nm using fluorescence microscopy. This ~10-fold improvement in resolution has resolved structures with significantly improved spatial resolution compared to wide-field microscopy (Figure 4.2) (Kanchanawong et al., 2010; Lambacher et al., 2016; Löscherberger et al., 2012; Shroff et al., 2013; Szymborska et al., 2013). A recent report of SMLM provided insights into the organisation of HCV structural proteins around the viral assembly site at lipid droplets (Figure 4.2F and G) (Eggert et al., 2014). The organisation of core and E2 around lipid droplets indicated a lower level of colocalisation than previously documented by conventional light microscopy (Eggert et al., 2014). Understanding the protein architecture within HCV RCs is now achievable with the improved resolving power of SMLM over wide-field microscopy.

An important component of the HCV replication complex is NS5A, a multifunctional phosphoprotein (Ross-Thriepland and Harris, 2015). It interacts with other non-structural proteins (Shirota et al., 2002), HCV RNA (Foster et al., 2010) and lipid droplets (Miyanari et al., 2007), along with cellular proteins (Hamamoto et al., 2005). As such, it is regularly used as a marker for replication complexes. The protein is regulated by phosphorylation, although the precise mechanisms by which it does so remain elusive (Ross-Thriepland and Harris, 2015). Recently, our lab has reported a complex multi-phosphorylation process in the regulation of NS5A function (Section 1.3.7.4) (Ross-Thriepland et al., 2015; Ross-Thriepland and Harris, 2014).

The critical functions NS5A plays during HCV genome replication are also highlighted by the development of the potent NS5A inhibitor daclatasvir (DCV), recently approved by the FDA for HCV therapy. Currently the mechanism of action is unknown as NS5A does not have any known enzymatic activity. Therefore multiple models for DCVs binding to NS5A have been proposed (Barakat et al., 2015; Kazmierski et al., 2014; Lambert et al., 2014; Nettles et al., 2014; O'Boyle et al., 2013) although the exact site of binding is still unknown.

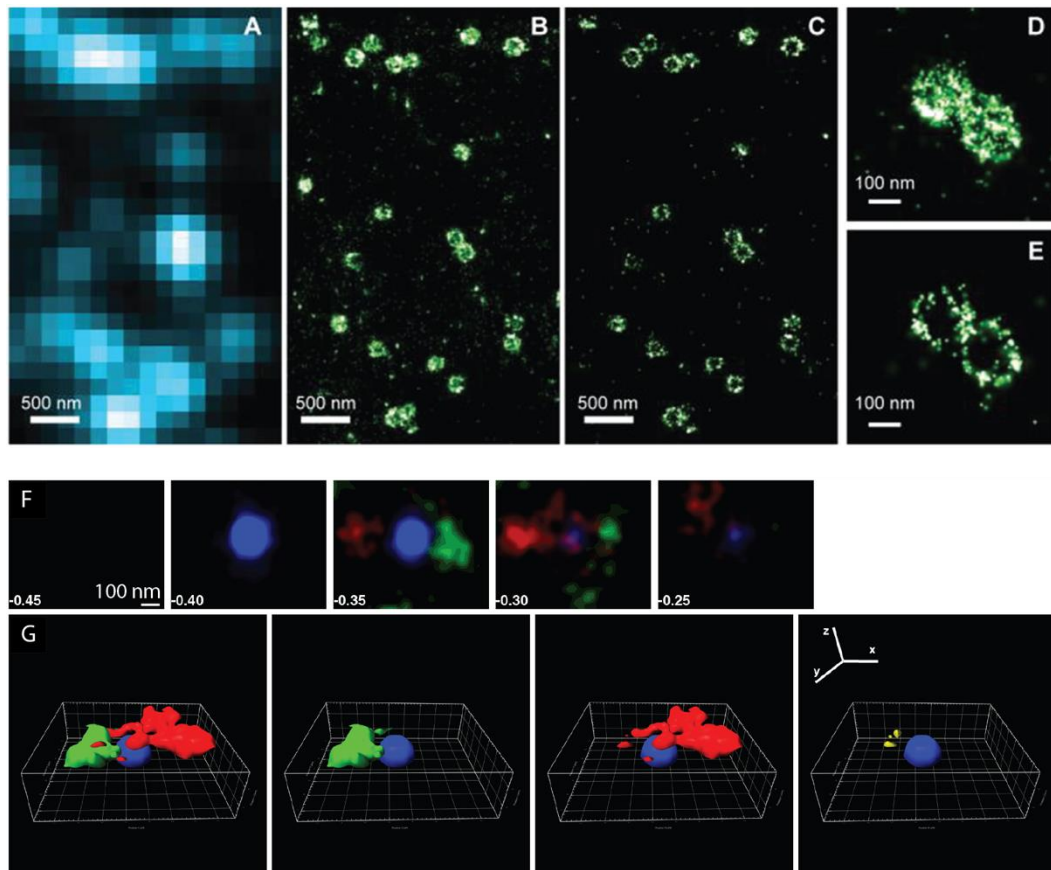


Figure 4.2: STORM microscopy of clathrin coated pits and HCV structural proteins.

A: Conventional direct immunofluorescence image of clathrin. B: Z-projection of 3D-STORM image from A. C: 50 nm thick x-y cross-section from B. D: Magnified Z-projection of two clathrin coated pits from B. E: Corresponding 100 nm thick x-y cross-section from D. F: Image stacks from 3D-STORM of HCV infected cells. Core protein (green), E2 protein (red), lipid droplet (blue). G: Corresponding 3D volume reconstruction from stacks in F. From left to right, all three channels, core and lipid droplet, E2 and lipid droplet then core-E2 colocalisation volume (yellow) and lipid droplet. Ruler hatch marks in 3D image correspond to 100 nm. A-E adapted from (Huang et al., 2008b). F-G adapted from (Eggert et al., 2014).

Cell based studies monitoring NS5A-GFP localisation from the NS3–5B polyprotein and SGR systems have revealed no accumulation of DMV or other virus-induced membrane structures in subcellular regions containing NS5A-GFP fluorescence (Berger et al., 2014; Reghellin et al., 2014). These studies indicated that DCV inhibits the formation of the membranous web without interfering with NS5A localisation, or its interactions with PI4KIII α (Berger et al., 2014). Although confusingly, DCV was found in a separate study to have no effect on preformed replication factories (McGivern et al., 2014).

Taking advantage of the improved resolution SMLM microscopy offers, this chapter was focussed on elucidating the NS5A and NS3 protein organisation within HCV replication complexes. By inhibiting NS5A functions through DCV treatment, or manipulating NS5A phosphorylation, this study aimed to better understand the roles of NS5A within the replication complex.

4.2 Localisation microscopy methods

4.2.1 Workflow for localisation microscopy

4.2.1.1 SMLM image acquisition

Localisation microscopy studies were carried out on a custom built super-resolution microscope at Leeds (Section 3.6.6). Preparation of samples followed the same protocol as immunofluorescence studies with additional coverslip cleaning (Section 3.6.5). Additionally, once samples were fixed and labelled they were imaged within three days, after which the quality of labelled antibodies deteriorated. Antibodies used in dSTORM imaging were directly labelled with an ~1:1 ratio of Alexa Fluor 647 (Section 3.6.4).

Prior to image acquisition, fiducials markers (gold nanoparticles of 100 nm or 150 nm (Section 3.6.6) for PALM and dSTORM, respectively) were applied to coverslips. Imaging of fiducials under the required excitation wavelength was performed to generate a calibration stack of the PSF distortion in x - y from the cylindrical lens using 50 nm steps in z (Figure 1.15). By performing a cross correlation (Guizar-Sicairos et al., 2008) between sample and bead PSFs, the molecular localisation of fluorescent events in z were obtained. These gold nanoparticles embedded in the sample were then used as fiducial markers to track drift during image acquisition.

Image acquisitions collected for each sample typically consisted of 11,000 frames (22,000 for 3D-PALM imaging). These were composed of 50 repeating sequences of 200 frames followed by 20 frames (Section 3.6.6). The 20 frame data sets were for monitoring image drift between acquisition of the 200 frame image sequences. Laser illumination powers were typically 30 mW or 50 mW for 561 nm and 647 nm wavelengths, respectively. To encourage blinking of either fluorescent proteins or dyes, 0–3 μ W 405 nm illumination was used as required.

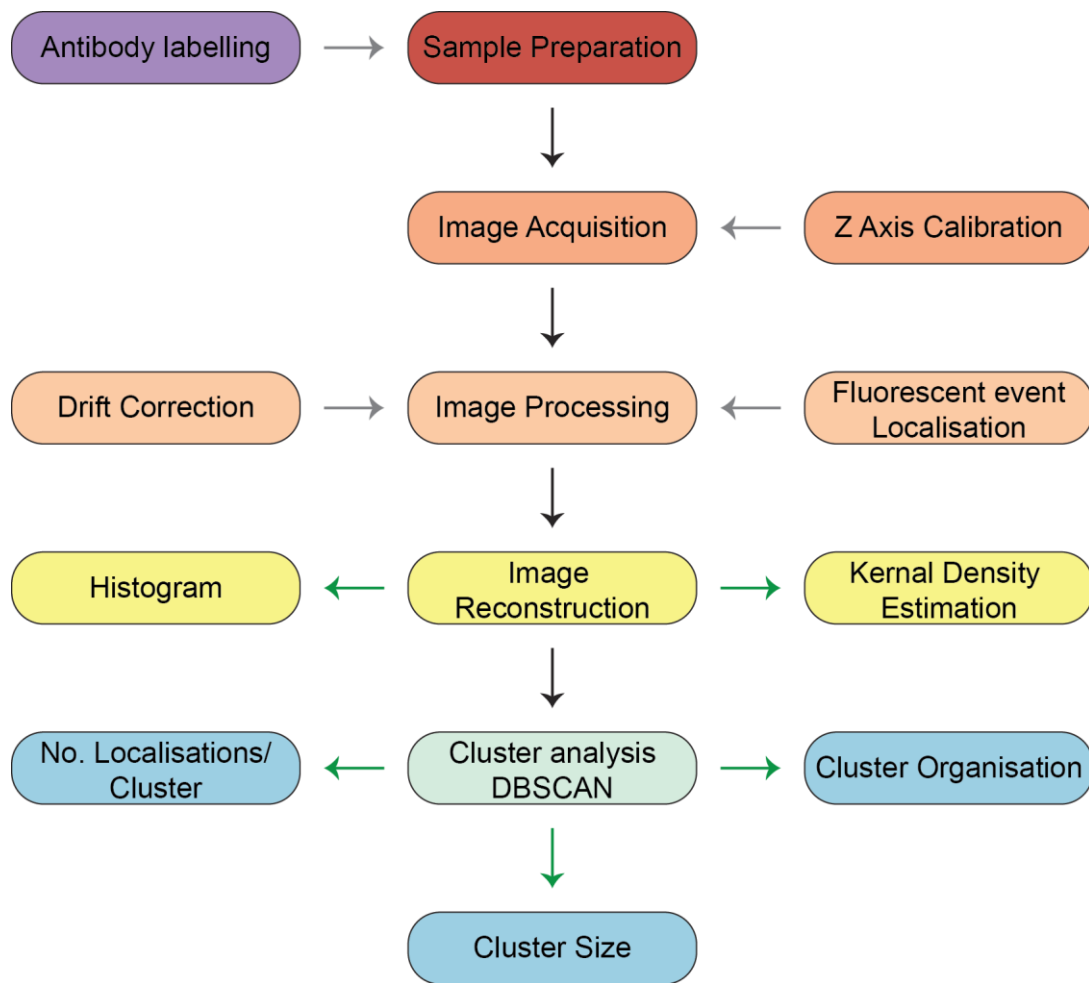


Figure 4.3: Flowchart of localisation microscopy image acquisition and processing. Black arrows indicate direction of workflow, grey arrows correspond to processes carried out during the current step, and green arrows represent output.

4.2.1.2 SMLM image processing

Fluorescent event localisation and drift correction were conducted in the palm3d software (<https://github.com/AndrewGYork/palm3d>) which uses the Python programming language (Oliphant, 2007; York et al., 2011). Image acquisition runs were loaded into the palm3d software and selection parameters determined empirically for each image collection to reduce false positive and false negative localisations. A Gaussian-Laplace filter ($\sigma = 4$) was applied to each data frame as a band-pass filter to remove slowly-varying background and quick-varying noise. The Laplacian is a 2D measure of the second spatial derivative of an image (Abramowitz and Stegun, 1964). It identifies regions of rapid intensity change, in this case the appearance of a single fluorescent event. Gaussian smoothing of the image beforehand reduces the sensitivity of the Laplacian to noise. Pixels in the filtered image were then selected according to intensity, typically 3–5 standard deviations above the mean. Candidate particles are then compared to the calibration stack to estimate the sub-pixel position in x , y and z . Routinely, 20 nm localisation precision was obtained in x - y and 30 nm in z . Localisation precision was measured from the standard deviation of the full width at half maximum from a source of multiple emitters, in this case gold fiducials (Hendrik Deschout et al., 2014).

After candidate selection and localisation, sample drift during acquisition was corrected. A single fiducial from the field of view was selected by filtering all localisations to a specified x - y - z position and minimum correlation strength between subsequent frames. Piecewise linear interpolation and Gaussian smoothing are then used to estimate drift over time.

4.2.1.3 SMLM image reconstruction

Once all fluorescent events have been localised and drift corrected, the molecular coordinates were plotted in a 3D histogram. The entire field of view was reconstructed with 100 nm pixel bins, within $\pm 1.5 \mu\text{m}$ of the imaging focus, from localisations with a cross-correlation strength above 0.4 to the calibration stack. Correction of the x and y coordinates with pre-determined correction factors, typically $x=106$ nm and $y=133$ nm, were applied before image reconstruction. These correction factors remove the distortion caused by the cylindrical lens and were determined from gold nanoparticles in the same microscope set-up as samples. Cropping and re-binning of histogram images is then used to inspect regions of interest.

To visualise localisations with Gaussian smoothing, kernel density estimation was conducted in R (R Core Team, 2013). The molecular coordinates were extracted from the palm3d output files (Appendix 3) and smoothed using a 3D Gaussian kernel (σ of 20 nm in x - y and 30 nm in z) on a regular grid. The Gaussian kernel bandwidth corresponds to the average localisation precision obtained. Grid spacing was chosen as 501 x 501 for the x and y dimensions to produce 10 nm pixels in the final image.

4.2.1.4 Analysis of protein clusters

The coordinate positions of localisations in x - y - z were extracted directly from palm3d output files into a Python NumPy array. Protein clusters were analysed using density-based spatial clustering of applications with noise (DBSCAN) analysis in Python (Appendix 4 and Appendix 5) (Figure 4.4). DBSCAN requires two parameters, the first is the minimum number of localisations within a cluster (minimum points), and the second is the size of the search radius (ϵ) (Figure 4.4). Localisations were assigned to clusters or noise based on their local density (Ester et al., 1996). DBSCAN identifies localisations as either a core, border or noise point (Figure 4.4). Core points contain the minimum number of localisations within the search radius, and are therefore in a cluster. Border points contain a core point within the search radius but do not have the minimum number of localisations to be a core point. Therefore these points are on the borders of clusters. Lastly, localisations which do not satisfy either DBSCAN parameter are termed noise.

The choice of DBSCAN parameters were carefully selected and optimised empirically according to some considerations. First, the choice of minimum points was selected as 20 for PALM and 30 for dSTORM. This ensured several protein molecules had to be within a cluster, and also accounted for each protein molecule being represented more than once, e.g. for blinking in dSTORM. Second, the search radius was informed from current knowledge on the size of replication factories (Ferraris et al., 2010; Romero-Brey et al., 2012). Therefore, the search radius (ϵ) was set to 150 nm, the size of smaller membranous structures produced by HCV infection. This was much higher than the average localisation precision of ~20 nm and ensured multiple, spatially separate localisations within the search radius. Visual inspection of DBSCAN clustering was conducted to ensure the minimum selection of false positives.

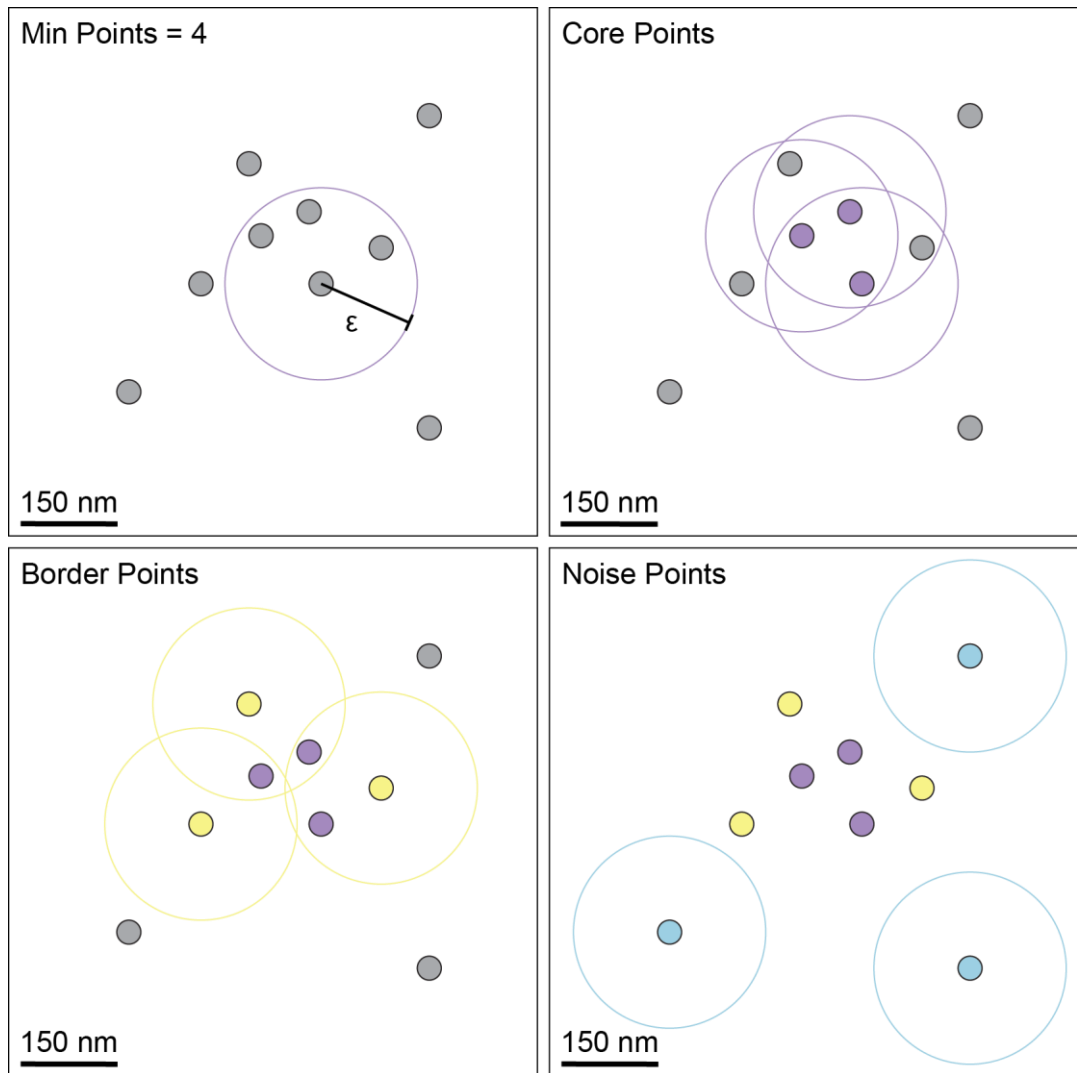


Figure 4.4: Schematic illustrating DBSCAN clustering of localisations.

Points are clustered based on local density. Two parameters are required for DBSCAN clustering. First, the number of points (min points) needed within a search radius, and secondly the size of the search radius (ϵ). DBSCAN scores points as either core points, which satisfy min points and ϵ ; border points, which have a core point within their search radius but do not have min points; or noise points, which fail both criteria. Core, border and noise points are shown in purple, yellow and blue, respectively.

Multiple characteristics were measured from clusters identified by DBSCAN analysis, such as the number of localisations per cluster, cluster size, and distance of localisations from the cluster centroid (Appendix 5). The measurements provided information about cluster size and the internal organisation of localisations. The cluster centroid is the geometric centre of localisations within a cluster. For each localisation within a cluster, the Euclidean distance to the centroid position of its cluster was calculated. The cluster size is reported as the mean pairwise Euclidean distance in *x-y* between localisations within a cluster. Graphical and statistical analysis was then conducted using GraphPad Prism.

4.2.2 NS5A-mEos3.2 cloning strategy

To undertake PALM imaging studies on the HCV replication complex, the photoswitchable fluorescent protein mEos3.2 (McKinney et al., 2009; Zhang et al., 2012) was engineered into domain III of NS5A (Figure 4.5). mEos3.2 was chosen because of its monomeric nature and superior photophysical properties over other fluorescent proteins. The coding sequence for mEos3.2 was PCR amplified (Appendix 1) introducing unique *Bam*HI and *Bcl*I restriction enzyme sites, at the N- and C-terminus respectively. PCR amplified mEos3.2 was ligated into NS5A using the unique restriction enzyme site *Bcl*I in pmSUB (Mair Hughes Thesis). *Bam*HI and *Bcl*I have compatible ligations sites. Colony PCR was used to screen constructs with the correct orientation of mEos3.2. To assess the replication kinetics of the NS5A-mEos3.2 fusion protein, the *Bam*HI and *Hpa*I restriction digestion fragment from pmSUB [NS5A-mEos3.2] was ligated into pmSGR-Feo-JFH1 creating pSGR-Feo-JFH1 [NS5A-mEos3.2]. All constructs were confirmed by restriction digestion and Sanger sequencing.

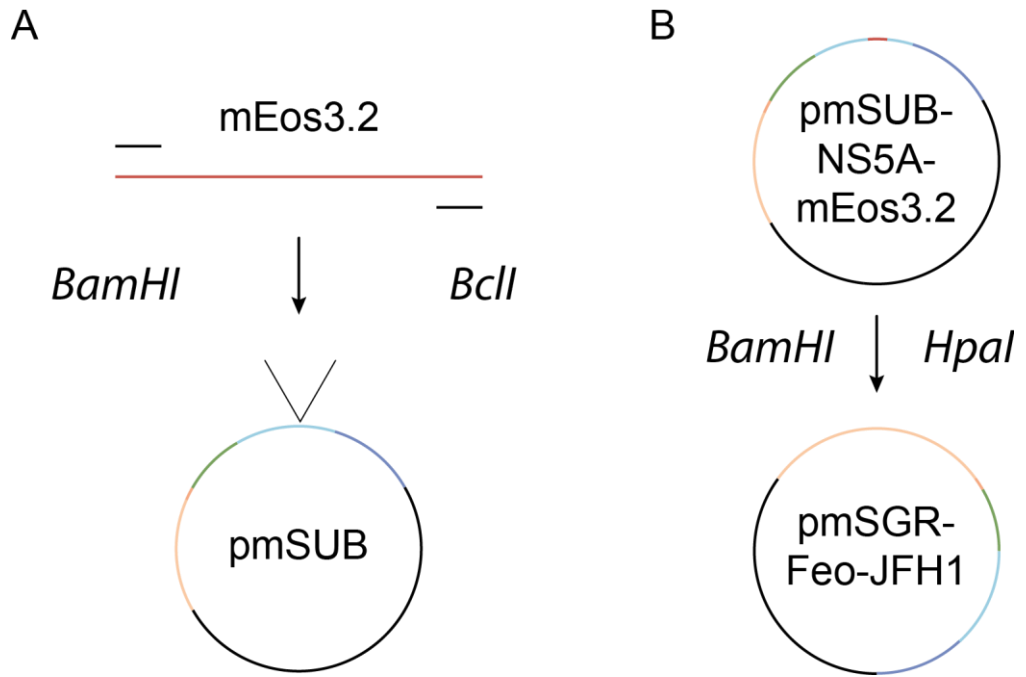


Figure 4.5: Illustration of NS5A-mEos3.2 cloning strategy.

A: mEos3.2 sequence was PCR amplified, introducing unique restriction enzyme sites at the N- and C-terminus. The PCR product was cloned into pmSUB using the unique *BclI* restriction enzyme site within domain III of NS5A. B: NS5A-mEos3.2 fusion protein was ligated into pmSGR-Feo-JFH1 using *BamHI* and *HpaI* creating pSGR-Feo-JFH1 [NS5A-mEos3.2]. Coding sequences for NS3, NS4B, NS5A, NS5B and mEos3.2 in yellow, green, light blue, dark blue and red, respectively.

4.3 Results

4.3.1 Characterisation of NS5A-mEos3.2 fusion protein

Introduction of the mEos3.2 fluorescent protein into domain III of NS5A did not affect HCV replication (Figure 4.6A). Luciferase signal increased for SGR-Feo-JFH1 [NS5A-mEos3.2] by $\sim 2\log_{10}$ up to 72 hours post infection (h.p.e) (Figure 4.6). The increase in luciferase signal, as a measure of replication, was the same as unaltered control RNA. In contrast there was no increase in luciferase signal for the replication deficient SGR-Feo-JFH1 [GND].

mEos3.2 maintains the ability to correctly fold when expressed as an internal insertion in domain III of NS5A (Figure 4.6B). This correlates with previous reports of fluorescent protein insertion (e.g. GFP) internally into NS5A (Eyre et al., 2014; D. M. Jones et al., 2007). The localisation of mEos3.2 fluorescent puncta is characteristic of NS5A, and colocalisation with antibody staining for NS5A was also observed. Both the luciferase kinetics and immunofluorescence data validate the SGR-Feo-JFH1 [NS5A-mEos3.2] construct for super-resolution imaging. A population of cells stably harbouring SGR-Feo-JFH1 [NS5A-mEos3.2] were selected and taken forward for super-resolution microscopy analysis.

4.3.2 Visualising NS5A-mEos3.2 by 3D-PALM

PALM imaging of NS5A-mEos3.2 showed clusters of molecules that were equivalent to the diffraction limited puncta observed by wide-field (Figure 4.7). Diffraction limited NS5A puncta in wide-field images were resolved as regions of dense localisations clustered into discrete structures. (Figure 4.7D and E arrows). These protein clusters were observed in the cytoplasm of SGR harbouring cells, amid a diffuse background of single molecule localisations. NS5A-mEos3.2 protein clusters were observed distributed throughout the cytoplasm at random.

NS5A-mEos3.2 protein clusters were identified from the diffuse single molecule background by DBSCAN analysis (Figure 4.8). Protein clusters identified from areas of dense NS5A-mEos3.2 localisations were typically between 90–140 nm in size, with a mean size of 123 ± 1.6 nm (Figure 4.8C and D). This size range correlated with the smaller DMV structures measured by electron microscopy during HCV infection (Romero-Brey et al., 2012). Image reconstruction and analysis of two independent cells identified >1,000 NS5A-mEos3.2 protein clusters, which contained around 59 localisations on average. From all the localisations in the reconstructed image, around 25% were classified as part of a cluster by DBSCAN analysis.

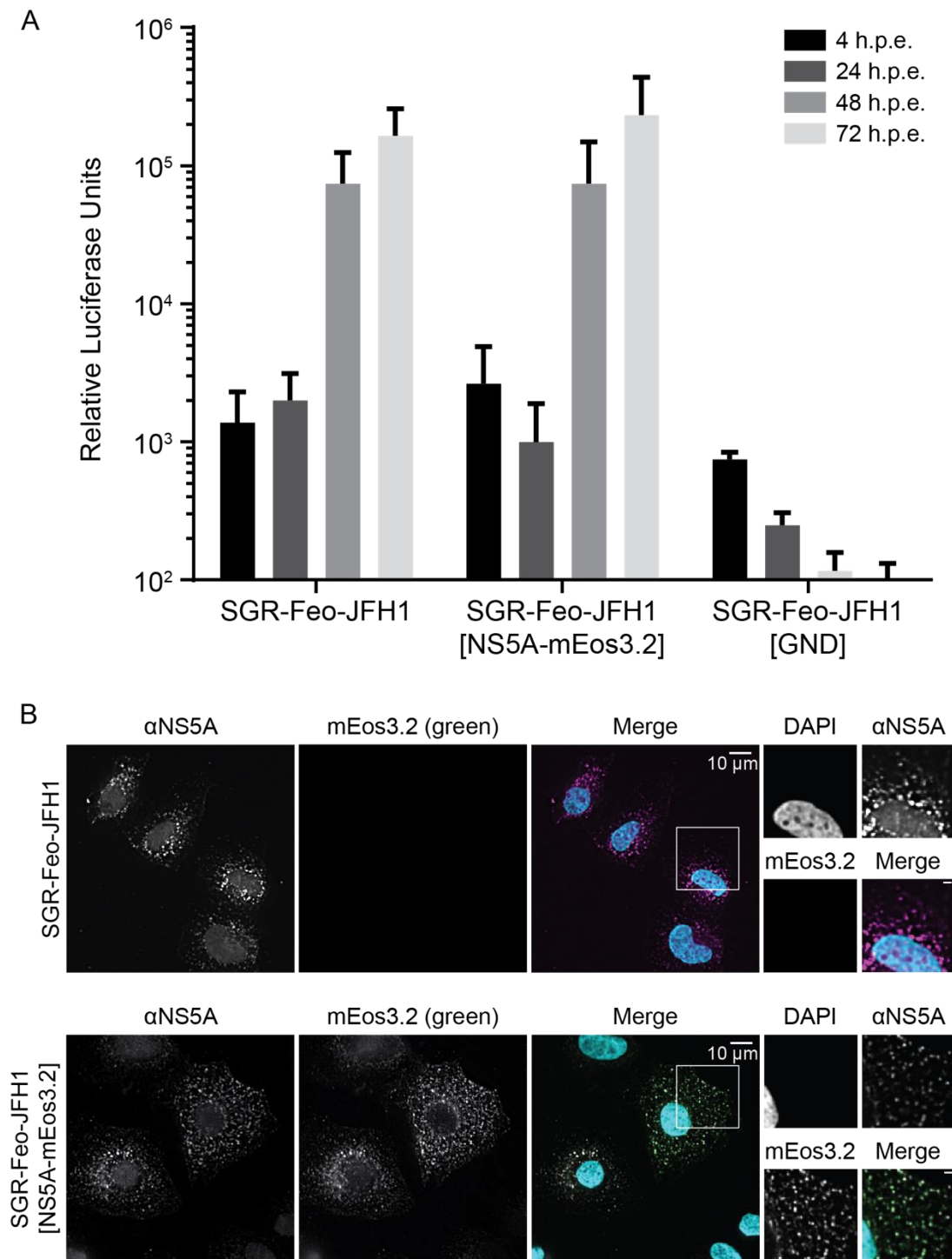


Figure 4.6: Characterisation of SGR-Feo-JFH1 [NS5A-mEos3.2].

A: Luciferase reporter values were measured up to 72 h.p.e. from transient electroporation of 5 μ g RNA into HuH7 cells. Comparison of mEos3.2 tagged NS5A to wildtype and polymerase deficient (GND) SGR controls. Data represent the mean \pm SD, $n=3$. B: Cells stably harbouring SGR-Feo-JFH1 or SGR-Feo-JFH1 [NS5A-mEos3.2] were fixed and labelled with anti-NS5A antibody and DAPI. White boxes indicate zoomed in regions with 2 μ m scale bars.

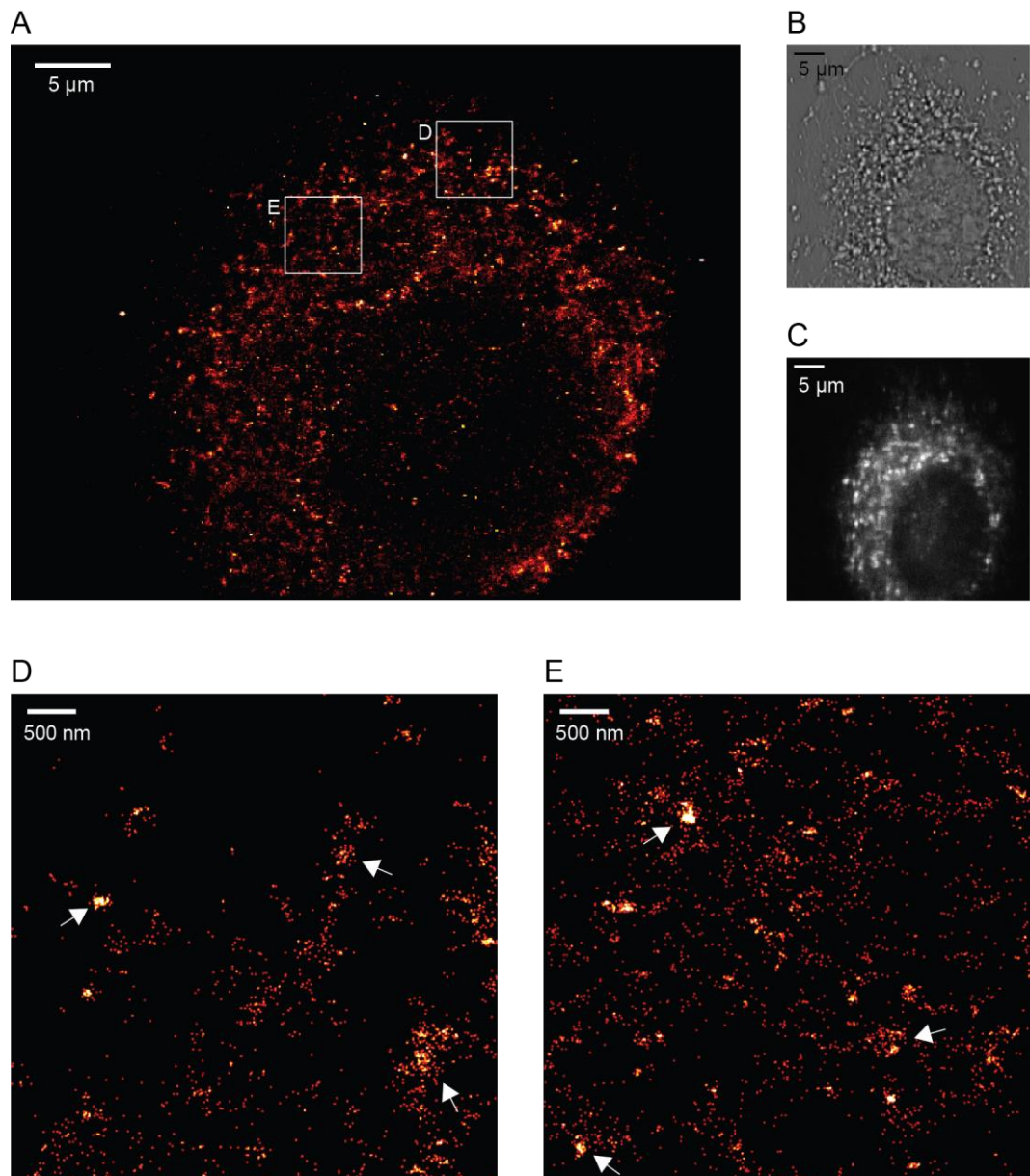


Figure 4.7: 3D-PALM imaging of SGR-Feo-JFH1 [NS5A-mEos3.2].

A: Sum of z slices, $3.9\ \mu\text{m}$ thick, from a representative 3D-PALM image reconstruction from a stable SGR-Feo-JFH1 [NS5A-mEos3.2] cell line. Image was reconstructed from 348,829 localisations using $100\ \text{nm}$ 3D histogram pixel bins. B: Bright-field image of cell in A. C: Wide-field image of cell in A. D and E: $5\ \mu\text{m}^2$ regions of interest from the cell cytoplasm after kernel density estimation ($\sigma = 20\ \text{nm}$ in x - y , $30\ \text{nm}$ in z) using $4\ \text{nm}$ pixels. Sum of z slices, $850\ \text{nm}$ thick. Arrows illustrate protein clusters. Scale bars are indicated.

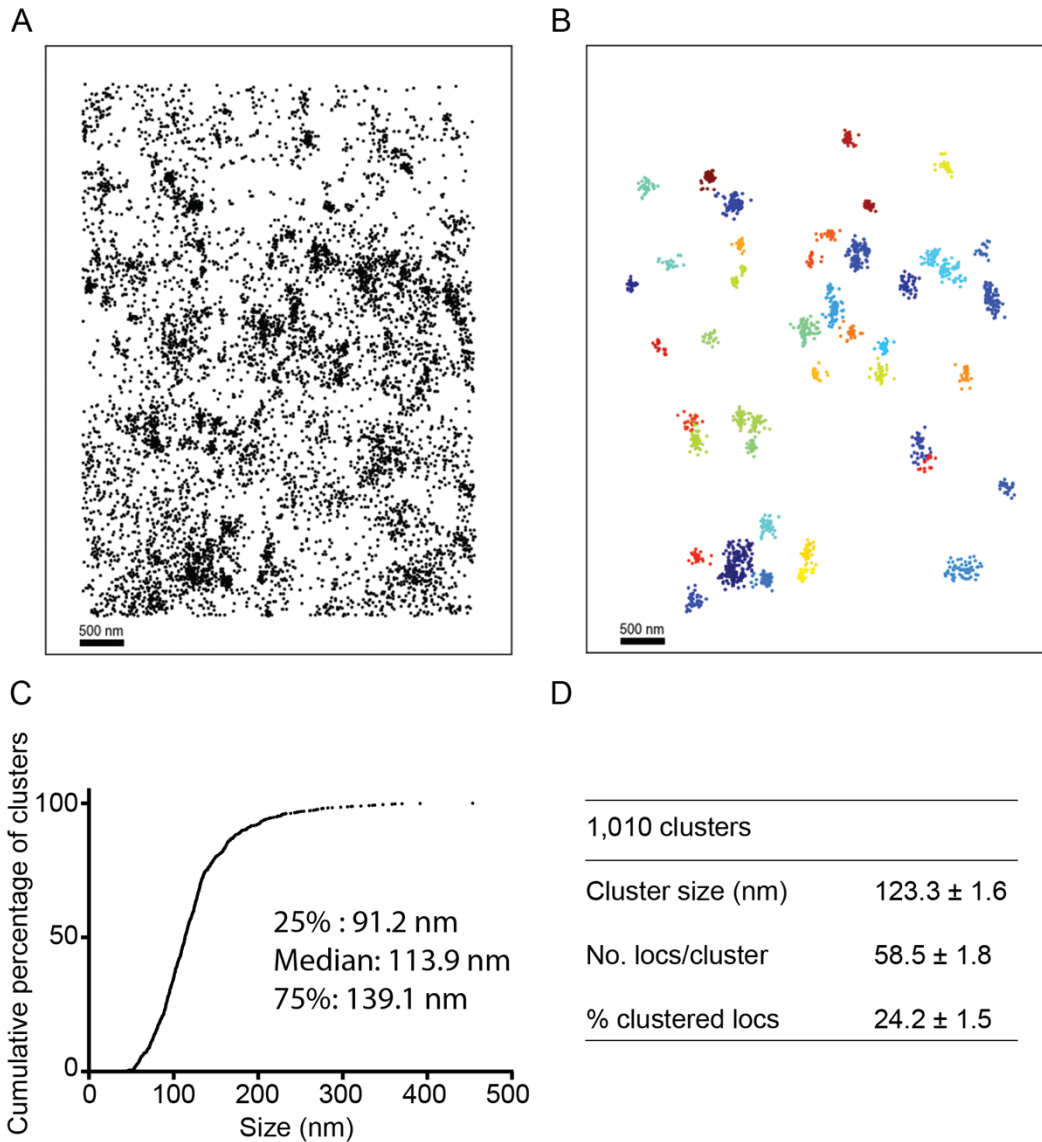


Figure 4.8: DBSCAN analysis of SGR-Feo-JFH1 [NS5A-mEos3.2] protein clusters.

A: Maximum z projection of representative region of interest from 3D-PALM image reconstruction of SGR-Feo-JFH1 [NS5A-mEos3.2] containing 7,968 localisations. B: Clusters identified from DBSCAN analysis of A (min points = 20, ϵ = 150 nm). 42 clusters containing 2,115 localisations are coloured according to their cluster identity. C: Cumulative percentage of cluster size from two independent cells. Median and percentile values are indicated. D: Summary of clusters from DBSCAN analysis, derived from 28 regions of interest from 2 independent cells. Data represent the mean \pm SEM.

4.3.3 Super-resolution imaging of untagged NS5A by dSTORM

NS5A produced during HCV infection was readily detected under a number of permeabilisation conditions (Figure 4.9). Discrete punctate structures were observed distributed throughout the cytoplasm of infected cells. Fluorescence intensity appeared greatest with Triton X-100 permeabilisation indicating a greater accessibility of antibodies to NS5A epitopes. This is likely a consequence of the non-selective extraction of lipids by Triton X-100, whereas saponin and digitonin preferentially form pores in the plasma membrane by binding cholesterol (Jamur and Oliver, 2010). All future antibody staining was conducted using Triton X-100 permeabilisation for NS protein detection.

Image reconstructions from dSTORM of antibody labelled NS5A resolved a greater number of clustered structures over 3D-PALM with a reduced single molecule population (Figure 4.10). NS5A protein clusters were more clearly defined as regions of dense localisations. The distribution of NS5A protein clusters throughout the cytoplasm was comparable to NS5A-mEos3.2. However, over twice as many fluorescence events were localised from 3D-dSTORM imaging compared to 3D-PALM. Additionally, these were obtained from a single data collection series compared to the two required to reconstruct a 3D-PALM image.

In contrast to 3D-PALM imaging, NS5A protein clusters were typically smaller in size, between 64–140 nm, with a mean of 113.8 ± 1.7 nm (Figure 4.11 and Figure 4.12). Although around 10 nm smaller in size, 3D-dSTORM protein clusters contained around 5-fold more localisations within each cluster than 3D-PALM (269 compared to 59). This discrepancy may be attributed to the greater number of localisations identified from antibody labelling, likely a result of multiple localisations from a single dye due to fluorescence blinking (Endesfelder et al., 2014). After fluorescence emission, fluorophores under dSTORM conditions may enter a “dark” state before a second excitation at a later time. This results in multiple localisations, and therefore multiple positions, being recorded for the same fluorophore (Dave et al., 2009). The differences in position of the detected fluorophore between PALM and dSTORM, genetic tag in domain III of NS5A vs antibody staining respectively, may alter the apparent cluster size (Huang et al., 2008b). The improved labelling density revealed that 65% of all observed localisations were identified as part of a cluster structure, compared to only 25% for 3D-PALM (Figure 4.12B).

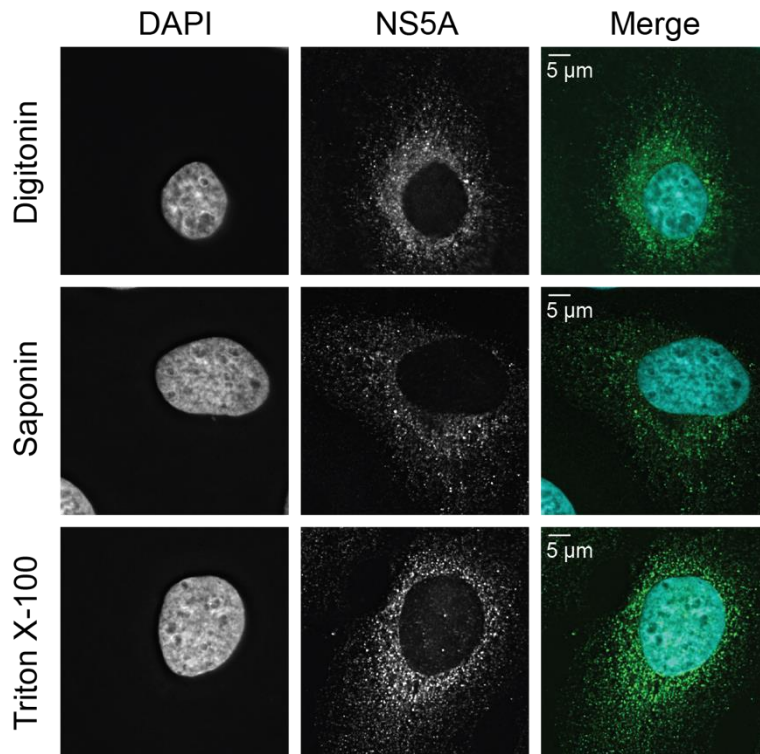


Figure 4.9: Optimisation of different permeabilisation conditions for antibody labelling of NS5A.

HuH7 cells were infected with JFHcc for 48 before permeabilisation with the indicated detergent and antibody detection of NS5A. Scale bars are indicated.

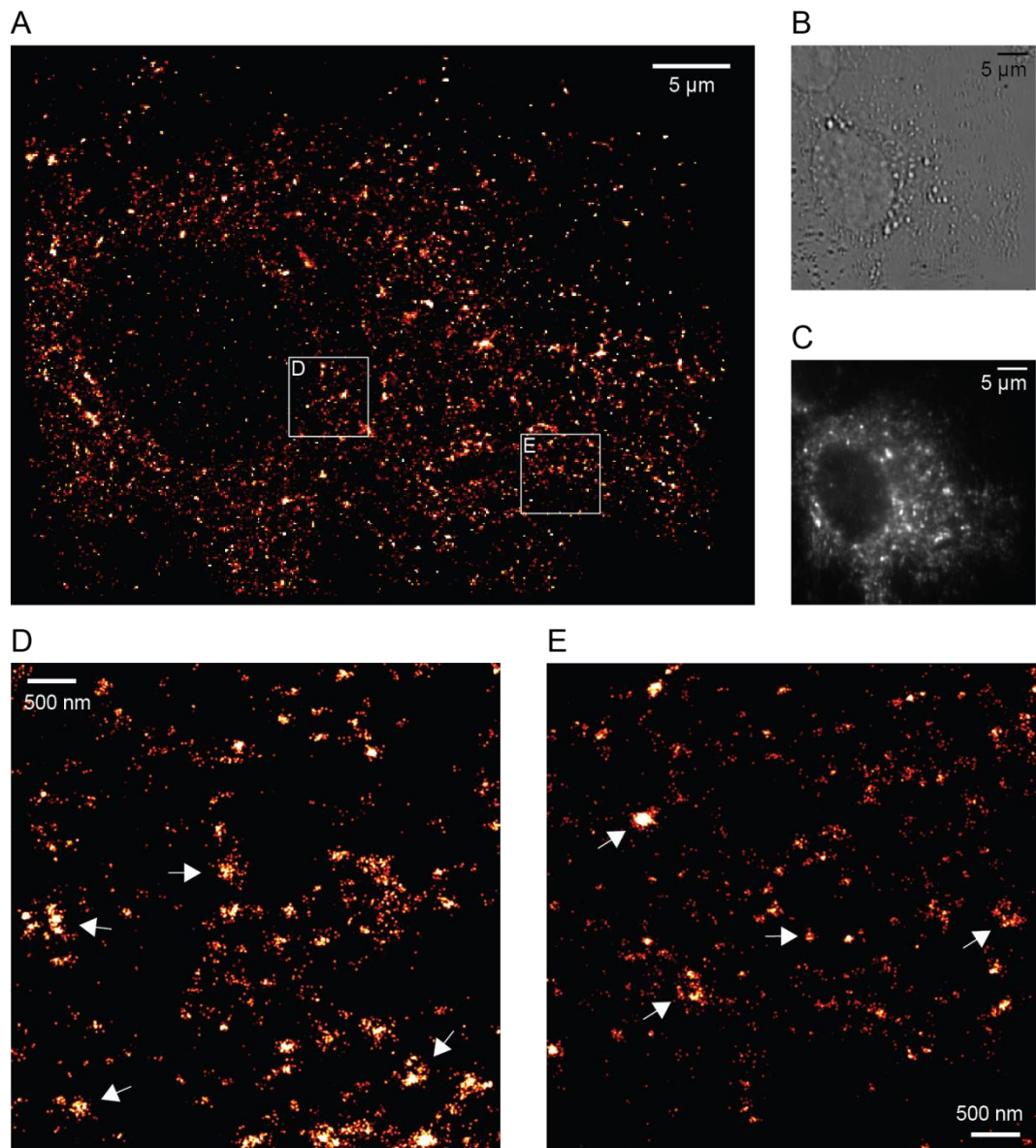


Figure 4.10: 3D-dSTORM imaging of antibody labelled NS5A.

Cells stably harbouring SGR-Neo-JFH1 were fixed and subjected to immunofluorescence staining for NS5A before 3D-dSTORM imaging. A: Sum of z slices, $3.9 \mu\text{m}$ thick, from a representative 3D-dSTORM image reconstruction. 873,185 localisations were binned into 100 nm pixels in a 3D histogram. B: Bright-field image of cell in A. C: Wide-field image of cell in A. D and E: $5 \mu\text{m}^2$ regions of interest after kernel density estimation ($\sigma = 20 \text{ nm}$ in x - y , 30 nm in z) with 4 nm pixel bins. Sum of z slices, 800 nm thick. Arrows illustrate clusters. Scale bars are indicated.

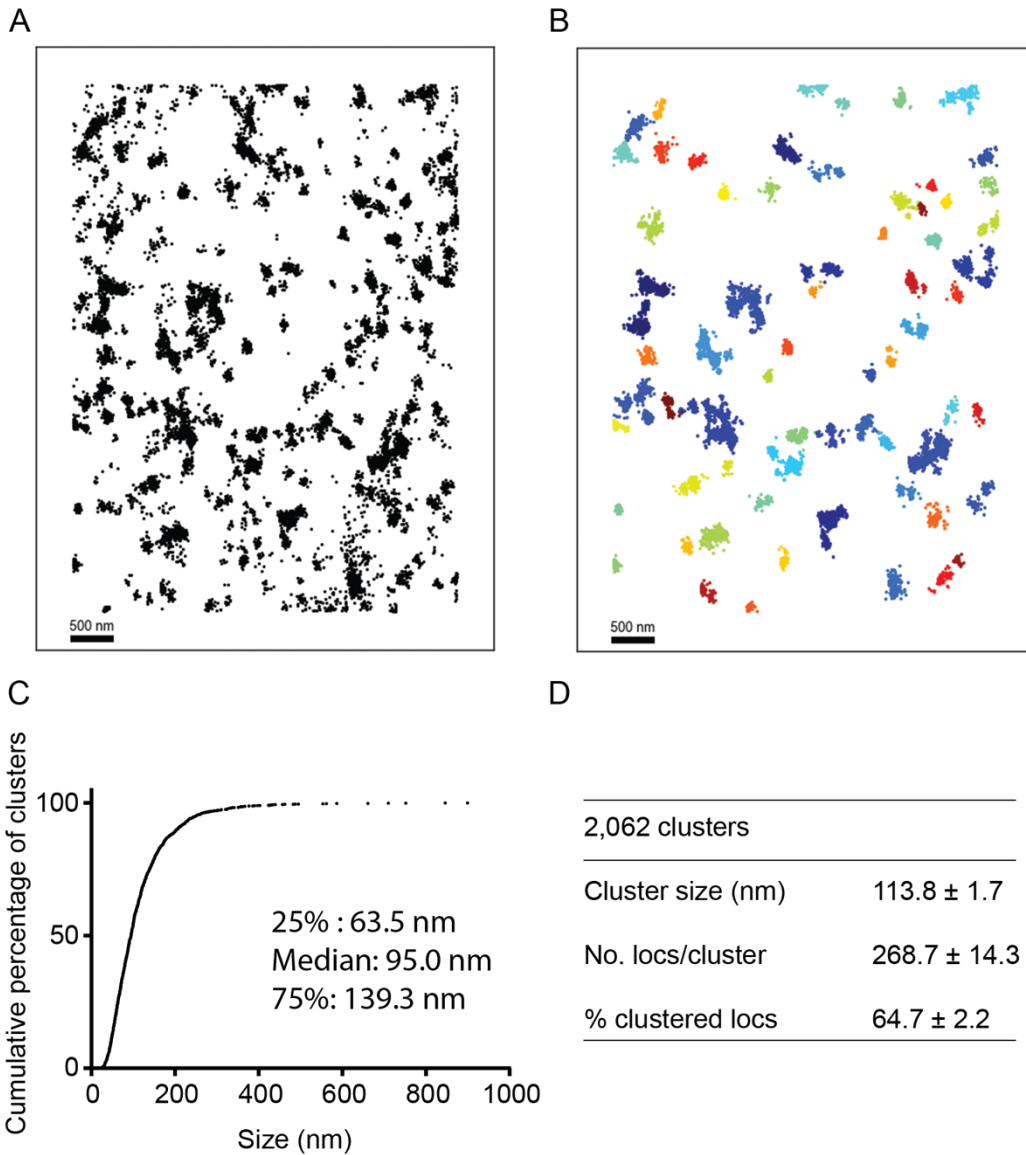


Figure 4.11: DBSCAN analysis of SGR-Neo-JFH1 antibody labelled NS5A protein clusters.

A: Maximum z projection of representative region of interest from 3D-dSTORM image reconstruction containing 15,721 localisations. B: Clusters identified from DBSCAN analysis of A (min points = 30, ϵ = 150 nm). 66 clusters containing 11,790 localisations are coloured according to their cluster identity. C: Cumulative percentage of cluster size from three independent cells. Median and percentile values are indicated. D: Summary of clusters from DBSCAN analysis, derived from 63 regions of interest from 3 independent cells. Data represent the mean \pm SEM.

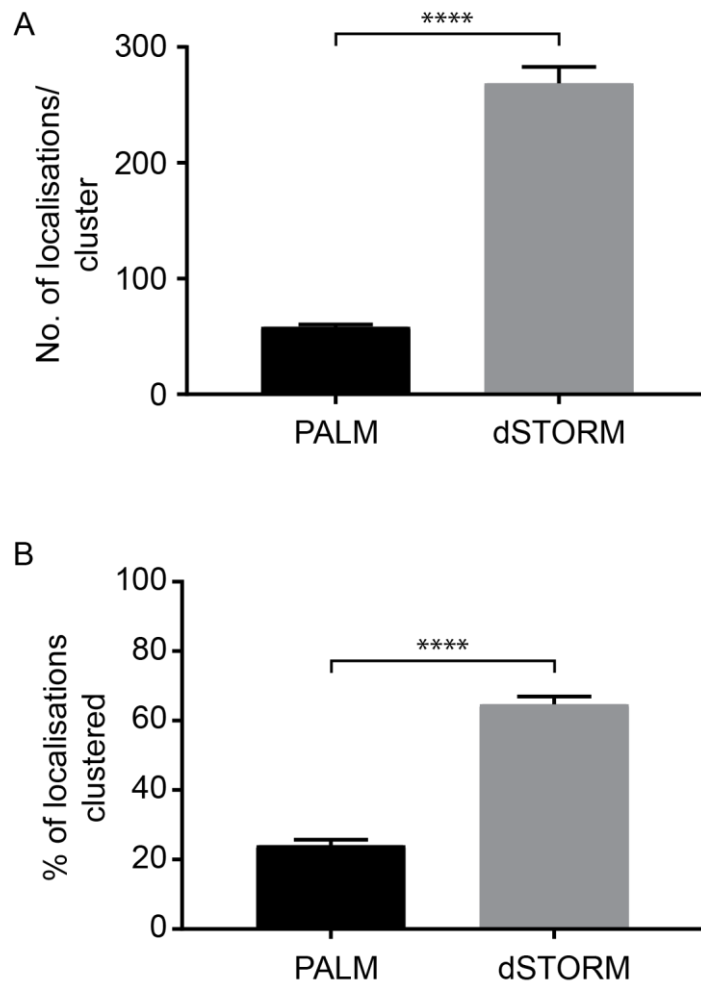


Figure 4.12: Comparison of cluster characteristics between PALM and dSTORM imaging.

A: The mean number of localisations in each cluster from PALM or dSTORM image reconstructions. B: The percentage of localisations assigned to a cluster by DBSCAN analysis. Error bars represent the SEM. **** $P < 0.0001$.

4.3.4 Comparison of NS5A protein clusters from different genotypes

NS5A from different genotypes were clustered into discrete regions of dense localisations comparable to genotype 2a (SGR-Neo-JFH1) (Figure 4.13 and Figure 4.14). Genotype 1b and 3a NS5A protein clusters were distributed throughout the cytoplasm (Figure 4.13D and Figure 4.14D).

Genotype 1b and genotype 3a NS5A localisations were organised into smaller protein clusters of 85.1 ± 1.3 nm and 76.9 ± 1.2 nm respectively (Figure 4.15). Genotype 3a protein clusters were the smallest on average and, along with genotype 1b, contained significantly fewer localisations than genotype 2a (Figure 4.15B). Although different to genotype 2a, there was no significant difference in the number of localisations per cluster, or the percentage of clustered localisations, between genotypes 1b and 3a (Figure 4.15B and C).

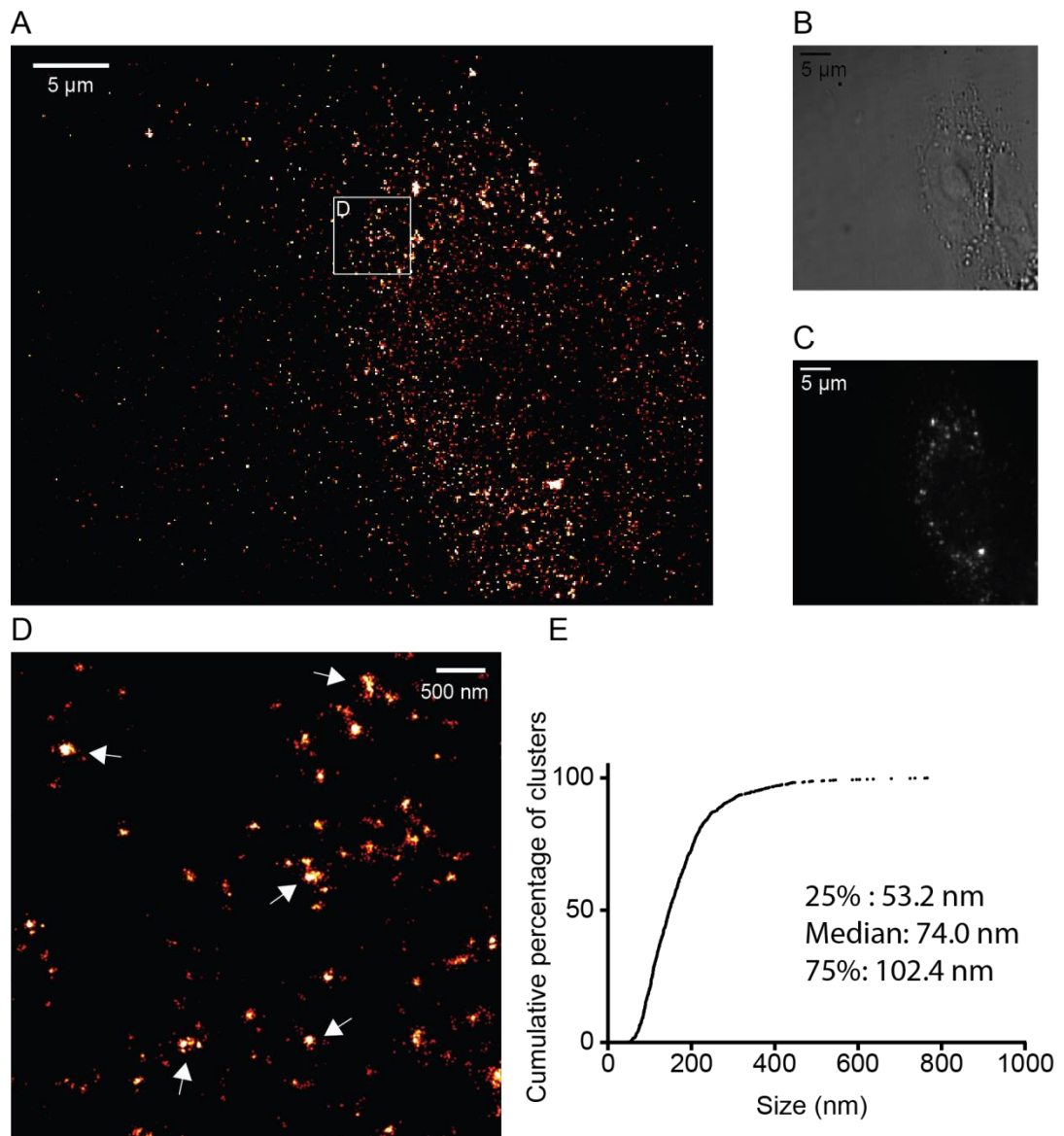


Figure 4.13: 3D-dSTORM image reconstruction of NS5A from genotype 1b.

Cells stably harbouring SGR-Neo-Con1 were fixed and subjected to immunofluorescence staining for NS5A before 3D-dSTORM imaging. A: Sum of z slices, 1.95 μm thick, from a representative 3D-dSTORM image reconstruction. 259,072 localisations were binned into 50 nm pixels in a 3D histogram. B: Bright-field image of cell in A. C: Wide-field image of cell in A. D: 5 μm² region of interest after kernel density estimation ($\sigma = 20$ nm in x-y, 30 nm in z) with 4 nm pixel bins. Sum of z slices, 850 nm thick. Arrows illustrate NS5A protein clusters. Scale bars are indicated. E: Cumulative percentage of cluster size from three independent cells. Median and percentile values are indicated.

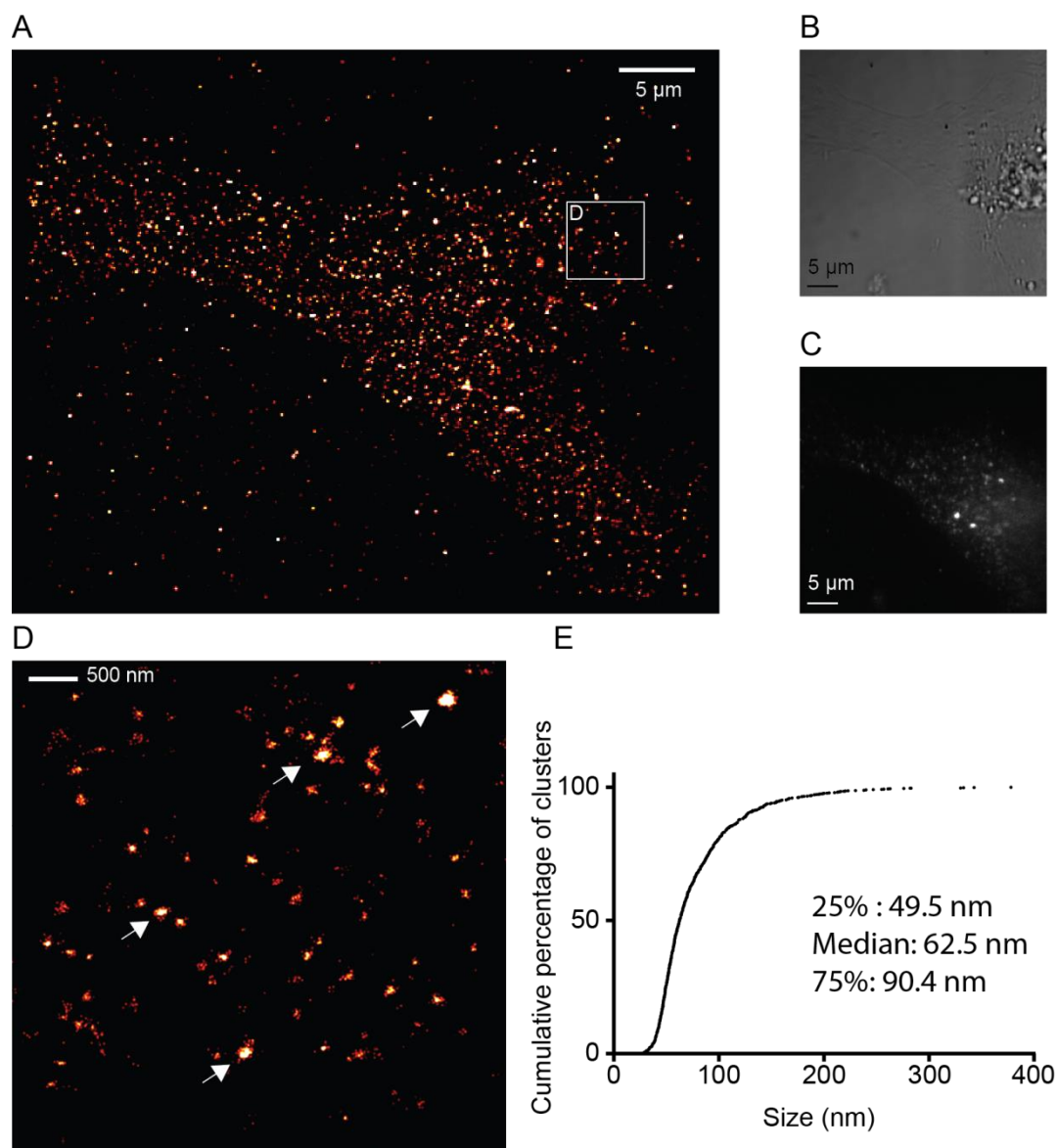


Figure 4.14: 3D-dSTORM image reconstruction of NS5A from genotype 3a.

Cells stably harbouring SGR-Neo-S52 were fixed and subjected to immunofluorescence staining for NS5A before 3D-dSTORM imaging. A: Sum of z slices, 1.7 μm thick, from a representative 3D-dSTORM image reconstruction. 426,071 localisations were binned into 50 nm pixels in a 3D histogram. B: Bright-field image of cell in A. C: Wide-field image of cell in A. D: 5 μm^2 region of interest after kernel density estimation ($\sigma = 20$ nm in x-y, 30 nm in z) with 4 nm pixel bins. Sum of z slices, 650 nm thick. Arrows illustrate NS5A protein clusters. Scale bars are indicated. E: Cumulative percentage of cluster size from three independent cells. Median and percentile values are indicated.

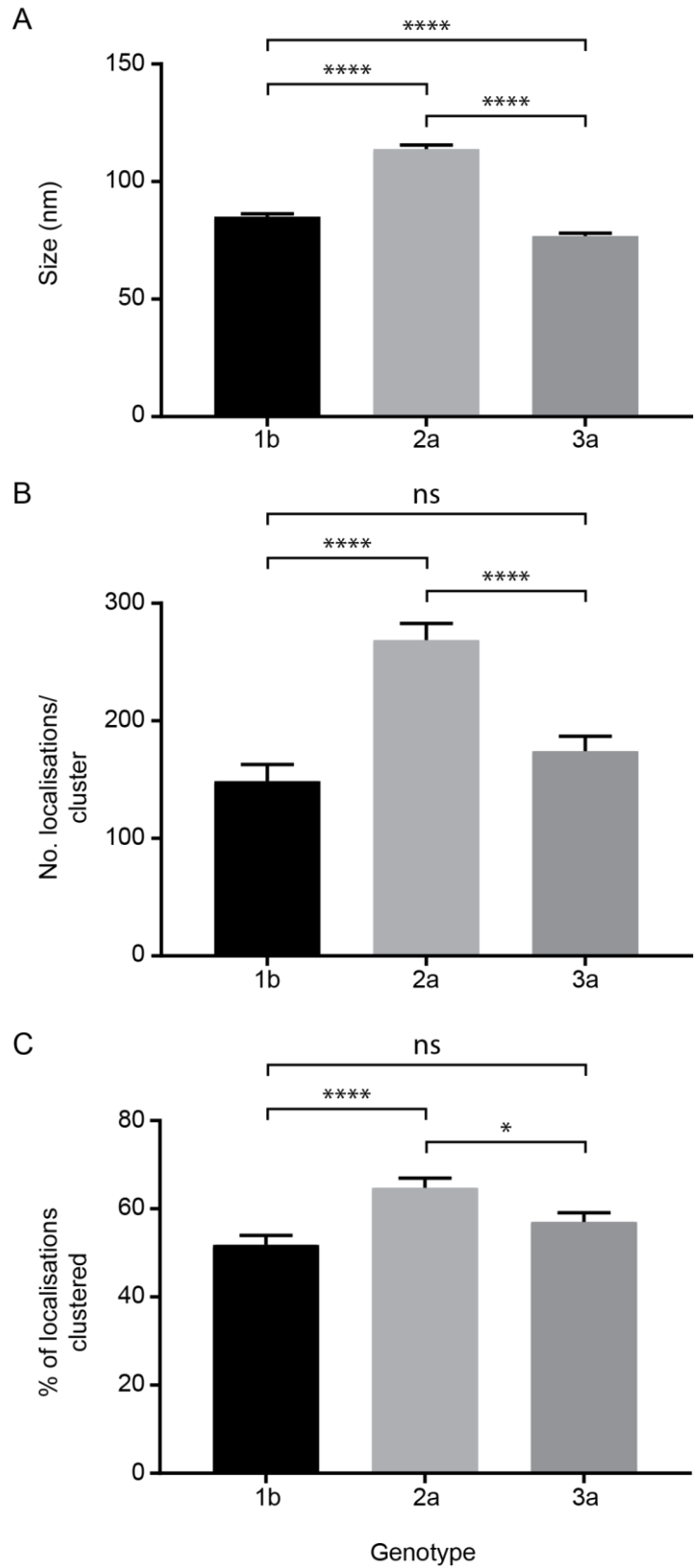


Figure 4.15: Comparison of NS5A protein clusters between genotypes.

A: The mean distance in x - y between localisations within clusters. B: Mean number of localisations within each NS5A protein cluster. C: The percentage of localisations contained within clusters. Error bars represent the SEM. * $P < 0.05$, **** $P < 0.0001$.

4.3.5 dSTORM of HCV infection

Clusters of NS5A localisations from HCV infected cells were resolved from diffraction limited NS5A foci in wide-field images (Figure 4.16). Consistent with SGR observations, NS5A protein clusters were distributed evenly throughout infected cells (Figure 4.16D).

In contrast to SGR samples, NS5A protein clusters at 24 h.p.i. were smaller with a size range between 63–110 nm. Although with a mean size around 20 nm smaller at 95.5 ± 1.5 nm, these protein clusters were still larger than those observed for genotype 1b and 3a SGRs by 10–20 nm. At 24 h.p.i., an early time after HCV infection, NS5A protein clusters contained around a third fewer localisations within each cluster than those from SGR harbouring cells. This also correlated with the lower percentage of localisations contained within clusters (Figure 4.17).

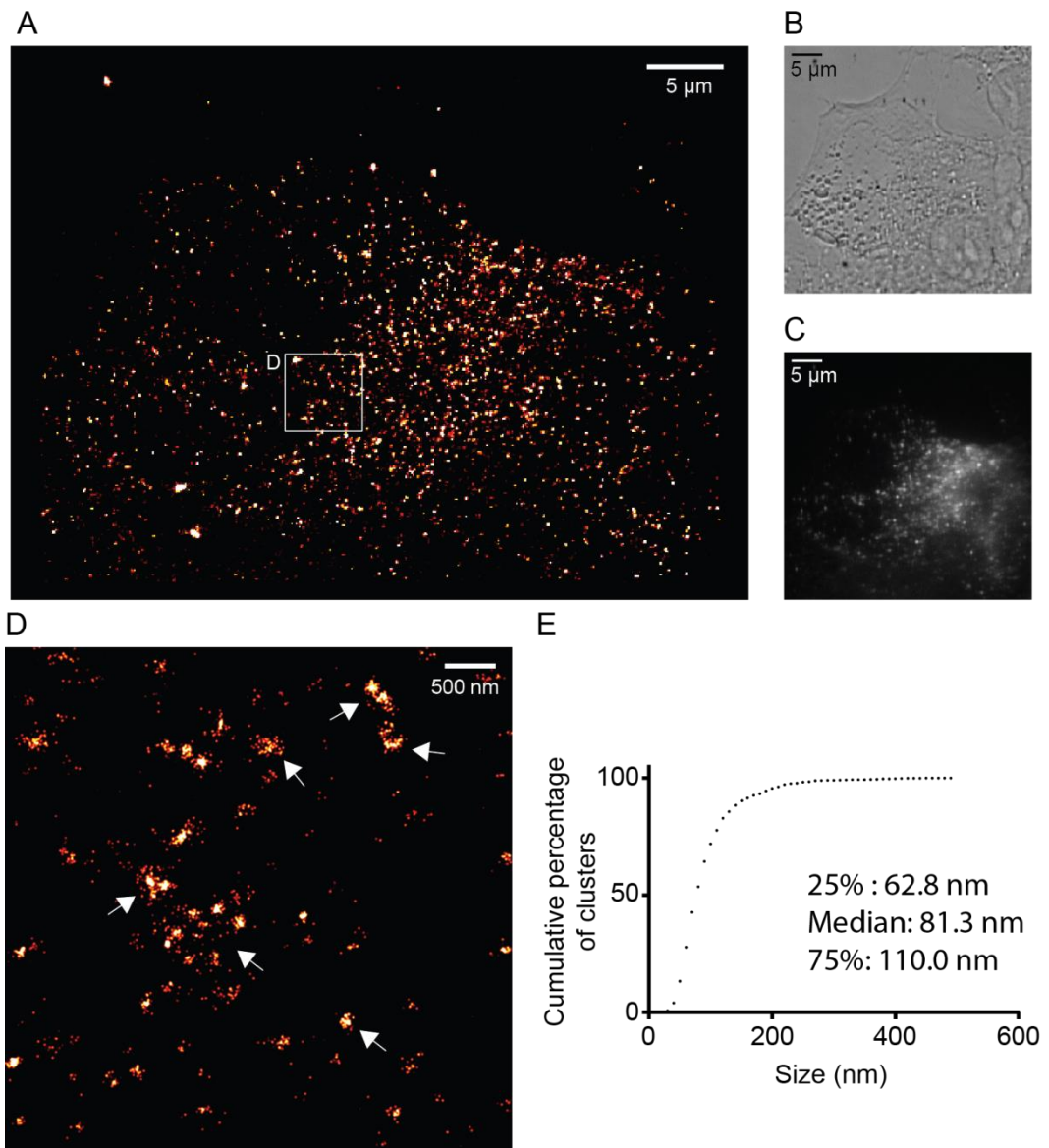


Figure 4.16: 3D-dSTORM imaging of NS5A in HuH7 cells infected with JFHcc.

HuH7 cell infected with JFHcc for 24 h before fixation and immunofluorescence labelling for NS5A. Samples were then imaged by 3D-dSTORM. A: Sum of z slices, 3.9 μm thick, from a representative 3D-dSTORM image reconstruction with 100 nm pixel bins in a 3D histogram from 199,451 localisations. B: Bright-field of cell in A. C: Wide-field of cell in A. D: 5 μm^2 region of interest after kernel density estimation ($\sigma = 20$ nm in x-y, 30 nm in z) with 4 nm pixel bins. Sum of z slices, 650 nm thick. Arrows illustrate NS5A protein clusters. Scale bars are indicated. E: Cumulative percentage of cluster size from three independent cells. Median and percentile values are indicated.

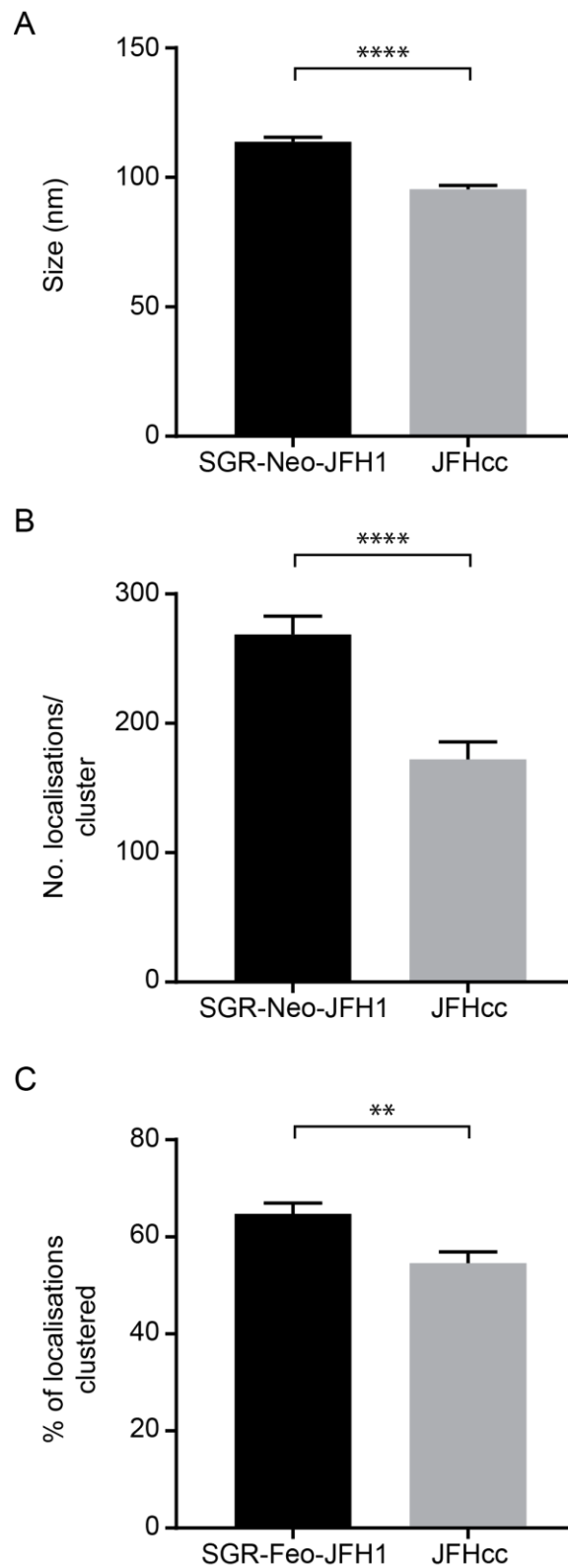


Figure 4.17: Comparison of NS5A protein clusters between SGR and virus replication.

A: The mean distance between localisations in x-y within clusters. B: Mean number of localisations within each NS5A protein cluster. C: The percentage of localisations contained within clusters. Error bars represent the SEM. ** $P < 0.01$, **** $P < 0.0001$.

4.3.6 Internal cluster organisation of NS5A

NS5A localisations within clusters are $\sim 95 \pm 2.5$ nm from the centroid position for virus infected cells (Figure 4.18). The centroid position is the geometric centre of an object, and corresponds to the mean position of all coordinates in all directions. The smaller clusters for virus infection produce a smaller distance from the centroid position than stable SGR harbouring cells. Distances were plotted as a frequency distribution with 5 nm bins (Figure 4.18). The peak of the skewed right distribution, the mode, corresponds to the most common distance of localisations from the centroid. This was calculated as 95 ± 2.5 nm and 125 ± 2.5 nm for virus and SGR NS5A protein clusters respectively. The lack of localisations within 100 nm of the centroid indicates a spherical cluster organisation with a hollow core. The following tail in the distribution corresponds to clusters of increasing size where the distance of localisations to the centroid increases. A closer inspection of individual clusters indicate that a number of elliptical clusters of differing sizes contain a hollow core (Figure 4.19). Additionally, some clusters were found to have a non-uniform shape (Figure 4.19, bottom panel arrows), and these were observed for both SGR-Neo-JFH1 harbouring and HCV infected cells. This subpopulation may be due to a specific membranous organisation during infections or due to undersampling of these clusters. From these observations, the internal diameter of NS5A protein clusters would be 190 nm and 250 nm for virus and SGR respectively.

4.3.7 NS5A clusters around lipid droplets

Fluorescence labelling of lipid droplets revealed an association with NS5A protein clusters (Figure 4.20). Observations with SGRs and HCV infected cells identified NS5A protein clusters surrounding regions in the reconstructed image absent of other NS5A localisations. Magnification of the corresponding bright-field region revealed light diffractive spherical structures that could be labelled with a lipid droplet dye (Figure 4.20A). Mapping of these putative lipid droplets onto the 3D-dSTORM image revealed a number of NS5A protein clusters in close association, or in neighbouring locations to lipid droplets (Figure 4.20B, circles and arrows, respectively). The association of NS5A with lipid droplets is well documented during the HCV lifecycle (Appel et al., 2008; Masaki et al., 2008; Zayas et al., 2016). Interestingly, the 3D-dSTORM imaging presented here revealed that discrete protein clusters are associated with lipid droplets whereas NS5A was previously thought to coat lipid droplets similar to core (Miyanari et al., 2007).

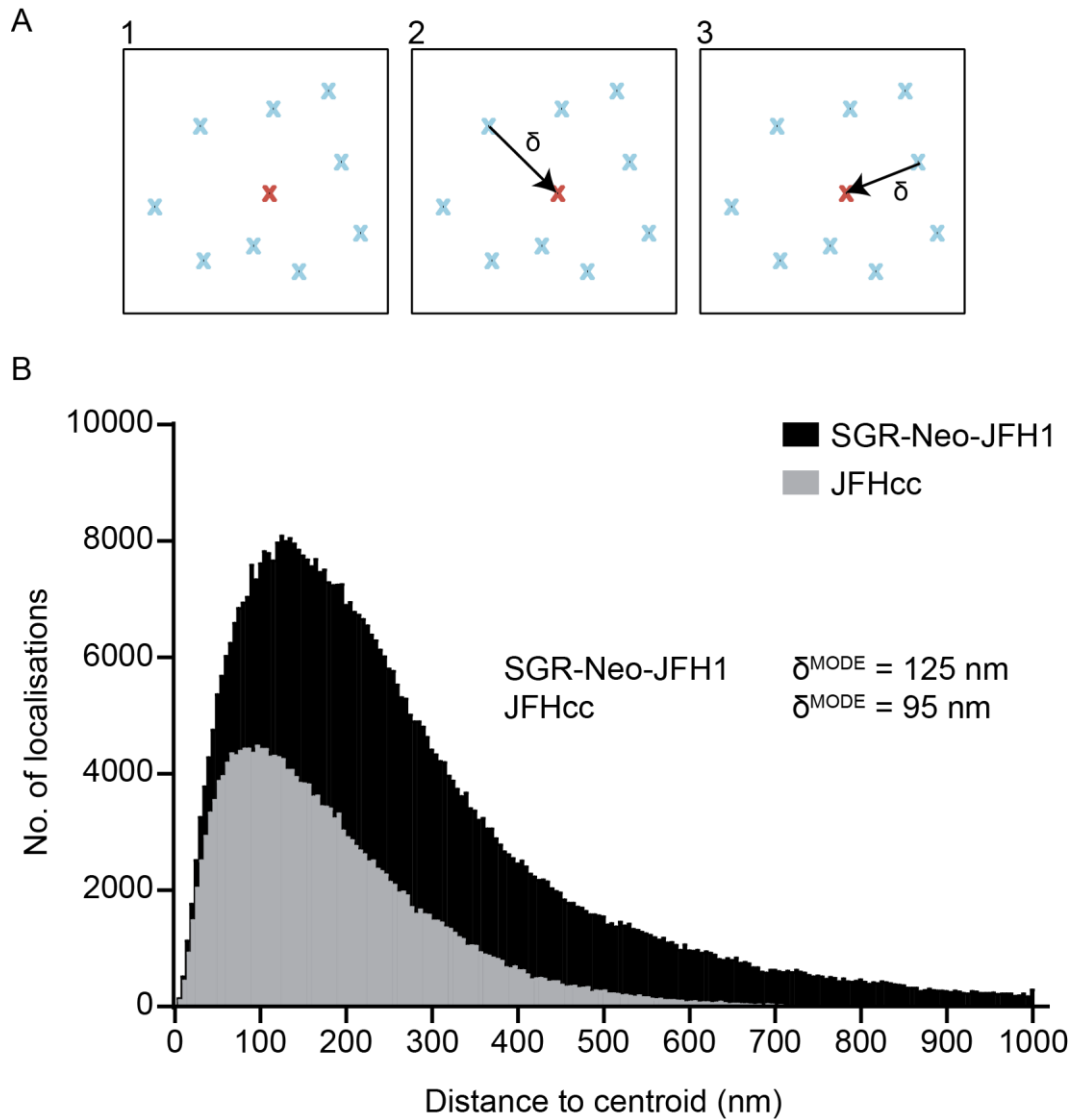


Figure 4.18: Distance of localisations in clusters from cluster centroid position.

A: Diagram illustrating Euclidean distance measurement of cluster localisation to centroid position. 1) Cluster centroid determined, red cross. 2) Euclidean distance (δ) between cluster localisation and centroid calculated, black arrow. 3) Euclidean measurement repeated for all localisations in every cluster. B: Euclidean distance histogram (5 nm bins) from localisation position to centroid. Data from 3 cells with 2,062 and 1,266 clusters containing 554,079 and 218,040 localisations for SGR-Neo-JFH1 and JFHcc respectively. The peak of the skewed right distribution (δ^{MODE}) for each sample is indicated.

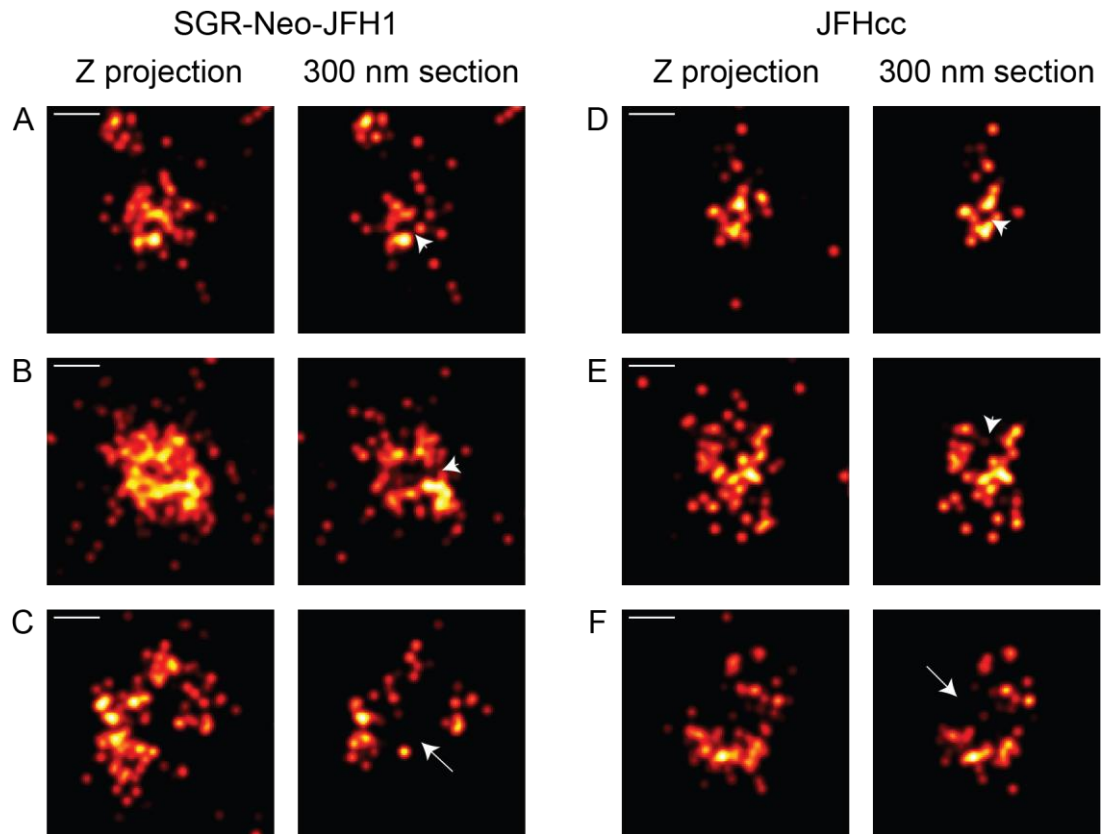


Figure 4.19: Architecture of individual protein clusters.

Individual clusters isolated from 3D-dSTORM reconstructed images. A-C from SGR-Neo-JFH1 harbouring HuH7 cells. D-F from JFHcc infected cells. Left panel; z projection through entire volume. Right panel; 300 nm thick cross-section. Arrow heads indicate hollow core structures of NS5A proteins clusters. Arrows highlight clusters with a non-elliptical shape. Kernel density estimation ($\sigma = 20$ nm for x-y, 30 nm for z) of localisation coordinates with a pixel size of 4 nm. Scale bar 100 nm.

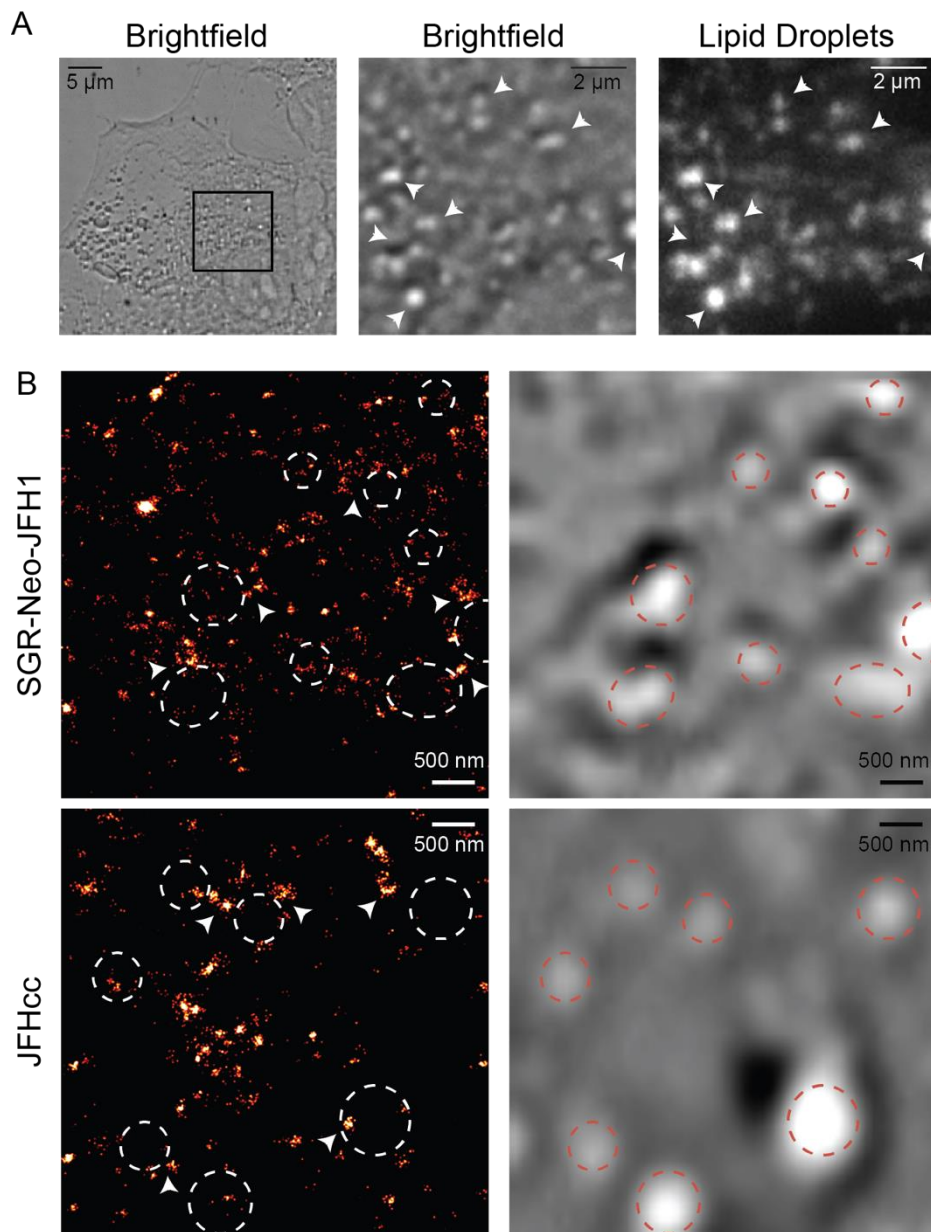


Figure 4.20: Association of NS5A protein clusters with lipid droplets.

A: Bright-field image of HuH7 cells infected with JFHcc for 24 h. Cells were labelled for lipid droplets. Box corresponds to panels on right of digitally enhanced bright-field and wide-field images. Arrows indicate positions of lipid droplets.

B: $5 \mu\text{m}^2$ regions of interest from SGR-Neo-JFH1 harbouring and JFHcc infected HuH7 cells, top and bottom panels respectively. Left panels, reconstructed 3D-dSTORM images after kernel density estimation ($\sigma = 20 \text{ nm}$ in x - y , 30 nm in z) with 4 nm pixel bins. Sum of z slices 800 nm and 650 nm thick for SGR-Neo-JFH1 and JFHcc, respectively. Right panels, correspond to digitally magnified bright-field region. Circles indicate putative lipid droplet locations. Arrows indicate NS5A protein clusters around the periphery, or closely associated, with putative lipid droplets. Scale bars are indicated.

4.3.8 NS3 clusters during HCV infection differ from NS5A

dSTORM imaging showed that NS3 protein clusters within cells infected with HCV are significantly smaller than NS5A protein clusters (Figure 4.21 and Figure 4.22). Both proteins are involved in the HCV replication complex and NS3 and NS5A puncta colocalise by wide-field microscopy with a Pearson correlation >0.85 (Ross-Thriepland and Harris, 2015). Similar to observations with NS5A, NS3 proteins clusters were resolved from diffraction limited puncta throughout the cytoplasm of infected cells. NS3 protein clusters were detected as dense regions of localisations within a comparable cellular distribution to NS5A (Figure 4.21D).

The mean size of NS3 protein clusters was 62.1 ± 1.0 nm with a size range from 45–72 nm. Interestingly, these sizes are closer to the observations of protein clusters from genotype 1b and 3a SGR studies than all previous genotype 2a NS5A sizes. Additionally, the quantity of NS3 localisations within clusters and the percentage of clusters observed were significantly lower than NS5A (Figure 4.22).

To understand the organisation of NS3 within protein clusters, the distance to the centroid position was calculated (Figure 4.23A). The distribution exhibited the same skewed right profile as NS5A but a minimum expected distance of ~ 55 nm was smaller than measured for NS5A. This smaller distance correlates with the measured size of NS3 clusters which are significantly smaller than NS5A (Figure 4.22). Closer inspection of individual NS3 clusters also revealed a hollow core phenotype, comparable to previous observations with NS5A but with a smaller overall hollow core size (Figure 4.23). This finding indicates the internal diameter between NS3 localisations within clusters is ~ 110 nm, which shares a hollow core phenotype like NS5A.

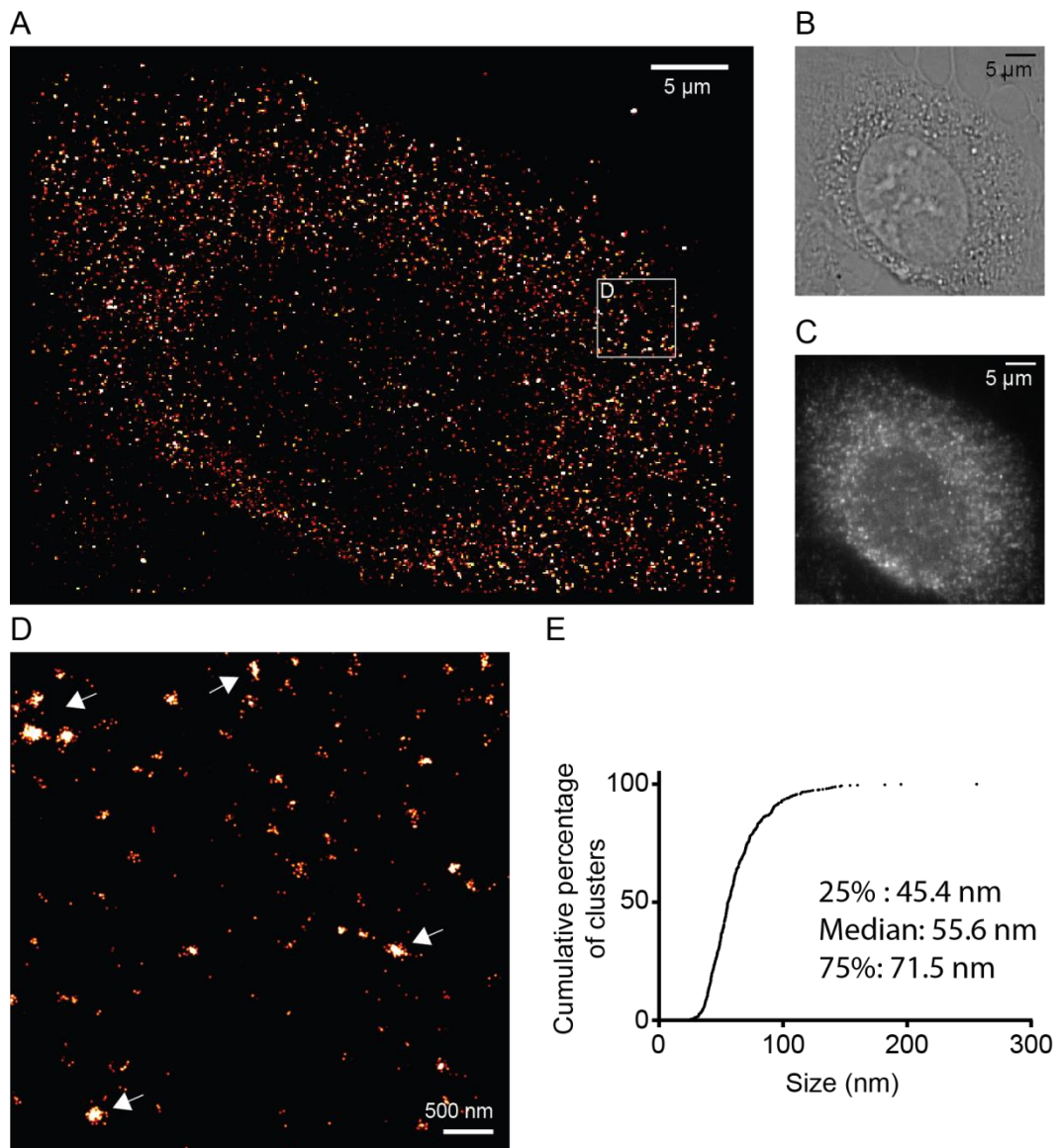


Figure 4.21: 3D-dSTORM imaging of NS3 in HuH7 cells infected with JFHcc.

HuH7 cell infected with JFHcc for 24 h before fixation and immunofluorescence labelling for NS3. Samples were then imaged by 3D-dSTORM. A: Sum of slices, 3.9 μm thick, from a representative 3D-dSTORM image reconstruction with 100 nm pixel bins in a 3D histogram from 289,015 localisations. B: Bright-field of cell in A. C: Wide-field of cell in A. D: 5 μm^2 region of interest after kernel density estimation ($\sigma = 20$ nm in x - y , 30 nm in z) with 4 nm pixel bins. Sum of z slices, 800 nm thick. Arrows illustrate NS3 protein clusters. Scale bars are indicated. E: Cumulative percentage of cluster size from two independent cells. Median and percentile values are indicated.

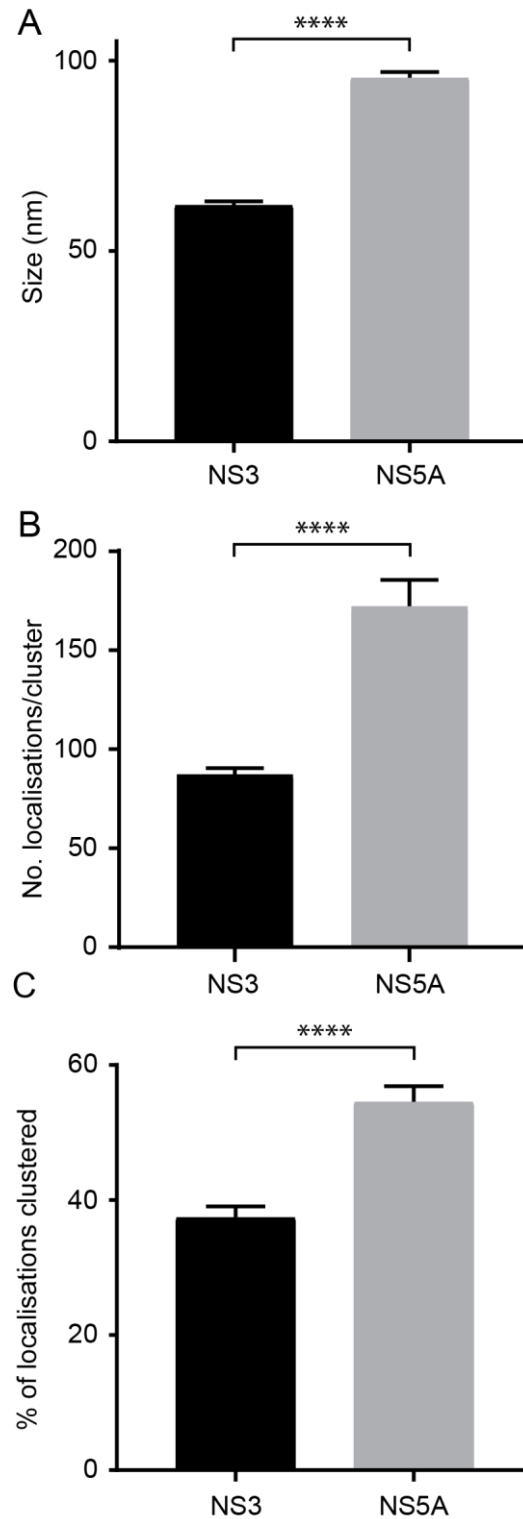


Figure 4.22: Comparison of NS3 and NS5A protein clusters 24 h.p.i. of HuH7 cells with JFHcc.

A: The mean distance between localisations in x-y within clusters. B: Mean number of localisations within each protein cluster. C: The percentage of localisations contained within clusters. Error bars represent the SEM. **** $P < 0.0001$.

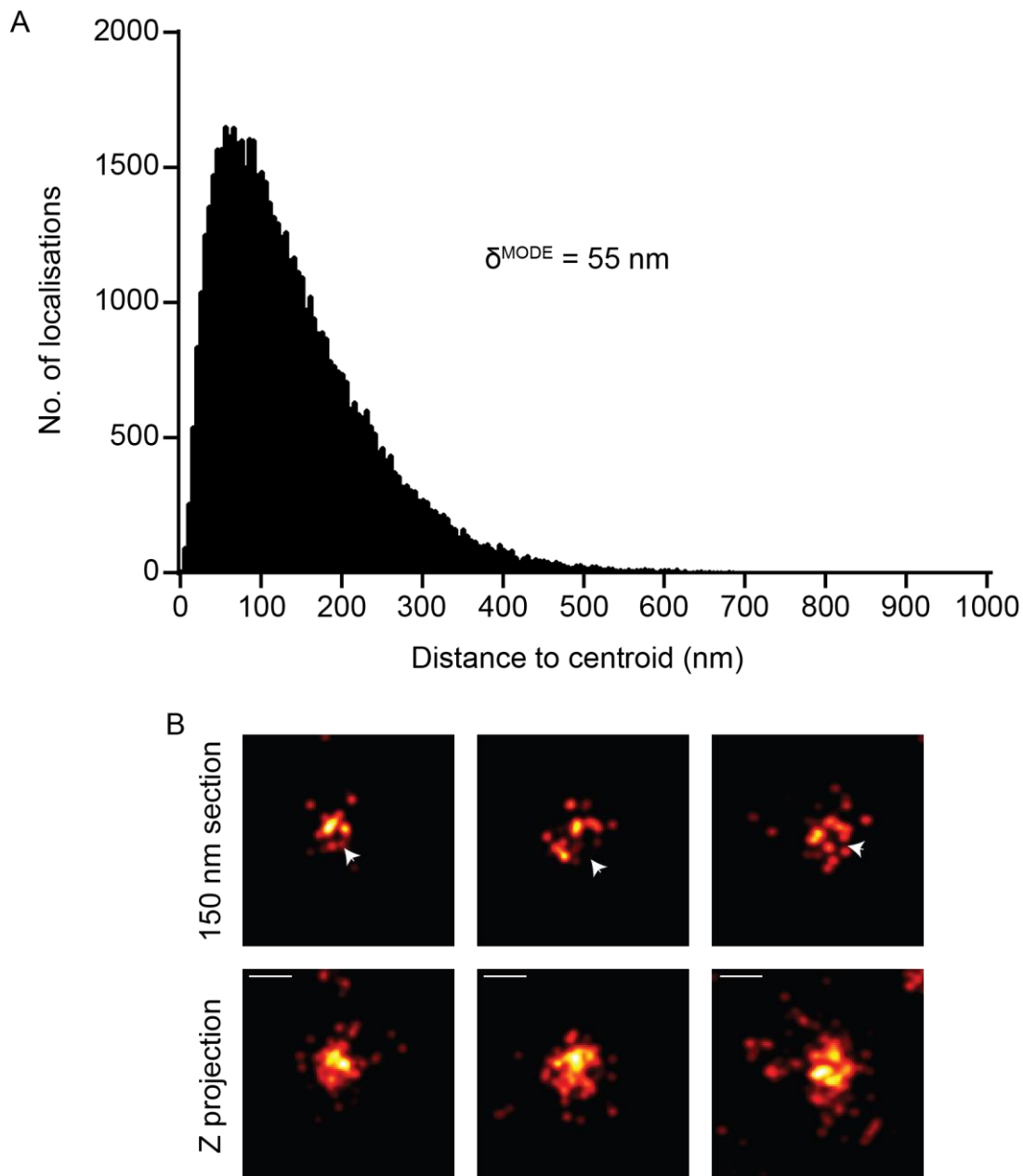


Figure 4.23: Distance of localisations in NS3 protein clusters from centroid position.

A: Euclidean distance histogram (5 nm bins) from localization position to cluster centroid. Data from 2 cells with 677 clusters containing 60,104 localisations. The peak of the skewed right distribution (δ^{MODE}) is indicated. B: Individual NS3 protein clusters isolated from 3D-dSTORM reconstructed images. Top panel, 150 nm cross section. Bottom panel, corresponding z projection. Arrow heads indicate hollow core structures of NS3 protein clusters. Scale bar 100 nm.

4.3.9 Effect of daclatasvir treatment

Inhibition of HCV infection with daclatasvir (DCV) results in the gradual accumulation of NS5A puncta in a perinuclear region (Figure 4.24). Daclatasvir is a potent inhibitor of NS5A function with an unknown mechanism of action. Prior to treatment with DCV, NS5A puncta are observed distributed through the cytoplasm as observed previously (Figure 4.9). After 6–8 h treatment with 1 nM daclatasvir, condensation and an overall loss of fluorescent signal was observed (Figure 4.24). This phenotype in virus infected cells corroborates previous findings in NS3–5B expressing cells (Chukkapalli and Randall, 2014) and replicon harbouring cells (Reghellin et al., 2014). Treatment of HCV infected cells with DCV for 8 h was sufficient to induce a distinct phenotype observed by conventional microscopy and was thus taken forward for 3D-dSTORM imaging.

Treatment of HCV infected cells with the NS5A inhibitor daclatasvir alters NS5A protein cluster morphology (Figure 4.25). Visual inspection of 3D-dSTORM images revealed little alteration in NS5A protein cluster morphology, but measurement of protein cluster size revealed a small but statistically significant reduction in cluster size (Figure 4.26A). In addition, , protein clusters contained a significant increase in the number of localisations contained within clusters indicating they contained a greater quantity of protein (Figure 4.26B). This finding correlated with a corresponding decrease in the single molecule localisation pool of NS5A with a higher percentage of localisations contained within clusters (Figure 4.26C).

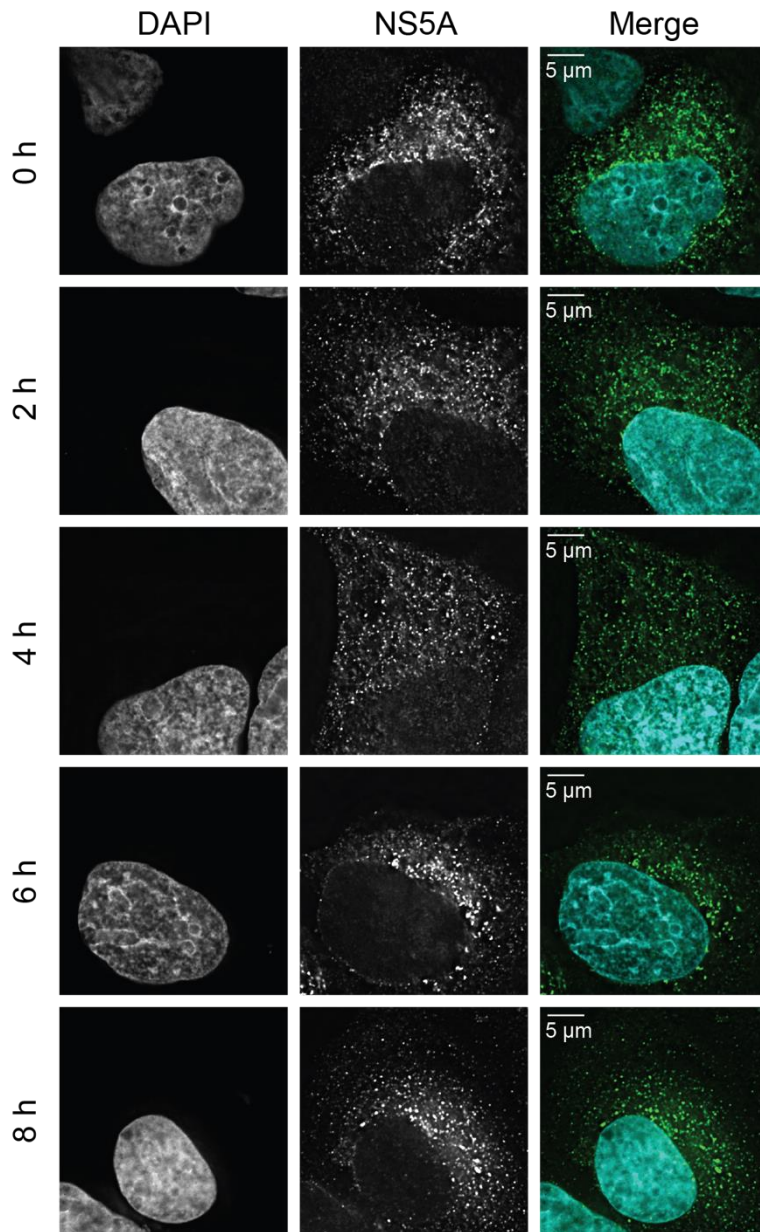


Figure 4.24: Alterations in NS5A distribution during daclatasvir treatment.

HuH7 cells were infected with JFHcc for 24 h before the addition of 1 nM DCV for the indicated time points. Cells were then fixed and processed for immunofluorescence staining with antibodies against NS5A. Scale bars are indicated.

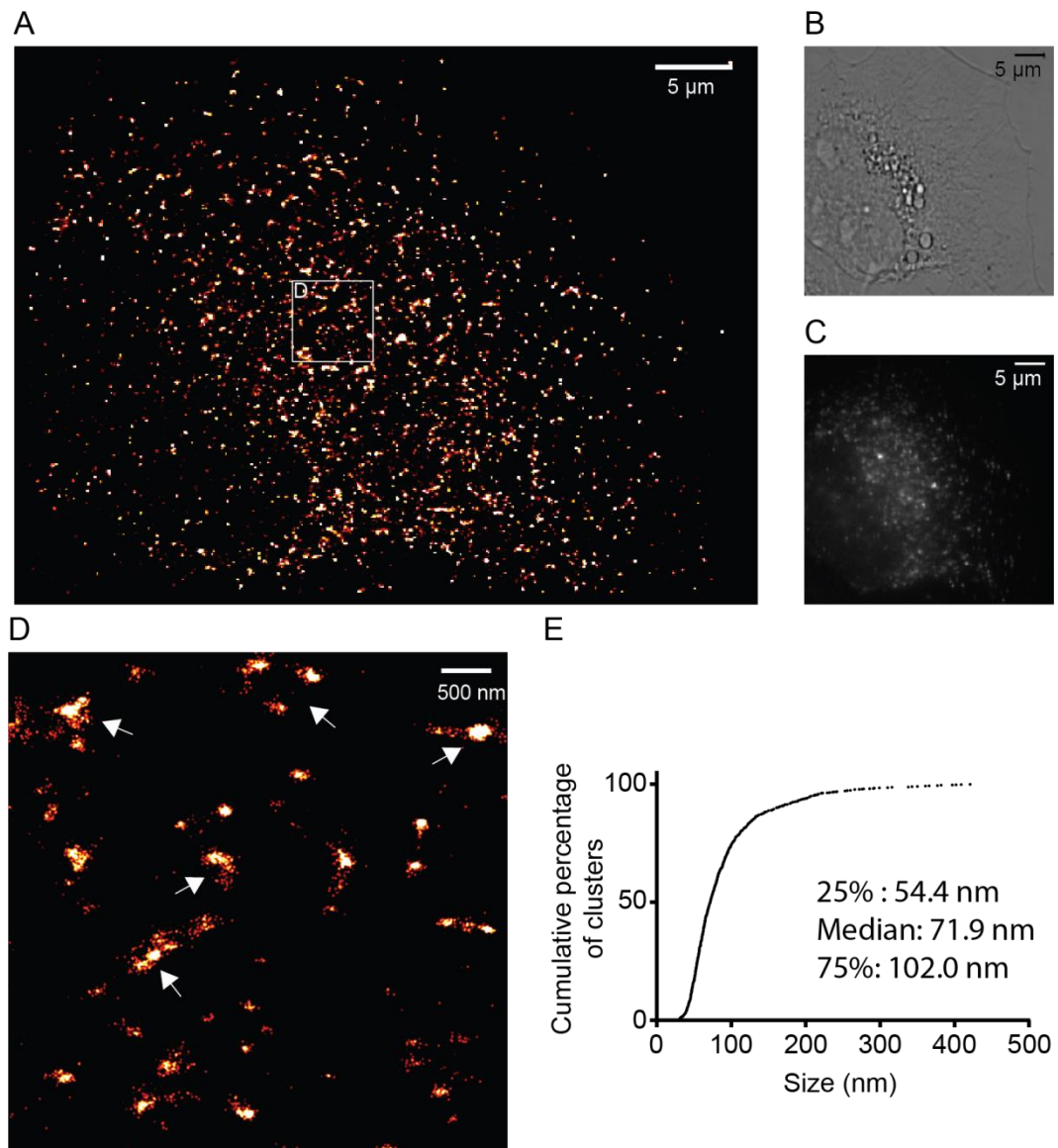


Figure 4.25: 3D-dSTORM imaging of NS5A in JFHcc infected cells treated with DCV.

HuH7 cells 24 h.p.i. with JFHcc were treated with 1 nM DCV for 8 hour before fixation and immunofluorescence labelling of NS5A. A: Sum of z slices, 3.9 μm thick, from a representative 3D-dSTORM image reconstruction from 587,570 localisations with 100 nm pixel bins in a 3D histogram. B: Bright-field image of cell in A. C: Wide-field image of cell in A. D: 5 μm^2 region of interest after kernel density estimation ($\sigma = 20$ nm in x-y, 30 nm in z) with 4 nm pixel bins. Sum of z slices, 800 nm thick. Arrows illustrate NS5A protein clusters. Scale bars are indicated. E: Cumulative percentage of cluster size from two independent cells. Median and percentile values are indicated.

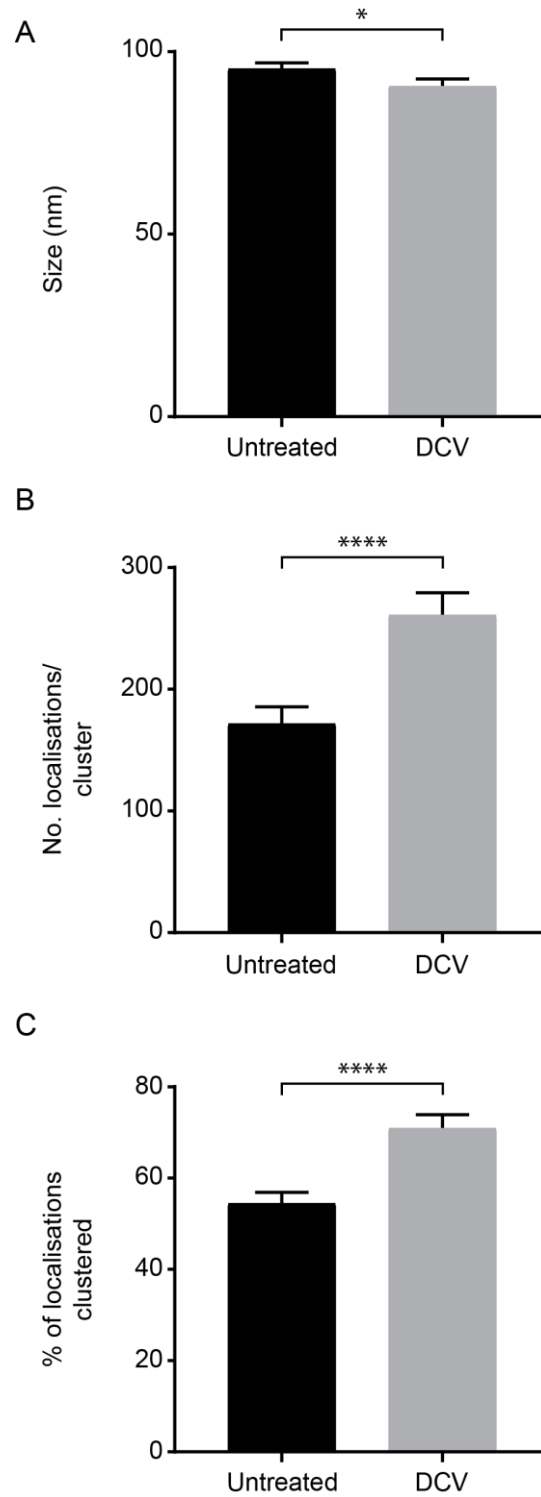


Figure 4.26: Comparison of NS5A protein clusters after treatment with DCV.

A: The mean distance in *x-y* between localisations within clusters. B: Mean number of localisations within each protein cluster. C: The percentage of localisations contained within clusters. Error bars represent the SEM. * $P < 0.05$, **** $P < 0.0001$.

4.3.10 NS5A phosphorylation mutants

Interference with NS5A phosphorylation alters the phenotype of NS5A protein clusters (Figure 4.27-3.30). NS5A is a multifunctional phosphoprotein that is regulated by phosphorylation with two species observed by SDS-PAGE, termed basal and hyperphosphorylated. The precise details of NS5A regulation by phosphorylation remain elusive and this section focused on characterising serine mutants previously described (Section 1.3.7.4) (Ross-Thriepland and Harris, 2014).

Analysis of NS5A puncta from wide-field images reveals that S146A, S146D and S225D all retain the diffuse distribution of NS5A protein clusters throughout the cytoplasm. S225A on the other hand exhibits a markedly different phenotype that is restricted to a perinuclear region. This phenotype was previously reported for NS5A and is additionally characterised by an impairment in replication (Ross-Thriepland and Harris, 2014).

The protein cluster size increased for both S146A and S146D mutations from 113.8 ± 1.7 nm for SGR-Neo-JFH1 to 137.1 ± 2.1 nm and 135.3 ± 1.7 nm for SGR-Neo-JFH1 [S146A] and SGR-Neo-JFH1 [S146D] respectively (Figure 4.31). The S146A mutant exhibits the biggest differences with ~30% more localisations in a cluster than wildtype, compared to ~15% more for S146D. Both mutants contain a greater number of clustered localisations than wildtype, although S146D has a larger single molecule population (Figure 4.31C).

Larger irregular-shaped fluorescence structures observed for S225A in a peri-nuclear region by wide-field appear to be formed from collections of small clusters grouping together when imaged by 3D-dSTORM (Figure 4.29A and D arrowheads). The S225D protein cluster size is smaller (104.8 ± 1.7 nm) than wildtype whereas the S225A is larger (132.0 ± 2.9 nm). However, both populations have more localisations within clusters and a greater percentage of clusters compared to wildtype (Figure 4.31).

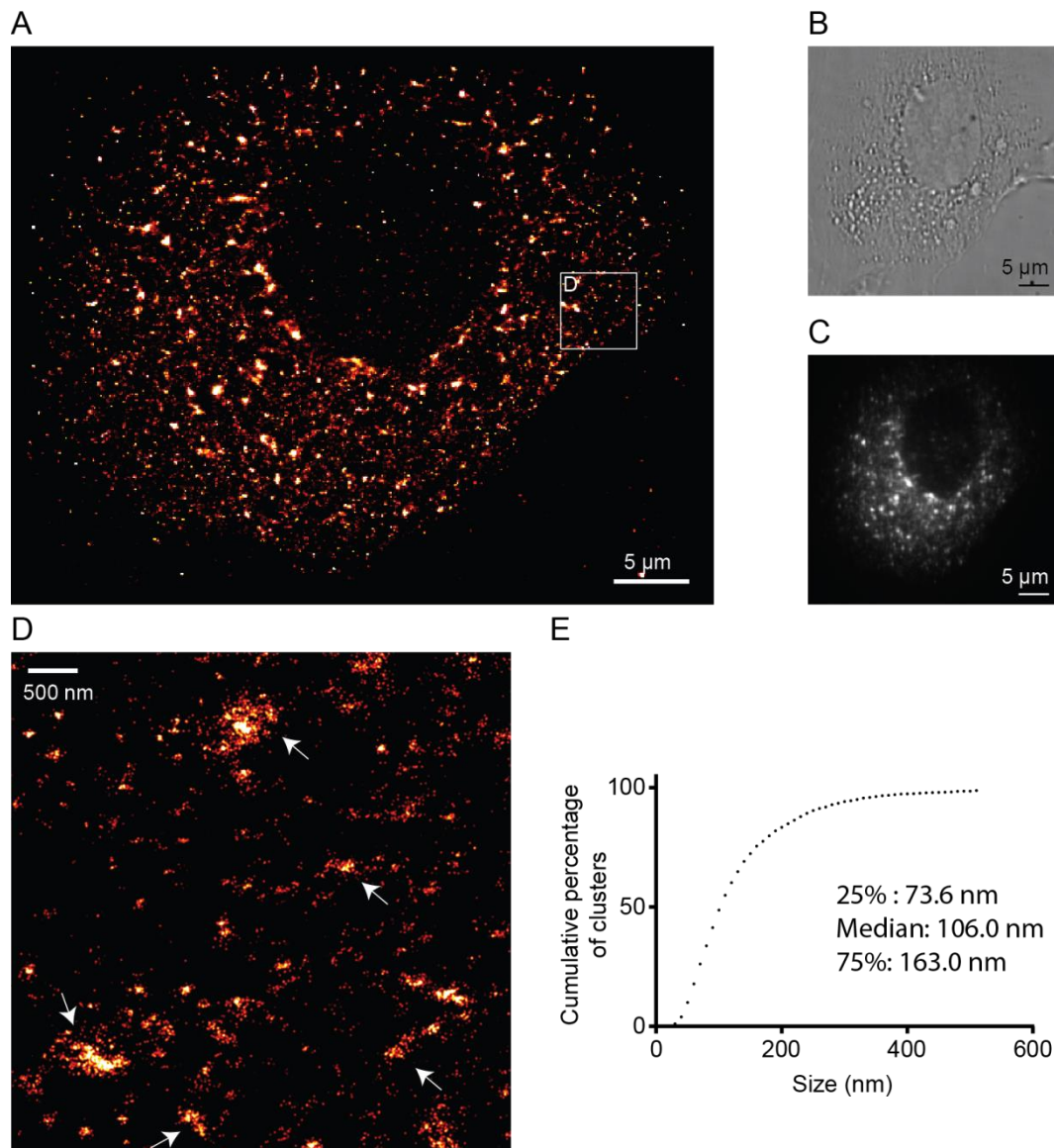


Figure 4.27: 3D-dSTORM imaging of SGR-Neo-JFH1 with S146A phosphorylation mutation.

Cells stably harbouring SGR-Neo-JFH1 [S146A] were fixed and processed for immunofluorescence. Cells were stained with NS5A antibody for 3D-dSTORM imaging. A: Sum of z slices, 3.9 μm thick, from a representative 3D-dSTORM image reconstruction with 100 nm pixel bins from 689,802 localisations in a 3D histogram. B: Bright-field image of cell in A. C: Wide-field image of cell in A. D: 5 μm^2 region of interest after kernel density estimation ($\sigma = 20$ nm in x - y , 30 nm in z) with 4 nm pixel bins. Sum of z slices, 800 nm thick. Arrows illustrate NS5A protein clusters. Scale bars are indicated. E: Cumulative percentage of cluster size from three independent cells. Median and percentile values are indicated.

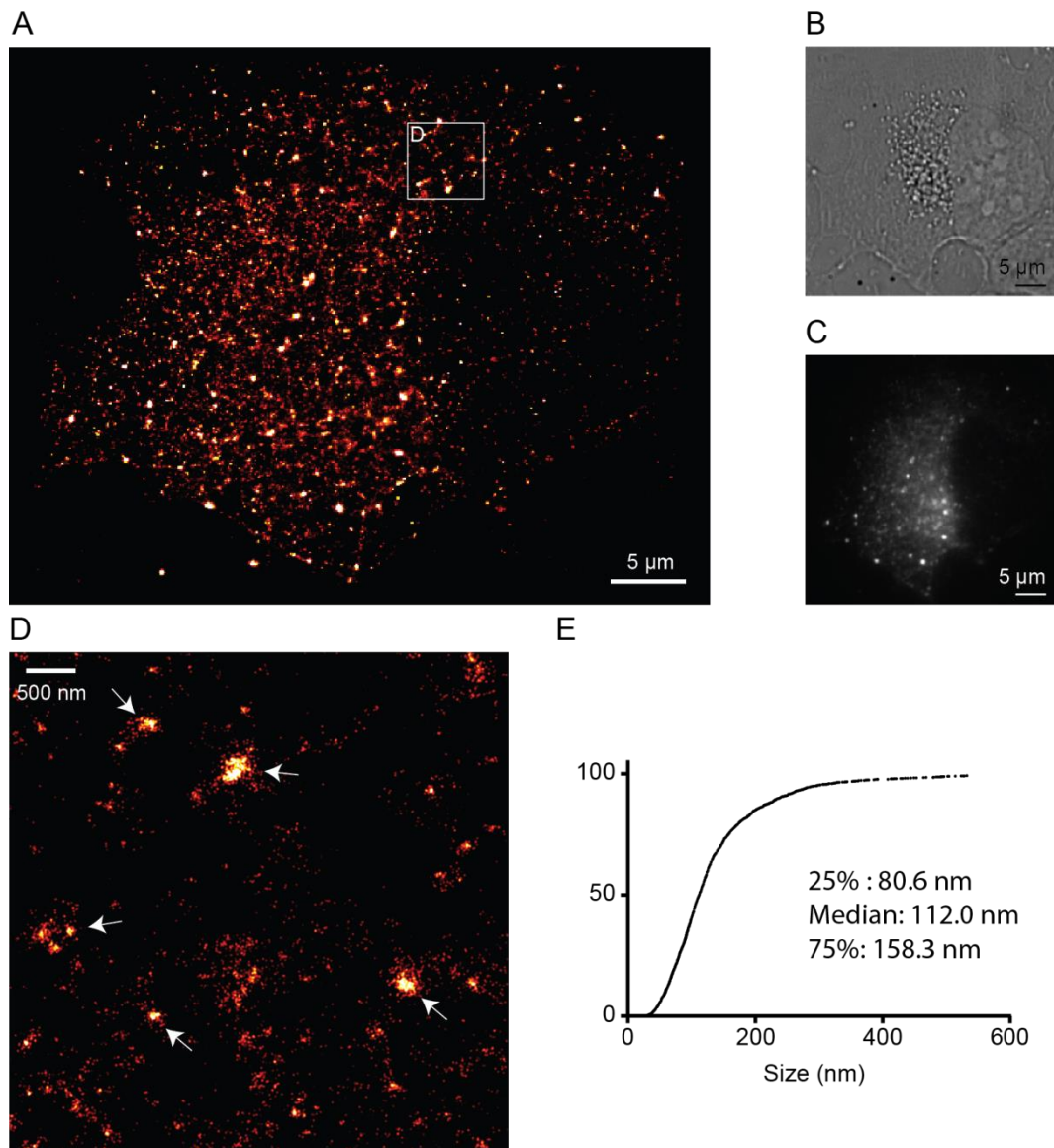


Figure 4.28: 3D-dSTORM imaging of SGR-Neo-JFH1 with S146D phosphorylation mutation.

Cells stably harbouring SGR-Neo-JFH1 [S146D] were fixed and processed for immunofluorescence. Cells were stained with NS5A antibody for 3D-dSTORM imaging. A: Sum of z slices, 3.9 μm thick, from a representative 3D-dSTORM image reconstruction with 100 nm pixel bins from 570,379 localisations in a 3D histogram. B: Bright-field image of cell in A. C: Wide-field image of cell in A. D: 5 μm^2 region of interest after kernel density estimation ($\sigma = 20$ nm in x - y , 30 nm in z) with 4 nm pixel bins. Sum of z slices, 650 nm thick. Arrows illustrate NS5A protein clusters. Scale bars are indicated. E: Cumulative percentage of cluster size from three independent cells. Median and percentile values are indicated.

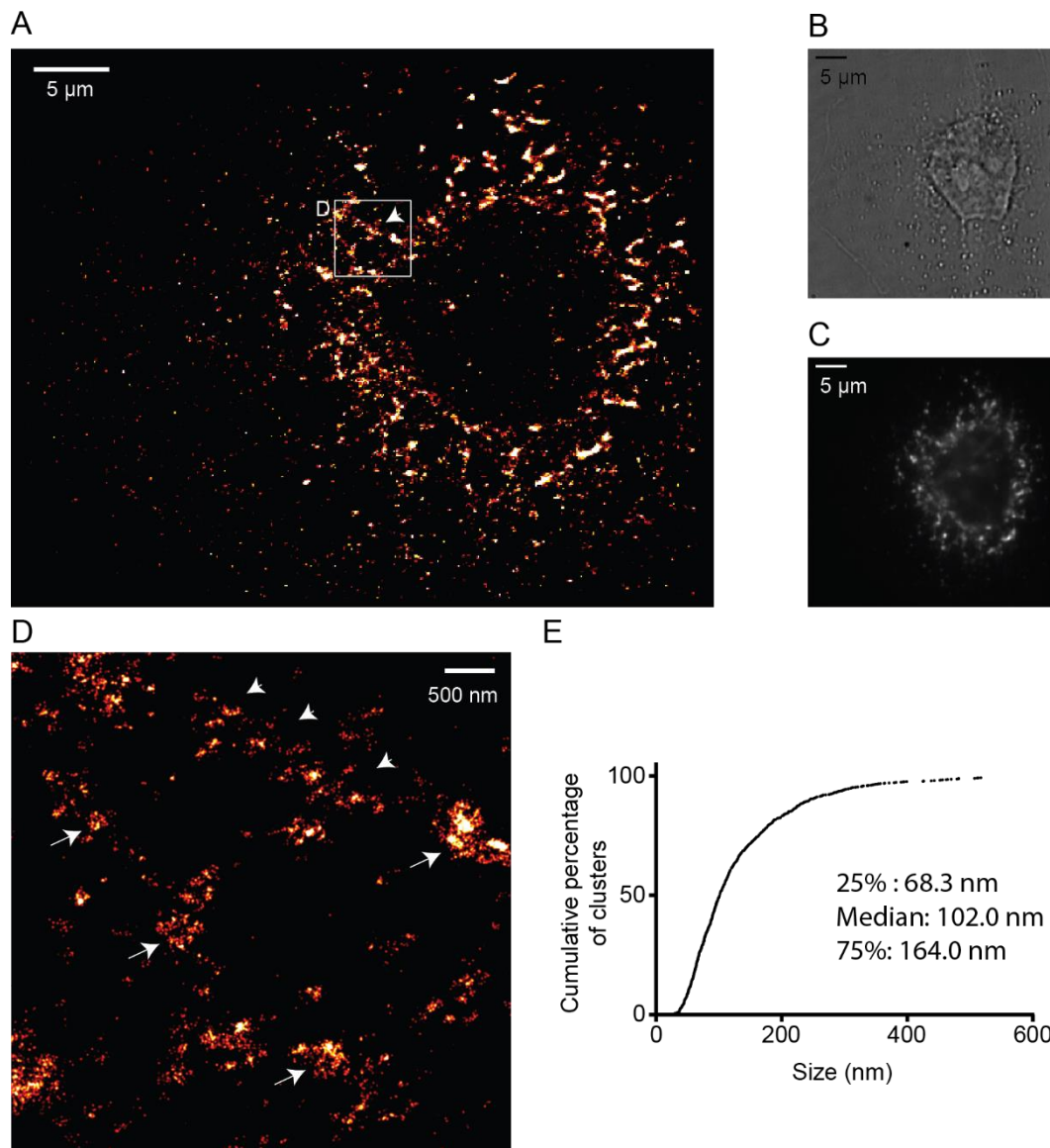


Figure 4.29: 3D-dSTORM imaging of SGR-Neo-JFH1 with S225A phosphorylation mutation.

Cells stably harbouring SGR-Neo-JFH1 [S225A] were fixed and processed for immunofluorescence. Cells were stained with NS5A antibody for 3D-dSTORM imaging. A: Sum of z slices, 3.9 μm thick, from a representative 3D-dSTORM image reconstruction with 100 nm pixel bins from 641,609 localisations in a 3D histogram. B: Bright-field of cell in A. C: Wide-field of cell in A. D: 5 μm^2 region of interest after kernel density estimation ($\sigma = 20$ nm in x-y, 30 nm in z) with 4 nm pixel bins. Sum of z slices, 800 nm thick. Arrows illustrate NS5A protein clusters. Scale bars are indicated. E: Cumulative percentage of cluster size from two independent cells. Median and percentile values are indicated.

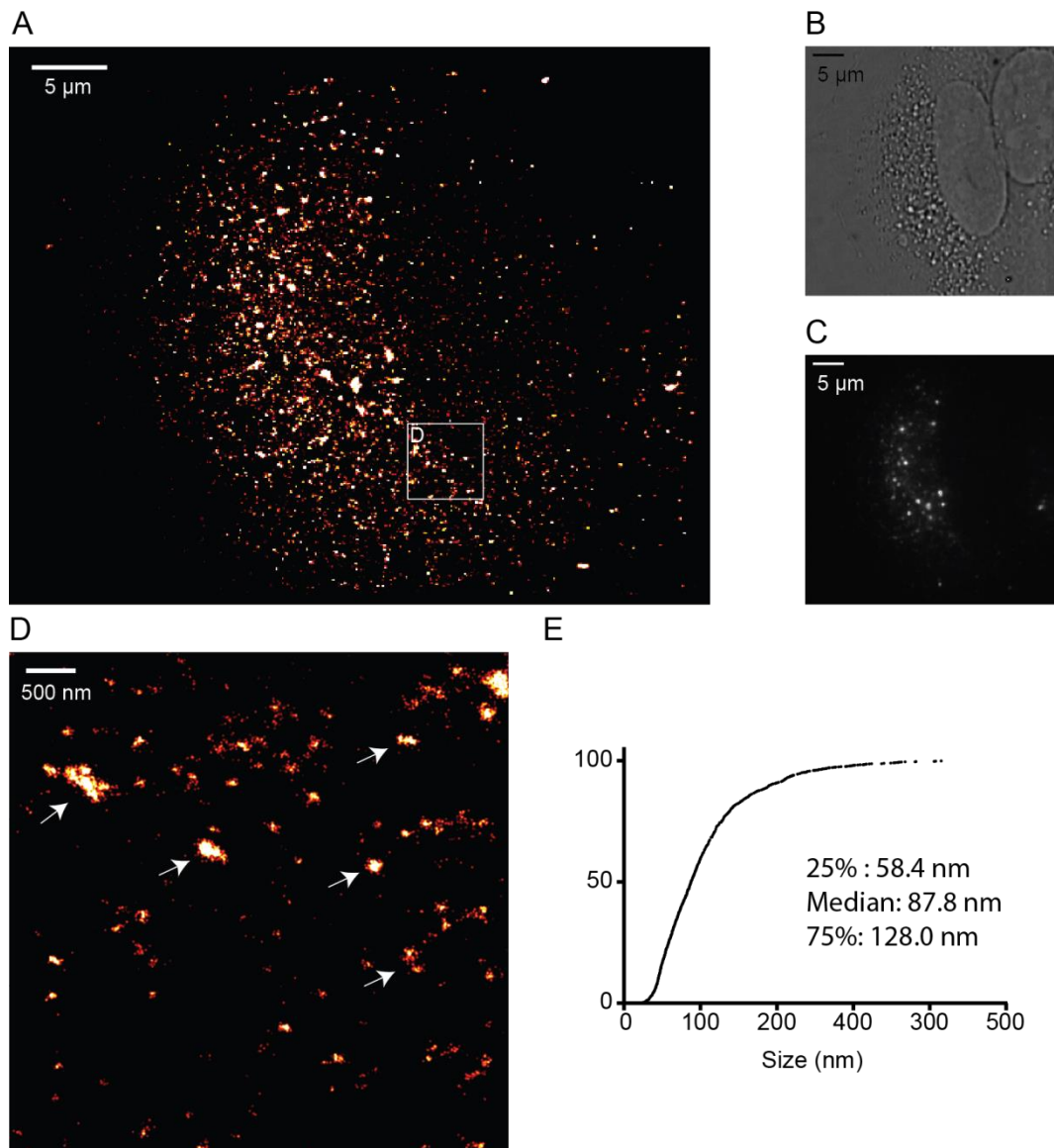


Figure 4.30: 3D-dSTORM imaging of SGR-Neo-JFH1 with S225D phosphorylation mutation.

Cells stably harbouring SGR-Neo-JFH1 [S225D] were fixed and processed for immunofluorescence. Cells were stained with NS5A antibody for 3D-dSTORM imaging. A: Sum of z slices, 3.9 μm thick, from a representative 3D-dSTORM image reconstruction with 100 nm pixel bins from 354,952 localisations in a 3D histogram. B: Bright-field of cell in A. C: Wide-field of cell in A. D: 5 μm^2 region of interest after kernel density estimation ($\sigma = 20$ nm in x-y, 30 nm in z) with 4 nm pixel bins. Sum of z slices, 800 nm thick. Arrows illustrate NS5A protein clusters. Scale bars are indicated. E: Cumulative percentage of cluster size from three independent cells. Median and percentile values are indicated.

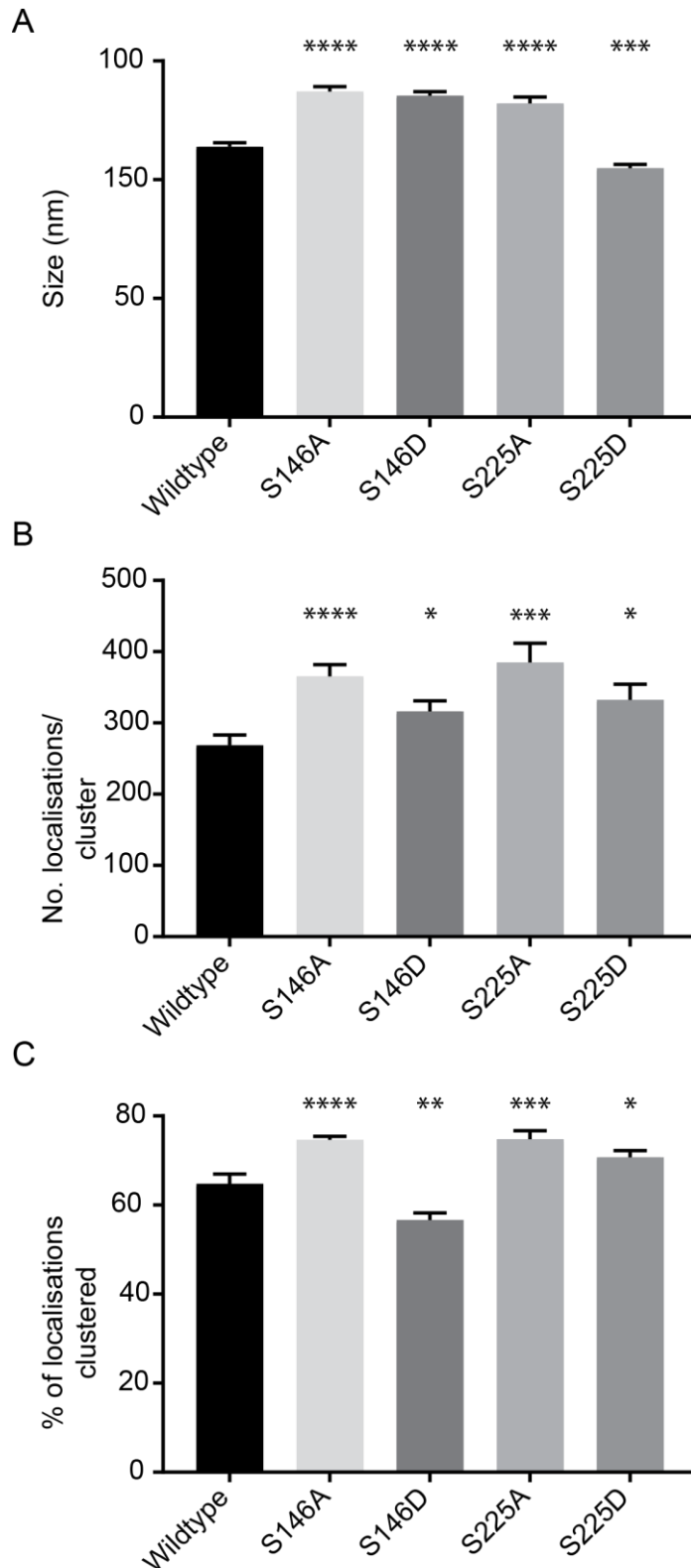


Figure 4.31: Comparison of NS5A phosphorylation mutation.

A: The mean distance in *x-y* between localisations within clusters. B: Mean number of localisations within each protein cluster. C: The percentage of localisations contained within clusters. Error bars represent the SEM. * $P < 0.05$, ** $P < 0.01$, *** $P < 0.001$, **** $P < 0.0001$, all compared to wildtype.

4.4 Discussion

Within this chapter, I set out to characterise the hepatitis C virus replication complex organisation and architecture, using the localisation microscopy techniques of 3D-PALM and 3D-dSTORM. A comparison between PALM and dSTORM demonstrated a reduced single molecule population and the observation of more protein cluster structures in dSTORM imaging (Figure 4.12). A key finding from this study was the clear difference in the organisation of NS5A and NS3 within clusters (Figure 4.18 and Figure 4.23), as well as the arrangement of protein clusters around lipid droplets (Figure 4.20). Additionally differences were seen between HCV genotypes; 2a was able to form larger and denser protein clusters than either 1b or 3a (Figure 4.15). Finally, interference of NS5A protein function by pharmacological inhibition (Figure 4.24), or manipulation of protein phosphorylation, both produced distinct phenotypes compared to wildtype (Figure 4.31).

4.4.1 DBSCAN analysis of clusters

Single molecule localisation microscopy offers the ability to study biological molecules and processes in the native environment from fluorescence imaging at the nanometer scale. In contrast to conventional microscopy, the resultant data is a multidimensional array of coordinates that can be plotted to render images with much higher resolution (Baddeley et al., 2010). However, image rendering has the potential to lose or obscure important information about the sample or produce spurious structures (Baddeley et al., 2010). Instead, exploring the mathematical relationship of localisation positions provides information at the single-molecule level and avoids the need for image rendering (Nicovich et al., 2017).

To identify clusters of localisations for further characterisation, the DBSCAN algorithm was used (Ester et al., 1996) (Figure 3.32D). DBSCAN identifies clusters by detecting density differences between clustered points and the background, making it particularly well-suited to SMLM (H. Deschout et al., 2014; Nicovich et al., 2017). In this study, the algorithm was able to efficiently identify clusters of varying density and size, which allowed its application across different sample conditions. DBSCAN analysis of SMLM images have been documented by a number of groups and prove a robust method of cluster identification in SMLM (Bar-On et al., 2012; Endesfelder et al., 2013; Itano et al., 2014; Nan et al., 2013; Pertsinidis et al., 2013). However, a drawback to DBSCAN is the requirement of user selected variables for the size of the search query (ϵ) and the number of points (min points).

A number of other clustering algorithms are available which have been applied to the study of SMLM and all define clusters differently. K-means clustering partitions data into a user defined number of clusters by classifying each point into the cluster with the nearest centroid (Lloyd, 1982). However, the number of potential clusters are often unknown in advance with SMLM and there is no theoretical way to find the optimum number (Lloyd, 1982). Additionally, K-means is a partitioning algorithm, therefore noise is incorporated into clusters. The mean shift is another centroid-based algorithm which locates the maxima of a density function (Fukunaga and Hostetler, 1975). A kernel function, typically Gaussian, is used to determine the weight of nearby points for re-estimation of the mean in an iterative process until convergence. This process can detect arbitrary shaped clusters like DBSCAN, however as an iterative process it is typically much slower and relies on a high data density that exhibits a well-defined gradient to the cluster center (Fukunaga and Hostetler, 1975).

Ripley's K and pair correlation functions (PCF) (Figure 3.32A–B) have been explored for SMLM clustering and provide information on the length-scale of clusters (Owen et al., 2010; Ripley, 1977; Sengupta et al., 2011; Sengupta and Lippincott-Schwartz, 2012). These measure the average number of extra localisations within a given radius of each point, providing a measure of the overall clustering and average cluster size in a sample or region of interest.

However, analysing the ensemble average undermines the benefits of SMLM when information about individual clusters provides information about the distribution of the underlying biology. Segmentation of individual clusters by Ripley's H function followed by interpolation to a regular grid and thresholding allows conventional image-analysis methods to be performed on SMLM data (Getis and Franklin, 1987; Owen et al., 2010). Adaptation using Bayesian inference produces optimal radius selection and threshold values after evaluating cluster segmentation against a model (Griffié et al., 2016; Rubin-Delanchy et al., 2015). However, this approach does require a high density of points across the image and suffers from the drawbacks of image rendering (Baddeley et al., 2010).

Another approach for image visualization, and more recently cluster segmentation, uses Voronoi and Delaunay diagrams (Figure 3.32E) (Andronov et al., 2016; Baddeley et al., 2010; Levet et al., 2015). These are formed of polygons with edges that are equidistant between neighbouring points. The area of polygons is inversely proportional to the local density and can be thresholded to identify clusters (Andronov et al., 2016; Levet et al., 2015).

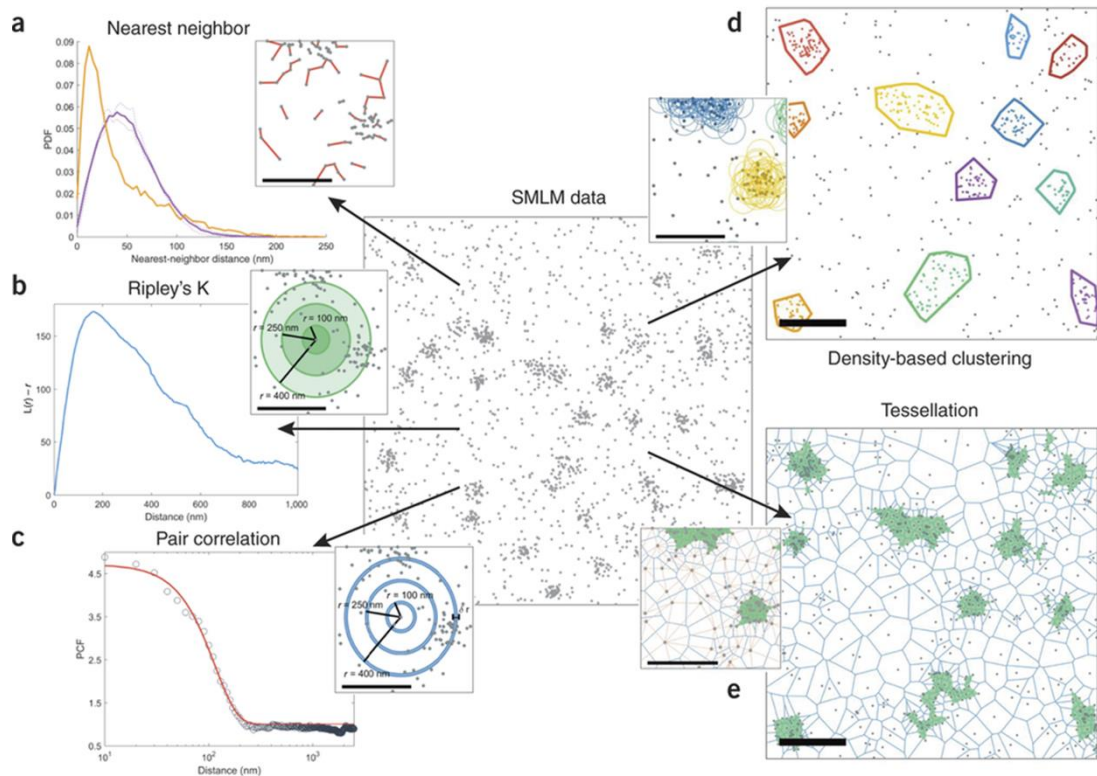


Figure 4.32: Diagrams illustrating different clustering algorithms.

A: Nearest-Neighbour measures pairwise distances (red lines, inset) between the closest neighbour points (Clark and Evans, 1954). The histogram of the measured data (orange) indicates shorter nearest-neighbour distances than a random distribution of points with the same density (purple). B: Ripley's K measures the point density for each point as a function of circle radius (green circle, inset) (Ripley, 1977). The peak at 170 nm indicates clustering at this length scale. C: The pair-correlation approach is similar to Ripley's K but the circles are replaced by concentric tori with width δr (inset, blue) (Sengupta et al., 2011). D: DBSCAN groups points together in a defined neighbourhood ϵ that have at least min points (Ester et al., 1996). Clustered points are coloured according to their cluster identity, noise points are grey. E: A mesh representation with Voronoi polygons (blue lines) and the Delaunay triangulation (orange lines, inset) (Andronov et al., 2016; Baddeley et al., 2010; Levet et al., 2015). Clusters can then be segmented based on the inverse relationship of density with polygon size (green). Reproduced from Nicovich et al., 2017.

A limitation to all the above approaches is the input of parameters or thresholds with which to segment images for analysis at some stage during the process. DBSCAN is also sensitive to parameter selection and choices should be made using domain knowledge. In this study the search radius was set to 150 nm, the size of smaller membrane structures produced by HCV. Adaptations to DBSCAN have been developed such as OPTICS (ordering points to identify clustering structure) (Ankerst et al., 1999) and DeLi-Clu (density-link clustering) (Achtert et al., 2006). These are designed to perform like DBSCAN but aim to eliminate the need to specify min points and ϵ . Continued investigations into clustering the SMLM produced here for HCV will explore these algorithms in the future to reduce user bias and characterise the data using different approaches.

4.4.2 The internal architecture of HCV replication complexes

A major aim of this investigation was to characterise the internal architecture of HCV replication complexes. The distance of localisations within clusters to the cluster centroid revealed two distinct distributions for NS5A and NS3. In both cases a defined minimum distance was observed which tailed off at increasing distance from the centroid; the minimum diameter was 110 ± 5 nm for NS3 and 190 ± 5 nm for NS5A.

All HCV proteins are known to be membrane associated (Moradpour et al., 2003), and this distribution of protein molecules likely corresponds to membrane associated NS3 and NS5A molecules around either the interior or exterior of DMV. Although the orientation of proteins with respect to membranes cannot be explicitly determined from these images, the sizes correlate well with the known size range of HCV DMV produced during infection (Ferraris et al., 2010; Romero-Brey et al., 2012). The identification of purified DMV containing HCV polymerase activity, which is resistant to protease and nuclease treatment before disruption of the membrane, suggests that HCV non-structural proteins are sequestered inside (Paul et al., 2013).

One explanation for the observed size differences between NS3 and NS5A are that each protein is associated with different DMV sizes. Although this is unlikely as the full complement of NS3–5B constitutes the replication complex and is required for genome replication (Lohmann et al., 1999), a high degree of colocalisation between NS3 and NS5A is observed by wide-field (Gosert et al., 2003; Ross-Thriepland and Harris, 2014), and specific interactions have been observed between the non-structural proteins (David et al., 2015; Paredes and Blight, 2008; Shimakami et al., 2004; Zhang et al., 2005).

A second explanation suggests that each protein is associated with the same DMV although some of the protein is localised to different sides of the membrane (Figure 4.34). In the model proposed, NS5A is localised to the exterior of DMV on the cytosolic side (Figure 4.34B). The theoretical distance of NS5A from the cluster centroid is approximately 102.1 nm. This is calculated from the measured distances of NS3 and the expected displacement distance of NS5A if antibody labelled and oriented on the opposite side of the membrane (Figure 4.34A). This theoretical distance is in good agreement with the measurements made by dSTORM of $95 \text{ nm} \pm 2.5 \text{ nm}$.

The association of NS5A on this side of the membrane has a number of consequences for HCV infection. Domain III of NS5A is reported to interact with core on lipid droplets (Appel et al., 2008; Masaki et al., 2008; Miyanari et al., 2007; Zayas et al., 2016). Accordingly, DMV are known to be in close association with lipid droplets (Romero-Brey et al., 2012), and protein clusters observed by dSTORM were also observed in close association (Section 4.3.7). The presentation of NS5A on the surface of DMV may facilitate the localisation of replication factories to sites of HCV assembly through interactions with core. In comparison, the remaining non-structural proteins inside the DMV are protected from cellular innate immune detection of replication intermediates such as double stranded RNA (Paul and Bartenschlager, 2015).

To experimentally validate this model a number of key experiments need to be explored. Firstly, multi-colour dSTORM imaging (Erdelyi et al., 2013; Lampe et al., 2012; Zhao et al., 2015) of NS5A and NS3 is required to confirm whether the protein clusters observed individually in this study are associated structures or independent from each other. Secondly, biochemical studies such as selective permeabilisation of the host cell membrane followed by either, immunofluorescence imaging, or protease digestion, would identify cytosolic exposed NS proteins in HCV infected cells.

Proteinase K protection assays have been reported for HCV sub-genomic replicon harbouring or infected cells (Miyanari et al., 2003; Paul et al., 2013; Quinkert et al., 2005). These studies identified that a small proportion, <5%, of each NS protein remains protease resistant before membrane disruption with detergents, yet accounts for the full replicase activity (Quinkert et al., 2005). Therefore, the HCV NS proteins are proposed to reside on both cytosolic exposed and cytosolic protected membranes. However, careful examination of the reported results indicate that NS5A is more susceptible to proteinase K digestion, and therefore

more exposed, than the other NS proteins when lower concentrations of proteinase K are used (Figure 4.33).

Immunogold labelling experiments of DMV in ultrathin sections, or purified from HCV infected cells, have previously been exploited to confirm the association of HCV NS proteins with virus induced membrane structures (Ferraris et al., 2010; Paul et al., 2013). However, the relative orientation of proteins about the purified membranes was not investigated extensively in these studies. Labelling of NS5A was observed on both the internal and external membrane faces, whereas NS3 and the majority of dsRNA was observed internally (Ferraris et al., 2010; Paul et al., 2013). Reproduction of both proteinase K and immunogold labelling experiments with a quantitative approach to determine the relative orientations of each NS protein should be investigated in the future to rigorously test the proposed model.

Along with 3D-dSTORM data presented here, the proteinase K and immunogold studies previously reported provide evidence in support of the model (Figure 4.34). The data indicate that the small proportion of each NS protein in a detergent sensitive environment provides replicase activity, explaining the requirement of NS3–5B for genome replication (Lohmann et al., 1999). The remaining NS5A, which is more susceptible to proteinase K digestion, is then oriented on the exterior of DMV in a cytosolic exposed environment facilitating interactions between NS5A and core for HCV assembly (Appel et al., 2008; Masaki et al., 2008; Miyanari et al., 2007; Zayas et al., 2016), or between other cellular proteins (Tripathi et al., 2013).

4.4.3 Association of protein clusters with lipid droplets

A second finding from dSTORM imaging was the identification of HCV NS5A protein clusters surrounding putative lipid droplets in SGR harbouring and virus infected cells (Figure 4.20). Although the location of lipid droplets were inferred from bright-field images, a number of protein clusters were observed in close proximity, either associated around the surface, or in the vicinity of proposed lipid droplets (Figure 4.20). This contrasts with previous reports by conventional light microscopy that show NS5A covering lipid droplets in a localisation similar to core (Miyanari et al., 2007).

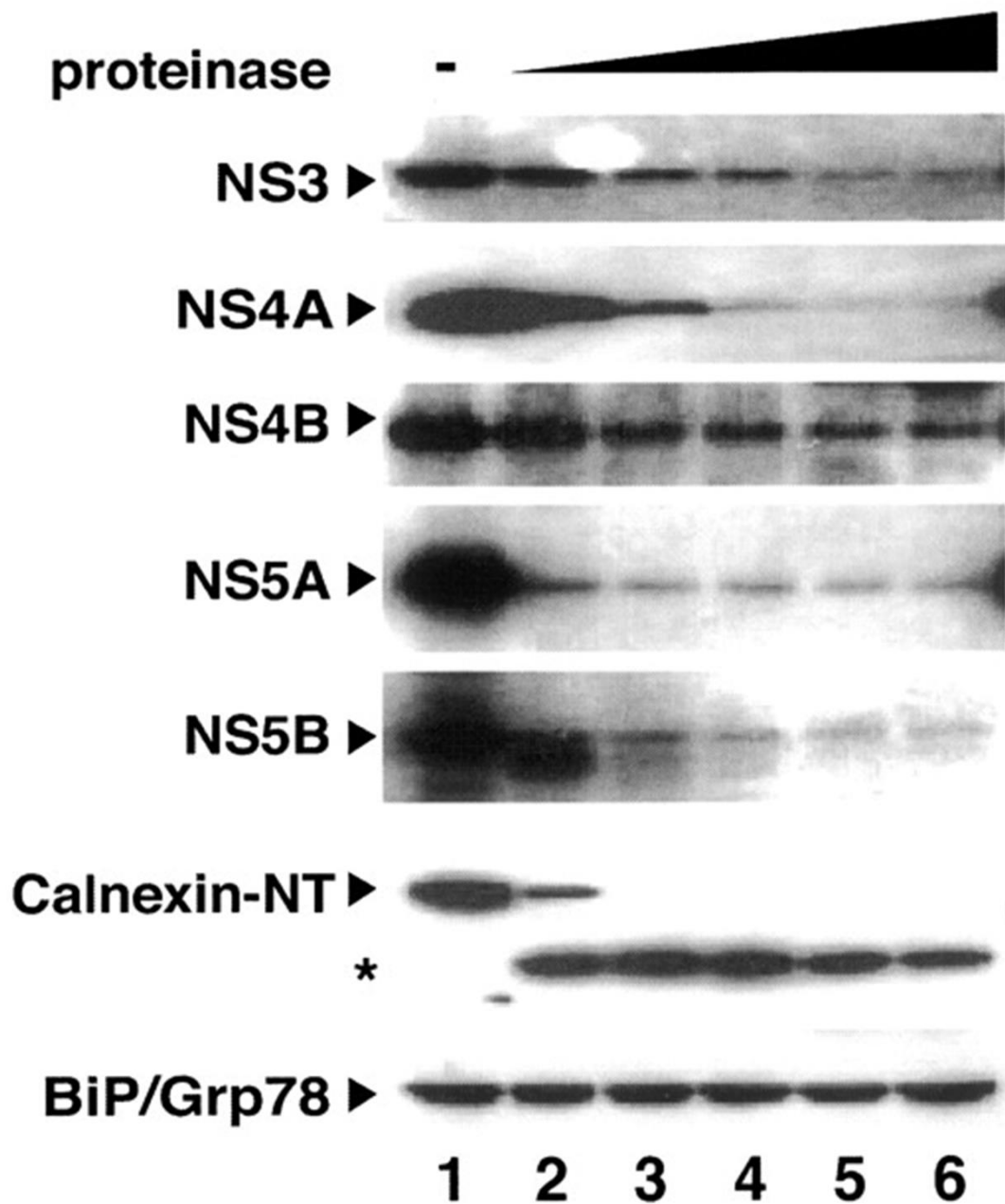


Figure 4.33: Susceptibility of NS proteins to proteinase K digestion. Digitonin permeabilised cells were incubated with proteinase K at varying concentrations (0 $\mu\text{g/ml}$ lane 1, 1 $\mu\text{g/ml}$ lane 2, 5 $\mu\text{g/ml}$ lane 3, 10 $\mu\text{g/ml}$ lane 4, 50 $\mu\text{g/ml}$ lane 5 and 100 $\mu\text{g/ml}$ lane 6). Asterisk denotes the position of calnexin NH_2 -terminal segment located in the ER lumen. BiP/Grp78 which is located in the ER lumen was used as a negative control for proteinase K digestion. Reproduced from (Miyanari et al., 2003).

It is well documented that HCV requires the lipid droplet as a scaffold for virion assembly (Ogawa et al., 2009; Paul et al., 2014). Light and electron microscopy studies have identified that DMVs are closely associated with the ER and lipid droplets in the membranous web (Egger et al., 2002; Romero-Brey et al., 2012; Targett-Adams et al., 2008a). Future studies exploiting multi-colour dSTORM with specific labelling of lipid droplets are required to confirm the association of HCV NS proteins. Three-colour super-resolution imaging of the HCV assembly site around lipid droplets have already been investigated with core and E2 labelling (Eggert et al., 2014).

These results from 3D-dSTORM in this study fit with the proposed model of HCV replication complexes in close association with lipid droplets, thereby allowing tight regulation of HCV replication and assembly (Masaki et al., 2008; Romero-Brey et al., 2012; Zayas et al., 2016).

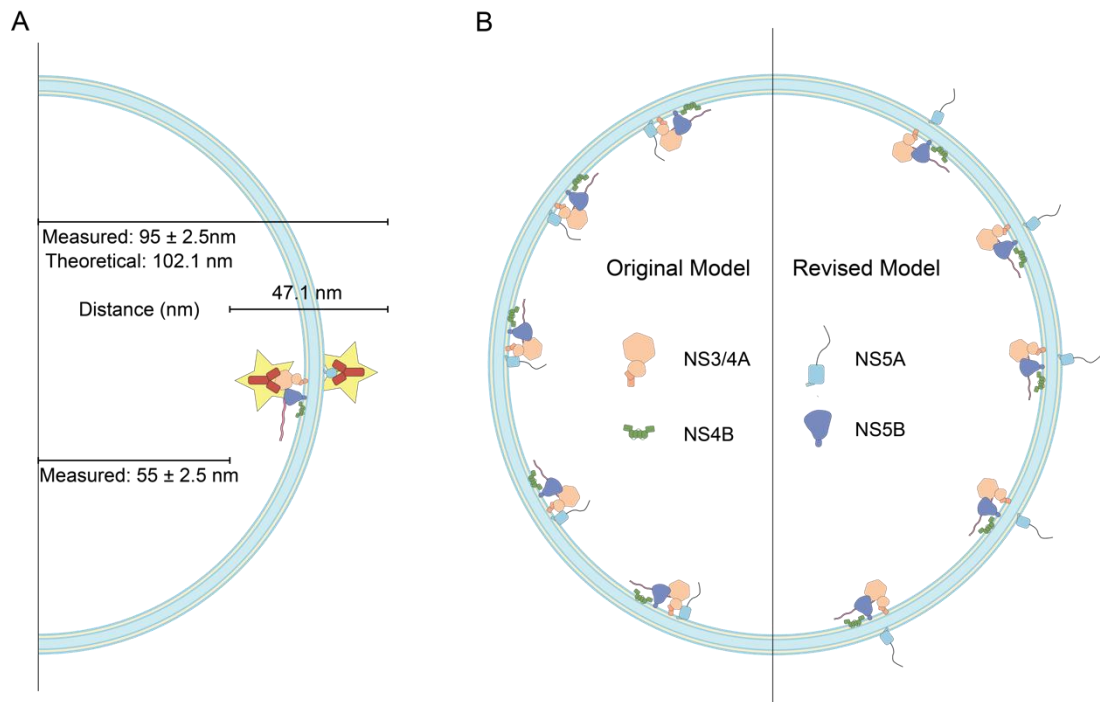


Figure 4.34: Revised model of HCV replication complex formation.

A: Illustration of non-structural protein organisation on different sides of DMV membrane with detection of proteins by labelled primary antibodies in dSTORM. The diameter of non-structural proteins was measured as the minimum diameter of a sphere occupied by the protein volume (Erickson, 2009), 5.5 nm for NS3 and 3.6 nm for NS5A domain I. Antibody (red) displacement of 10 nm (Huang et al., 2008b), and average localisation precision (yellow) of 20 nm are indicated. The fluorescent dye is assumed to be centrally located on the antibody during random labelling of amines. Double membrane vesicle diameter of 8 nm corresponds to two 4 nm thick ER membranes (Mitra et al., 2004). The measured and theoretical distances to the cluster centroid are indicated. B: Left, original model of HCV non-structural proteins in a macromolecular protein assembly inside DMV. Right, revised model of non-structural protein organisation around DMV as informed from dSTORM imaging. Images are drawn to scale.

4.4.4 HCV replication complexes are organised differently between genotypes

An investigation of NS5A protein clusters from different genotypes revealed distinct differences. Both genotype 1b and 3a were observed in protein clusters smaller than the previously characterised genotype 2a, which also contained more NS5A localisations.

The epitope for the 9E10 antibody has been localised to residues 414–428 of NS5A domain III which are 100% conserved between the genotypes used in this study (Galli et al., 2013; Scheel et al., 2012). Therefore, the differences in protein cluster size observed are likely not due to changes in antibody affinity but represent phenotypic differences in the organisation of NS5A between different genotypes.

The genotype 2a isolate, JFH1, is currently the only isolate which undergoes the full replication cycle in cell culture without the addition of cell culture adaptive mutations (Wakita et al., 2005). Both genotype 1b and 3a SGRs require selective pressure to obtain cell populations harbouring SGRs for each genotype (Lohmann et al., 1999; Saeed et al., 2012). Therefore, JFH1 is much more efficient in establishing replication in cell culture than other genotypes. The precise mechanisms for this are not understood but the identification of larger and denser NS5A protein clusters for genotype 2a compared to 1b or 3a, in stable SGR harbouring cells, indicate a more efficient and robust establishment of replication complexes (Figure 4.15). Additionally, this efficiency of DMV formation may be an attribute associated with NS5A alone. Expression of NS5A in cells is reported to induce formation of DMV in the absence of other non-structural proteins (Paul et al., 2013; Romero-Brey et al., 2012).

This hypothesis is also supported by the increased NS5A cluster sizes observed in replicon compared to virus infection. Cells stably harbouring replicons have an average protein cluster diameter of 250 ± 5 nm. Accordingly, at later times post infection larger (~300 nm) multi-membrane vesicles were observed within infected cells (Romero-Brey et al., 2012).

4.4.5 Effect of daclatasvir treatment

The extremely potent NS5A inhibitor DCV currently has an unknown mechanism of action as NS5A does not have a known enzymatic activity. Current models propose that DCV binding to NS5A alters its dimerisation state, ultimately disrupting HCV RC formation (Berger et al., 2014; McGivern et al., 2014) or RNA binding (Ascher et al., 2014). A number of NS5A dimer conformations have been proposed based on the X-ray crystallographic structures of domain I (Lambert et al., 2014; Love et al., 2009; Tellinghuisen et al., 2005), and the symmetrical structures of daclatasvir and related inhibitors. Molecular dynamic simulation studies indicate that this interaction may occur at the dimer interface in close association with the cell membrane (Lambert et al., 2014). However, which, if any, dimer conformations are functional during HCV infection remains to be experimentally determined.

The increased quantity of NS5A localisations observed within protein clusters after DCV treatment fit the current hypothesis that DCV binding stabilises a dimer of NS5A, thereby trapping and/or immobilising NS5A in an inactive replication complex (Berger et al., 2014; Gao et al., 2010). 72 h treatments with DCV result in a condensed and immobile phenotype of NS5A puncta suggesting stalling of replication assembly at an early step (Chukkapalli and Randall, 2014).

Expansion of the studies presented here for virus infection and daclatasvir treatment are required to monitor how protein cluster size changes during the course of infection, and how NS5A is altered during the earlier hours following daclatasvir treatment, for example at 2 or 4 h. Correspondingly, HCV virion production is inhibited as early as 2 h after treatment of cells with DCV (McGivern et al., 2014). This has been proposed to occur through some displacement of NS5A from lipid droplets, or inhibition of RNA binding which uncouple transfer of HCV RNA from replication complexes to core (Ascher et al., 2014) A precise description of lipid droplet positions was beyond the scope of this investigation but two-colour imaging approaches using NS5A and lipid droplet staining are under investigation to address how the organisation of NS5A in protein clusters around lipid droplets is altered upon inhibition with DCV.

4.4.6 Roles of phosphorylation during HCV infection

Manipulation of NS5A phosphorylation resulted in a number of phenotypic differences in NS5A proteins cluster organisation by 3D-dSTORM. Mutations of S146 to either ablate phosphorylation at the site with an alanine, or mimic with an aspartate resulted in increased NS5A cluster sizes which contained more localisations than wildtype. In transient replication assays both S146 mutants are capable of wildtype replication, but a reduction in the hyperphosphorylated species is observed (Ross-Thriepland and Harris, 2014). The molecular details and purpose of hyperphosphorylation within cells remain elusive. Genotype 1b appears to be dependent on hyperphosphorylation for efficient replication, whereas this is not the case for genotype 2a (Appel et al., 2005; Neddermann et al., 2004). Intriguingly, in all genotypes except 2a and 1a, S146 is an alanine (Ross-Thriepland and Harris, 2014). Therefore, this phosphorylatable serine may provide an additional level of replication control such as the regulation of NS5A dimer formation (Ross-Thriepland and Harris, 2014).

Mutation of S225 had a more pronounced impact on NS5A, with an accumulation of NS5A in a perinuclear region (Figure 4.29) (Ross-Thriepland et al., 2015). These were observed as groups of clusters localised in a similar region. The absence of S225A distributed throughout the cytoplasm indicates a deficient trafficking and mobility function of NS5A. Accordingly, the association of replication complexes with actin filaments and microtubules are reported to depend on NS3 and NS5A (Lai et al., 2008). The impaired but competent replication kinetics for this mutant indicate that S225A retains the ability to form active replication complexes (Ross-Thriepland and Harris, 2014). The deficiency of this mutant may be associated with a reduced re-localisation and interaction with lipid droplets. Accordingly, the quantity of lipid droplets in S225A replicating cells was significantly lower than wildtype and the corresponding S225D (Ross-Thriepland et al., 2015). To quantify the association of S225A with lipid droplets, 2-colour dSTORM imaging methods are currently under investigation to simultaneously visualise both NS5A and lipid droplet in SMLM.

4.4.7 Model of HCV replication complexes

The data reported in this chapter from localisation microscopy analysis of SGR harbouring and HCV infected cells has provided additional information on the organisation and architecture of the HCV replication complex. From our findings a revised model of HCV replication complex organisation is proposed (Figure 4.35).

dSTORM imaging indicates that NS3 may be associated on the membrane on the interior of DMV, whereas NS5A is localised on the exterior (Figure 4.34; Figure 4.35, step 2). Inhibition of NS5A with DCV may arrest replication complex assembly (Figure 4.35, step 2) (Berger et al., 2014). The observed close association of replication complexes with lipid droplets may be instigated by interactions of NS5A with core (Appel et al., 2008; Masaki et al., 2008; Miyanari et al., 2007; Zayas et al., 2016). Thus positioning replication complexes spatially adjacent to sites of HCV virion assembly (Figure 4.35, steps 3–4). Close association of replication factories with lipid droplets facilitates the transport of HCV RNA into sites of virion assembly. The precise mechanism of this step remains elusive but is proposed to involve the RNA binding properties of NS5A (Foster et al., 2010), along with its known interactions with other non-structural proteins (David et al., 2015; Shimakami et al., 2004) and core (Masaki et al., 2008; Miyanari et al., 2007; Zayas et al., 2016), thereby bridging the space between replication complexes and sites of assembly. Alteration of the NS5A conformation and reduction of RNA binding by DCV (Ascher et al., 2014), reduces the transport of RNA from replication complexes to sites of assembly thus producing a rapid arrest in virion production (McGivern et al., 2014).

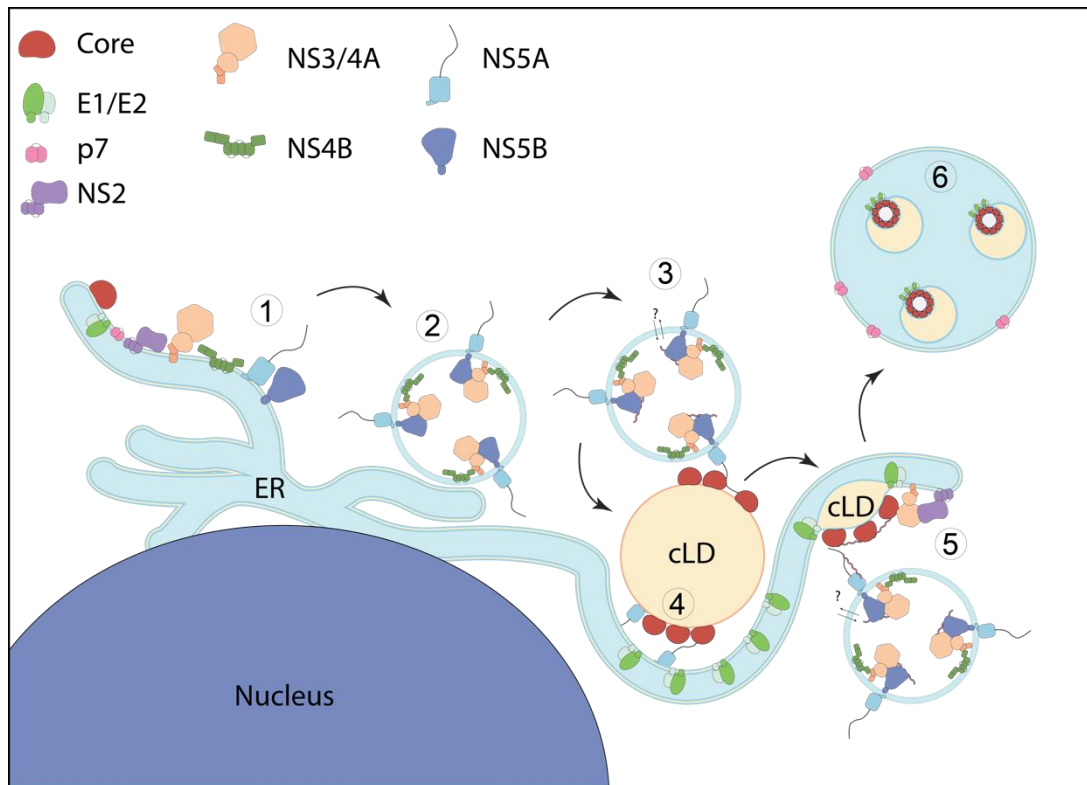


Figure 4.35: Model of HCV replication.

Step 1: HCV polyprotein is translated and cleaved into individual proteins on the ER. Step 2: Formation of HCV replication factories with NS5A on exterior and NS3/4A, NS4B and NS5B on the interior. Step 3–4: NS5A interactions with core mediate close association of replication factories with sites of virus assembly. Step 5: NS5A mediated transport of RNA to core at sites of HCV assembly. Step 6: Budding of HCV virions into the ER and trafficking through endosome-Golgi pathway releasing progeny virions.

**Chapter 5 - The PI3P binding protein
DFCP1 is required for HCV replication
complex formation**

5.1 Aims and Objectives

The manipulation and repurposing of cellular membranes for virus propagation is common amongst all positive strand RNA viruses studied to date (Romero-Brey and Bartenschlager, 2014). However, the origin of HCV replication factories and the corresponding cellular interaction partners remain poorly defined.

The autophagosome biogenesis pathway has the potential to supply the DMVs required for HCV replication. However, the precise mechanisms with which HCV interacts with the autophagy machinery remain poorly defined.

To address this, a combination of pharmacological inhibition, genetic ablation and fluorescence imaging were used. The data presented here correspond to the imaging studies undertaken in the investigation, excluding the live cell imaging. All other experimentation was carried out by Bjorn-Patrick Mohl and is reported alongside this microscopy analysis in Mohl et al. 2016.

5.2 Introduction

The production of double and multi-membrane vesicles is a well-documented phenotype of HCV infection both in cell culture and patients (Ait-Goughoulte et al., 2008; Dreux et al., 2009; Rautou et al., 2011; Sir et al., 2008). The large quantities of vesicles produced during infection have commonly been referred to as the “membranous web”, a convoluted system of vesicles in a perinuclear region of infected cells (Figure 1.10, Figure 4.1) (Egger et al., 2002). This clustering of vesicles, mainly double-membraned vesicles (DMVs), is proposed to be the site of HCV genome replication (Gosert et al., 2003; Miyanari et al., 2003). Recent studies, along with work presented here in Chapter 3, have sought to characterise these structures in molecular detail to better understand their role during the HCV lifecycle (Paul et al., 2013; Pérez-Berná et al., 2016; Romero-Brey et al., 2012).

The double membranous architecture of these vesicles has led to the hypothesis that these structures are derived from the cellular process of autophagy. Importantly this process, which is normally involved in maintaining cell homeostasis, is characterised by the formation of DMVs, termed autophagosomes (Tanida, 2011). During times of nutrient starvation or stress these DMVs subsequently fuse with lysosomes facilitating the degradation and re-cycling of the vesicular contents. In higher eukaryotes, autophagy can also be utilised by the cell for development, immunity and eliminating intracellular microorganisms (Choi et al., 2013; Deretic et al., 2013).

The unfolded protein response (UPR) is one method of autophagy induction whereby ER stress results in DMV formation which sequester misfolded proteins (Ding et al., 2007; Ron and Walter, 2007). HCV has been shown to induce the UPR (Chan and Egan, 2005; Ke and Chen, 2011; S. Li et al., 2009; Shinohara et al., 2013), and this process was proposed as the subsequent induction of autophagy by HCV as inhibition of the UPR results in a decrease of HCV RNA levels (Sir et al., 2008). However, more recent work in the lab identified the induction of autophagy at 4 h post infection with the UPR not observed until 48 h (Mohl et al., 2012). Critically, although autophagy is induced by HCV, the fusion of autophagosomes with lysosomes is inhibited (Sir et al., 2008).

A growing body of evidence points to autophagy as an important process in HCV replication. This parallels with observations for other positive strand RNA viruses where subversion of autophagy facilitates viral propagation (Romero-Brey and Bartenschlager, 2014), a notable example is poliovirus (Taylor and Kirkegaard, 2007). Downregulation or chemical inhibition of proteins involved in autophagosome

formation such as Atg5, Atg7, Atg4B, LC3 and Beclin1 all result in reduced HCV replication (Dreux et al., 2009; Mizui et al., 2010; Sir et al., 2008). Additional reports also suggest that HCV may upregulate autophagy proteins during its lifecycle, specifically Beclin1 by NS5A (Shrivastava et al., 2012). Sucrose gradient fractionation experiments have identified autophagosome-like membranes co-purifying with NS3 and NS5A, and immunogold labelling of EM sections revealed the presence of NS5A and dsRNA within LC3 positive DMVs (Ferraris et al., 2010).

Other precipitation studies have isolated LC3 containing vesicles and shown they contain NS5A, NS5B and remain productive for HCV RNA generation (Sir et al., 2012). Direct interactions between proteins have been observed biochemically through immunoprecipitation of NS4B and p7 (Aweya et al., 2013; Su et al., 2011) and yeast two-hybrid studies of NS5B (Guévin et al., 2010) which identified Vps34, Beclin1 and Atg5 interaction partners, respectively.

Although strong biochemical evidence exists for direct protein interactions, conflicting data exists for colocalisation of proteins in microscopy studies. Studies using the GFP-LC3 fusion protein have provided evidence to support (Guévin et al., 2010; Sir et al., 2012) or contest (Ait-Goughoulte et al., 2008; Dreux et al., 2009) the idea that HCV replication complexes are found on autophagosomes. However, the analysis of studies using transient expression of LC3 should be interpreted with caution as overexpression can cause re-localisation of LC3 into protein aggregates (Kuma et al., 2007). Data from our lab using endogenous staining of LC3 and NS5A suggest that replication complexes are not on autophagosomes (Mohl et al., 2012). This data agreed with previous findings that identified the Atg4B and Beclin1 proteins as important for initial HCV RNA translation, however they were no longer required once infection is established (Dreux et al., 2009).

Despite the current understanding about the “membranous web” and the interplay between HCV and autophagy, the biogenesis of the HCV replication complex remains to be fully elucidated. The expression of NS4B or NS5A alone within cells results in the production of DMVs, however no single protein is sufficient and the full complement of NS proteins are required for complete “membranous web” formation (Egger et al., 2002; Paul et al., 2013; Reiss et al., 2011; Romero-Brey et al., 2012; Su et al., 2011). It is currently thought that the DMVs are derived from ER membranes as EM studies have observed a close association between these two structures (Romero-Brey et al., 2012). This parallels with autophagy where the maturation of autophagosomes is reported to stem from specialised domains of the

ER (Axe et al., 2008; Bernales et al., 2006). In particular the recruitment of the class III phosphatidylinositol 3-kinase (PI3K) complex to mitochondrial-associated ER membranes (MAM) produces phosphatidylinositol 3-phosphate (PI3P) (Hamasaki et al., 2013). The PI3K complex subsequently generates a PI3P-rich region for recruitment of additional effector proteins, such as the double-FYVE-containing protein 1 (DFCP1) and WD-repeat protein-interacting phosphoinositide (WIPI) (Karanasios et al., 2013; Koyama-Honda et al., 2013; Polson et al., 2010; Ridley et al., 2001). Binding of these proteins gives rise to cup-like protrusions from the ER, called omegasomes, which provide the scaffold for expansion of the isolation membrane (phagophore); the membrane domain from which autophagosomes are produced (Axe et al., 2008; Polson et al., 2010). Recently the link between these effector proteins and the lipidation of LC3 (microtubule-associated protein light chain 3) with phosphatidylethanolamine (PE), a key process for the expansion and closure of the phagophore, has been elucidated (Dooley et al., 2014).

5.4 Results

It was shown previously that HCV enhances the activity of class I PI3K by our lab (Street et al., 2004) and others (He et al., 2002). However, the importance of this has yet to be elucidated during HCV infection. The first step during autophagosome formation is the local production of PI3P on the ER membrane by the class III PI3K Vps34 (vacuolar protein sorting 34). Treatment of cells stably expressing a sub-genomic replicon with the well-known inhibitor of PI3K, wortmannin, resulted in a progressive loss of LC3-II over time, indicative of Vps34 inhibition, and a concurrent loss in NS5A protein and luciferase reporter levels (Mohl et al., 2016). These findings confirmed the requirement of HCV for autophagy, specifically the production of PI3P by Vps34, during infection.

DFCP1 (double-FYVE-containing protein 1), and other PI3P binding proteins are then recruited to the local PI3P pool produced by Vps34 (Karanasios et al., 2013; Koyama-Honda et al., 2013; Polson et al., 2010; Ridley et al., 2001). These proteins provide the scaffold for expansion and closure of the ER membrane into autophagosomes (Axe et al., 2008; Dooley et al., 2014; Polson et al., 2010). Therefore, the role of these autophagosome biogenesis proteins during the HCV lifecycle was investigated by siRNA-mediated silencing in stable cell lines and during virus infection. Efficient silencing of either protein resulted in a loss of HCV replication in genotype 1b and 2a comparable to the HCV inhibitors cyclosporin A and daclatasvir (Mohl et al., 2016). These observations suggest that HCV replication is dependent on a functional autophagosome biogenesis pathway involving Vps34 and DFPC1.

5.4.1 Validation of an mCherry-DFCP1 expression construct

To address whether the HCV replication complex associates with DFPC1, an mCherry-DFCP1 expression construct was constructed by B.-P. Mohl (Mohl et al., 2016) from an existing EGFP-DFCP1 expression plasmid (Axe et al., 2008), and its functionality validated (Figure 5.1).

After induction of autophagy by thapsigargin, an increase in the appearance of LC3 puncta was observed which exhibited overlapping fluorescence signals with the mCherry-DFCP1 (Figure 5.1). In comparison, both the LC3 and mCherry-DFCP1 staining from DMSO or wortmannin treated cells were more diffuse and exhibited minimal colocalisation. Wortmannin is a well-known inhibitor of autophagy (Mohl et al., 2012), whereas thapsigargin is an inhibitor of the ER Ca^{2+} -ATPase which induces ER stress and the induction of autophagy (Ogata et al., 2006).

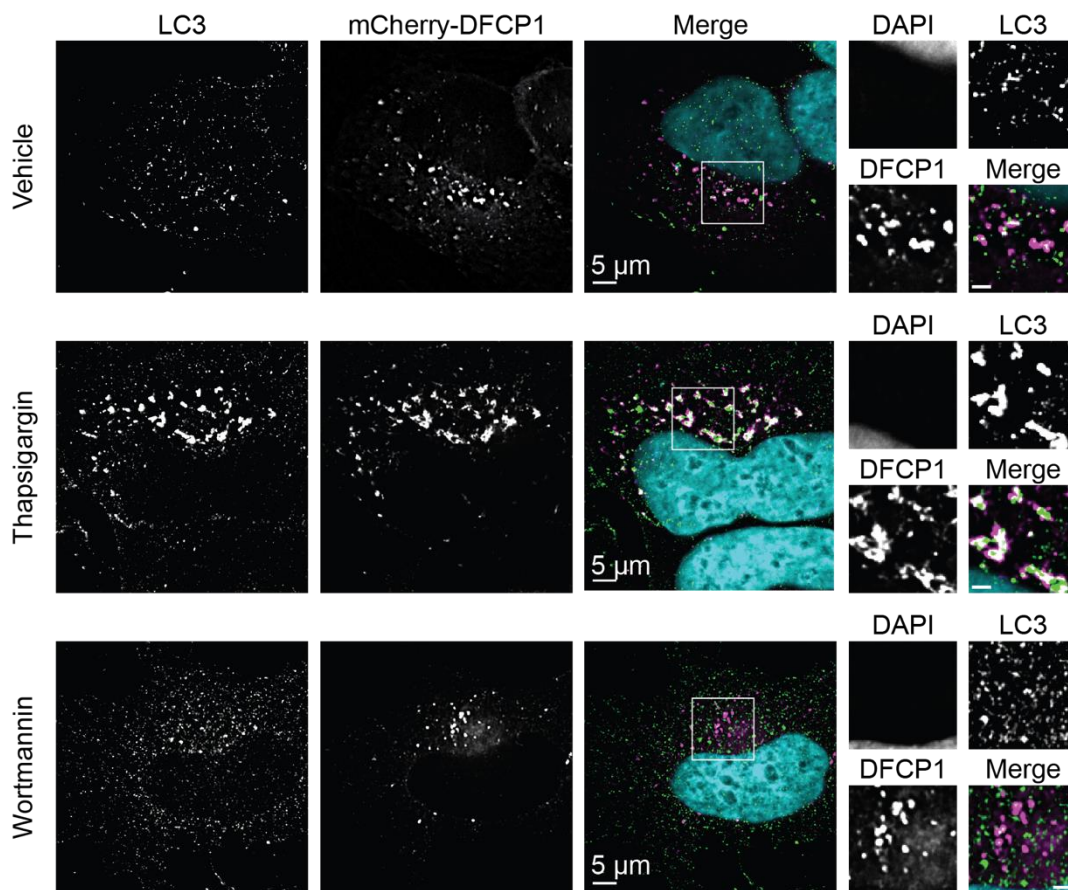


Figure 5.1: Validation of an mCherry-DFCP1 construct as a marker for autophagosome formation.

HuH7 cells were transfected with an mCherry-DFCP1 expression plasmid for forty-eight hours. Cells were then treated with vehicle (DMSO), thapsigargin (3 μM) or wortmannin (1 μM) for 3 h before fixation and autophagosome and nuclear staining with an LC3 antibody and DAPI. Scale bars, 5 μm . White boxes indicate magnified regions.

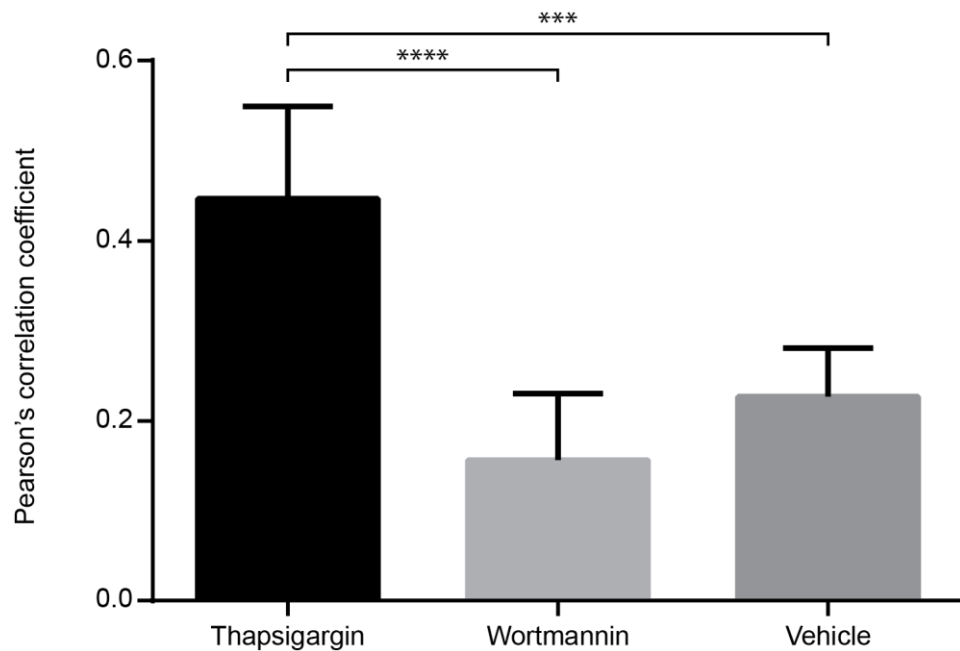


Figure 5.2: Colocalisation analysis from mCherry-DFCP1 expression plasmid validation.

The mean Pearson correlation coefficient was determined from vehicle, thapsigargin and wortmannin treatment, from 6, 8 and 8 cells, respectively. Data represent the mean \pm SD. Statistical significance measured by Welch's unpaired *t*-test, *** $P < 0.0005$, **** $P < 0.0001$.

The quantification confirmed the observations that there was a significant difference in fluorescence signal overlap between LC3 and mCherry-DFCP1 in autophagy stimulated and inhibited cells (Figure 5.2). The observation that mCherry-DFCP1 localises to cytoplasmic puncta and colocalises with LC3 after the induction of autophagy, validate this construct for future microscopy studies.

5.4.2 HCV replication complexes do not stably associate with DFPC1 during infection

To address whether HCV replication complexes are associated with DFPC1 during infection, the localisation of NS5A (as a marker for replication complexes) and DFPC1 was investigated. There was no observable colocalisation of NS5A puncta with DFPC1 in cells replicating HCV (Figure 5.3). The absence of colocalisation was also observed in cells treated with the alternative PI3K inhibitor 3-methyladenine (3MA). Intriguingly, the inhibition of PI3K in these cells did not block the process of virus-induced autophagy previously shown with wortmannin (Mohl et al., 2016).

The observation of NS5A puncta distributed throughout the cell is characteristic of NS5A localisation and confirmed HCV positive cells. Consistent with the induction of autophagy by HCV following infection, mCherry-DFCP1 localised to cytoplasmic puncta similar to uninfected cells treated with thapsigargin (Figure 5.1).

The absence of any colocalisation between DFCP1 and HCV replication complexes suggest no direct interaction occurs between these two partners. This is supported in part by the inability to successfully pull-down either protein by co-immunoprecipitation (data not shown). However, an alternative hypothesis is that the interaction between DFCP1 and replication complexes are only required during the establishment of infection, therefore any interaction might be transient and short-lived. Accordingly, omegasomes are transient structures early in the process of autophagosome formation (Axe et al., 2008). This idea is supported by previously published work indicating that autophagy is required for the translation of incoming HCV genomes (Dreux et al., 2009). It was later shown that HCV translation requires active HCV RNA synthesis (Liu et al., 2012), which in turn requires a functional autophagosome biogenesis pathway (Mohl et al., 2016).

To investigate the potential transient interaction between DFCP1 and NS5A, live cell imaging was carried out on mCherry-DFCP1 transfected cells ((Mohl et al., 2016); Figures 6 and 7), subsequently infected with a HCV derivative containing an NS5A-GFP fusion at 24 hours post infection (Mohl et al., 2016; Schaller et al., 2007). This analysis revealed a sub-population of puncta containing both NS5A and DFCP1. Over a period of 8 min there was the progressive accumulation of NS5A and DFCP1 into a distinct structure containing both proteins, followed by their eventual dissociation into two distinct structures (Mohl et al., 2016). These observations were comparable to the previously reported transient interaction of DFCP1 with LC3 in the formation of autophagosomes (Axe et al., 2008) and provide strong evidence to support the hypothesis that a short-lived interaction between replication complexes (NS5A) and omegasomes (DFCP1) are required in autophagosome formation.

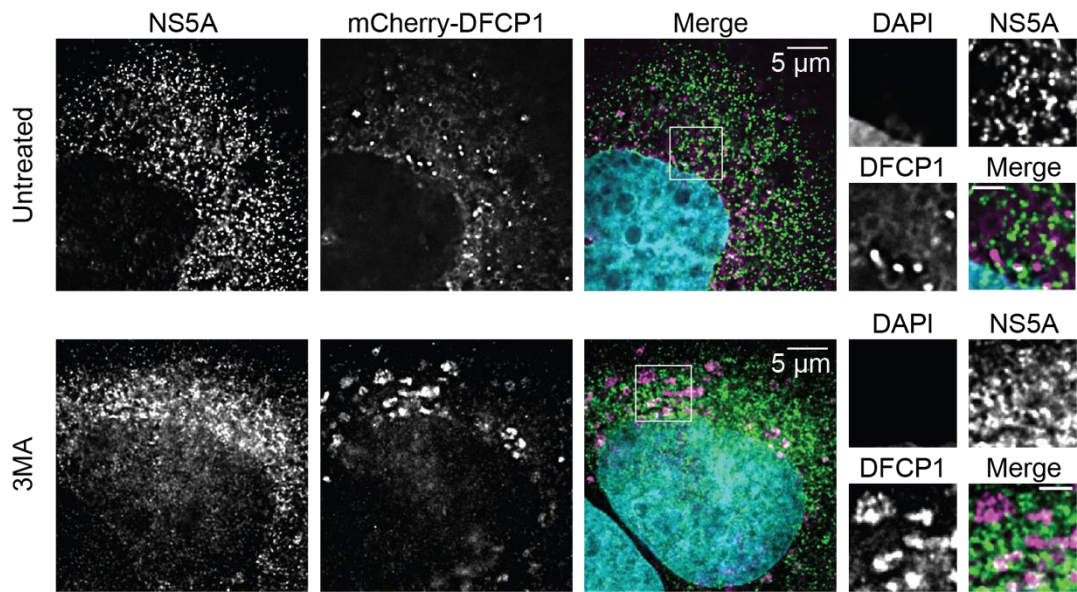


Figure 5.3: HCV replication complexes do not stably colocalise with mCherry-DFCP1.

HuH7 cells were transfected with mCherry-DFCP1 for 48 h prior to infection with Jc1 (Pietschmann et al., 2006) (0.5 f.f.u./cell) for 24 h. Before fixation, cells were treated with or without 0.1 mM 3-methyladenine (3MA) and subsequently stained for HCV replication complexes (NS5A) and nuclei (DAPI). Scale bars in insets 2 μ m. White boxes indicate magnified regions.

5.4.3 Incomplete colocalisation is observed between DFCP1 with NS5A or NS4B expression constructs

This observed association between replication complexes and omegasomes might be a core function of one of the non-structural proteins. To investigate which HCV proteins contribute to the interaction, cells were transfected with different non-structural expression plasmids in combination with mCherry-DFCP1 (Figure 5.4).

All proteins were localised in bright punctate structures with a diffuse background staining throughout the cell. NS5A puncta were distributed evenly throughout the cytoplasm while NS4B-GFP was constrained to a more perinuclear region (Figure 5.4). In all cases there was limited or incomplete colocalisation between the non-structural protein and DFCP1. The degree of colocalisation for each expression plasmid combination was subsequently derived using Mander's overlap coefficients (Figure 5.5) NS3/5A colocalisation from cells stably expressing a SGR and target/DAPI overlap were used as positive and negative controls respectively.

The expression construct data from at least 10 individual cells indicate that around 15–20% of NS5A puncta colocalise with DFCP1 and up to 40% of DFCP1 overlaps with NS5A staining (Figure 5.5). For NS4B, ~20–30% of protein overlapped with DFCP1 and vice versa. During this analysis, differences were also observed between NS5A and NS4B. More NS4B signal overlapped with DFCP1 than NS5A, however DFCP1 colocalised more with NS5A (Figure 5.5). The known interaction between NS3 and NS5A results in at least 75% signal overlap for each protein with the other, whilst <5% of any target overlaps with DAPI staining (Figure 5.5).

This quantitative data indicate that, albeit at low levels, there is a significant colocalisation of either NS5A or NS4B with DFCP1, compared to the negative control, when expressed together within cells.

5.4.4 Expression of WIPI2b, another PI3P effector protein in autophagosome formation

Investigations so far have looked exclusively at DFCP1, but the formation of autophagosomes involves multiple proteins, and protein complex interactions. In order to investigate if HCV replication complexes also interact with WIPI2b, a GFP-WIPI2b fusion protein expression construct was obtained (Dooley et al., 2014) and transfected into HuH7 cells (Figure 5.6). WIPI2b has been reported to link LC3 conjugation, a key step in the maturation of autophagosomes, with PI3P synthesis at sites of autophagosome formation, by recruiting the LC3-conjugating

Atg12-5-16L1 complex (Dooley et al., 2014). Comparable to the reported phenotype, GFP-WIPI2b was distributed throughout the cytoplasm of transfected cells with an apparent ER localisation (Figure 5.6). After the stimulation of starvation-induced autophagy by Earle's balanced salt solution (EBSS), discrete punctate structures could be observed within cells in a perinuclear region that were absent from wortmannin treated cells (white arrows in Figure 5.6).

These initial experiments confirmed the ability of WIPI2b to be recruited to, punctate structures in HuH7 cells during starvation-induced autophagy. However, a major drawback from these experiments was the high expression levels of this protein in transfected cells. This made analysis challenging as only a limited number of discrete puncta were discernible above the background in stimulated cells. Additionally, a high GFP signal was still observed in a perinuclear region of cells treated with the PI3K inhibitor wortmannin. Considering the distribution of NS5A in HCV infected cells, an interpretation of colocalisation between these two proteins would be complicated by the high expression and background signal of GFP-WIPI2b. To address this, a cell line which stably expresses GFP-WIPI2b at low levels is currently under investigation. Unfortunately due to time constraints in this project a stable cell population for further investigation has not yet been established.

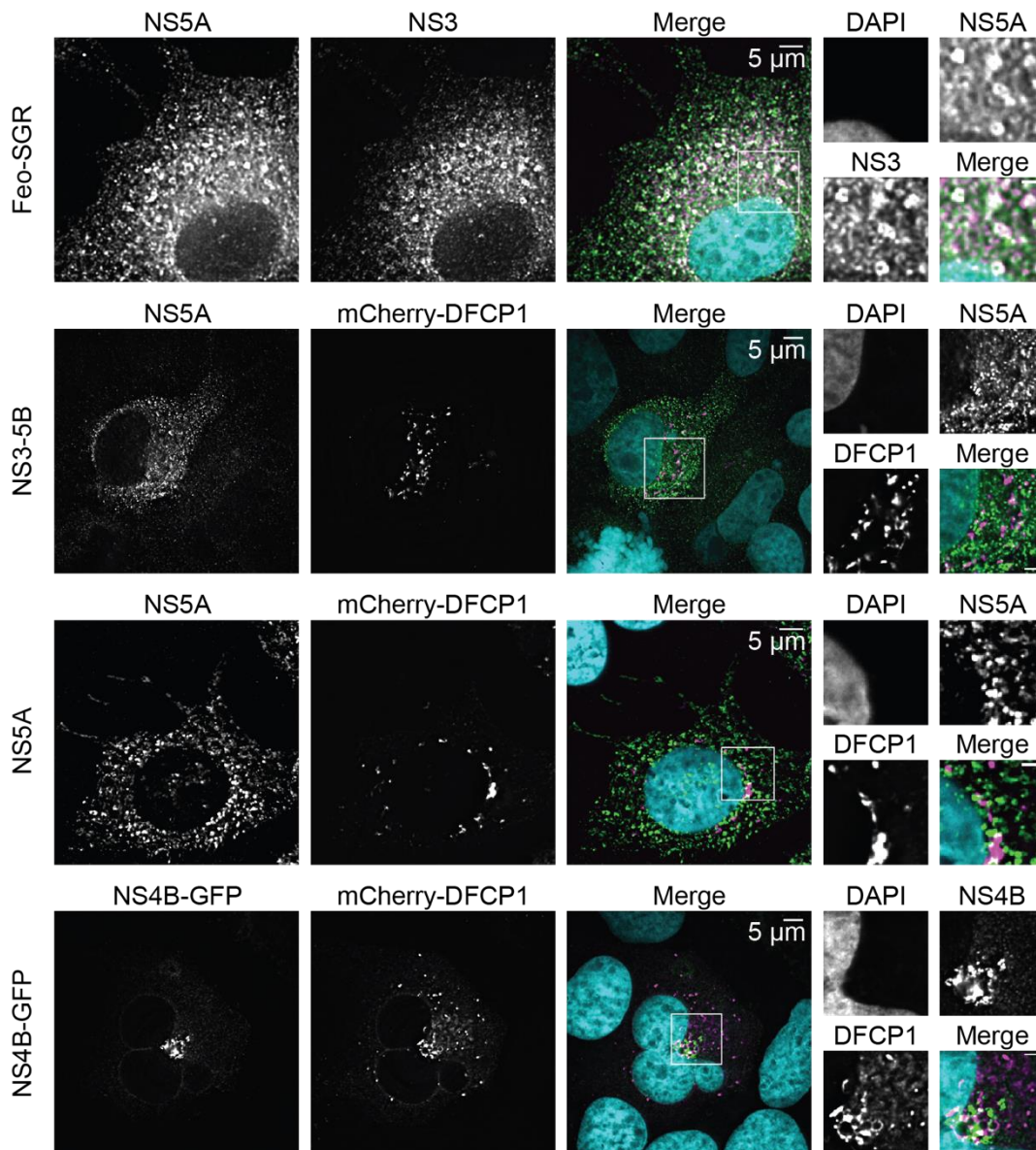


Figure 5.4: Incomplete colocalisation between NS5A or NS4B with DFACP1, either expressed alone or in the context of NS3–5B.

HuH7 cells were transfected with expression plasmids for mCherry-DFACP1 and JFH-1 NS3-5B or NS5A or NS4B-GFP for 48 h. Cells were fixed and NS5A detected by indirect immunofluorescence. Scale bar in inset 2 µm. White boxes indicate magnified regions. Arrows highlight regions of fluorescence overlap between the two channels.

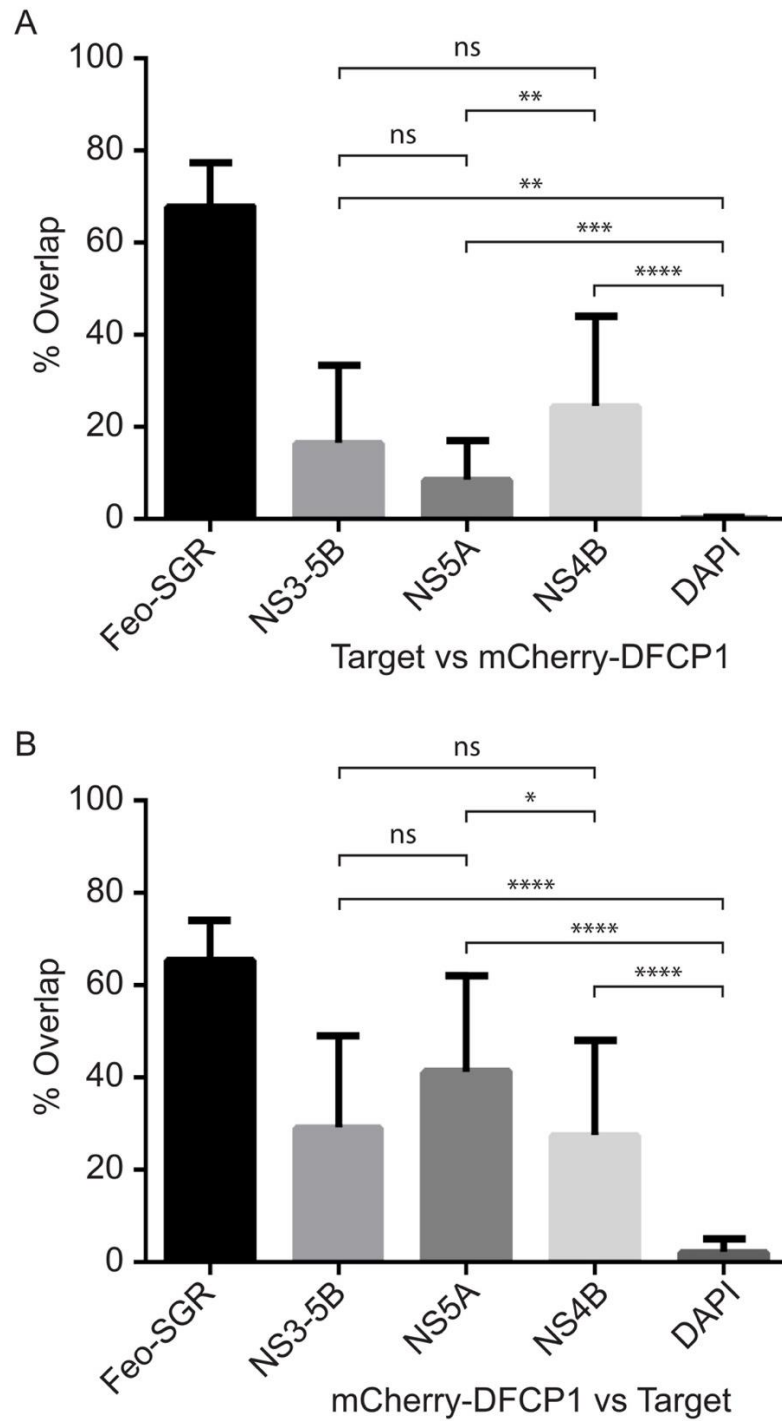


Figure 5.5: Colocalisation analysis of DFCP1 and non-structural protein expression constructs.

Mander's overlap coefficients were determined from >10 cells for each expression construct combination. Data represent the mean \pm SD. Statistical significance measured by Welch's unpaired *t*-test, * $P < 0.05$, ** $P < 0.005$, *** $P < 0.0005$, **** $P < 0.0001$.

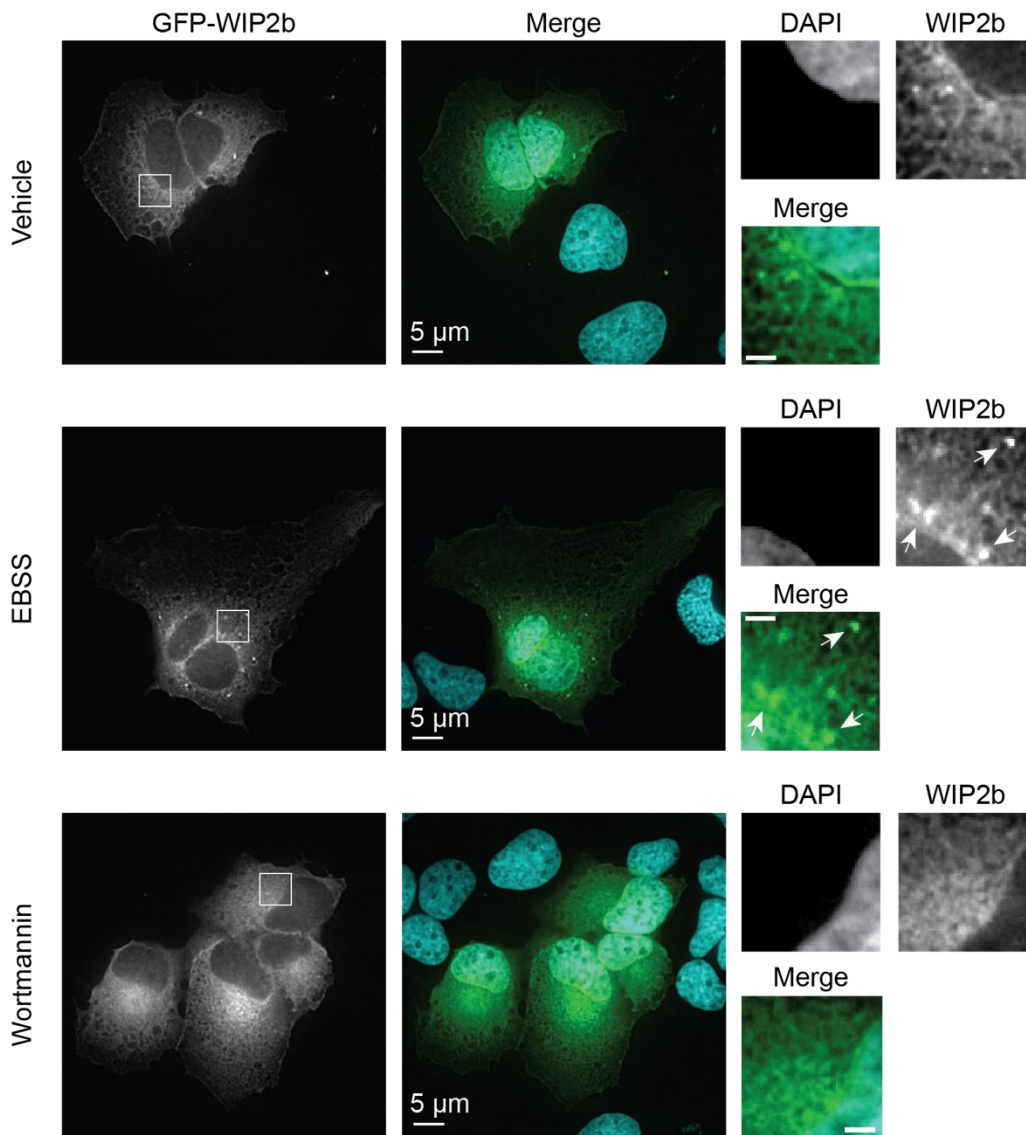


Figure 5.6: Transient expression of GFP-WIP2b.

HuH7 cells were transfected with GFP-WIP2b for 48 h before vehicle, starvation-induced stimulation or pharmacological inhibition of autophagy with DMSO, EBSS or wortmannin, respectively. Scale bar in insets 3 μm. White boxes indicate digitally magnified region. White arrows highlight discrete GFP-WIP2b puncta.

5.5 Discussion

The results from this study provide strong evidence to support that an intact autophagosome biogenesis pathway is required in the formation of HCV replication complexes. The characteristic membranous web produced upon HCV infection was shown in an elegant EM study (Romero-Brey et al., 2012) to be mostly composed of DMVs derived from, or closely associated with, the ER. The similarities between HCV DMVs and autophagosomes strongly indicate they arise via a common biogenesis pathway. In agreement with this hypothesis, both pharmacological inhibition and siRNA mediated gene silencing revealed that the class III PI3K Vps34, and PI3P effector DFCP1, are key requirements for HCV replication (Mohl et al., 2016).

The role of DFCP1 in HCV replication is previously undocumented, and the findings reported here confirm a previously reported role of Vps34 (Su et al., 2011). Taken together with the observation that HCV upregulates Beclin1 expression (Shrivastava et al., 2012) and that the corresponding inhibition studies reduce HCV replication (Dreux et al., 2009), the formation of the class III PI3K complex (Vps34-Vps15-Beclin1-Atg14L) appears to be critical for the establishment of HCV infection. It is worth noting however that a separate study found no effect of Vps34 inhibition or silencing (Sir et al., 2012). Considering the diverse ways of autophagy induction and the stimulation of the UPR by HCV, the redundancy in autophagosome biogenesis may explain this observation.

The mCherry-DFCP1 expression plasmid constructed for this study was comparable to a previously reported EGFP-DFCP1 expression construct (Axe et al., 2008), and therefore a powerful tool for understanding the roles of omegasomes within cells using fluorescence microscopy. The investigation of both fixed and live cell imaging strongly suggest that DFCP1 is involved in the early stages of HCV replication, however it is not stably associated with HCV structures and therefore is only required for replication complex formation. A finding corroborated by previously documented studies showing an involvement of Atg4B and Beclin1 in initial HCV RNA translation (Dreux et al., 2009). The transient colocalisation of HCV replication complexes (NS5A) with DFCP1 is reminiscent of the LC3-DFCP1 interaction previously reported (Axe et al., 2008). In both cases fluorescent puncta association and dissociation occurs over a 10 min period.

This study's findings also agree with previously published literature regarding the involvement of NS5A and NS4B in DMV generation (Paul et al., 2013; Romero-Brey et al., 2012) as both proteins partially colocalise with DFCP1 when expressed within

cells. The colocalisation patterns, which at first were confusing, can be explained by the expression levels and localisation patterns of each protein. NS5A was localised throughout the cytoplasm whilst NS4B is constrained to a perinuclear region, a distribution most similar to DFCP1. Therefore a significant portion of NS5A occupies cytoplasmic space that DFCP1 does not.

Previous reports have shown a direct interaction between HCV non-structural proteins and the autophagic machinery, in particular NS4B with Vps34 (Su et al., 2011) and NS5B with Atg5 (Guévin et al., 2010). Unfortunately, previous attempts within the lab (co-immunoprecipitation studies conducted by Bjorn-Patrick Mohl) have failed to provide any biochemical evidence in support of a direct interaction between HCV proteins and DFCP1. Nonetheless, the live cell imaging would suggest that any interaction or association between the HCV non-structural proteins and DFCP1 would be short-lived. Therefore, biochemical investigations that enable detection of transient interactions, such as protein crosslinking (Yakovlev, 2009; Yang et al., 2010) and label transfer approaches (Horney et al., 2001; Lapinsky and Johnson, 2015), are better suited to addressing if there is a direct interaction between HCV and DFCP1.

Finally, the roles of another PI3P effector downstream of PI3K in autophagosome formation, WIPI2b were investigated. Of particular note is the recent report of a direct association between WIPI2b and Atg16L1 (Dooley et al., 2014) therein linking the production of PI3P with the lipidation of LC3, a key step in the formation of autophagosomes. The results so far suggest that although viable, the expression levels of the GFP-WIPI2b from the expression construct require fine tuning to reproducibly observe omegasomes by fluorescence microscopy. Unfortunately due to time restrictions of this project work into this area is ongoing, with efforts towards selecting a stable cell line expressing GFP-WIPI2b at levels suitable for future experimentation.

The manipulation and subversion of autophagy is a well-documented phenotype for multiple viral infections. A noteworthy example is that of poliovirus which produces autophagosome-like vesicles to serve as a scaffold for RNA replication (Taylor and Kirkegaard, 2007). Additionally a more recent study identified the nsp6 protein from coronaviruses and the nsp5-7 protein from arterivirus recruiting Vps34 and DFCP1 to the ER resulting in omegasome formation (Cottam et al., 2011). Furthermore, a closely related virus to HCV, Dengue virus, has been shown to replicate and translate on amphisomes which arise from the fusion of autophagosomes with endosomes (Lee et al., 2008; Panyasrivanit et al., 2009). However, the final

membrane architecture of these structures is distinct from HCV (Welsch et al., 2009).

All together these results are in agreement with a model of the HCV replication complex formation requiring and utilising the cellular process of autophagy. The HCV non-structural proteins, shortly after translation on the ER, likely associate with the omegasome nucleation machinery, in particular the class III PI3K Vps34 (Figure 5.7). The subsequent production of PI3P recruits DFCP1, possibly WIPI2b — although not confirmed, leading to LC3 lipidation and phagophore expansion. During this process the non-structural proteins form replication complexes in the developing DMV, eventually resulting in full autophagosome production. By a yet unknown method, autophagosomes containing HCV non-structural proteins are diverted away from degradation by lysosome fusion, lose their lipidated LC3 (Sir et al. 2012 observe colocalisation of NS5A and NS5B with LC3, whereas no such colocalisation has been observed previously by our lab Mohl et al. 2012), and become dedicated HCV DMVs within the membranous web.

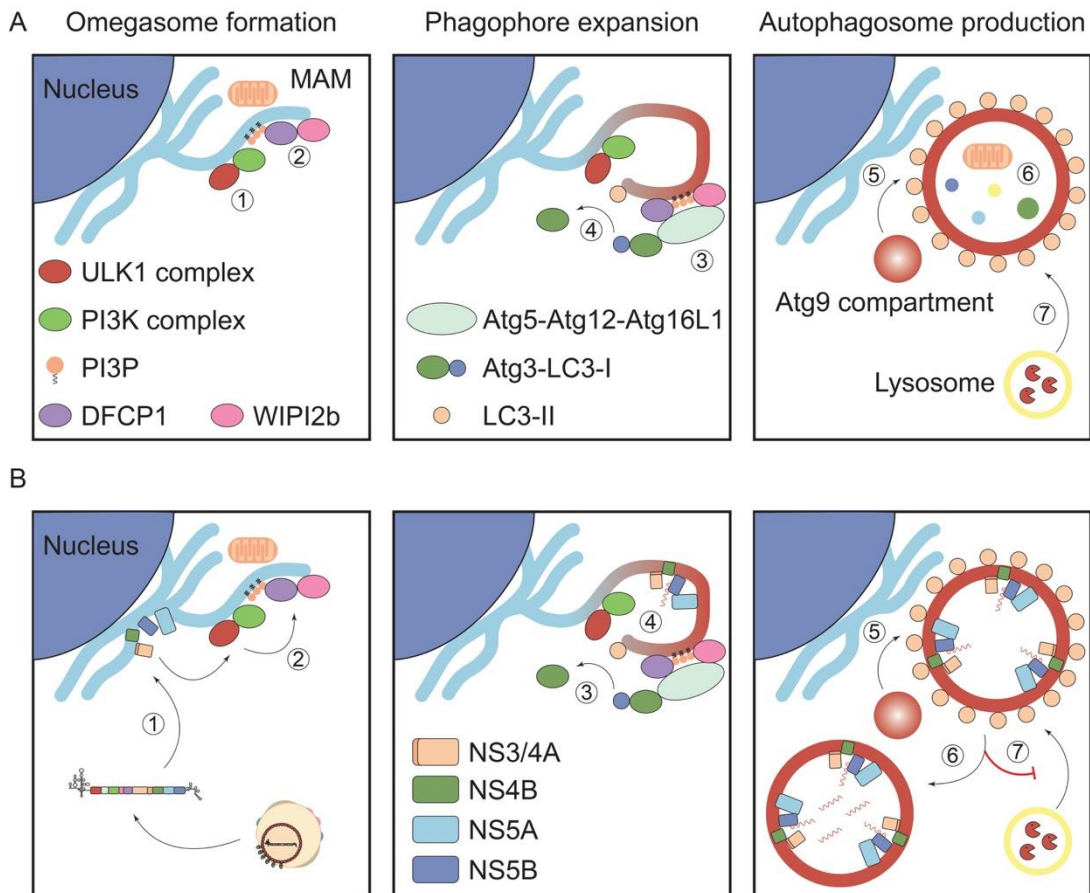


Figure 5.7: Model of HCV replication complex formation using the autophagosome biogenesis pathway.

A: autophagosome biogenesis within cells. 1) ULK1 and PI3K complexes recruited to curved mitochondrial-associated ER membranes (MAM). 2) DFCP1 and WIPI2b recruitment to PI3P-rich membrane. 3) Recruitment of Atg5-Atg12-Atg16L1 complex and Atg3-LC3-I. 4) Lipidation of LC3-I onto phosphatidylethanolamine producing LC3-II. 5) Phagophore membrane expansion from Atg9 containing vesicles. 6) Engulfment of cytoplasmic contents and autophagosome closure. 7) Fusion with lysosomes for degradation.

Chapter 6 - Developing fluorescence microscopy tools to study HCV infection

6.1 Aims and Objectives

Fluorescence microscopy has become a powerful and widely used technique in the study of biological processes. The development of strategies to fluorescently label particular targets, typically with antibodies or fluorescent proteins, has enabled a direct visualisation of cellular processes (Stadler et al., 2013). This ultimately leads to a better understanding of target localisation, interaction partners, signalling pathways and more.

Several strategies exist to label proteins and RNA in cells, as discussed below. The main goal of the research in this chapter was to develop a range of novel tools to visualise HCV protein and RNA in cells.

Part I focusses on methods to label HCV non-structural proteins through either genetic incorporation of fusion proteins as reporters, or the selection of non-antibody binding proteins to the HCV polymerase.

Part II discusses the incorporation of a modified nucleotide into HCV RNA to monitor the localisation of actively replicating HCV RNA in cells.

6.3 Part I – Detection of HCV non-structural proteins

6.3.1 Fusion proteins as reporters on protein localisation

The genetic incorporation of fluorescent proteins (FPs) and epitope tags into target proteins has become a routine approach for protein detection, particularly in the study of proteins in living cells or when antibodies to the endogenous protein are unavailable. This was first demonstrated using the green fluorescent protein (GFP) derived from the jellyfish *Aequorea victoria* (Chalfie et al., 1994). However, because of its size (238 amino acids) this can result in aberrant or defective protein function and localisation within cells (Margolin, 2012). In addition, viruses have compressed genomes which can encode multi-functional proteins or overlapping open reading frames (Belshaw et al., 2007). Alternatively, small epitope tags, such as the FLAG tag (Hopp et al., 1988), require less sequence space to encode, but require subsequent detection with antibodies. The use of larger tags such as FPs (e.g. GFP ~27 kDa) are more problematic as the size and shape may interfere with the native protein structure or function (Snapp, 2005).

More recently, the tetracysteine (TC) tag, a six residue natural amino acid sequence was developed (Griffin et al., 1998). Tetracysteine tags are small peptide sequences that fold into a hairpin structure and bind fluorescent arsenical derivatives (Griffin et al., 1998). Since its first description, additional modifications have been made to improve its binding properties, and its size has increased to 12 amino acids (Adams et al., 2002; Martin et al., 2005). The tetracysteine tag has been reported functional in a number of proteins at the N or C terminus and as an internal protein tag (Andresen et al., 2004; Counihan et al., 2011; Eyre et al., 2014). Protein in live cells can be labelled by adding the dye to cells, which is taken up and binds to the TC tag, allowing the labelled protein to be imaged. The small size of the tag also makes it attractive for super-resolution microscopy (Lelek et al., 2012). An additional benefit is the absence of fluorescence from the arsenical derivative until it binds to the TC tag (Griffin et al., 1998).

The study of many important virus infections has been facilitated by the TC tag. These include the investigation of HCV core and NS5A protein trafficking in cells during infection (Coller et al., 2012; Counihan et al., 2011; Eyre et al., 2014). Epitope tag incorporation has proven successful for other HCV proteins, including E2 (Eggert et al., 2014), p7 (Vieyres et al., 2013), NS2 (Stapleford and Lindenbach, 2011) and NS4B (Paul et al., 2013). However, there is a distinct lack of functional fusion proteins for NS3 and NS5B. Protein expression constructs for NS3 and

NS5B with GFP or FLAG tags are reported (Chatel-Chaix et al., 2011; Wu et al., 2008), however these are expressed outside the natural NS3–5B polyprotein.

Transposon mutagenesis studies can probe the ability of protein domains to tolerate tag insertions. Recent reports of transposon insertions into the HCV genome have revealed areas considered non-essential for protein function, defined by their ability to tolerate small 15 nucleotide insertions (Arumugaswami et al., 2008; Remenyi et al., 2014). The findings from these studies indicate that epitope tags may be tolerated at insertion sites between amino acids 1023–1035 (N-terminus of NS3), and 3010–3016 (before the C-terminal transmembrane domain of NS5B) (Figure 6.1); amino acid numbering corresponds to the JFH-1 genome sequence.

Thus it should be possible to use this information to generate and characterise NS3 and NS5B TC tagged constructs (Sections 6.4.1 and 6.5.1).

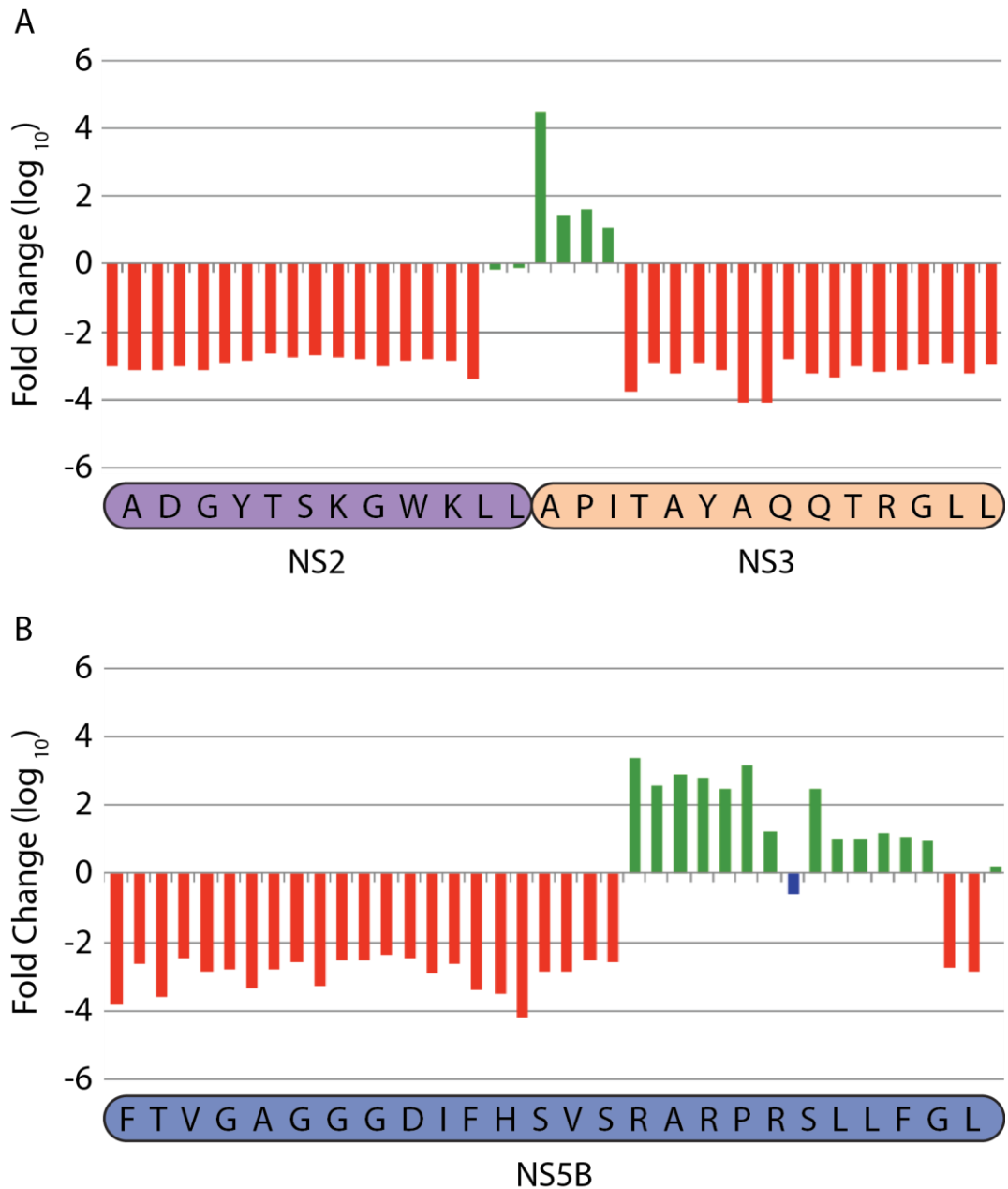


Figure 6.1: Tetracysteine tag cloning sites identified from transposon mutagenesis studies.

A: Transposon insertion sites in sub-region of NS2–3 coding sequence.
 B: Transposon insertion sites in sub-region of NS5B coding sequence. Schematic of HCV region is shown below each graph with amino acid sequence. Lethal, attenuated and tolerated phenotypes are shown as red, blue and green bars respectively. Adapted from (Arumugaswami et al., 2008).

6.3.2 Non-antibody binding reagents

Antibodies are the most widely used binding proteins, with applications in research, diagnosis and therapy. Nonetheless, they have a number of limitations. They require inoculation of animals with a target protein for their generation and are large multimeric proteins (~150 kDa) that require disulphide bonds for stability. With regard to super-resolution microscopy, the size of antibodies is another consideration as they position the detected fluorophore around 10 nm away from the intended target. In comparison, other labelling methods such as nanobodies (Ries et al., 2012), aptamers (de Castro et al., 2016), or non-antibody binding proteins (Tiede et al., 2014), are attractive alternatives due to their small size and alternative selection procedures.

Nanobodies are a variable single-domain antibody, composed of homodimeric heavy-chains without light chains (Muyldermans, 2013). As such they have comparable binding properties to conventional antibodies but are much smaller in size, ~15 kDa (Figure 6.2). This makes them attractive candidates for super-resolution imaging, over antibodies, due to the closer positioning of the detected fluorophore to the target (Platonova et al., 2015; Pleiner et al., 2015; Ries et al., 2012). However, they still require the inoculation of animals for their generation. In particular, nanobodies are only produced by a small number of animals, namely Tylopoda (camels, dromedaries and llamas) and sharks (Flajnik et al., 2011).

Aptamers are short oligonucleotide sequences that are engineered to bind a target ligand. They are identified from a library of sequences using the systematic evolution of ligands by exponential enrichment (SELEX), an *in vitro* selection technique (Ellington and Szostak, 1990; Oliphant et al., 1989; Tuerk and Gold, 1990). Aptamers are much smaller than antibodies (~15 kDa; Figure 6.2) (Lupold et al., 2002; Wilner et al., 2012) and therefore have been exploited for super-resolution imaging studies (de Castro et al., 2016; Opazo et al., 2012).

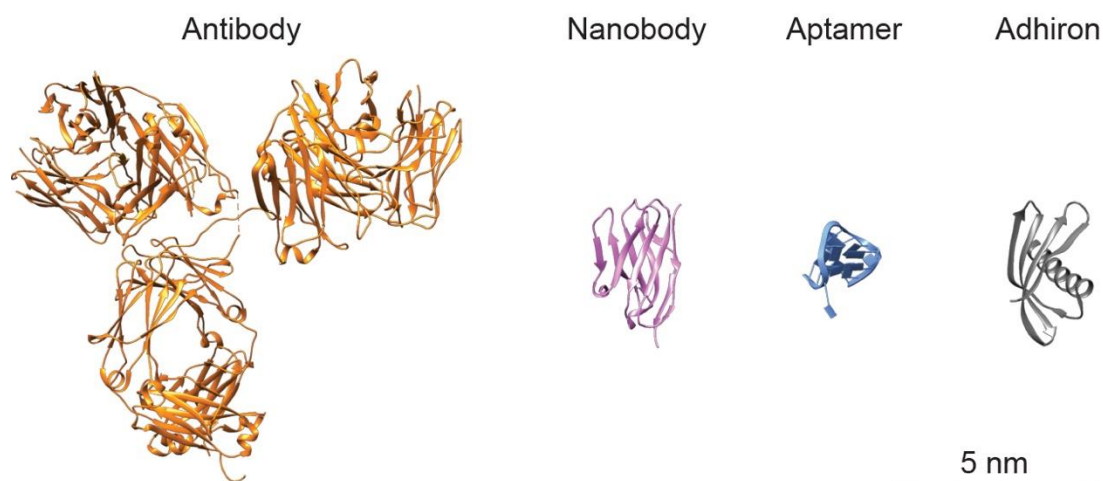


Figure 6.2: Size comparison between protein binding molecules.

Crystal structures of an antibody (orange), nanobody (pink), aptamer (blue) and Adhiron (grey). PDB ID no.'s: 1HZH, 3K1K, 3QLP, 4N6T respectively. Images are displayed to scale.

The selection of aptamers to HCV is well documented with targets including core (Shi et al., 2014; Stewart et al., 2016), both envelope proteins (Chen et al., 2015; Yang et al., 2013), the non-structural proteins NS2 (Gao et al., 2014), NS3 (Fukuda et al., 2000), NS5A (X. Yu et al., 2014), NS5B (Lee et al., 2013), and the HCV IRES (Kikuchi et al., 2003). Although these studies were focused on the applications of aptamers as therapeutic agents, they exemplify the ability of selection techniques to identify unique and specific binders to particular targets. However, to our knowledge, no selection of non-antibody binding proteins has been conducted towards HCV proteins.

Non-antibody binding proteins have been generated from a range of different scaffolds, and inserted variable peptide sequences within these proteins are designed to recognise specific ligands. Some of these include designed ankyrin repeat proteins (Binz et al., 2003), reprobodies (Lee et al., 2012), anticalins (Schlehuber and Skerra, 2005), fibronectins (Koide et al., 1998), affibodies (Nord et al., 1995) and engineered Kunitz domains (Nixon and Wood, 2006). Recently, a novel scaffold, termed the Adhiron (or affimer), has been characterised at the University of Leeds (Tiede et al., 2014).

The Adhiron scaffold is derived from plant cysteine protease inhibitors called phytocystatins (Kondo et al., 1991), which are small (~100 amino acid), monomeric proteins with high solubility and stability. In place of the inhibitory sequences, two

variable 9 amino acid loops have been inserted resulting in a library of potential non-antibody binding proteins from 1.3×10^{10} clones (Tiede et al., 2014). Specific and high affinity binders to a target protein can be selected by screening the Adhiron library against an immobilised target (Figure 6.3). Once identified, binders can be expressed and purified to high levels in bacteria and specifically labelled by modification of unique cysteines engineered into the scaffold backbone — for example, fluorophore conjugation using a maleimide derivative. Therefore Adhiron provide an excellent alternative to antibodies for protein detection.

Given the various potential approaches to derive novel binders to NS5B, and the expertise at Leeds, we have therefore attempted to raise Adhiron to NS5B (Section 6.5.4) for use in fluorescent labelling. Although our lab has previously produced a polyclonal antiserum against NS5B, this serum recognises non-specific cellular proteins by western blot and immunofluorescence. Thus, the generation of Adhiron to NS5B would be a useful tool to investigate the localisation of this protein in cells.

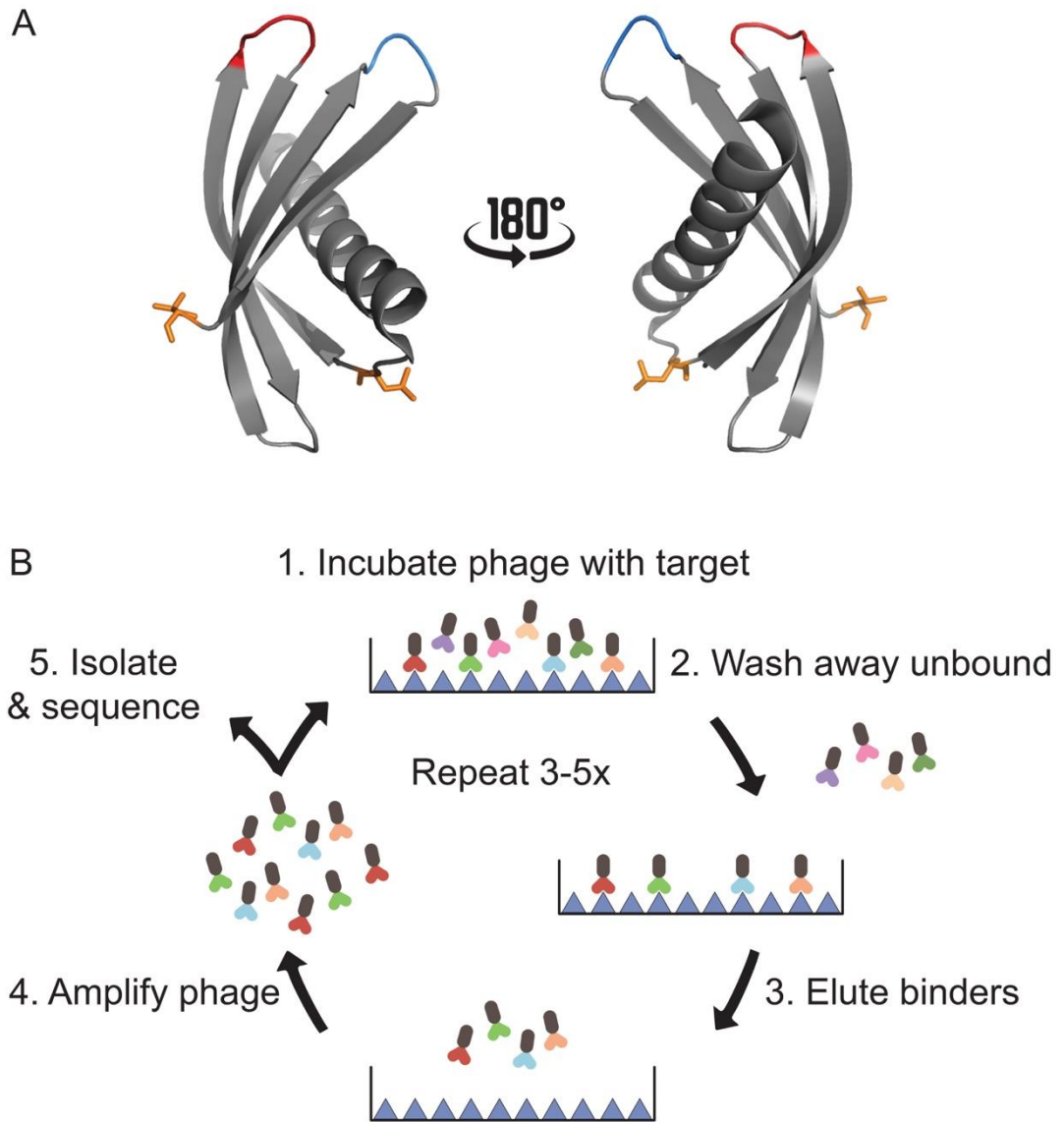


Figure 6.3: Adhiron scaffold and phage display procedure.

A: Crystal structure (PDB ID no. 4N6T) of Adhiron scaffold in grey. Variable loops 1 and 2 are coloured red and blue respectively. Residues in scaffold modified to cysteines for site specific labelling in orange. B: Phage display screening procedure. 1) Phage library incubated with target protein. 2) Unbound phage washed away 3) Elution of Adhiron binders. 4) Eluted phage amplified and re-incubated with target in further panning rounds. 5) After 3–5 selection rounds, eluted phage isolated and sequenced.

6.4 Part I – Cloning strategies

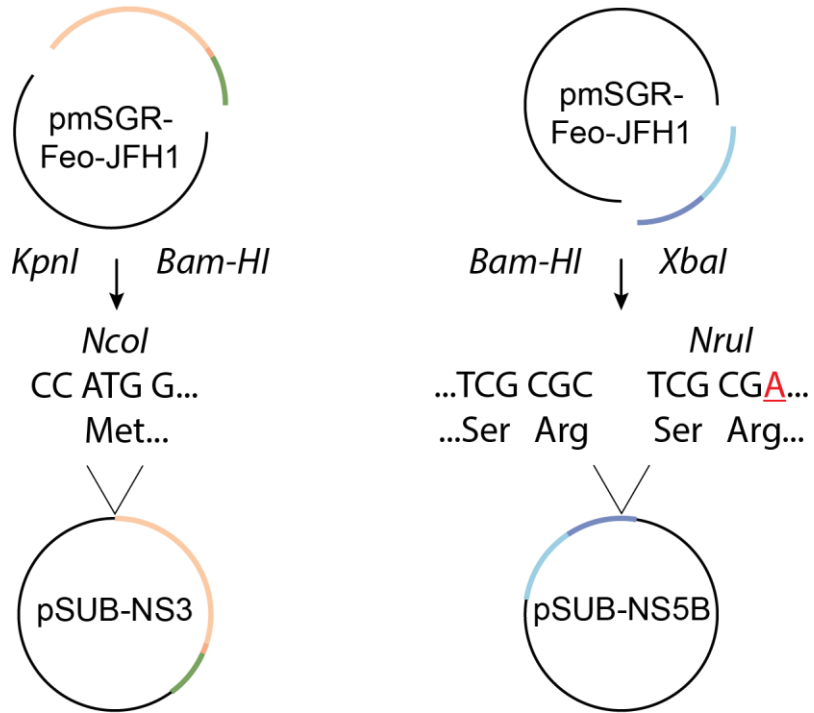
6.4.1 Tetracysteine tag cloning into NS3 and NS5B

To facilitate our investigations on the structure and architecture of the HCV replication complex, the TC tag was engineered into both NS3 and NS5B. In each case a sub-clone containing either the NS3 or NS5B coding region was generated, termed pSUB-NS3 and pSUB-NS5B respectively (Figure 6.4A). pSUB-NS3 contains a single copy of the *NcoI* restriction enzyme site at the N-terminus of NS3. Using site-directed mutagenesis, a unique restriction site was introduced into the NS5B coding region within pSUB-NS5B. The single nucleotide mutation, C to A, created an *NruI* restriction enzyme site within NS5B without altering the protein coding sequence, termed NS5B [*NruI*]. This internal restriction enzyme site is immediately prior to the C-terminal transmembrane domain of NS5B.

To introduce the TC tag into either NS3 or NS5B, each target gene was amplified by PCR with primers containing the optimised TC tag (FLNCCPGCCMEP; Appendix 1) (Figure 6.4B). PCR products were then cloned into pSUB-NS3 or pSUB-NS5B using the unique restriction enzyme sites. To characterise the fitness of these TC-tagged proteins during HCV replication, each was cloned into SGR-Feo-JFH1 to monitor luciferase expression as an indirect measure of sub-genomic replicon replication; SGR-Feo-JFH1 [NS3-TC] and SGR-Feo-JFH1 [NS5B-TC] respectively. The introduction of *NruI* into NS5B did not alter the protein coding sequence; however it is possible that RNA interactions required for HCV replication are altered by this modification. Therefore an NS5B SGR containing *NruI* was created to determine the consequence of this RNA modification, termed SGR-Feo-JFH1 [*NruI*].

All constructs were confirmed by analytical digest and Sanger sequencing.

A



B

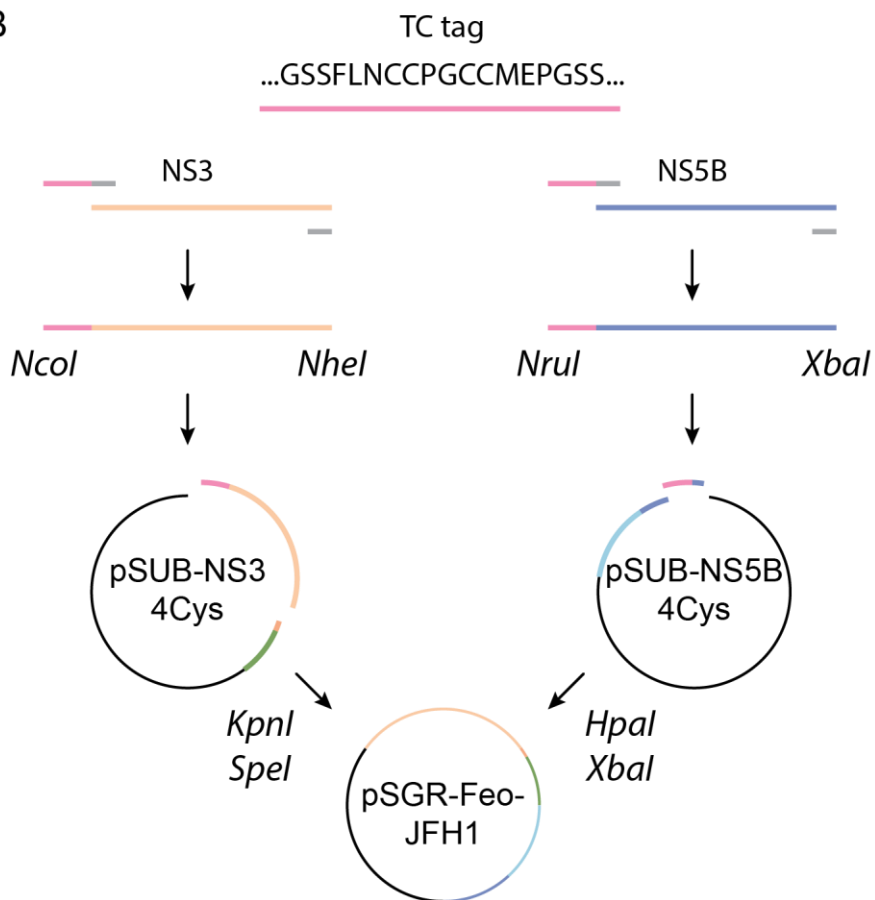


Figure 6.4: NS3 and NS5B tetracysteine tag cloning strategies.

A: Generation of sub-clones containing unique restriction sites from NS3–4B and NS5A–5B regions. pmSGR was digested with either *KpnI* and *BamHI* or *BamHI* and *XbaI* before ligation into pLITMUS28i with the corresponding restriction sites to generate pSUB-NS3 and pSUB-NS5B respectively. pSUB-NS3 contains the unique restriction site *NcoI* for TC tag insertion into NS3. pSUB-NS5B was modified by site-directed mutagenesis to introduce the unique restriction site *NruI* into NS5B, without altering the protein coding sequence. B: Introduction of the TC tag into NS3 and NS5B. Optimised TC tag sequence, including flexible linker regions on either end (pink), was introduced into NS3 and NS5B sequences using PCR (Appendix 1). The resultant PCR fragments were cloned into pSUB-NS3 or pSUB-NS5B using *NcoI* and *NheI* or *NruI* and *XbaI* respectively. Tagged protein constructs were then cloned into pmSGR using *KpnI* and *SpeI* or *HpaI* and *XbaI* for NS3 and NS5B respectively. Coding sequences for NS3, NS4B, NS5A and NS5B in yellow, green, light blue and dark blue, respectively.

6.4.2 NS5B Δ C21 expression construct

In order to select Adhirons against NS5B, a C-terminal hexa-histidine affinity tagged expression construct was purified from *E. coli* (Simister et al., 2009) (Section 3.4.2). A corresponding expression construct, containing a defective polymerase active site (GDD to GND), was engineered by replacing the *NcoI* and *AscI* gene fragment from the expression construct with the corresponding fragment from SGR-Feo-JFH1 [GND].

6.4.3 Cloning of Adhiron expression constructs

To express, purify and fluorescently label Adhirons, sequences were PCR amplified and cloned into pET11b with a C-terminal hexa-histidine tag (Figure 6.5). A two-step PCR process was conducted with Adhiron primers 1–4 (Appendix 1), generating 2 PCR products. This introduced two cysteines into the Adhiron backbone, first a substitution of leucine 26, and secondly the addition of a cysteine prior to the hexa-histidine tag at the C-terminus. The two PCR fragments were then combined and amplified using SOE PCR, before ligation into pET11b. All constructs were confirmed by restriction digestion and Sanger sequencing.

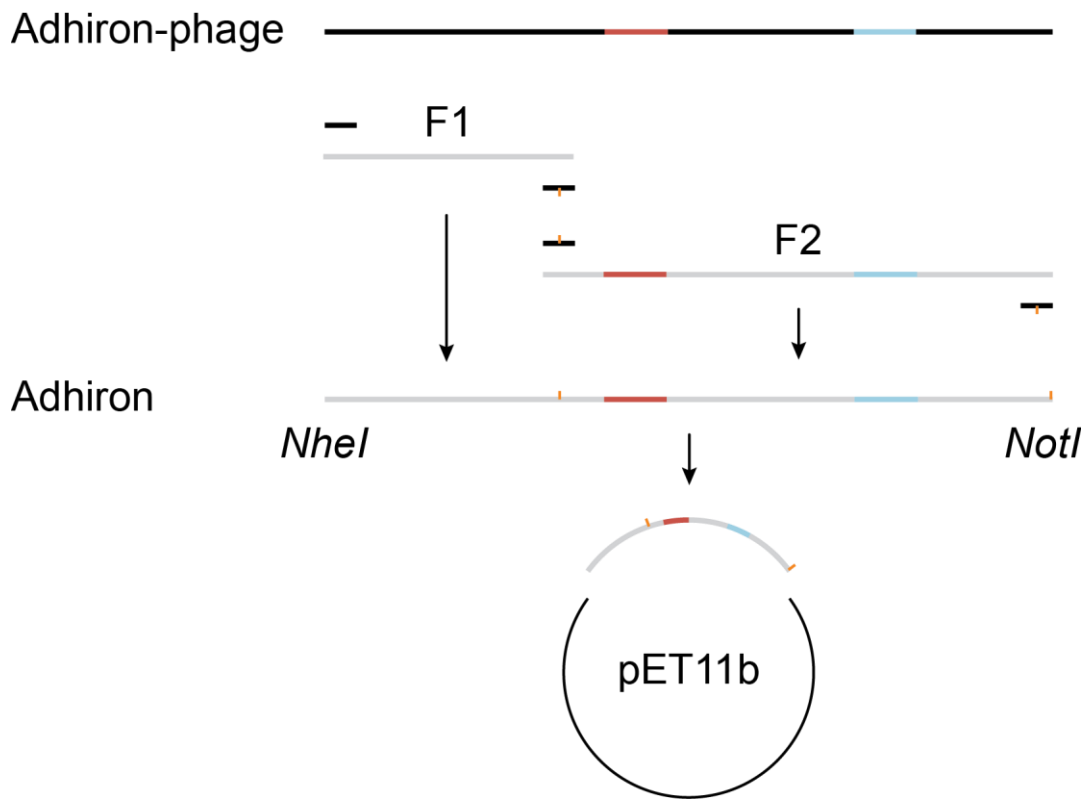


Figure 6.5: Adhiron cloning strategy.

Adhiron sequences were amplified by PCR in two fragments (F1 and F2), simultaneously introducing cysteines (orange) into Adhiron backbone (Appendix 1). PCR products were then combined by splice overlap extension PCR to yield full Adhiron sequence containing unique restriction sites and modified cysteine residues. Final PCR product was subsequently cloned into pET11b using *NheI* and *NotI* restriction sites.

6.5 Part I – Results

6.5.1 Replicative fitness of TC-tagged SGRs

Introducing the TC-tag affected the replication fitness of HCV SGR (Figure 6.6). Luciferase expression levels from SGRs correlate with HCV RNA copy numbers, and therefore provide a measure of HCV replication fitness (Krieger et al., 2001). While luciferase signal was observed 4 h.p.e. of the RNA for the control SGR-Feo-JFH1, neither SGR-Feo-JFH1 [NS3-TC] nor SGR-Feo-JFH1 [NS5B-TC] showed any increase in luciferase signal for up to 72 h.p.e. Their replication kinetics were thus similar to the polymerase deficient control SGR-Feo-JFH1 [GND] for which no increase in luciferase was observed at 48 and 72 h.p.e.

The selection of HuH7 cells stably expressing TC-tagged SGRs also proved unsuccessful (data not shown). Due to the limited number of viable insertion sites identified by transposon mutagenesis studies, no additional investigations exploiting the introduction of reporters were conducted. Instead the selection of Adhirons to NS5B was explored.

6.5.2 Expression and purification of NS5B Δ C21

To screen the Adhiron library against the HCV polymerase, NS5B was expressed and purified from *E. coli* using an expression construct containing a 21 amino acid deletion at the C-terminus, termed NS5B Δ C21 (Simister et al., 2009). The polymerase fold of NS5B was shown previously to be unaffected by the transmembrane domain deletion by crystallography and *in vitro* polymerase activity assays (Simister et al., 2009).

Fractions collected from NS5B Δ C21 expression and purification were analysed by SDS-PAGE (Figure 6.7A and B). Lysates from IPTG induced bacteria contained an abundant protein band with an apparent molecular weight around 58 kDa (ExpASY Protparam predicted molecular weight of 64.2 kDa), which was insoluble under initial lysis conditions (Figure 6.7A and B, lanes 1–3), consistent with previous studies (Simister et al., 2009). Resuspension and sonication of the lysate pellet yielded soluble NS5B (lane 4) which was then bound to Ni²⁺-charged Sepharose. However, a significant portion of expressed NS5B remained insoluble after this step (lane 5). After washing of immobilised NS5B, protein was eluted (lane 11).

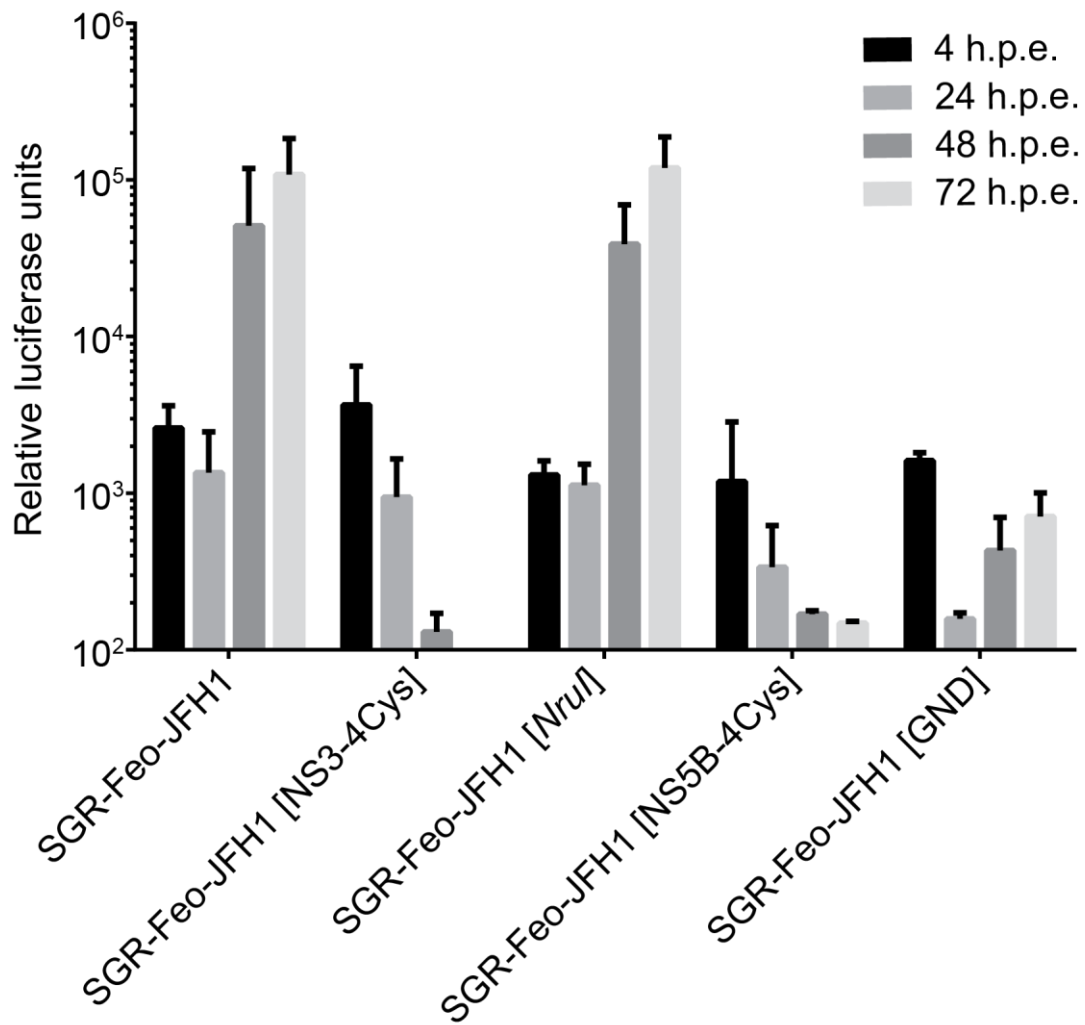


Figure 6.6: Replication of TC-tagged SGR constructs.

Luciferase reporter values were measured up to 72 h.p.e. from transient electroporation (Section 3.5.2) of 5 μ g SGR RNA into HuH7 cells. Comparison of TC tagged constructs to wildtype and polymerase deficient (GND) SGR controls. Data represent the mean \pm SD, n=3.

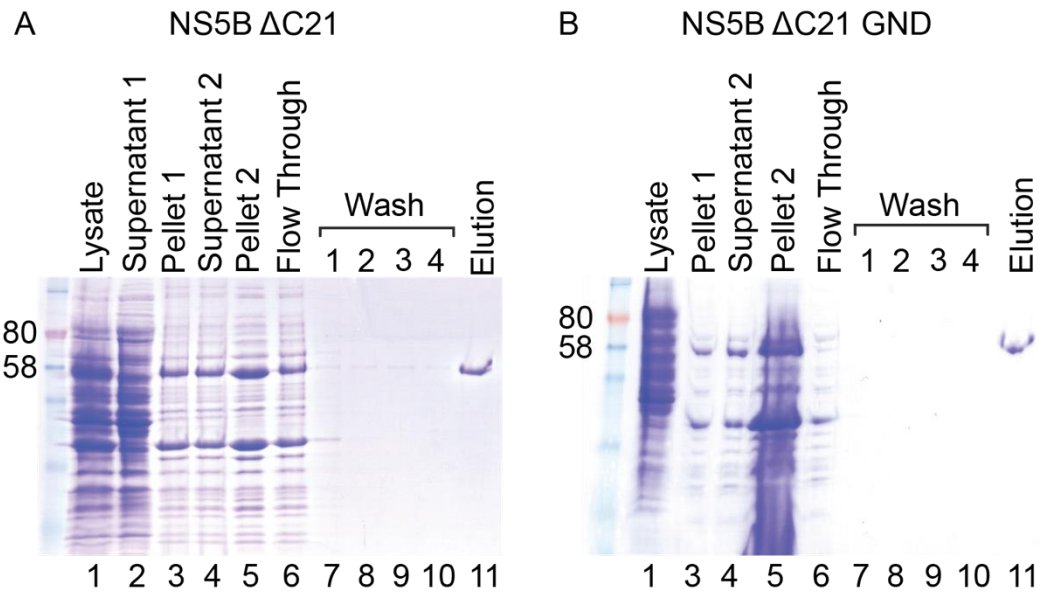


Figure 6.7: NS5B Δ C21 protein purification.

A: Coomassie stain of SDS-PAGE analysis from Ni^{2+} -affinity purification of NS5B Δ C21 (Section 3.4.2). Induced cell pellets were lysed (lane 1) and insoluble material pelleted (lanes 2–3). Insoluble pellet was re-suspended and sonicated to solubilise NS5B Δ C21 (lanes 4–5). Soluble NS5B Δ C21 was loaded onto Ni^{2+} charged resin (lane 6). Bound NS5B Δ C21 was washed in buffer containing 50 mM imidazole (lanes 7–10) before elution in buffer containing 250 mM imidazole (lane 11).

B: NS5B Δ C21 GND was purified as in A. Molecular weight markers in kDa are indicated.

6.5.3 Purified NS5B Δ C21 exhibits polymerase activity

The identity of purified NS5B Δ C21 was confirmed by western blotting using the in house anti-NS5B polyclonal serum (Figure 6.8A). Protein bands were detected by NS5B serum and control antibody (anti-hexa-histidine tag) at the predicted molecular weight.

NS5B Δ C21 purified from *E. coli* displayed polymerase activity confirming the purification of correctly folded and functional protein (Figure 6.8B). The polymerase activity was measured by incorporation of [α -³²P]-CTP into HCV transcripts from *de novo* initiation by NS5B Δ C21. An approximately 20-fold increase in radioactivity was observed from transcripts derived from NS5B Δ C21 reactions over the polymerase deficient control. The low levels of radioactivity observed for NS5B Δ C21 [GND] represent background signal from transcript purification.

The selection of Adhirons that bind to and recognise NS5B in HCV infected cells requires a correctly folded target protein that displays native epitopes. Purified protein can often be incorrectly folded or inactive when expressed using *E. coli* (Khow and Suntrarachun, 2012). Fractions of purified, active polymerase were taken forward for screening against the Adhiron library to identify novel and specific high affinity binding proteins.

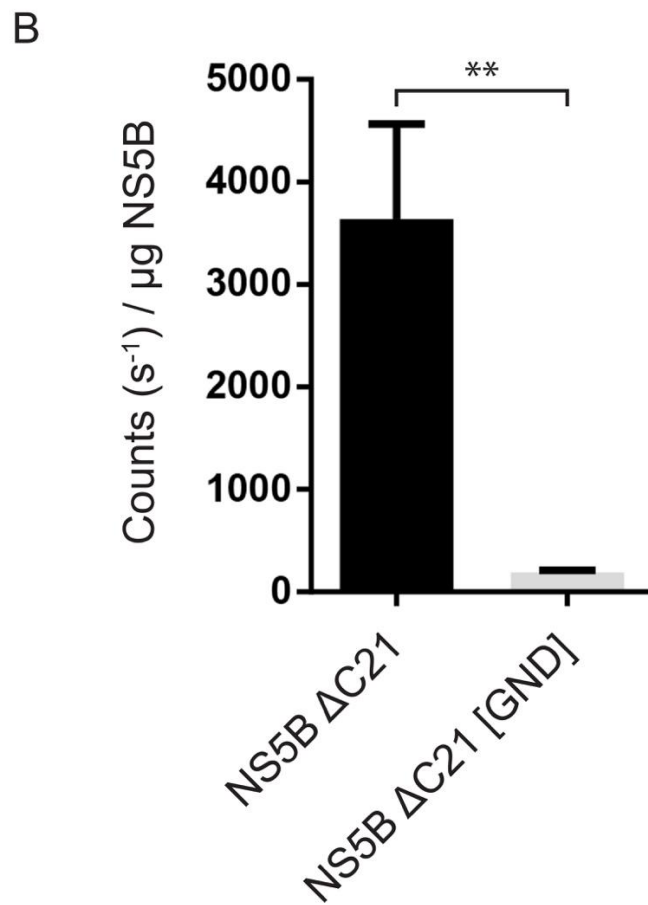
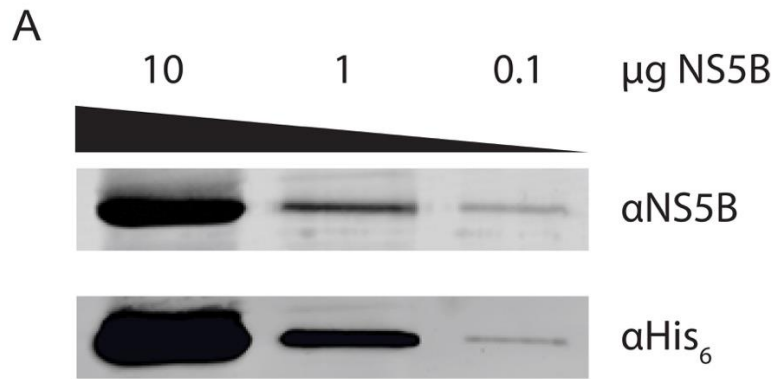


Figure 6.8: Purified NS5B ΔC21 is correctly folded and functional.

A: western blot analysis from SDS-PAGE of purified NS5B ΔC21. Quantity of pure protein per lane and antibody identity is indicated. B: Liquid scintillation counting of *in vitro* polymerase assay products. 150 nM of pure NS5B ΔC21, or GND mutant, were incubated with JFH1 [GND] template RNA in the presence of [α -³²P]-CTP. Incorporation of ³²P into HCV transcripts, after 1 h incubation, was measured from purified transcripts by liquid scintillation counting. Data represent mean \pm SD, n=3.

** $P < 0.005$.

6.5.4 Five Adhirons were identified from NS5B Δ C21 screening

After three selection rounds of the Adhiron library against NS5B Δ C21, seven Adhiron-phage were identified as potential binders from 32 colonies (Figure 6.9A). An arbitrary cut-off of 0.2 absorbance units was used to identify Adhiron binders, this corresponds to an approximately 4-fold increase in absorbance over the negative control. The increase in absorbance at 620 nm from the horseradish peroxidase reaction product indicates binding of Adhiron-phage to NS5B Δ C21.

Sequencing of the variable loops from the seven adhiron-phage identified five unique binders (Figure 6.9B). In two pairs of Adhirons, Adhirons 10 and 27 and Adhirons 16 and 17, the sequence of the variable loops were identical. Each of the five remaining Adhirons had unique variable loops with no apparent consensus sequence or common amino acid properties observed from the primary amino acid sequence.

Adhiron 28 had 11 amino acids in variable loop 1 compared to 9 in the remaining Adhirons (Figure 6.9B). The Adhiron library was constructed by splice overlap extension (SOE) of two PCR products (Horton et al., 1990; Tiede et al., 2014), creating two variable loops containing nine random amino acids. The longer loop in Adhiron 28 is most likely a result of miss-matched PCR product overlap or polymerase error during the Adhiron library construction and suggests that the phage library may be larger than first predicted, although how much larger is currently unknown (Tiede et al., 2014). Protein BLAST (Altschul et al., 1990) alignments were conducted using the adhiron variable loops against human and HCV proteins to identify potential NS5B interaction partners based on the Adhiron protein sequence (Espadaler et al., 2005), however no complete alignments were observed (data not shown).

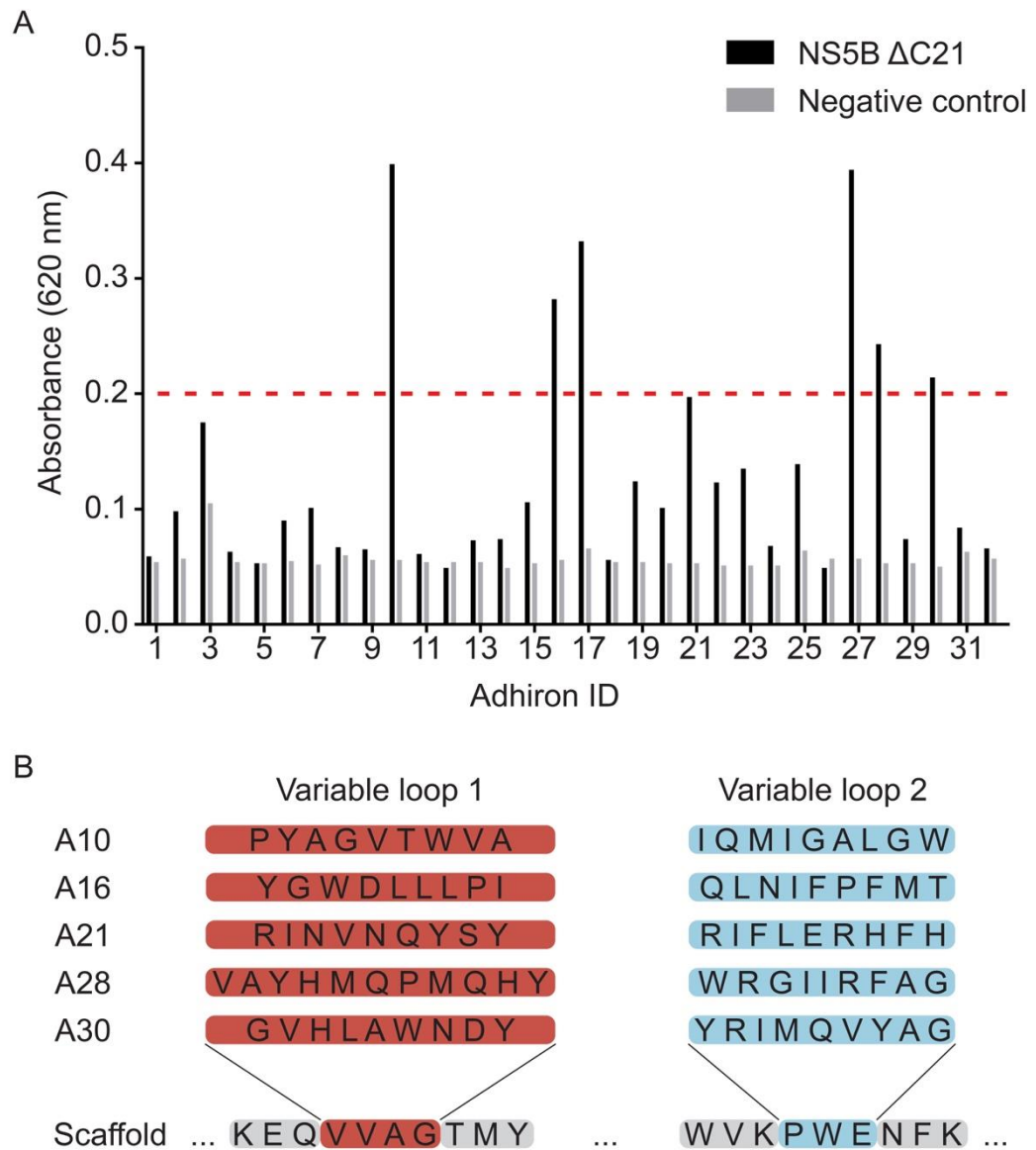


Figure 6.9: Adhirons identified from phage display screening against NS5B Δ C21.

A: Horseradish peroxidase based phage-ELISA. Isolated Adhiron-phage from the third selection round were incubated with target protein in a phage-ELISA. Horseradish peroxidase activity was measured by 620 nm absorbance of reaction product. Biotinylated, NS5B Δ C21 plasmid-deficient, BL21 (DE3) cell lysate was used as a negative control. Dashed red line indicates arbitrary cut-off of 0.2 absorbance units used in Adhiron selection. B: Amino acid sequence of variable loops from Adhirons identified as NS5B Δ C21 binders. Adhirons were screened and identified by the Leeds Adhiron BioScreening group (Section 3.4.4) (Tiede et al., 2014).

6.5.5 Expression and purification of Adhiron

Each of the five Adhiron identified from screening were expressed to high levels from *E. coli* (Figure 6.10). An abundant protein band with apparent molecular weight around 11 kDa, matching the expected molecular weight (Table 6.1), was observed from bacterial expression trials after IPTG induction.

Four of the five Adhiron were successfully purified using Ni²⁺-affinity purification (Figure 6.11 lanes 8–10). Purified Adhiron in elution fractions (lanes 8–10) contained little or no contaminants consistent with previous reports (Tiede et al., 2014). During the purification procedure, Adhiron 21 precipitated from solution after elution from the Ni²⁺-resin indicating protein aggregation or insolubility. The introduction of nine amino acid variable loops into a scaffold may cause self-interaction or destabilise the scaffold (Tiede, personal communication), therefore Adhiron 21 was no longer investigated and is discussed no further. The other four Adhiron had no observable precipitation and were taken forward for cysteine labelling.

Adhiron	Molecular weight (kDa)	Extinction coefficient ($M^{-1} cm^{-1}$)	Isoelectric point
A10	12.26	22585	7.13
A16	12.50	17085	6.75
A21	12.63	13075	8.53
A28	12.78	18575	8.53
A30	12.48	20065	7.16

Table 6.1: Properties of Adhiron as computed by the ExPASy ProtParam bioinformatics tool. Extinction coefficients presented are for Adhiron with reduced cysteines.

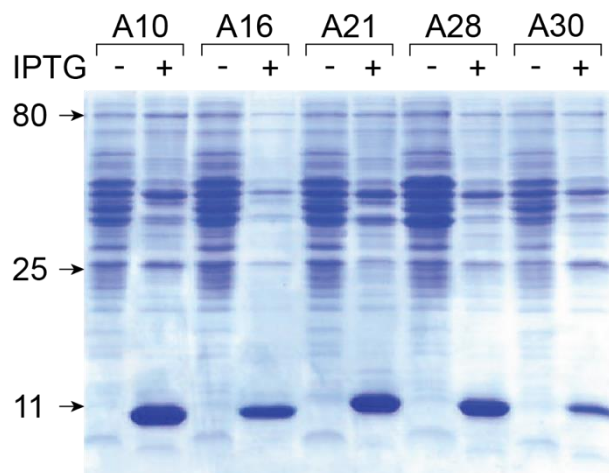


Figure 6.10: Expression of Adhiron from pET11b in BL21(DE3) cells.

Cells were grown to an OD_{600} of 0.6–0.8 at 37 °C before induction of expression using 0.1 mM IPTG for 4 h at RT. Pellets from uninduced (- lanes) or induced (+ lanes) cells were lysed and analysed by Coomassie stain of SDS-PAGE. Molecular weight markers in kDa are indicated.

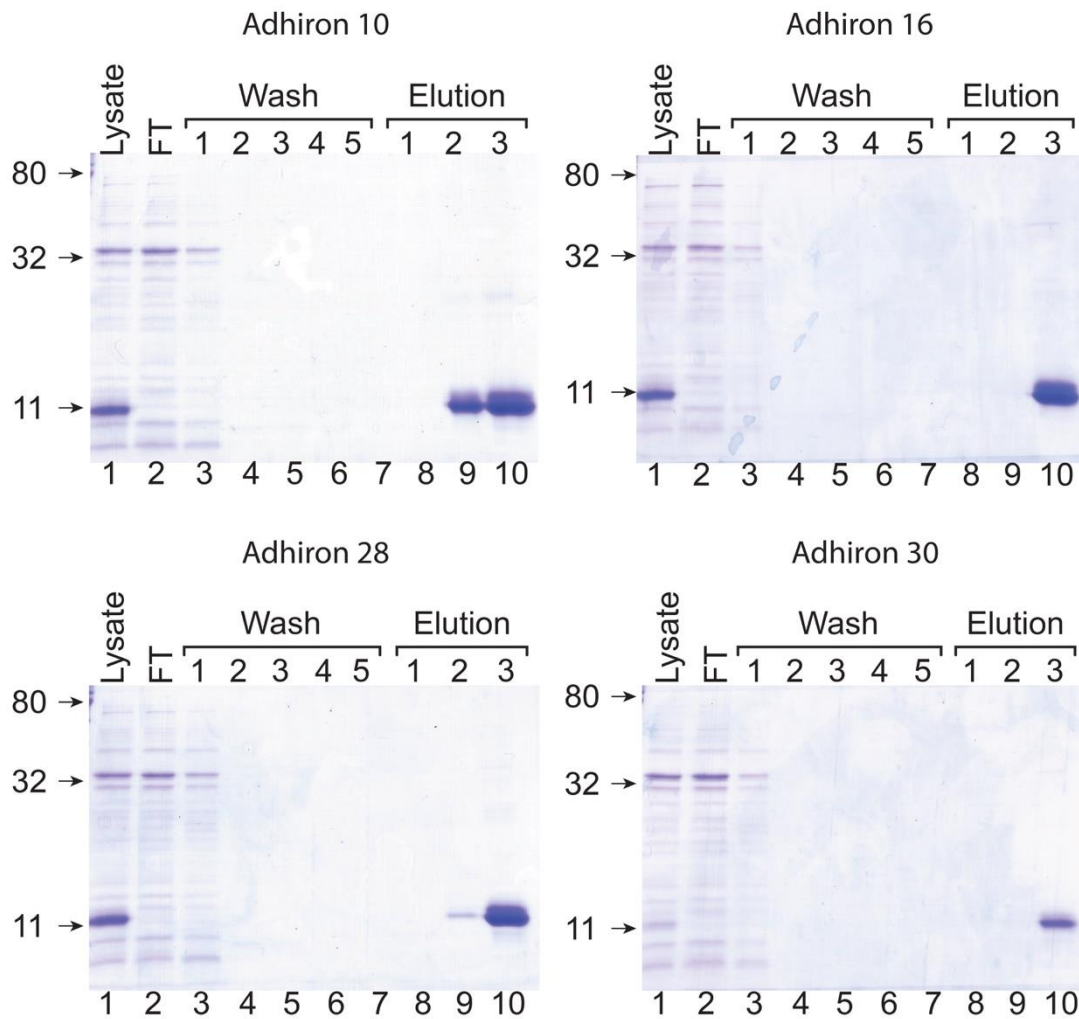


Figure 6.11: Adhiron purification fractions analysed by Coomassie stain of SDS-PAGE.

Adhiron expressed from BL21 DE3 cells were lysed (lane 1) and loaded onto Ni^{2+} -charged resin collecting flow through (FT; lane 2). Bound Adhiron were washed in buffer containing 100 mM imidazole (lanes 3–7) before elution in buffer containing 300 mM imidazole (lanes 8–10). Fractions from Ni^{2+} -affinity purification were analysed by SDS-PAGE. Molecular weight markers in kDa are indicated.

6.5.6 Adhirons were labelled with Alexa Fluor 647

Fluorescence imaging of Alexa 647-labelled Adhirons run on an SDS-PAGE gel confirmed that Alexa Fluor 647 had been conjugated to cysteines on the Adhiron scaffold (Figure 6.12). Western blot analysis with an antibody to the Adhiron hexa-histidine tag confirmed the identity of the Adhiron band. In some cases two closely resolved bands were observed, and is due to incomplete denaturation of the Adhiron stable protein fold before SDS-PAGE analysis (Christian Tiede, personal communication). Regardless, the presence of 647 nm fluorescent protein bands demonstrate successful labelling of purified Adhirons. Labelled Adhirons were taken forward to assess their binding and detection of NS5B in cells.

6.5.7 Purified Adhirons do not bind native NS5B

No fluorescence signal corresponding to NS5B was observed in cells stably harbouring SGR-Feo-JFH1 (Figure 6.13A). No observable 647 nm fluorescence signal was observed for Adhiron 28 or 30, in any cell which had high levels of NS5A expression (Figure 6.13A). In contrast a weak fluorescence signal was observed for Adhiron 10 and 16 in cells.

For Adhiron 10, this was mostly confined to the nucleus, a cellular compartment not occupied by HCV, and therefore likely represents cross-reactivity with cellular polymerases. This is supported by the observation that there is an identical weak fluorescence signal in replicon and virus naïve cells (Figure 6.13B). Additionally, in both replicon harbouring and naïve cells, a weak and diffuse signal was observed throughout the cytoplasm. However, this was significantly lower than signal observed with NS5A staining.

Adhiron 16 exhibited a similar weak fluorescence signal in the nucleus as found for Adhiron 10. However, it also stained discrete puncta or ring-like structures in the cytoplasm (Figure 6.13A). Ring structures are a reported phenotype for HCV core (Miyanari et al., 2007) and suggested that Adhiron 16 might be specifically detecting NS5B. However, comparable fluorescence structures were observed in the cytoplasm of naïve HuH7 cells (Figure 6.13B). Therefore, this is not a real phenotype and corresponds to non-specific binding of Adhiron 16 to a cellular structure, possibly proteins on, or the surface of lipid droplets directly.

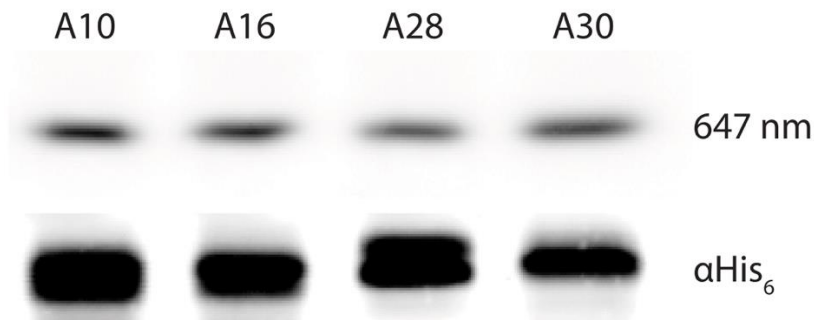


Figure 6.12: Alexa Fluor 647 labelling of Adhiron cysteines.

Adhiron cysteines were labelled by incubation with Alexa Fluor 647 C₂ maleimide for 16 h at RT in the dark following reduction of Adhiron cysteines using TCEP resin. SDS-PAGE analysis of labelled Adhiron was imaged for 647 nm fluorescence or by western blot using anti-hexa-histidine antibody.

Despite the observed binding of Adhiron to NS5B Δ C21 in the phage-ELISA (Figure 6.9), no fluorescence signal was detected by microscopy to native NS5B. SGR-Feo-JFH1 harbouring cells were analysed as they constitutively express NS5B to high levels as part of the NS3–5B polyprotein (Wyles et al., 2009). Expression of SGRs within cells was confirmed by immunofluorescence staining for NS5A, a marker for replication complexes.

Labelled Adhiron were also unable to detect purified NS5B Δ C21 blotted onto PVDF membranes (Figure 6.14A). For each membrane containing NS5B Δ C21, no fluorescence signal was detected when incubated with labelled Adhiron. The presence of NS5B was confirmed using the anti-NS5B polyclonal serum, and the quantity of Adhiron applied to detect NS5B was readily detected when applied directly to membranes (Figure 6.14B). Combined with the immunofluorescence, these experiments strongly indicate that none of the identified Adhiron from Section 6.5.4 are able to bind native NS5B.

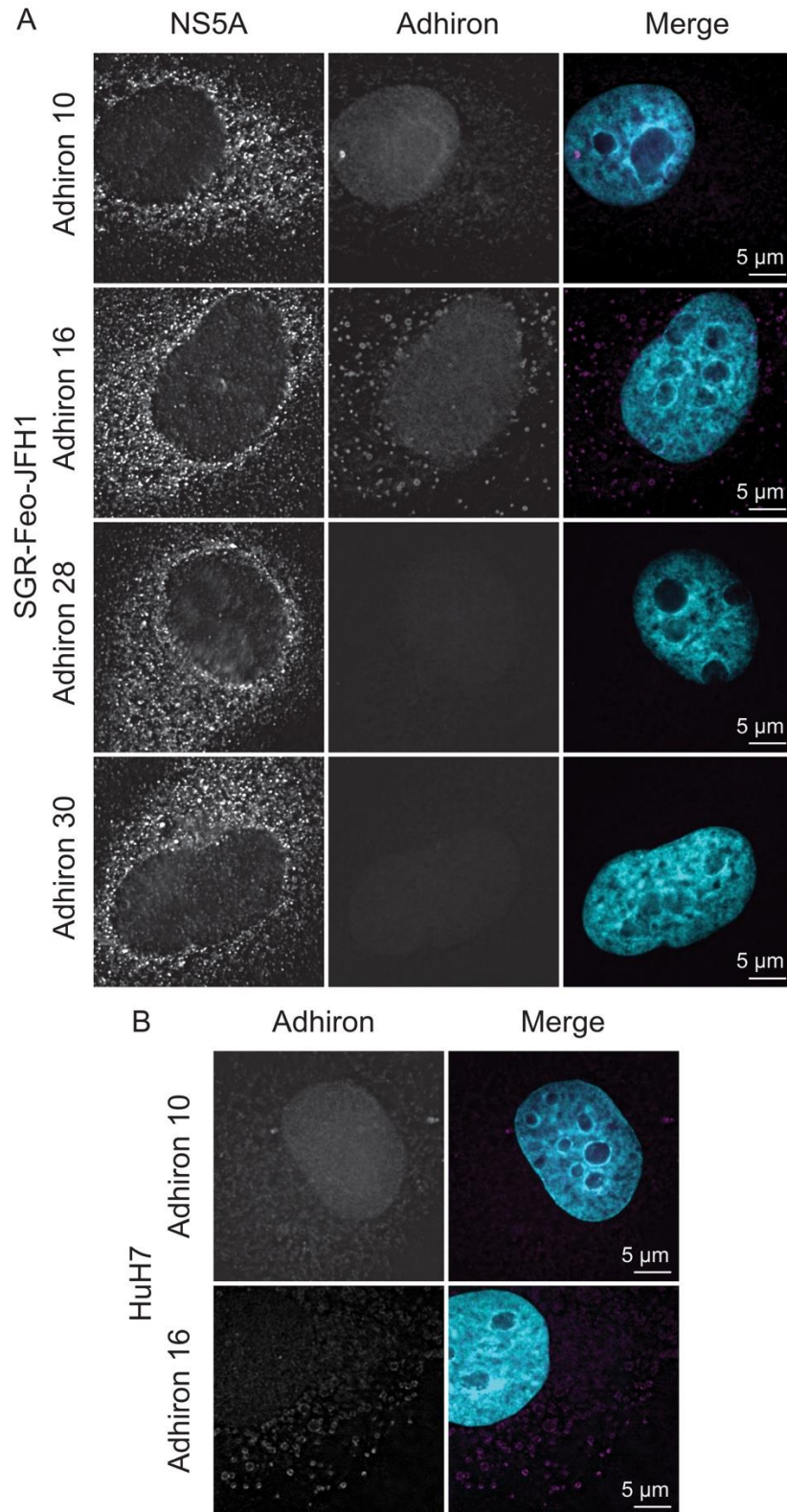


Figure 6.13: Validation of Adhiron as non-antibody binding proteins for fluorescence microscopy detection of NS5B.

A: HuH7.5 cells stably harbouring SGR-Feo-JFH1 were fixed and labelled with anti-NS5A antibody, 647-labelled Adhiron and DAPI. B: Naïve HuH7 cells were fixed and labelled as in A. Scale bars are indicated.

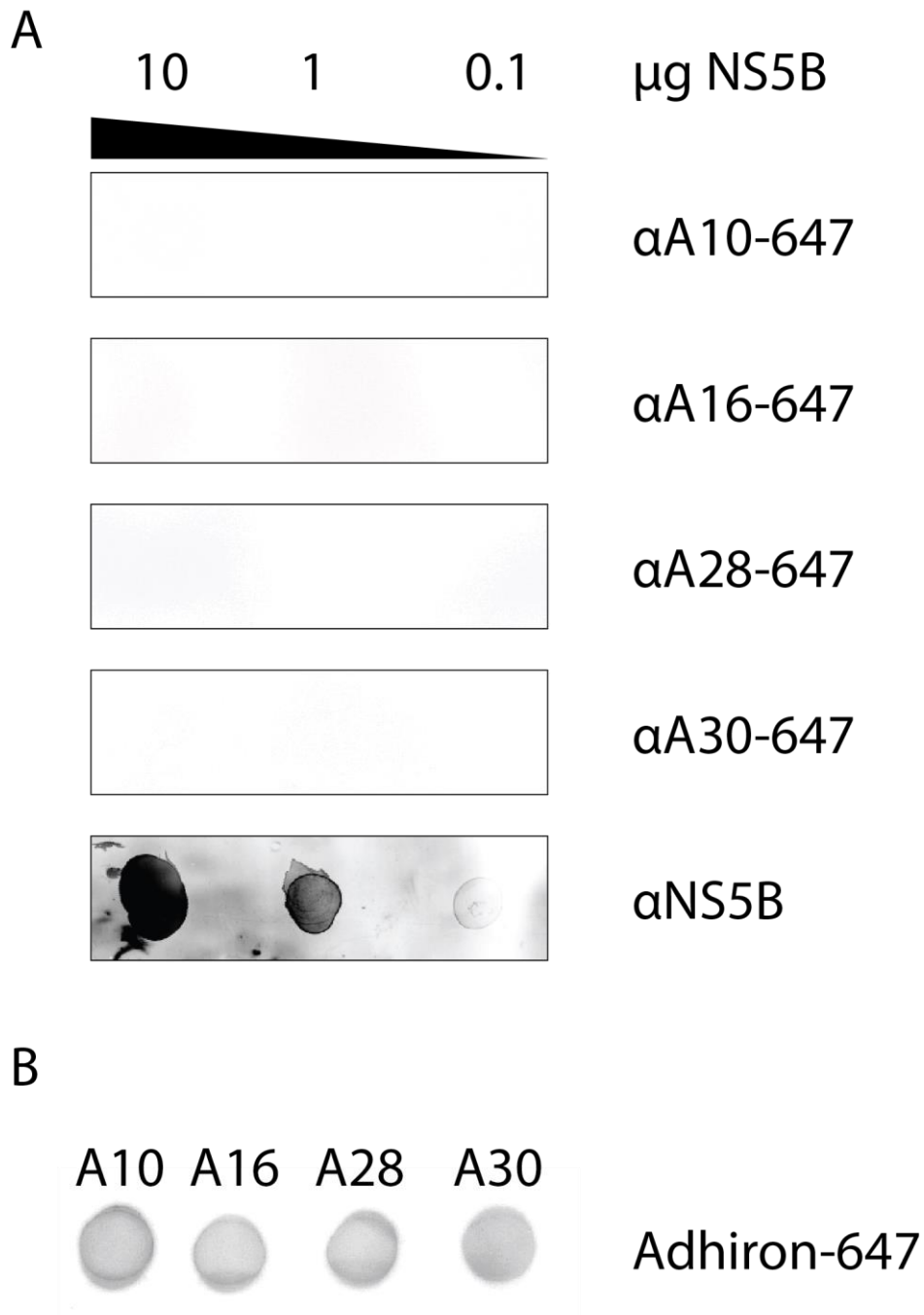


Figure 6.14: *In vitro* binding of 647-labelled Adhiron to purified NS5B ΔC21 .

A: Purified NS5B ΔC21 was blotted onto PVDF membranes in 10-fold dilutions before the membrane was incubated with 647-labelled Adhiron (5 μg) or anti-NS5B antibody. Membranes were imaged for 647 nm fluorescence or by western blot for primary antibody detection. B: 5 μg of 647-labelled Adhiron were dotted onto PVDF membranes prior to 647 nm fluorescence detection.

6.6 Part I – Discussion

In part I of this chapter I attempted to develop multiple different approaches to visualise HCV non-structural proteins that would then be suitable for super-resolution imaging. These included engineering TC-tagged fusion proteins of NS3 and NS5B, and identifying specific and high affinity non-antibody binding proteins to the HCV polymerase. Unfortunately, none of these approaches gave reliable detection of the specific target and could not be taken forward for super-resolution imaging.

6.6.1 Characterisation of TC-tagged NS3 and NS5B proteins

To the best of our knowledge, there are currently no reported fusion proteins for the detection of NS3 or NS5B during active HCV replication. Fusion protein expression constructs are reported for each protein (Chatel-Chaix et al., 2011; Wu et al., 2008) which provide methods to visualise the localisation of both proteins in cells. However these would be supplied outside the native NS3-5B context during virus replication and may not fully represent the entire process accurately.

The TC tagged constructs generated in this study were unable to replicate, with no detectable luciferase signal from transient electroporation. The absence of luciferase activity for NS3-TC or NS5B-TC indicates that the TC tag is somehow interfering with protein function during HCV replication. The N-terminal helix of NS3 and the C-terminal transmembrane domain of NS5B are both reported to be critical for membrane association (He et al., 2012; Lee et al., 2004). Accordingly, the TC tag is inserted directly upstream from each of these protein domains.

Although the transposon mutagenesis studies indicated these regions were able to tolerate small 5 amino acid insertions (Figure 6.1), the TC tag is bigger at 18 amino acids and may be sufficiently large to impair protein function. This is corroborated in part by the inability of G418 selection, using the neomycin phosphotransferase-luciferase reporter fusion protein expressed by SGR-Feo-JFH1, to select for a population of cells capable of HCV replication (data not shown).

In comparison, the NS5A protein of HCV is well documented to tolerate epitope tag insertions (Amako et al., 2009; D. M. Jones et al., 2007; Masaki et al., 2008; McCormick et al., 2006; Moradpour et al., 2004) including the tetracysteine tag (Eyre et al., 2014). The inability of NS3 or NS5B to tolerate small peptide insertions reiterate the critical roles these proteins have in the virus lifecycle, with limited or no genetic flexibility.

Future studies will investigate if other epitope tags, such as the FLAG, HA or myc tag, can be inserted at the sites used in this study to produce functional NS3 and NS5B constructs. Alternatively, the direct insertion of the desired epitope tag into the protein coding sequence, for example by using Tn7-transposon mutagenesis (Zordan et al., 2015), subverts the need to independently verify each epitope tag.

6.6.2 Selection of Adhirons targeted towards NS5B

Without functional NS5B fusion proteins, there is currently no method available at the University of Leeds, to detect the HCV polymerase by fluorescence microscopy. Monoclonal antibodies to NS5B are reported for genotype 1 (Nikonov et al., 2008), however they were unsuccessful in our hands for the detection of genotype 2 NS5B (data not shown). Previously, an anti-NS5B polyclonal serum was raised in house to genotype 2 NS5B; however the quality of the raised serum was insufficient for fluorescence and super-resolution microscopy. Therefore, a library of Adhirons, were screened against purified NS5B to identify specific and high-affinity binding proteins.

The attempt to find Adhirons that specifically bound to and recognised NS5B, was unsuccessful in this investigation. A number of potential binders were identified by Adhiron screening (Figure 6.9), however these failed to detect native NS5B expressed during active HCV replication (Figure 6.13), or purified, unbiotinylated, NS5B from *E. coli* (Figure 6.14).

Adhirons have been successfully raised to numerous targets typically with high affinities, indicating their broad application to multiple target proteins (Kyle et al., 2015; Rawlings et al., 2015; Tiede et al., 2014). During this investigation, only 32 potential binders were selected for analysis from the final panning round which identified 5 unique binders for characterisation. A repeat of the final selection step with characterisation of many more binders may identify novel Adhiron binders to NS5B.

It is possible that the Adhirons raised recognise an epitope on NS5B that does not exist on native protein. To screen for Adhirons, NS5B was surface biotinylated and immobilised, therefore a surface biotin may occlude or block an epitope. Alternatively, the presence of small quantities of contaminants in the original preparation may be the Adhiron target. However, no contaminants were unobserved by SDS-PAGE analysis and pre-screening of the Adhiron library with naïve bacterial lysate was conducted to reduce this possibility.

Another possibility is the orientation or presentation of the Adhiron on the phage capsid may display the variable binding loops in a unique conformation not adopted in the Adhiron scaffold alone. Additionally, part of the phage capsid protein itself may, in combination with the Adhiron variable loops, bind an epitope of NS5B. Lastly, there is always a chance that Adhiron will never be raised successfully against a target. Some proteins are poorly immunogenic and present limited epitopes, although the generation of antibodies to NS5B, both in house and against different HCV genotypes (Nikonov et al., 2008), and aptamers (Lee et al., 2013), suggest NS5B displays detectable epitopes.

6.7 Part II – Metabolically labelling HCV RNA

6.7.1 Visualising RNA transcription within cells

The HCV non-structural proteins are a critical component of replication complexes, directly involved in replication of the viral genome. However, viral proteins are often multifunctional, as is the case of NS5A (Ross-Thriepland and Harris, 2015), and therefore not all protein is involved in HCV genome replication. The visualisation of HCV RNA localisation therefore provides an alternative marker for replication complexes.

Historically, the detection of RNA in cells uses fluorescence *in situ* hybridisation (FISH) (Langer-Safer et al., 1982). A fluorescently labelled complementary nucleotide probe binds to the target sequence, enabling visualisation of RNA localisation (Li et al., 2013).

Another approach reported recently uses the RNA aptamer Spinach, which binds a fluorophore resembling the fluorophore in GFP (Paige et al., 2011). This RNA-fluorophore complex emits green fluorescence comparable to enhanced GFP. The genetic incorporation of Spinach into target RNA sequences allows live cell imaging of RNA localisation (Paige et al., 2011). Another genetic approach was described recently for HCV using the MS2 bacteriophage stem loop engineered into the HCV untranslated region (Fiches et al., 2016). HCV RNA was then observed indirectly by subsequent recruitment of an MS2-Coat-mCherry fusion protein to the MS2 RNA stem loop.

The major drawback to these approaches is their detection of total RNA containing the relevant sequence. In the case of HCV, and other virus infections, a subpopulation of these may be exhausted or inactive replication complexes.

The incorporation of modified nucleotides into newly synthesised RNA is an alternative to the above described techniques and offers an approach to visualise sites of active RNA transcription. Original methods to label new RNA transcripts were described through the incorporation of 5-bromouridine 5'-triphosphate (BrUTP) (Haukenes et al., 1997). In the presence of the host cell RNA synthesis inhibitor actinomycin D (AD), BrUTP incorporation into viral transcripts has been demonstrated for a number of virus infections, including HCV (El-Hage and Luo, 2003; Sir et al., 2012). AD binds to RNA transcription initiation sites and prevents cellular RNA polymerase elongation, without affecting viral polymerases (Sobell, 1985). However, cells are impermeable to BrUTP and therefore require methods to provide BrUTP into the cell cytoplasm, either by transfection (Haukenes et al.,

1997), permeabilisation (Wei et al., 1999) or microinjection (Wansink et al., 1993). Additionally, BrUTP itself is non-fluorescent; therefore antibody detection is required for visualisation.

Bio-orthogonal chemistry, defined as reactions that can occur without interfering with biological processes, have provided new methodologies to functionalise target molecules within the complex environment of cells (Sletten and Bertozzi, 2009). An investigation of RNA transcription *in vivo* illustrates how this can be applied to RNA labelling by a Sharpless-Meldal copper (I)-catalysed Huisgen cycloaddition reaction, often referred to as a “click” reaction (Jao and Salic, 2008). This was subsequently applied to the study of virus infections comparable to original methodology using BrUTP (Hagemeijer et al., 2012; Kalveram et al., 2011; Reid et al., 2015).

A key advantage of this approach over BrUTP labelling is the direct conjugation of an azide-modified fluorophore onto the substrate 5-ethynyl uridine (5EU). Additionally, eukaryotic cells are able to uptake the substrate directly from growth medium eliminating the need for transfection. Therefore, the goal of part II in this chapter was to develop tools for fluorescence detection of actively replicating HCV genomes through incorporation of 5EU (Section 6.8).

6.8 Part II – Results

6.8.1 HCV replication is unaffected by actinomycin D or 5-ethynyl uridine treatment of cells

HCV replication was unaffected by cellular RNA transcription inhibition (Figure 6.15A). No reduction in luciferase activity was detected, compared to control cells, up to 8 h after treatment with actinomycin D (AD). At 24 h, a reduction in luciferase compared to the control was observed with a concurrent increase in luciferase of control cells over earlier time-points (Figure 6.15A). The discrepancy between untreated and treated after 24 h treatment is a consequence of cell number and viability (data not shown). Therefore, an 8 h time period exists within which to incorporate 5EU into viral transcripts before deleterious effects on cell viability.

Additionally, no effect on HCV replication was observed with 5-ethynyl uridine treatment of cells stably harbouring SGR-Feo-JFH1 (Figure 6.15B). After 24 h treatment with 5EU, no decrease in luciferase signal was observed compared to untreated cells. Therefore, HCV replication and cell growth are unaffected by the incorporation of 5EU into RNA transcripts.

6.8.2 5-ethynyl uridine is incorporated into cellular RNA transcripts

The localisation of 5EU incorporated into cellular RNA transcripts in HuH7 cells was visualised using click chemistry with an azide-modified fluorophore (Figure 6.16A). RNA was localised to the nucleus of labelled cells, in particular to bright nuclear sub-regions. These bright sub-regions were absent for histone 3 staining and contained the nucleolar protein fibrillarin. The presence of 5EU within these fibrillarin-positive structures is consistent with the nucleolus, a site of high RNA transcription within eukaryotic cells (Tollervey et al., 1991).

Cells grown in the absence of 5EU exhibited no fluorescence signal in the nucleus, confirming the successful incorporation of, and specificity of azides for, 5EU (Figure 6.16B). Additionally, inhibition of cells with AD produced a phenotype comparable to cells grown in the absence of 5EU. Therefore, AD treatment is sufficient to shut-down cell transcription and no 5EU was incorporated into cellular transcripts.

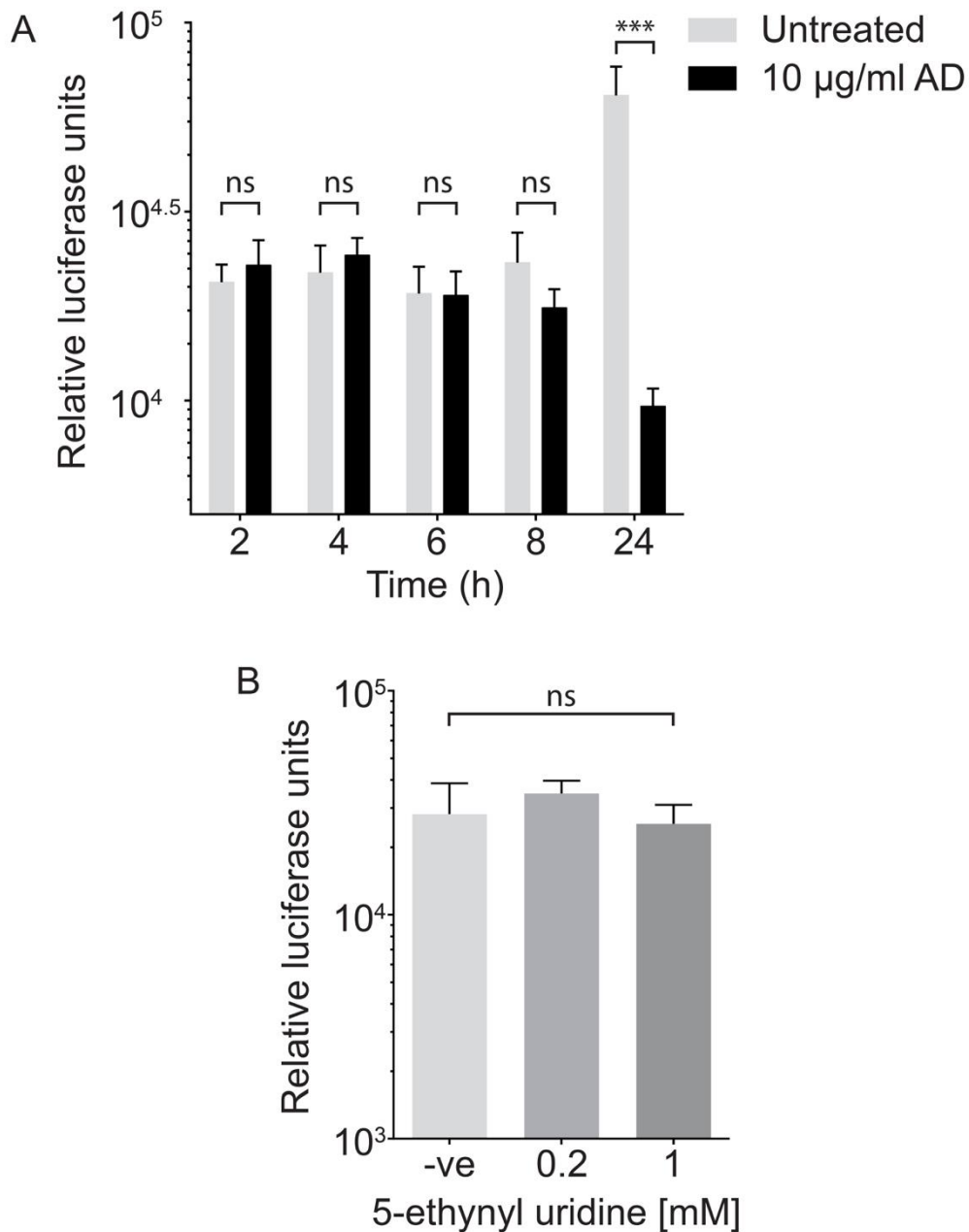


Figure 6.15: SGR-Feo-JFH1 replication in the presence of actinomycin D or 5EU.

A: HuH7.5 cells stably harbouring SGR-Feo-JFH1 were incubated with or without 10 µg/ml actinomycin D for the indicated times. Cells were subsequently lysed and luciferase activity measured. B: Cells stably harbouring SGR-Feo-JFH1 were incubated with or without 5EU for 24 h before cell lysis and measurement of luciferase activity. Data represent the mean ± SD, $n \geq 3$. *** $P < 0.0005$.

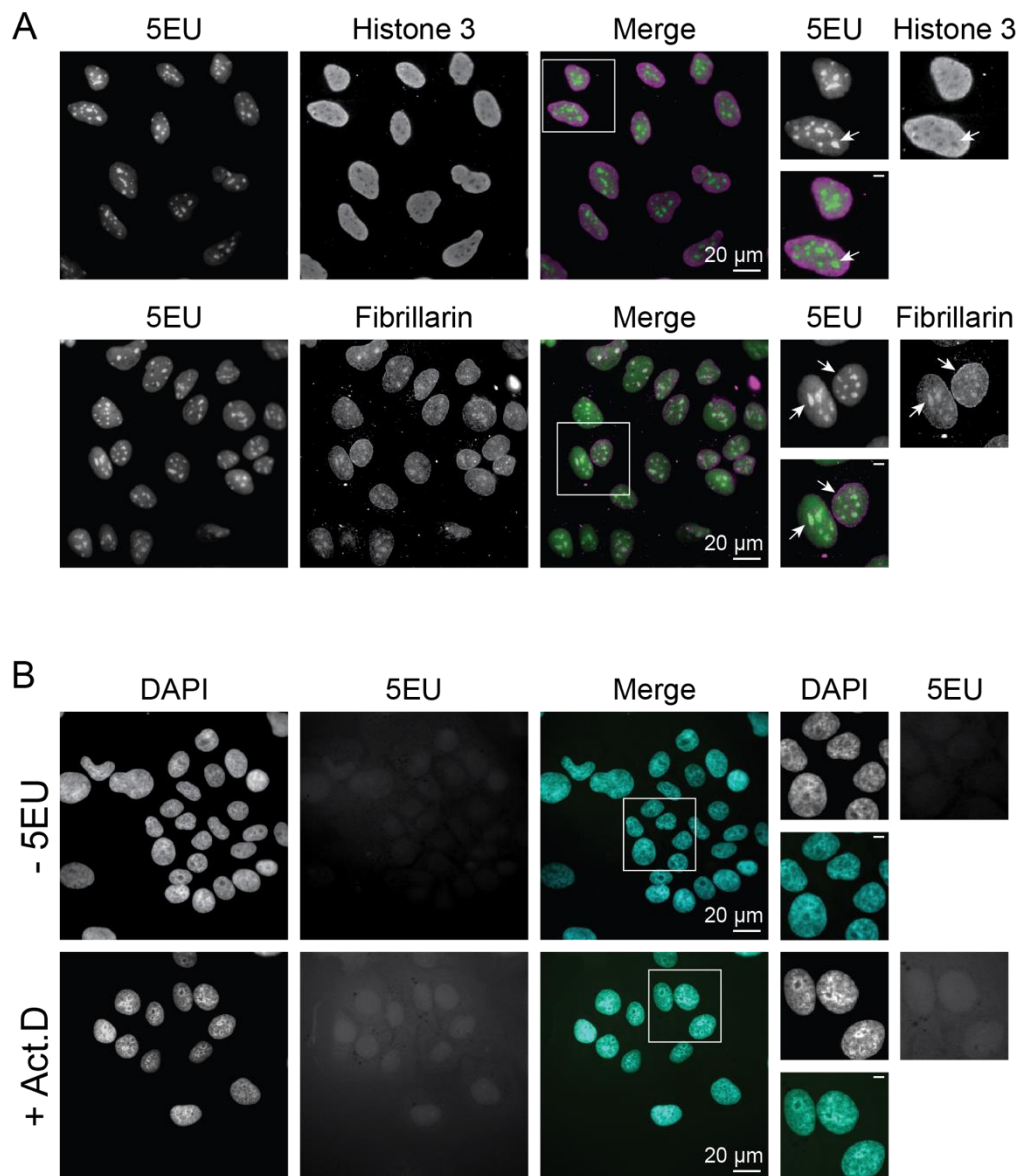


Figure 6.16: Localisation of 5EU incorporated into cellular transcripts.

A: HuH7 cells were treated with 1 mM 5EU for 2 h and incorporation into RNA transcripts visualised with Alexa Fluor 488-azide using click chemistry. Nuclear compartments were labelled with either histone 3 or fibrillarin antibodies. B: HuH7 cells were grown in the absence of 5EU or in the presence of 1 mM 5EU and 10 µg/ml AD. 5EU incorporated into RNA transcripts was visualised as in A. White boxes indicate magnified regions. Scale bars are indicated.

6.8.3 5EU was not incorporated into HCV RNA

No fluorescence signal was observed for 5EU incorporation into newly transcribed HCV genomes in cells stably harbouring SGR-Feo-JFH1 (Figure 6.17). Previous reports using BrUTP identified cytoplasmic puncta within infected cells (El-Hage and Luo, 2003; Shi et al., 2003; Sir et al., 2012). However, no such phenotype was observed for cells stably expressing replicons at high levels, confirmed by cytoplasmic NS5A staining. After 6 and 8 h 5EU incorporation, some weak fluorescence was observed as small nuclear speckles within cells (Figure 6.17). Therefore, despite AD mediated inhibition of transcription a small amount of 5EU is still incorporated into cellular transcripts. These nuclear speckles confirm that 5EU was still processed and incorporated by the cell under these conditions; however it was not incorporated into HCV RNA.

Additionally, in cells transiently expressing SGR-Feo-JFH1, no cytoplasmic fluorescence signal was observed at 24 or 48 h.p.e., after incubation of cells with 5EU (Figure 6.18). However, the nuclear speckles of 5EU were observed comparable to the stable cells. Transiently replicating SGRs undergo high levels of translation and replication in order to establish replication (Krieger et al., 2001). In comparison, cells stably harbouring SGRs may only undergo sufficient replication to be maintained within the cell population.

Lastly, no fluorescence signal for 5EU was detected in cells infected with HCV (Figure 6.19). NS5A positive cells displayed no cytoplasmic 5EU fluorescence after 8 h 5EU incorporation at either 24 or 48 h.p.i. HCV positive cells were confirmed by immunofluorescence staining for NS5A as a marker for the replication complex.

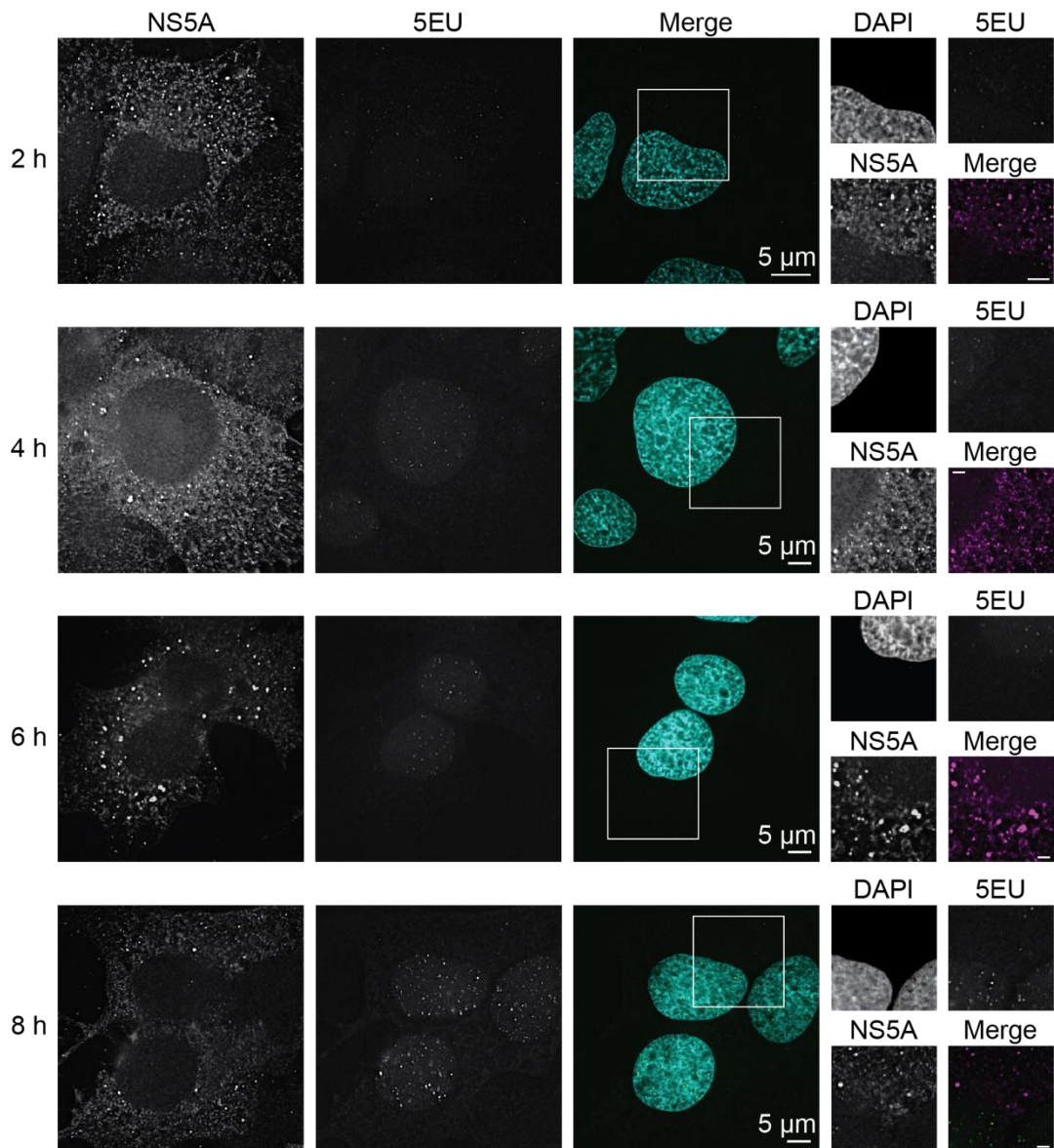


Figure 6.17: 5EU labelling of HCV RNA in cells stably harbouring SGRs.

HuH7 cells stably harbouring SGR-Feo-JFH1 were treated with 10 µg/ml AD for 30 min prior to incubation with 1 mM 5EU in the presence of AD. At the indicated times cells were fixed and 5EU detected by click chemistry before immunofluorescence labelling of NS5A. White boxes indicate magnified regions with 2 µm scale bars.

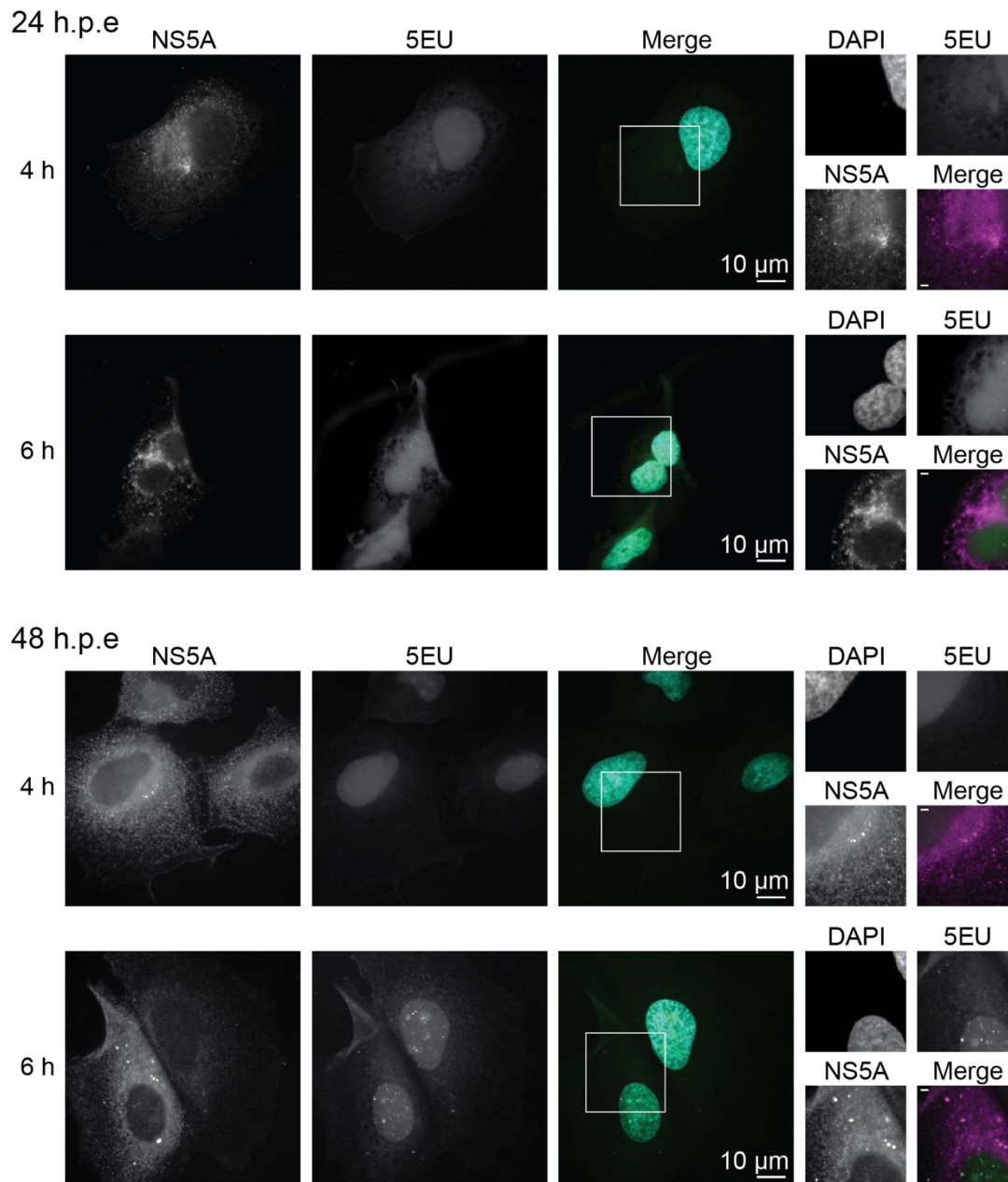


Figure 6.18: 5EU incorporation into transiently replicating SGR-Feo-JFH1 RNA.

HuH7 cells were electroporated with 5 μ g of SGR-Feo-JFH1 RNA and grown for either 24 or 48 h. Cells were then incubated with growth medium containing 1 mM 5EU and 10 μ g/ml AD for the indicated times after a 30 min pre-treatment with AD. Cells were then fixed and processed for immunofluorescence. 5EU incorporation and SGR-Feo-JFH1 positive cells were detected with fluorophore azide and NS5A staining respectively. White boxes indicate magnified regions with 2 μ m scale bars.

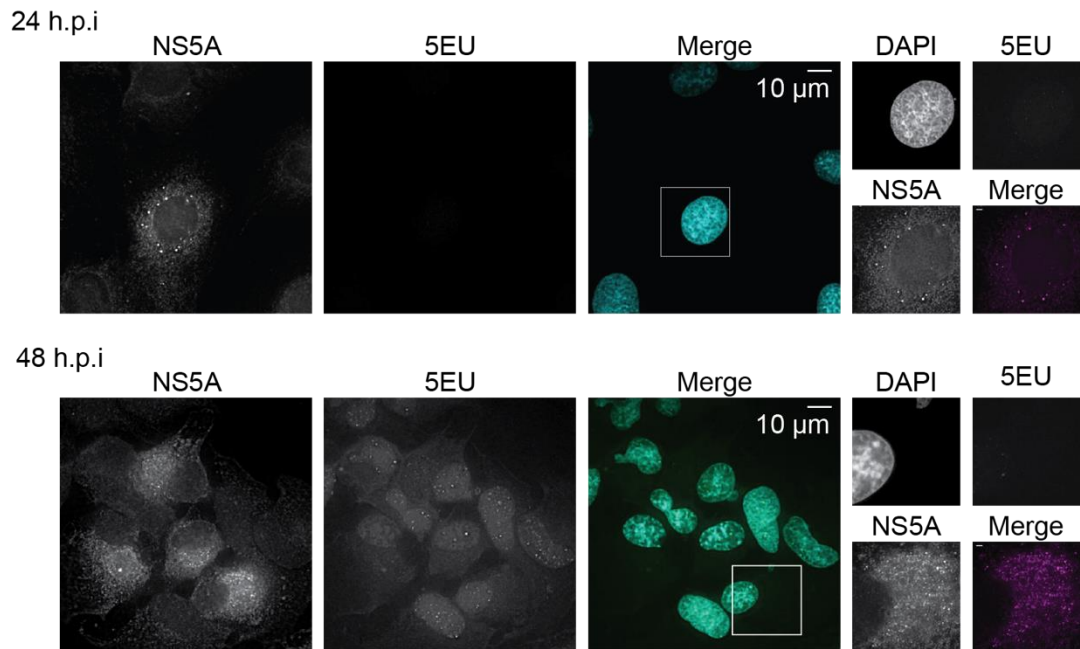


Figure 6.19: 5EU incorporation into HCV genomes during virus infection.

HuH7 cells were infected with JFHcc for 24 or 48 h. 1 mM 5EU and 10 µg/ml AD were then added to the culture medium for 8 h after a 30 min pre-treatment with AD. Cells were processed for immunofluorescence with 5EU detected by fluorophore azide and HCV positive cells identified by NS5A staining. White boxes indicate magnified regions with 2 µm scale bars.

6.9 Part II – Discussion

In the second part of this chapter I attempted to visualise the localisation of HCV RNA in cells. Incorporating 5-ethynyl uridine into HCV transcripts was unfortunately unsuccessful with no detectable fluorescence puncta in HCV harbouring cells under all experimental conditions tested. The incorporation and detection of 5EU into HCV RNA has been recently reported using RNA isolation and qPCR analysis of whole cell lysates (Masaki et al., 2015). In comparison to fluorescence microscopy, qPCR analysis amplifies RNA to enable detection. Consequently, in these studies HCV RNA may have incorporated 5EU however the signal was below a useful threshold.

Actively replicating HCV RNA localisation has been reported before using BrUTP with the SGR system (El-Hage and Luo, 2003; Shi et al., 2003; Sir et al., 2012). However, other groups, Romero-Brey et al (2012), have reported the detection of HCV RNA using BrUTP, 5EU or antibody labelling was not achievable. Of note, BrUTP is detected with primary and secondary antibodies. Therefore antibody-mediated signal amplification with BrUTP may bring fluorescence signal above a detectable threshold.

A recent study has demonstrated total HCV RNA localisation and trafficking within cells through the recruitment of mCherry-capsid protein to MS2 stem loops encoded in the HCV genome (Fiches et al., 2016). However, a major limitation of this approach was the substantial fitness cost. Studies from our lab have corroborated this finding with replication deficient Spinach tagged HCV constructs (data not shown).

Chapter 7 - Conclusions and future perspectives

The subversion of cellular membranes by HCV has been well documented for over 10 years. The viral determinants responsible are individually well characterized but the precise arrangement of non-structural proteins within the membranous web remains elusive. This study set out to gain a detailed understanding of viral protein organisation with replication factories, using advances in light microscopy to resolve structures previously obscured by the diffraction of light.

A major finding from this investigation was the difference in NS3 and NS5A organisation within protein clusters, and the association of HCV replication factories with lipid droplets. From these findings a model of HCV protein arrangement within DMV was proposed (Figure 4.34). The HCV non-structural proteins NS3/4A, NS4B and NS5B are membrane associated and contained inside DMV where HCV genome replication occurs. NS5A is proposed to face the cytosol, arranged on the outside of DMV, allowing interactions with core located on lipid droplets. This brings replication factories into close association with sites of virus assembly.

Currently, 2-colour imaging has not been achieved at Leeds due to additional technical requirements in image processing. However, this is an important next step in confirming or disputing the proposed model. Two colour imaging has been reported using dSTORM (van den Dries et al., 2013), and image processing to correct chromatic aberration of different channels provide methods for complete correction and image reconstruction (Erdelyi et al., 2013).

Another important component of HCV replication factories not investigated in this study is the lipid species that compose the HCV DMV. DMV undergo virus-mediated alteration to form membrane structures that have an altered PI4P, cholesterol and sphingolipids composition (Berger et al., 2009; Paul et al., 2013). Approaches to fluorescently label lipids have been reported using GFP-tagged PI4P binding proteins (Balla et al., 2005), PI4P antibodies (Ross-Thriepland and Harris, 2015), fluorescent cholesterol analogues (Maxfield and Wüstner, 2012), and lipid droplet dyes (Eggert et al., 2014). Future studies should look to exploit these approaches in 2-colour SMLM.

Additionally, the HCV RNA is an important component of replication factories that warrants additional investigation. Efforts to fluorescently label HCV RNA with modified nucleotides have so far proved unsuccessful, although similar methodology using BrUTP is reported (Shi et al., 2003). Alternatively, *in situ* hybridisation for the detection of total RNA and has been successfully demonstrated for HCV (Li et al., 2013; Shiogama et al., 2013).

Although the mechanism of action for DCV inhibition remains undefined, temporal associations with NS5A appear to be important. Early inhibition of virus release after DCV treatment was observed before replication factory disruption (Berger et al., 2014; McGivern et al., 2014). Monitoring the different populations of NS5A should be investigated in the future. The SNAP/CLIP tags are an enzymatic labelling strategy compatible with pulse chase fluorescence experiments. These have been incorporated into functional NS5A SGR to monitor temporal and trafficking functions (Eyre et al., 2014; Ross-Thriepland et al., 2015). Additionally the application of SNAP/CLIP tagging strategy has been demonstrated for super resolution imaging (Stagge et al., 2013).

Analysis of different genotypes also identified differences in NS5A protein cluster organisation. However, differences were also observed between SGR and virus infection in genotype 2a. Therefore an investigation of NS5A protein cluster organisation in genotype 1 infections is required. Culture adaptation of HCV isolates has produced genotype 1a infectious clones which should be explored in future studies (Li et al., 2015, 2012; Yi et al., 2006).

Analysis of SMLM images was performed using a clustering algorithm which identifies regions of high local density amid background noise (Ester et al., 1996). This gave superior results over other clustering algorithms such as hierarchical DBSCAN which grouped clusters together (data not shown) (Campello et al., 2013). DBSCAN is limited in its application when there is a large amount of varying density in a sample (Section 4.4.1). Although carefully controlled by parameter selection in this study, improvements of DBSCAN should be explored in the future. For example, OPTICS (ordering points to identify the clustering structure) (Ankerst et al., 1999) overcomes this weakness by describing how densely packed clusters are and thus accounts for varying density.

Along with the advances in SMLM, a number of developments have occurred in correlative imaging approaches. The power of correlative light and electron microscopy was demonstrated for HCV to identify HCV proteins within DMV (Romero-Brey et al., 2012). Techniques are now becoming available which combine SMLM with EM (Johnson et al., 2015; Watanabe et al., 2011). The advantage of these approaches are the ability to localise proteins at the nanoscale by SMLM with subsequent correlation to the cellular ultrastructure observed by EM. Currently methods have used resin embedding (Johnson et al., 2015; Watanabe et al., 2011), although applications with cryoelectron microscopy are under investigation (Wolff et al., 2016). An alternative to EM is soft X-ray microscopy

which can image cell architecture in intact, whole cells. Correlative approaches with conventional light microscopy will likely lead the way for correlative super-resolution approaches (Carzaniga et al., 2014; Hagen et al., 2012).

The organisation of non-structural proteins in HCV replication factories have been further defined in this study, however the biogenesis of HCV DMV remains elusive. The identification of DFCP1 as a cellular factor essential for HCV replication indicates the requirement of the autophagosome biogenesis machinery. However, additional questions have been raised from this study, for example, what interactions dictate the association with autophagy? How does HCV inhibit autophagosome lysosome fusion? Future methodologies should explore earlier steps in the autophagy biogenesis pathway to determine the cellular interactions required by HCV.

Chapter 8 - References

- A. Schwentker, M., Bock, H., Hofmann, M., Jakobs, S., Bewersdorf, J., Eggeling, C., Hell, S.W., 2007. Wide-field subdiffraction RESOLFT microscopy using fluorescent protein photoswitching. *Microsc. Res. Tech.* 70, 269–280. doi:10.1002/jemt.20443
- Abbe, E., 1873. Beiträge zur Theorie des Mikroskops und der mikroskopischen Wahrnehmung. *Arch. Für Mikrosk. Anat.* 9, 413–418. doi:10.1007/BF02956173
- Abbondanzieri, E.A., Greenleaf, W.J., Shaevitz, J.W., Landick, R., Block, S.M., 2005. Direct observation of base-pair stepping by RNA polymerase. *Nature* 438, 460–465. doi:10.1038/nature04268
- Abramowitz, M., Stegun, I.A., 1964. *Handbook of Mathematical Functions: With Formulas, Graphs, and Mathematical Tables*. Courier Corporation.
- Achtert, E., Böhm, C., Kröger, P., 2006. DeLi-Clu: Boosting Robustness, Completeness, Usability, and Efficiency of Hierarchical Clustering by a Closest Pair Ranking, in: *Proceedings of the 10th Pacific-Asia Conference on Advances in Knowledge Discovery and Data Mining, PAKDD'06*. Springer-Verlag, Berlin, Heidelberg, pp. 119–128. doi:10.1007/11731139_16
- Adams, S.R., Campbell, R.E., Gross, L.A., Martin, B.R., Walkup, G.K., Yao, Y., Llopis, J., Tsien, R.Y., 2002. New Biarsenical Ligands and Tetracysteine Motifs for Protein Labeling in Vitro and in Vivo: Synthesis and Biological Applications. *J. Am. Chem. Soc.* 124, 6063–6076. doi:10.1021/ja017687n
- Afdhal, N., Zeuzem, S., Kwo, P., Chojkier, M., Gitlin, N., Puoti, M., Romero-Gomez, M., Zarski, J.-P., Agarwal, K., Buggisch, P., Foster, G.R., Bräu, N., Buti, M., Jacobson, I.M., Subramanian, G.M., Ding, X., Mo, H., Yang, J.C., Pang, P.S., Symonds, W.T., McHutchison, J.G., Muir, A.J., Mangia, A., Marcellin, P., 2014. Ledipasvir and Sofosbuvir for Untreated HCV Genotype 1 Infection. *N. Engl. J. Med.* 370, 1889–1898. doi:10.1056/NEJMoa1402454
- Agnello, V., Abel, G., Elfahal, M., Knight, G.B., Zhang, Q.X., 1999. Hepatitis C virus and other flaviviridae viruses enter cells via low density lipoprotein receptor. *Proc. Natl. Acad. Sci. U. S. A.* 96, 12766–12771.
- Airy, G.B., 1835. On the Diffraction of an Object-glass with Circular Aperture. *Trans. Camb. Philos. Soc.* 5, 283.
- Ait-Goughoulte, M., Kanda, T., Meyer, K., Ryerse, J.S., Ray, R.B., Ray, R., 2008. Hepatitis C Virus Genotype 1a Growth and Induction of Autophagy. *J. Virol.* 82, 2241–2249. doi:10.1128/JVI.02093-07
- Albecka, A., Montserret, R., Krey, T., Tarr, A.W., Diesis, E., Ball, J.K., Descamps, V., Duverlie, G., Rey, F., Penin, F., Dubuisson, J., 2011. Identification of new functional regions in hepatitis C virus envelope glycoprotein E2. *J. Virol.* 85, 1777–1792. doi:10.1128/JVI.02170-10
- Aligo, J., Jia, S., Manna, D., Konan, K.V., 2009. Formation and function of hepatitis C virus replication complexes require residues in the carboxy-terminal

- domain of NS4B protein. *Virology* 393, 68–83. doi:10.1016/j.virol.2009.07.033
- Alter, H.J., Seeff, L.B., 2000. Recovery, persistence, and sequelae in hepatitis C virus infection: a perspective on long-term outcome. *Semin. Liver Dis.* 20, 17–35.
- Altschul, S.F., Gish, W., Miller, W., Myers, E.W., Lipman, D.J., 1990. Basic local alignment search tool. *J. Mol. Biol.* 215, 403–410. doi:10.1016/S0022-2836(05)80360-2
- Amako, Y., Igloi, Z., Mankouri, J., Kazlauskas, A., Saksela, K., Dallas, M., Peers, C., Harris, M., 2013. Hepatitis C Virus NS5A Inhibits Mixed Lineage Kinase 3 to Block Apoptosis. *J. Biol. Chem.* 288, 24753–24763. doi:10.1074/jbc.M113.491985
- Amako, Y., Sarkeshik, A., Hotta, H., Yates, J., Siddiqui, A., 2009. Role of Oxysterol Binding Protein in Hepatitis C Virus infection. *J. Virol.* 83, 9237–9246. doi:10.1128/JVI.00958-09
- Andresen, M., Schmitz-Salue, R., Jakobs, S., 2004. Short Tetracysteine Tags to β -Tubulin Demonstrate the Significance of Small Labels for Live Cell Imaging. *Mol. Biol. Cell* 15, 5616–5622. doi:10.1091/mbc.E04-06-0454
- Andresen, M., Stiel, A.C., Fölling, J., Wenzel, D., Schönle, A., Egner, A., Eggeling, C., Hell, S.W., Jakobs, S., 2008. Photoswitchable fluorescent proteins enable monochromatic multilabel imaging and dual color fluorescence nanoscopy. *Nat. Biotechnol.* 26, 1035–1040. doi:10.1038/nbt.1493
- Andronov, L., Lutz, Y., Vonesch, J.-L., Klaholz, B.P., 2016. SharpViSu: integrated analysis and segmentation of super-resolution microscopy data. *Bioinformatics* 32, 2239–2241. doi:10.1093/bioinformatics/btw123
- Ankerst, M., Breunig, M.M., Kriegel, H., Sander, J., 1999. OPTICS: Ordering Points To Identify the Clustering Structure. ACM Press, pp. 49–60.
- Appel, N., Pietschmann, T., Bartenschlager, R., 2005. Mutational analysis of hepatitis C virus nonstructural protein 5A: potential role of differential phosphorylation in RNA replication and identification of a genetically flexible domain. *J. Virol.* 79, 3187–3194. doi:10.1128/JVI.79.5.3187-3194.2005
- Appel, N., Zayas, M., Miller, S., Krijnse-Locker, J., Schaller, T., Friebe, P., Kallis, S., Engel, U., Bartenschlager, R., 2008. Essential role of domain III of nonstructural protein 5A for hepatitis C virus infectious particle assembly. *PLoS Pathog.* 4, e1000035. doi:10.1371/journal.ppat.1000035
- Appleby, T.C., Perry, J.K., Murakami, E., Barauskas, O., Feng, J., Cho, A., Fox, D., Wetmore, D.R., McGrath, M.E., Ray, A.S., Sofia, M.J., Swaminathan, S., Edwards, T.E., 2015. Viral replication. Structural basis for RNA replication by the hepatitis C virus polymerase. *Science* 347, 771–775. doi:10.1126/science.1259210
- Ariumi, Y., Kuroki, M., Maki, M., Ikeda, M., Dansako, H., Wakita, T., Kato, N., 2011. The ESCRT system is required for hepatitis C virus production. *PloS One* 6, e14517. doi:10.1371/journal.pone.0014517
- Arumugaswami, V., Remenyi, R., Kanagavel, V., Sue, E.Y., Ho, T.N., Liu, C., Fontanes, V., Dasgupta, A., Sun, R., 2008. High-Resolution Functional Profiling of Hepatitis C Virus Genome. *PLOS Pathog* 4, e1000182. doi:10.1371/journal.ppat.1000182
- Ascher, D.B., Wielens, J., Nero, T.L., Doughty, L., Morton, C.J., Parker, M.W., 2014. Potent hepatitis C inhibitors bind directly to NS5A and reduce its affinity for RNA. *Sci. Rep.* 4, 4765. doi:10.1038/srep04765
- Aweya, J.J., Mak, T.M., Lim, S.G., Tan, Y.-J., 2013. The p7 protein of the hepatitis C virus induces cell death differently from the influenza A virus viroporin M2. *Virus Res.* 172, 24–34. doi:10.1016/j.virusres.2012.12.005
- Axe, E.L., Walker, S.A., Manifava, M., Chandra, P., Roderick, H.L., Habermann, A., Griffiths, G., Ktistakis, N.T., 2008. Autophagosome formation from membrane compartments enriched in phosphatidylinositol 3-phosphate and

- dynamically connected to the endoplasmic reticulum. *J. Cell Biol.* 182, 685–701. doi:10.1083/jcb.200803137
- Baddeley, D., Cannell, M.B., Soeller, C., 2010. Visualization of localization microscopy data. *Microsc. Microanal. Off. J. Microsc. Soc. Am. Microbeam Anal. Soc. Microsc. Soc. Can.* 16, 64–72. doi:10.1017/S143192760999122X
- Bai, Y., Zhou, K., Doudna, J.A., 2013. Hepatitis C virus 3'UTR regulates viral translation through direct interactions with the host translation machinery. *Nucleic Acids Res.* 41, 7861–7874. doi:10.1093/nar/gkt543
- Bankwitz, D., Steinmann, E., Bitzegeio, J., Ciesek, S., Friesland, M., Herrmann, E., Zeisel, M.B., Baumert, T.F., Keck, Z., Fong, S.K.H., Pécheur, E.-I., Pietschmann, T., 2010. Hepatitis C virus hypervariable region 1 modulates receptor interactions, conceals the CD81 binding site, and protects conserved neutralizing epitopes. *J. Virol.* 84, 5751–5763. doi:10.1128/JVI.02200-09
- Banterle, N., Bui, K.H., Lemke, E.A., Beck, M., 2013. Fourier ring correlation as a resolution criterion for super-resolution microscopy. *J. Struct. Biol.* 183, 363–367. doi:10.1016/j.jsb.2013.05.004
- Barakat, K.H., Anwar-Mohamed, A., Tuszyński, J.A., Robins, M.J., Tyrrell, D.L., Houghton, M., 2015. A Refined Model of the HCV NS5A protein bound to daclatasvir explains drug-resistant mutations and activity against divergent genotypes. *J. Chem. Inf. Model.* 55, 362–373. doi:10.1021/ci400631n
- Bar-On, D., Wolter, S., van de Linde, S., Heilemann, M., Nudelman, G., Nachliel, E., Gutman, M., Sauer, M., Ashery, U., 2012. Super-resolution Imaging Reveals the Internal Architecture of Nano-sized Syntaxin Clusters. *J. Biol. Chem.* 287, 27158–27167. doi:10.1074/jbc.M112.353250
- Barouch-Bentov, R., Neveu, G., Xiao, F., Beer, M., Bekerman, E., Schor, S., Campbell, J., Boonyaratanakornkit, J., Lindenbach, B., Lu, A., Jacob, Y., Einav, S., 2016. Hepatitis C Virus Proteins Interact with the Endosomal Sorting Complex Required for Transport (ESCRT) Machinery via Ubiquitination To Facilitate Viral Envelopment. *mBio* 7, e01456-16. doi:10.1128/mBio.01456-16
- Bartenschlager, R., Ahlborn-Laake, L., Mous, J., Jacobsen, H., 1994. Kinetic and structural analyses of hepatitis C virus polyprotein processing. *J. Virol.* 68, 5045–5055.
- Bartenschlager, R., Lohmann, V., Penin, F., 2013. The molecular and structural basis of advanced antiviral therapy for hepatitis C virus infection. *Nat. Rev. Microbiol.* 11, 482–496. doi:10.1038/nrmicro3046
- Bartenschlager, R., Lohmann, V., Wilkinson, T., Koch, J.O., 1995. Complex formation between the NS3 serine-type proteinase of the hepatitis C virus and NS4A and its importance for polyprotein maturation. *J. Virol.* 69, 7519–7528.
- Bates, M., Huang, B., Dempsey, G.T., Zhuang, X., 2007. Multicolor super-resolution imaging with photo-switchable fluorescent probes. *Science* 317, 1749–1753. doi:10.1126/science.1146598
- Belda, O., Targett-Adams, P., 2012. Small molecule inhibitors of the hepatitis C virus-encoded NS5A protein. *Virus Res.* 170, 1–14. doi:10.1016/j.virusres.2012.09.007
- Belema, M., Nguyen, V.N., Bachand, C., Deon, D.H., Goodrich, J.T., James, C.A., Lavoie, R., Lopez, O.D., Martel, A., Romine, J.L., Ruediger, E.H., Snyder, L.B., St Laurent, D.R., Yang, F., Zhu, J., Wong, H.S., Langley, D.R., Adams, S.P., Cantor, G.H., Chimalakonda, A., Fura, A., Johnson, B.M., Knipe, J.O., Parker, D.D., Santone, K.S., Fridell, R.A., Lemm, J.A., O'Boyle, D.R., Colonna, R.J., Gao, M., Meanwell, N.A., Hamann, L.G., 2014. Hepatitis C virus NS5A replication complex inhibitors: the discovery of daclatasvir. *J. Med. Chem.* 57, 2013–2032. doi:10.1021/jm401836p

- Belshaw, R., Pybus, O.G., Rambaut, A., 2007. The evolution of genome compression and genomic novelty in RNA viruses. *Genome Res.* 17, 1496–1504. doi:10.1101/gr.6305707
- Benga, W.J.A., Krieger, S.E., Dimitrova, M., Zeisel, M.B., Parnot, M., Lupberger, J., Hildt, E., Luo, G., McLauchlan, J., Baumert, T.F., Schuster, C., 2010. Apolipoprotein E interacts with hepatitis C virus nonstructural protein 5A and determines assembly of infectious particles. *Hepatology* 51, 43–53. doi:10.1002/hep.23278
- Berger, C., Romero-Brey, I., Radujkovic, D., Terreux, R., Zayas, M., Paul, D., Harak, C., Hoppe, S., Gao, M., Penin, F., Lohmann, V., Bartenschlager, R., 2014. Daclatasvir-Like Inhibitors of NS5A Block Early Biogenesis of Hepatitis C Virus-Induced Membranous Replication Factories, Independent of RNA Replication. *Gastroenterology* 147, 1094–1105.e25. doi:10.1053/j.gastro.2014.07.019
- Berger, K.L., Cooper, J.D., Heaton, N.S., Yoon, R., Oakland, T.E., Jordan, T.X., Mateu, G., Grakoui, A., Randall, G., 2009. Roles for endocytic trafficking and phosphatidylinositol 4-kinase III alpha in hepatitis C virus replication. *Proc. Natl. Acad. Sci. U. S. A.* 106, 7577–7582. doi:10.1073/pnas.0902693106
- Bernales, S., McDonald, K.L., Walter, P., 2006. Autophagy Counterbalances Endoplasmic Reticulum Expansion during the Unfolded Protein Response. *PLOS Biol* 4, e423. doi:10.1371/journal.pbio.0040423
- Betzig, E., Patterson, G.H., Sougrat, R., Lindwasser, O.W., Olenych, S., Bonifacino, J.S., Davidson, M.W., Lippincott-Schwartz, J., Hess, H.F., 2006. Imaging Intracellular Fluorescent Proteins at Nanometer Resolution. *Science* 313, 1642–1645. doi:10.1126/science.1127344
- Binz, H.K., Stumpp, M.T., Forrer, P., Amstutz, P., Plückthun, A., 2003. Designing repeat proteins: well-expressed, soluble and stable proteins from combinatorial libraries of consensus ankyrin repeat proteins. *J. Mol. Biol.* 332, 489–503.
- Blanchard, E., Belouzard, S., Goueslain, L., Wakita, T., Dubuisson, J., Wychowski, C., Rouillé, Y., 2006. Hepatitis C virus entry depends on clathrin-mediated endocytosis. *J. Virol.* 80, 6964–6972. doi:10.1128/JVI.00024-06
- Blight, K.J., Kolykhalov, A.A., Rice, C.M., 2000. Efficient initiation of HCV RNA replication in cell culture. *Science* 290, 1972–1974.
- Blight, K.J., McKeating, J.A., Rice, C.M., 2002. Highly Permissive Cell Lines for Subgenomic and Genomic Hepatitis C Virus RNA Replication. *J. Virol.* 76, 13001–13014. doi:10.1128/JVI.76.24.13001-13014.2002
- Blight, K.J., Rice, C.M., 1997. Secondary structure determination of the conserved 98-base sequence at the 3' terminus of hepatitis C virus genome RNA. *J. Virol.* 71, 7345–7352.
- Bock, H., Geisler, C., Wurm, C.A., Middendorff, C. von, Jakobs, S., Schönle, A., Egner, A., Hell, S.W., Eggeling, C., 2007. Two-color far-field fluorescence nanoscopy based on photoswitchable emitters. *Appl. Phys. B* 88, 161–165. doi:10.1007/s00340-007-2729-0
- Bolte, S., Cordelieres, F.P., 2006. A guided tour into subcellular colocalization analysis in light microscopy. *J. Microsc.* 224, 213–232.
- Borawski, J., Troke, P., Puyang, X., Gibaja, V., Zhao, S., Mickanin, C., Leighton-Davies, J., Wilson, C.J., Myer, V., Cornellataracido, I., Baryza, J., Tallarico, J., Joberty, G., Bantscheff, M., Schirle, M., Bouwmeester, T., Mathy, J.E., Lin, K., Compton, T., Labow, M., Wiedmann, B., Gaither, L.A., 2009. Class III phosphatidylinositol 4-kinase alpha and beta are novel host factor regulators of hepatitis C virus replication. *J. Virol.* 83, 10058–10074. doi:10.1128/JVI.02418-08
- Born, M., Wolf, E., 2000. *Principles of Optics: Electromagnetic Theory of Propagation, Interference and Diffraction of Light.* CUP Archive.

- Boulant, S., Montserret, R., Hope, R.G., Ratinier, M., Targett-Adams, P., Lavergne, J.-P., Penin, F., McLauchlan, J., 2006. Structural Determinants That Target the Hepatitis C Virus Core Protein to Lipid Droplets. *J. Biol. Chem.* 281, 22236–22247. doi:10.1074/jbc.M601031200
- Boulant, S., Vanbelle, C., Ebel, C., Penin, F., Lavergne, J.-P., 2005. Hepatitis C Virus Core Protein Is a Dimeric Alpha-Helical Protein Exhibiting Membrane Protein Features. *J. Virol.* 79, 11353–11365. doi:10.1128/JVI.79.17.11353-11365.2005
- Bradford, M.M., 1976. A rapid and sensitive method for the quantitation of microgram quantities of protein utilizing the principle of protein-dye binding. *Anal. Biochem.* 72, 248–254.
- Bradley, D.W., Maynard, J.E., Popper, H., Cook, E.H., Ebert, J.W., McCaustland, K.A., Schable, C.A., Fields, H.A., 1983. Posttransfusion non-A, non-B hepatitis: physicochemical properties of two distinct agents. *J. Infect. Dis.* 148, 254–265.
- Bradley, D.W., McCaustland, K.A., Cook, E.H., Schable, C.A., Ebert, J.W., Maynard, J.E., 1985. Posttransfusion non-A, non-B hepatitis in chimpanzees. Physicochemical evidence that the tubule-forming agent is a small, enveloped virus. *Gastroenterology* 88, 773–779.
- Brass, V., Berke, J.M., Montserret, R., Blum, H.E., Penin, F., Moradpour, D., 2008. Structural determinants for membrane association and dynamic organization of the hepatitis C virus NS3-4A complex. *Proc. Natl. Acad. Sci. U. S. A.* 105, 14545–14550. doi:10.1073/pnas.0807298105
- Brazzoli, M., Bianchi, A., Filippini, S., Weiner, A., Zhu, Q., Pizza, M., Crotta, S., 2008. CD81 Is a Central Regulator of Cellular Events Required for Hepatitis C Virus Infection of Human Hepatocytes. *J. Virol.* 82, 8316–8329. doi:10.1128/JVI.00665-08
- Bressanelli, S., Tomei, L., Rey, F.A., Francesco, R.D., 2002. Structural Analysis of the Hepatitis C Virus RNA Polymerase in Complex with Ribonucleotides. *J. Virol.* 76, 3482–3492. doi:10.1128/JVI.76.7.3482-3492.2002
- Brimacombe, C.L., Grove, J., Meredith, L.W., Hu, K., Syder, A.J., Flores, M.V., Timpe, J.M., Krieger, S.E., Baumert, T.F., Tellinghuisen, T.L., Wong-Staal, F., Balfe, P., McKeating, J.A., 2011. Neutralizing Antibody-Resistant Hepatitis C Virus Cell-to-Cell Transmission. *J. Virol.* 85, 596–605. doi:10.1128/JVI.01592-10
- Brown, E.A., Zhang, H., Ping, L.H., Lemon, S.M., 1992. Secondary structure of the 5' nontranslated regions of hepatitis C virus and pestivirus genomic RNAs. *Nucleic Acids Res.* 20, 5041–5045.
- Burbelo, P.D., Dubovi, E.J., Simmonds, P., Medina, J.L., Henriquez, J.A., Mishra, N., Wagner, J., Tokarz, R., Cullen, J.M., Iadarola, M.J., Rice, C.M., Lipkin, W.I., Kapoor, A., 2012. Serology-enabled discovery of genetically diverse hepaciviruses in a new host. *J. Virol.* 86, 6171–6178. doi:10.1128/JVI.00250-12
- Campello, R.J.G.B., Moulavi, D., Sander, J., 2013. Density-Based Clustering Based on Hierarchical Density Estimates, in: Pei, J., Tseng, V.S., Cao, L., Motoda, H., Xu, G. (Eds.), *Advances in Knowledge Discovery and Data Mining: 17th Pacific-Asia Conference, PAKDD 2013, Gold Coast, Australia, April 14-17, 2013, Proceedings, Part II*. Springer Berlin Heidelberg, Berlin, Heidelberg, pp. 160–172.
- Camus, G., Herker, E., Modi, A.A., Haas, J.T., Ramage, H.R., Farese, R.V., Ott, M., 2013. Diacylglycerol Acyltransferase-1 Localizes Hepatitis C Virus NS5A Protein to Lipid Droplets and Enhances NS5A Interaction with the Viral Capsid Core. *J. Biol. Chem.* 288, 9915–9923. doi:10.1074/jbc.M112.434910
- Carzaniga, R., Domart, M.-C., Collinson, L.M., Duke, E., 2014. Cryo-soft X-ray tomography: a journey into the world of the native-state cell. *Protoplasma* 251, 449–458. doi:10.1007/s00709-013-0583-y

- Catanese, M.T., Uryu, K., Kopp, M., Edwards, T.J., Andrus, L., Rice, W.J., Silvestry, M., Kuhn, R.J., Rice, C.M., 2013. Ultrastructural analysis of hepatitis C virus particles. *Proc. Natl. Acad. Sci. U. S. A.* 110, 9505–9510. doi:10.1073/pnas.1307527110
- Chalfie, M., Tu, Y., Euskirchen, G., Ward, W.W., Prasher, D.C., 1994. Green fluorescent protein as a marker for gene expression. *Science* 263, 802–805. doi:10.1126/science.8303295
- Chan, S.-W., Egan, P.A., 2005. Hepatitis C virus envelope proteins regulate CHOP via induction of the unfolded protein response. *FASEB J. Off. Publ. Fed. Am. Soc. Exp. Biol.* 19, 1510–1512. doi:10.1096/fj.04-3455fje
- Chao, T.-C., Su, W.-C., Huang, J.-Y., Chen, Y.-C., Jeng, K.-S., Wang, H.-D., Lai, M.M.C., 2012. Proline-serine-threonine phosphatase-interacting protein 2 (PSTPIP2), a host membrane-deforming protein, is critical for membranous web formation in hepatitis C virus replication. *J. Virol.* 86, 1739–1749. doi:10.1128/JVI.06001-11
- Chatel-Chaix, L., Melançon, P., Racine, M.-È., Baril, M., Lamarre, D., 2011. Y-Box-Binding Protein 1 Interacts with Hepatitis C Virus NS3/4A and Influences the Equilibrium between Viral RNA Replication and Infectious Particle Production. *J. Virol.* 85, 11022–11037. doi:10.1128/JVI.00719-11
- Chatterji, U., Lim, P., Bobardt, M.D., Wieland, S., Cordek, D.G., Vuagniaux, G., Chisari, F., Cameron, C.E., Targett-Adams, P., Parkinson, T., Gallay, P.A., 2010. HCV resistance to cyclosporin A does not correlate with a resistance of the NS5A–cyclophilin A interaction to cyclophilin inhibitors. *J. Hepatol.* 53, 50–56. doi:10.1016/j.jhep.2010.01.041
- Chen, F., Chen, S.-C., Zhou, J., Chen, Z.-D., Chen, F., 2015. Identification of Aptamer-Binding Sites in Hepatitis C Virus Envelope Glycoprotein E2. *Iran. J. Med. Sci.* 40, 63–67.
- Chen, I., Howarth, M., Lin, W., Ting, A.Y., 2005. Site-specific labeling of cell surface proteins with biophysical probes using biotin ligase. *Nat. Methods* 2, 99–104. doi:10.1038/nmeth735
- Chen, S.L., Morgan, T.R., 2006. The natural history of hepatitis C virus (HCV) infection. *Int. J. Med. Sci.* 3, 47–52.
- Chen, Y., Wang, S., Yi, Z., Tian, H., Aliyari, R., Li, Y., Chen, G., Liu, P., Zhong, J., Chen, X., Du, P., Su, L., Qin, F.X.-F., Deng, H., Cheng, G., 2014. Interferon-inducible cholesterol-25-hydroxylase inhibits hepatitis C virus replication via distinct mechanisms. *Sci. Rep.* 4, 7242. doi:10.1038/srep07242
- Chen, Y.-C., Su, W.-C., Huang, J.-Y., Chao, T.-C., Jeng, K.-S., Machida, K., Lai, M.M.C., 2010. Polo-Like Kinase 1 Is Involved in Hepatitis C Virus Replication by Hyperphosphorylating NS5A. *J. Virol.* 84, 7983–7993. doi:10.1128/JVI.00068-10
- Choi, A.M.K., Ryter, S.W., Levine, B., 2013. Autophagy in Human Health and Disease. *N. Engl. J. Med.* 368, 651–662. doi:10.1056/NEJMra1205406
- Choo, Q.L., Kuo, G., Weiner, A.J., Overby, L.R., Bradley, D.W., Houghton, M., 1989. Isolation of a cDNA clone derived from a blood-borne non-A, non-B viral hepatitis genome. *Science* 244, 359–362.
- Choo, Q.L., Weiner, A.J., Overby, L.R., Kuo, G., Houghton, M., Bradley, D.W., 1990. Hepatitis C virus: the major causative agent of viral non-A, non-B hepatitis. *Br. Med. Bull.* 46, 423–441.
- Chukkapalli, V., Randall, G., 2014. Hepatitis C virus replication compartment formation: mechanism and drug target. *Gastroenterology* 146, 1164–1167. doi:10.1053/j.gastro.2014.03.017
- Ciczora, Y., Callens, N., Penin, F., Pécheur, E.-I., Dubuisson, J., 2007. Transmembrane domains of hepatitis C virus envelope glycoproteins: residues involved in E1E2 heterodimerization and involvement of these domains in virus entry. *J. Virol.* 81, 2372–2381. doi:10.1128/JVI.02198-06

- Cieśla, J., Frączyk, T., Rode, W., 2011. Phosphorylation of basic amino acid residues in proteins: important but easily missed. *Acta Biochim. Pol.* 58, 137–148.
- Clark, P.J., Evans, F.C., 1954. Distance to Nearest Neighbor as a Measure of Spatial Relationships in Populations. *Ecology* 35, 445–453. doi:10.2307/1931034
- Cocquerel, L., Op de Beeck, A., Lambot, M., Roussel, J., Delgrange, D., Pillez, A., Wychowski, C., Penin, F., Dubuisson, J., 2002. Topological changes in the transmembrane domains of hepatitis C virus envelope glycoproteins. *EMBO J.* 21, 2893–2902. doi:10.1093/emboj/cdf295
- Coelmont, L., Hanouille, X., Chatterji, U., Berger, C., Snoeck, J., Bobardt, M., Lim, P., Vliegen, I., Paeshuyse, J., Vuagniaux, G., Vandamme, A.-M., Bartenschlager, R., Gallay, P., Lippens, G., Neyts, J., 2010. DEB025 (Alisporivir) inhibits hepatitis C virus replication by preventing a cyclophilin A induced cis-trans isomerisation in domain II of NS5A. *PloS One* 5, e13687. doi:10.1371/journal.pone.0013687
- Cohen, P., 2000. The regulation of protein function by multisite phosphorylation – a 25 year update. *Trends Biochem. Sci.* 25, 596–601. doi:10.1016/S0968-0004(00)01712-6
- Coller, K.E., Berger, K.L., Heaton, N.S., Cooper, J.D., Yoon, R., Randall, G., 2009. RNA Interference and Single Particle Tracking Analysis of Hepatitis C Virus Endocytosis. *PLOS Pathog* 5, e1000702. doi:10.1371/journal.ppat.1000702
- Coller, K.E., Heaton, N.S., Berger, K.L., Cooper, J.D., Saunders, J.L., Randall, G., 2012. Molecular Determinants and Dynamics of Hepatitis C Virus Secretion. *PLoS Pathog.* 8. doi:10.1371/journal.ppat.1002466
- Corby, J., Biener, G., Raicu, V., Frick, D., 2016. FRET studies examining the interaction of hepatitis C NS3 helicase and human DEXD/H box helicases. *FASEB J.* 30, 600.23-600.23.
- Cordek, D.G., Croom-Perez, T.J., Hwang, J., Hargittai, M.R.S., Subba-Reddy, C.V., Han, Q., Lodeiro, M.F., Ning, G., McCrory, T.S., Arnold, J.J., Koc, H., Lindenbach, B.D., Showalter, S.A., Cameron, C.E., 2014. Expanding the Proteome of an RNA Virus by Phosphorylation of an Intrinsically Disordered Viral Protein. *J. Biol. Chem.* 289, 24397–24416. doi:10.1074/jbc.M114.589911
- Corless, L., Crump, C.M., Griffin, S.D.C., Harris, M., 2010. Vps4 and the ESCRT-III complex are required for the release of infectious hepatitis C virus particles. *J. Gen. Virol.* 91, 362–372. doi:10.1099/vir.0.017285-0
- Cottam, E.M., Maier, H.J., Manifava, M., Vaux, L.C., Chandra-Schoenfelder, P., Gerner, W., Britton, P., Ktistakis, N.T., Wileman, T., 2011. Coronavirus nsp6 proteins generate autophagosomes from the endoplasmic reticulum via an omegasome intermediate. *Autophagy* 7, 1335–1347. doi:10.4161/auto.7.11.16642
- Counihan, N.A., Rawlinson, S.M., Lindenbach, B.D., 2011. Trafficking of Hepatitis C Virus Core Protein during Virus Particle Assembly. *PLOS Pathog* 7, e1002302. doi:10.1371/journal.ppat.1002302
- Cristofari, G., Ivanyi-Nagy, R., Gabus, C., Boulant, S., Lavergne, J.-P., Penin, F., Darlix, J.-L., 2004. The hepatitis C virus Core protein is a potent nucleic acid chaperone that directs dimerization of the viral (+) strand RNA in vitro. *Nucleic Acids Res.* 32, 2623–2631. doi:10.1093/nar/gkh579
- Dao Thi, V.L., Granier, C., Zeisel, M.B., Guérin, M., Mancip, J., Granio, O., Penin, F., Lavillette, D., Bartenschlager, R., Baumert, T.F., Cosset, F.-L., Dreux, M., 2012. Characterization of hepatitis C virus particle subpopulations reveals multiple usage of the scavenger receptor BI for entry steps. *J. Biol. Chem.* 287, 31242–31257. doi:10.1074/jbc.M112.365924

- Dave, R., Terry, D.S., Munro, J.B., Blanchard, S.C., 2009. Mitigating Unwanted Photophysical Processes for Improved Single-Molecule Fluorescence Imaging. *Biophys. J.* 96, 2371–2381. doi:10.1016/j.bpj.2008.11.061
- David, N., Yaffe, Y., Hagoel, L., Elazar, M., Glenn, J.S., Hirschberg, K., Sklan, E.H., 2015. The interaction between the Hepatitis C proteins NS4B and NS5A is involved in viral replication. *Virology* 475, 139–149. doi:10.1016/j.virol.2014.10.021
- Davis, M., Sagan, S.M., Pezacki, J.P., Evans, D.J., Simmonds, P., 2008. Bioinformatic and physical characterizations of genome-scale ordered RNA structure in mammalian RNA viruses. *J. Virol.* 82, 11824–11836. doi:10.1128/JVI.01078-08
- de Castro, M.A.G., Rammner, B., Opazo, F., 2016. Aptamer Stainings for Super-resolution Microscopy. *Methods Mol. Biol.* Clifton NJ 1380, 197–210. doi:10.1007/978-1-4939-3197-2_17
- Deretic, V., Saitoh, T., Akira, S., 2013. Autophagy in infection, inflammation and immunity. *Nat. Rev. Immunol.* 13, 722–737. doi:10.1038/nri3532
- Deschout, H., Zanicchi, F.C., Mlodzianoski, M., Diaspro, A., Bewersdorf, J., Hess, S.T., Braeckmans, K., 2014. Precisely and accurately localizing single emitters in fluorescence microscopy. *Nat. Methods* 11, 253–266. doi:10.1038/nmeth.2843
- Diamond, D.L., Syder, A.J., Jacobs, J.M., Sorensen, C.M., Walters, K.-A., Proll, S.C., McDermott, J.E., Gritsenko, M.A., Zhang, Q., Zhao, R., Metz, T.O., Li, D.G.C., Waters, K.M., Smith, R.D., Rice, C.M., Katze, M.G., 2010. Temporal Proteome and Lipidome Profiles Reveal Hepatitis C Virus-Associated Reprogramming of Hepatocellular Metabolism and Bioenergetics. *PLOS Pathog* 6, e1000719. doi:10.1371/journal.ppat.1000719
- Diao, J., Pantua, H., Ngu, H., Komuves, L., Diehl, L., Schaefer, G., Kapadia, S.B., 2012. Hepatitis C virus induces epidermal growth factor receptor activation via CD81 binding for viral internalization and entry. *J. Virol.* 86, 10935–10949. doi:10.1128/JVI.00750-12
- Diaz, O., Delers, F., Maynard, M., Demignot, S., Zoulim, F., Chambaz, J., Trépo, C., Lotteau, V., André, P., 2006. Preferential association of Hepatitis C virus with apolipoprotein B48-containing lipoproteins. *J. Gen. Virol.* 87, 2983–2991. doi:10.1099/vir.0.82033-0
- Ding, W.-X., Ni, H.-M., Gao, W., Yoshimori, T., Stolz, D.B., Ron, D., Yin, X.-M., 2007. Linking of Autophagy to Ubiquitin-Proteasome System Is Important for the Regulation of Endoplasmic Reticulum Stress and Cell Viability. *Am. J. Pathol.* 171, 513–524. doi:10.2353/ajpath.2007.070188
- Donahue, J.G., Muñoz, A., Ness, P.M., Brown, D.E., Yawn, D.H., McAllister, H.A., Reitz, B.A., Nelson, K.E., 1992. The declining risk of post-transfusion hepatitis C virus infection. *N. Engl. J. Med.* 327, 369–373. doi:10.1056/NEJM199208063270601
- Dooley, H.C., Razi, M., Polson, H.E.J., Girardin, S.E., Wilson, M.I., Tooze, S.A., 2014. WIPI2 Links LC3 Conjugation with PI3P, Autophagosome Formation, and Pathogen Clearance by Recruiting Atg12–5–16L1. *Mol. Cell* 55, 238–252. doi:10.1016/j.molcel.2014.05.021
- Dreux, M., Gastaminza, P., Wieland, S.F., Chisari, F.V., 2009. The autophagy machinery is required to initiate hepatitis C virus replication. *Proc. Natl. Acad. Sci.* 106, 14046–14051. doi:10.1073/pnas.0907344106
- Drummer, H.E., Boo, I., Pountourios, P., 2007. Mutagenesis of a conserved fusion peptide-like motif and membrane-proximal heptad-repeat region of hepatitis C virus glycoprotein E1. *J. Gen. Virol.* 88, 1144–1148. doi:10.1099/vir.0.82567-0
- Dubuisson, J., Hsu, H.H., Cheung, R.C., Greenberg, H.B., Russell, D.G., Rice, C.M., 1994. Formation and intracellular localization of hepatitis C virus

envelope glycoprotein complexes expressed by recombinant vaccinia and Sindbis viruses. *J. Virol.* 68, 6147–6160.

- Dutartre, H., Bussetta, C., Boretto, J., Canard, B., 2006. General catalytic deficiency of hepatitis C virus RNA polymerase with an S282T mutation and mutually exclusive resistance towards 2'-modified nucleotide analogues. *Antimicrob. Agents Chemother.* 50, 4161–4169. doi:10.1128/AAC.00433-06
- Duvignaud, J.-B., Savard, C., Fromentin, R., Majeau, N., Leclerc, D., Gagné, S.M., 2009. Structure and dynamics of the N-terminal half of hepatitis C virus core protein: An intrinsically unstructured protein. *Biochem. Biophys. Res. Commun.* 378, 27–31. doi:10.1016/j.bbrc.2008.10.141
- Dyba, M., Jakobs, S., Hell, S.W., 2003. Immunofluorescence stimulated emission depletion microscopy. *Nat. Biotechnol.* 21, 1303–1304. doi:10.1038/nbt897
- Egger, D., Wölk, B., Gosert, R., Bianchi, L., Blum, H.E., Moradpour, D., Bienz, K., 2002. Expression of Hepatitis C Virus Proteins Induces Distinct Membrane Alterations Including a Candidate Viral Replication Complex. *J. Virol.* 76, 5974–5984. doi:10.1128/JVI.76.12.5974-5984.2002
- Eggert, D., Rösch, K., Reimer, R., Herker, E., 2014. Visualization and Analysis of Hepatitis C Virus Structural Proteins at Lipid Droplets by Super-Resolution Microscopy. *PLOS ONE* 9, e102511. doi:10.1371/journal.pone.0102511
- Einav, S., Elazar, M., Danieli, T., Glenn, J.S., 2004. A nucleotide binding motif in hepatitis C virus (HCV) NS4B mediates HCV RNA replication. *J. Virol.* 78, 11288–11295. doi:10.1128/JVI.78.20.11288-11295.2004
- El Omari, K., Iourin, O., Kadlec, J., Sutton, G., Harlos, K., Grimes, J.M., Stuart, D.I., 2014. Unexpected structure for the N-terminal domain of hepatitis C virus envelope glycoprotein E1. *Nat. Commun.* 5, 4874. doi:10.1038/ncomms5874
- Elazar, M., Liu, P., Rice, C.M., Glenn, J.S., 2004. An N-Terminal Amphipathic Helix in Hepatitis C Virus (HCV) NS4B Mediates Membrane Association, Correct Localization of Replication Complex Proteins, and HCV RNA Replication. *J. Virol.* 78, 11393–11400. doi:10.1128/JVI.78.20.11393-11400.2004
- El-Hage, N., Luo, G., 2003. Replication of hepatitis C virus RNA occurs in a membrane-bound replication complex containing nonstructural viral proteins and RNA. *J. Gen. Virol.* 84, 2761–2769. doi:10.1099/vir.0.19305-0
- Ellington, A.D., Szostak, J.W., 1990. In vitro selection of RNA molecules that bind specific ligands. *Nature* 346, 818–822. doi:10.1038/346818a0
- Endesfelder, U., Finan, K., Holden, S.J., Cook, P.R., Kapanidis, A.N., Heilemann, M., 2013. Multiscale spatial organization of RNA polymerase in *Escherichia coli*. *Biophys. J.* 105, 172–181. doi:10.1016/j.bpj.2013.05.048
- Endesfelder, U., Malkusch, S., Fricke, F., Heilemann, M., 2014. A simple method to estimate the average localization precision of a single-molecule localization microscopy experiment. *Histochem. Cell Biol.* 141, 629–638. doi:10.1007/s00418-014-1192-3
- Erdelyi, M., Rees, E., Metcalf, D., Schierle, G.S.K., Dudas, L., Sinko, J., Knight, A.E., Kaminski, C.F., 2013. Correcting chromatic offset in multicolor super-resolution localization microscopy. *Opt. Express* 21, 10978. doi:10.1364/OE.21.010978
- Erickson, H.P., 2009. Size and Shape of Protein Molecules at the Nanometer Level Determined by Sedimentation, Gel Filtration, and Electron Microscopy. *Biol. Proced. Online* 11, 32–51. doi:10.1007/s12575-009-9008-x
- Espadaler, J., Romero-Isart, O., Jackson, R.M., Oliva, B., 2005. Prediction of protein-protein interactions using distant conservation of sequence patterns and structure relationships. *Bioinformatics* 21, 3360–3368. doi:10.1093/bioinformatics/bti522
- Esser-Nobis, K., Romero-Brey, I., Ganten, T.M., Gouttenoire, J., Harak, C., Klein, R., Schemmer, P., Binder, M., Schnitzler, P., Moradpour, D., Bartenschlager, R., Polyak, S.J., Stremmel, W., Penin, F., Eisenbach, C.,

- Lohmann, V., 2013. Analysis of hepatitis C virus resistance to silibinin *in vitro* and *in vivo* points to a novel mechanism involving nonstructural protein 4B. *Hepatology*. Baltimore, Md 57, 953–963. doi:10.1002/hep.26260
- Ester, M., Kriegel, H.-P., Sander, J., Xiaowei, X., 1996. A density-based algorithm for discovering clusters in large spatial databases with noise. *Proc. Second Int. Conf. Knowl. Discov. Data Min.* 226–231.
- Evans, M.J., Rice, C.M., Goff, S.P., 2004. Phosphorylation of hepatitis C virus nonstructural protein 5A modulates its protein interactions and viral RNA replication. *Proc. Natl. Acad. Sci. U. S. A.* 101, 13038–13043. doi:10.1073/pnas.0405152101
- Evans, M.J., von Hahn, T., Tschernig, D.M., Syder, A.J., Panis, M., Wölk, B., Hatzioannou, T., McKeating, J.A., Bieniasz, P.D., Rice, C.M., 2007. Claudin-1 is a hepatitis C virus co-receptor required for a late step in entry. *Nature* 446, 801–805. doi:10.1038/nature05654
- Eyre, N.S., Fiches, G.N., Aloia, A.L., Helbig, K.J., McCartney, E.M., McErlean, C.S.P., Li, K., Aggarwal, A., Turville, S.G., Beard, M.R., 2014. Dynamic Imaging of the Hepatitis C Virus NS5A Protein during a Productive Infection. *J. Virol.* 88, 3636–3652. doi:10.1128/JVI.02490-13
- Fahmy, A.M., Labonté, P., 2017. The autophagy elongation complex (ATG5-12/16L1) positively regulates HCV replication and is required for wild-type membranous web formation. *Sci. Rep.* 7, 40351. doi:10.1038/srep40351
- Farci, P., Alter, H.J., Shimoda, A., Govindarajan, S., Cheung, L.C., Melpolder, J.C., Sacher, R.A., Shih, J.W., Purcell, R.H., 1996. Hepatitis C virus-associated fulminant hepatic failure. *N. Engl. J. Med.* 335, 631–634. doi:10.1056/NEJM199608293350904
- Faria, S.C., Ganesan, K., Mwangi, I., Shiehorteza, M., Viamonte, B., Mazhar, S., Peterson, M., Kono, Y., Santillan, C., Casola, G., Sirlin, C.B., 2009. MR imaging of liver fibrosis: current state of the art. *Radiogr. Rev. Publ. Radiol. Soc. N. Am. Inc* 29, 1615–1635. doi:10.1148/rg.296095512
- Farquhar, M.J., Harris, H.J., Diskar, M., Jones, S., Mee, C.J., Nielsen, S.U., Brimacombe, C.L., Molina, S., Toms, G.L., Maurel, P., Howl, J., Herberg, F.W., IJzendoorn, S.C.D. van, Balfe, P., McKeating, J.A., 2008. Protein Kinase A-Dependent Step(s) in Hepatitis C Virus Entry and Infectivity. *J. Virol.* 82, 8797–8811. doi:10.1128/JVI.00592-08
- Farquhar, M.J., Hu, K., Harris, H.J., Davis, C., Brimacombe, C.L., Fletcher, S.J., Baumert, T.F., Rappoport, J.Z., Balfe, P., McKeating, J.A., 2012. Hepatitis C virus induces CD81 and claudin-1 endocytosis. *J. Virol.* 86, 4305–4316. doi:10.1128/JVI.06996-11
- Feinstone, S.M., Kapikian, A.Z., Purcell, R.H., Alter, H.J., Holland, P.V., 1975. Transfusion-associated hepatitis not due to viral hepatitis type A or B. *N. Engl. J. Med.* 292, 767–770. doi:10.1056/NEJM197504102921502
- Feld, J.J., 2014. Interferon-free strategies with a nucleoside/nucleotide analogue. *Semin. Liver Dis.* 34, 37–46. doi:10.1055/s-0034-1371009
- Feld, J.J., Jacobson, I.M., Hézode, C., Asselah, T., Ruane, P.J., Gruener, N., Abergel, A., Mangia, A., Lai, C.-L., Chan, H.L.Y., Mazzotta, F., Moreno, C., Yoshida, E., Shafran, S.D., Towner, W.J., Tran, T.T., McNally, J., Osinusi, A., Svarovskaia, E., Zhu, Y., Brainard, D.M., McHutchison, J.G., Agarwal, K., Zeuzem, S., 2015. Sofosbuvir and Velpatasvir for HCV Genotype 1, 2, 4, 5, and 6 Infection. *N. Engl. J. Med.* 373, 2599–2607. doi:10.1056/NEJMoa1512610
- Felmlee, D.J., Sheridan, D.A., Bridge, S.H., Nielsen, S.U., Milne, R.W., Packard, C.J., Caslake, M.J., McLauchlan, J., Toms, G.L., Neely, R.D.G., Bassendine, M.F., 2010. Intravascular transfer contributes to postprandial increase in numbers of very-low-density hepatitis C virus particles. *Gastroenterology* 139, 1774–1783, 1783–6. doi:10.1053/j.gastro.2010.07.047

- Fernández-Suárez, M., Baruah, H., Martínez-Hernández, L., Xie, K.T., Baskin, J.M., Bertozzi, C.R., Ting, A.Y., 2007. Redirecting lipoic acid ligase for cell surface protein labeling with small-molecule probes. *Nat. Biotechnol.* 25, 1483–1487. doi:10.1038/nbt1355
- Ferrari, E., He, Z., Palermo, R.E., Huang, H.-C., 2008. Hepatitis C Virus NS5B Polymerase Exhibits Distinct Nucleotide Requirements for Initiation and Elongation. *J. Biol. Chem.* 283, 33893–33901. doi:10.1074/jbc.M803094200
- Ferraris, P., Beaumont, E., Uzbekov, R., Brand, D., Gaillard, J., Blanchard, E., Roingeard, P., 2012. Sequential biogenesis of host cell membrane rearrangements induced by hepatitis C virus infection. *Cell. Mol. Life Sci.* 70, 1297–1306. doi:10.1007/s00018-012-1213-0
- Ferraris, P., Blanchard, E., Roingeard, P., 2010. Ultrastructural and biochemical analyses of hepatitis C virus-associated host cell membranes. *J. Gen. Virol.* 91, 2230–2237. doi:10.1099/vir.0.022186-0
- Feuerstein, S., Solyom, Z., Aladag, A., Favier, A., Schwarten, M., Hoffmann, S., Willbold, D., Brutscher, B., 2012. Transient Structure and SH3 Interaction Sites in an Intrinsically Disordered Fragment of the Hepatitis C Virus Protein NS5A. *J. Mol. Biol.* 420, 310–323. doi:10.1016/j.jmb.2012.04.023
- Fiches, G.N., Eyre, N.S., Aloia, A.L., Van Der Hoek, K., Betz-Stablein, B., Luciani, F., Chopra, A., Beard, M.R., 2016. HCV RNA traffic and association with NS5A in living cells. *Virology* 493, 60–74. doi:10.1016/j.virol.2016.02.016
- Fitzgerald, J.E., Lu, J., Schnitzer, M.J., 2012. Estimation theoretic measure of resolution for stochastic localization microscopy. *Phys. Rev. Lett.* 109, 48102. doi:10.1103/PhysRevLett.109.048102
- Flajnik, M.F., Deschacht, N., Muyldermans, S., 2011. A Case Of Convergence: Why Did a Simple Alternative to Canonical Antibodies Arise in Sharks and Camels? *PLOS Biol* 9, e1001120. doi:10.1371/journal.pbio.1001120
- Fölling, J., Bossi, M., Bock, H., Medda, R., Wurm, C.A., Hein, B., Jakobs, S., Eggeling, C., Hell, S.W., 2008. Fluorescence nanoscopy by ground-state depletion and single-molecule return. *Nat. Methods* 5, 943–945. doi:10.1038/nmeth.1257
- Foster, T.L., Belyaeva, T., Stonehouse, N.J., Pearson, A.R., Harris, M., 2010. All Three Domains of the Hepatitis C Virus Nonstructural NS5A Protein Contribute to RNA Binding. *J. Virol.* 84, 9267–9277. doi:10.1128/JVI.00616-10
- Foy, E., Li, K., Wang, C., Sumpter, R., Ikeda, M., Lemon, S.M., Gale, M., 2003. Regulation of Interferon Regulatory Factor-3 by the Hepatitis C Virus Serine Protease. *Science* 300, 1145–1148. doi:10.1126/science.1082604
- Fridell, R.A., Qiu, D., Valera, L., Wang, C., Rose, R.E., Gao, M., 2011. Distinct Functions of NS5A in Hepatitis C Virus RNA Replication Uncovered by Studies with the NS5A Inhibitor BMS-790052. *J. Virol.* 85, 7312–7320. doi:10.1128/JVI.00253-11
- Fridell, R.A., Qiu, D., Wang, C., Valera, L., Gao, M., 2010. Resistance Analysis of the Hepatitis C Virus NS5A Inhibitor BMS-790052 in an In Vitro Replicon System. *Antimicrob. Agents Chemother.* 54, 3641–3650. doi:10.1128/AAC.00556-10
- Friebe, P., Bartenschlager, R., 2002. Genetic analysis of sequences in the 3' nontranslated region of hepatitis C virus that are important for RNA replication. *J. Virol.* 76, 5326–5338.
- Friebe, P., Lohmann, V., Krieger, N., Bartenschlager, R., 2001. Sequences in the 5' nontranslated region of hepatitis C virus required for RNA replication. *J. Virol.* 75, 12047–12057. doi:10.1128/JVI.75.24.12047-12057.2001
- Fujita, N., Itoh, T., Omori, H., Fukuda, M., Noda, T., Yoshimori, T., 2008. The Atg16L complex specifies the site of LC3 lipidation for membrane biogenesis in autophagy. *Mol. Biol. Cell* 19, 2092–2100. doi:10.1091/mbc.E07-12-1257

- Fukuda, K., Vishnuvardhan, D., Sekiya, S., Hwang, J., Kakiuchi, N., Taira, K., Shimotohno, K., Kumar, P.K.R., Nishikawa, S., 2000. Isolation and characterization of RNA aptamers specific for the hepatitis C virus nonstructural protein 3 protease. *Eur. J. Biochem.* 267, 3685–3694. doi:10.1046/j.1432-1327.2000.01400.x
- Fukunaga, K., Hostetler, L., 1975. The estimation of the gradient of a density function, with applications in pattern recognition. *IEEE Trans. Inf. Theory* 21, 32–40. doi:10.1109/TIT.1975.1055330
- Fukushi, S., Kurihara, C., Ishiyama, N., Hoshino, F.B., Oya, A., Katayama, K., 1997. The sequence element of the internal ribosome entry site and a 25-kilodalton cellular protein contribute to efficient internal initiation of translation of hepatitis C virus RNA. *J. Virol.* 71, 1662–1666.
- Furse, S., Brooks, N.J., Seddon, A.M., Woscholski, R., Templer, R.H., Tate, E.W., Gaffney, P.R.J., Ces, O., 2012. Lipid membrane curvature induced by distearoyl phosphatidylinositol 4-phosphate. *Soft Matter* 8, 3090–3093. doi:10.1039/C2SM07358G
- Galli, A., Scheel, T.K.H., Prentoe, J.C., Mikkelsen, L.S., Gottwein, J.M., Bukh, J., 2013. Analysis of hepatitis C virus core/NS5A protein co-localization using novel cell culture systems expressing core-NS2 and NS5A of genotypes 1–7. *J. Gen. Virol.* 94, 2221–2235. doi:10.1099/vir.0.053868-0
- Gao, M., Nettles, R.E., Belema, M., Snyder, L.B., Nguyen, V.N., Fridell, R.A., Serrano-Wu, M.H., Langley, D.R., Sun, J.-H., O'Boyle, D.R., Lemm, J.A., Wang, C., Knipe, J.O., Chien, C., Colonno, R.J., Grasela, D.M., Meanwell, N.A., Hamann, L.G., 2010. Chemical genetics strategy identifies an HCV NS5A inhibitor with a potent clinical effect. *Nature* 465, 96–100. doi:10.1038/nature08960
- Gao, Y., Yu, X., Xue, B., Zhou, F., Wang, X., Yang, D., Liu, N., Xu, L., Fang, X., Zhu, H., 2014. Inhibition of Hepatitis C Virus Infection by DNA Aptamer against NS2 Protein. *PLOS ONE* 9, e90333. doi:10.1371/journal.pone.0090333
- Gastaminza, P., Cheng, G., Wieland, S., Zhong, J., Liao, W., Chisari, F.V., 2008. Cellular Determinants of Hepatitis C Virus Assembly, Maturation, Degradation, and Secretion. *J. Virol.* 82, 2120–2129. doi:10.1128/JVI.02053-07
- Gastaminza, P., Dryden, K.A., Boyd, B., Wood, M.R., Law, M., Yeager, M., Chisari, F.V., 2010. Ultrastructural and biophysical characterization of hepatitis C virus particles produced in cell culture. *J. Virol.* 84, 10999–11009. doi:10.1128/JVI.00526-10
- Gawlik, K., Gallay, P.A., 2014. HCV core protein and virus assembly: what we know without structures. *Immunol. Res.* 60, 1–10. doi:10.1007/s12026-014-8494-3
- Gentsch, J., Brohm, C., Steinmann, E., Friesland, M., Menzel, N., Vieyres, G., Perin, P.M., Frentzen, A., Kaderali, L., Pietschmann, T., 2013. Hepatitis C Virus p7 is Critical for Capsid Assembly and Envelopment. *PLOS Pathog* 9, e1003355. doi:10.1371/journal.ppat.1003355
- Germi, R., Crance, J.-M., Garin, D., Guimet, J., Lortat-Jacob, H., Ruigrok, R.W.H., Zarski, J.-P., Drouet, E., 2002. Cellular glycosaminoglycans and low density lipoprotein receptor are involved in hepatitis C virus adsorption. *J. Med. Virol.* 68, 206–215. doi:10.1002/jmv.10196
- Getis, A., Franklin, J., 1987. Second-Order Neighborhood Analysis of Mapped Point Patterns. *Ecology* 68, 473–477. doi:10.2307/1938452
- Giepmans, B.N.G., Adams, S.R., Ellisman, M.H., Tsien, R.Y., 2006. The fluorescent toolbox for assessing protein location and function. *Science* 312, 217–224. doi:10.1126/science.1124618
- Goffard, A., Callens, N., Bartosch, B., Wychowski, C., Cosset, F.-L., Montpellier, C., Dubuisson, J., 2005. Role of N-linked glycans in the functions of hepatitis C

- virus envelope glycoproteins. *J. Virol.* 79, 8400–8409. doi:10.1128/JVI.79.13.8400-8409.2005
- Goh, P.-Y., Tan, Y.-J., Lim, S.P., Lim, S.G., Tan, Y.H., Hong, W.J., 2001. The Hepatitis C Virus Core Protein Interacts with NS5A and Activates Its Caspase-Mediated Proteolytic Cleavage. *Virology* 290, 224–236. doi:10.1006/viro.2001.1195
- Gosert, R., Egger, D., Lohmann, V., Bartenschlager, R., Blum, H.E., Bienz, K., Moradpour, D., 2003. Identification of the Hepatitis C Virus RNA Replication Complex in Huh-7 Cells Harboring Subgenomic Replicons. *J. Virol.* 77, 5487–5492. doi:10.1128/JVI.77.9.5487-5492.2003
- Gosert, R., Jendrszczok, W., Berke, J.M., Brass, V., Blum, H.E., Moradpour, D., 2005. Characterization of Nonstructural Protein Membrane Anchor Deletion Mutants Expressed in the Context of the Hepatitis C Virus Polyprotein. *J. Virol.* 79, 7911–7917. doi:10.1128/JVI.79.12.7911-7917.2005
- Gouttenoire, J., Penin, F., Moradpour, D., 2010. Hepatitis C virus nonstructural protein 4B: a journey into unexplored territory. *Rev. Med. Virol.* 20, 117–129. doi:10.1002/rmv.640
- Grakoui, A., McCourt, D.W., Wychowski, C., Feinstone, S.M., Rice, C.M., 1993. A second hepatitis C virus-encoded proteinase. *Proc. Natl. Acad. Sci. U. S. A.* 90, 10583–10587.
- Griffié, J., Shannon, M., Bromley, C.L., Boelen, L., Burn, G.L., Williamson, D.J., Heard, N.A., Cope, A.P., Owen, D.M., Rubin-Delanchy, P., 2016. A Bayesian cluster analysis method for single-molecule localization microscopy data. *Nat. Protoc.* 11, 2499–2514. doi:10.1038/nprot.2016.149
- Griffin, B.A., Adams, S.R., Tsien, R.Y., 1998. Specific Covalent Labeling of Recombinant Protein Molecules Inside Live Cells. *Science* 281, 269–272. doi:10.1126/science.281.5374.269
- Griffin, S., Clarke, D., McCormick, C., Rowlands, D., Harris, M., 2005. Signal Peptide Cleavage and Internal Targeting Signals Direct the Hepatitis C Virus p7 Protein to Distinct Intracellular Membranes. *J. Virol.* 79, 15525–15536. doi:10.1128/JVI.79.24.15525-15536.2005
- Griffin, S.D.C., Beales, L.P., Clarke, D.S., Worsfold, O., Evans, S.D., Jaeger, J., Harris, M.P.G., Rowlands, D.J., 2003. The p7 protein of hepatitis C virus forms an ion channel that is blocked by the antiviral drug, Amantadine. *FEBS Lett.* 535, 34–38.
- Gross, D.A., Silver, D.L., 2014. Cytosolic lipid droplets: from mechanisms of fat storage to disease. *Crit. Rev. Biochem. Mol. Biol.* 49, 304–326. doi:10.3109/10409238.2014.931337
- Gu, M., Rice, C.M., 2010. Three conformational snapshots of the hepatitis C virus NS3 helicase reveal a ratchet translocation mechanism. *Proc. Natl. Acad. Sci.* 107, 521–528. doi:10.1073/pnas.0913380107
- Guévin, C., Manna, D., Bélanger, C., Konan, K.V., Mak, P., Labonté, P., 2010. Autophagy protein ATG5 interacts transiently with the hepatitis C virus RNA polymerase (NS5B) early during infection. *Virology* 405, 1–7. doi:10.1016/j.virol.2010.05.032
- Guizar-Sicairos, M., Thurman, S.T., Fienup, J.R., 2008. Efficient subpixel image registration algorithms. *Opt. Lett.* 33, 156–158.
- Gustafsson, M.G., 2000. Surpassing the lateral resolution limit by a factor of two using structured illumination microscopy. *J. Microsc.* 198, 82–87.
- Gustafsson, M.G., Agard, D.A., Sedat, J.W., 1999. I5M: 3D widefield light microscopy with better than 100 nm axial resolution. *J. Microsc.* 195, 10–16.
- Gustafsson, M.G.L., 2005. Nonlinear structured-illumination microscopy: Wide-field fluorescence imaging with theoretically unlimited resolution. *Proc. Natl. Acad. Sci. U. S. A.* 102, 13081–13086. doi:10.1073/pnas.0406877102
- Gustafsson, M.G.L., Shao, L., Carlton, P.M., Wang, C.J.R., Golubovskaya, I.N., Cande, W.Z., Agard, D.A., Sedat, J.W., 2008. Three-dimensional resolution

- doubling in wide-field fluorescence microscopy by structured illumination. *Biophys. J.* 94, 4957–4970. doi:10.1529/biophysj.107.120345
- Gutierrez, M.G., Master, S.S., Singh, S.B., Taylor, G.A., Colombo, M.I., Deretic, V., 2004. Autophagy is a defense mechanism inhibiting BCG and *Mycobacterium tuberculosis* survival in infected macrophages. *Cell* 119, 753–766. doi:10.1016/j.cell.2004.11.038
- Hadziyannis, S.J., Sette, H., Morgan, T.R., Balan, V., Diago, M., Marcellin, P., Ramadori, G., Bodenheimer, H., Bernstein, D., Rizzetto, M., Zeuzem, S., Pockros, P.J., Lin, A., Ackrill, A.M., PEGASYS International Study Group, 2004. Peginterferon-alpha2a and ribavirin combination therapy in chronic hepatitis C: a randomized study of treatment duration and ribavirin dose. *Ann. Intern. Med.* 140, 346–355.
- Hagemeyer, M.C., Vonk, A.M., Monastyrska, I., Rottier, P.J.M., Haan, C.A.M. de, 2012. Visualizing Coronavirus RNA Synthesis in Time by Using Click Chemistry. *J. Virol.* 86, 5808–5816. doi:10.1128/JVI.07207-11
- Hagen, C., Guttman, P., Klupp, B., Werner, S., Rehbein, S., Mettenleiter, T.C., Schneider, G., Grünewald, K., 2012. Correlative VIS-fluorescence and soft X-ray cryo-microscopy/tomography of adherent cells. *J. Struct. Biol.* 177, 193–201. doi:10.1016/j.jsb.2011.12.012
- Haid, S., Pietschmann, T., Pécheur, E.-I., 2009. Low pH-dependent Hepatitis C Virus Membrane Fusion Depends on E2 Integrity, Target Lipid Composition, and Density of Virus Particles. *J. Biol. Chem.* 284, 17657–17667. doi:10.1074/jbc.M109.014647
- Hamamoto, I., Nishimura, Y., Okamoto, T., Aizaki, H., Liu, M., Mori, Y., Abe, T., Suzuki, T., Lai, M.M.C., Miyamura, T., Moriishi, K., Matsuura, Y., 2005. Human VAP-B is involved in hepatitis C virus replication through interaction with NS5A and NS5B. *J. Virol.* 79, 13473–13482. doi:10.1128/JVI.79.21.13473-13482.2005
- Hamasaki, M., Furuta, N., Matsuda, A., Nezu, A., Yamamoto, A., Fujita, N., Oomori, H., Noda, T., Haraguchi, T., Hiraoka, Y., Amano, A., Yoshimori, T., 2013. Autophagosomes form at ER-mitochondria contact sites. *Nature* 495, 389–393. doi:10.1038/nature11910
- Han, Q., Manna, D., Belton, K., Cole, R., Konan, K.V., 2013. Modulation of hepatitis C virus genome encapsidation by nonstructural protein 4B. *J. Virol.* 87, 7409–7422. doi:10.1128/JVI.03523-12
- Handschumacher, R.E., Harding, M.W., Rice, J., Drugge, R.J., Speicher, D.W., 1984. Cyclophilin: a specific cytosolic binding protein for cyclosporin A. *Science* 226, 544–547.
- Hanoulle, X., Badillo, A., Verdegem, D., Penin, F., Lippens, G., 2010. The domain 2 of the HCV NS5A protein is intrinsically unstructured. *Protein Pept. Lett.* 17, 1012–1018.
- Hanoulle, X., Badillo, A., Wieruszkeski, J.-M., Verdegem, D., Landrieu, I., Bartenschlager, R., Penin, F., Lippens, G., 2009a. Hepatitis C virus NS5A protein is a substrate for the peptidyl-prolyl cis/trans isomerase activity of cyclophilins A and B. *J. Biol. Chem.* 284, 13589–13601. doi:10.1074/jbc.M809244200
- Hanoulle, X., Verdegem, D., Badillo, A., Wieruszkeski, J.-M., Penin, F., Lippens, G., 2009b. Domain 3 of non-structural protein 5A from hepatitis C virus is natively unfolded. *Biochem. Biophys. Res. Commun.* 381, 634–638. doi:10.1016/j.bbrc.2009.02.108
- Harke, B., Keller, J., Ullal, C.K., Westphal, V., Schönle, A., Hell, S.W., 2008. Resolution scaling in STED microscopy. *Opt. Express* 16, 4154–4162.
- Harris, H.J., Davis, C., Mullins, J.G.L., Hu, K., Goodall, M., Farquhar, M.J., Mee, C.J., McCaffrey, K., Young, S., Drummer, H., Balfe, P., McKeating, J.A., 2010. Claudin association with CD81 defines hepatitis C virus entry. *J. Biol. Chem.* 285, 21092–21102. doi:10.1074/jbc.M110.104836

- Haukenes, G., Szilvay, A.M., Brokstad, K.A., Kanestrøm, A., Kalland, K.H., 1997. Labeling of RNA transcripts of eukaryotic cells in culture with BrUTP using a liposome transfection reagent (DOTAP). *BioTechniques* 22, 308–312.
- Hazuda, D.J., Burroughs, M., Howe, A.Y.M., Wahl, J., Venkatraman, S., 2013. Development of boceprevir: a first-in-class direct antiviral treatment for chronic hepatitis C infection. *Ann. N. Y. Acad. Sci.* 1291, 69–76. doi:10.1111/nyas.12218
- He, Y., Nakao, H., Tan, S.-L., Polyak, S.J., Neddermann, P., Vijaysri, S., Jacobs, B.L., Katze, M.G., 2002. Subversion of Cell Signaling Pathways by Hepatitis C Virus Nonstructural 5A Protein via Interaction with Grb2 and P85 Phosphatidylinositol 3-Kinase. *J. Virol.* 76, 9207–9217. doi:10.1128/JVI.76.18.9207-9217.2002
- He, Y., Weng, L., Li, R., Li, L., Toyoda, T., Zhong, J., 2012. The N-terminal helix $\alpha 0$ of hepatitis C virus NS3 protein dictates the subcellular localization and stability of NS3/NS4A complex. *Virology* 422, 214–223. doi:10.1016/j.virol.2011.10.021
- Heilemann, M., van de Linde, S., Schüttpeitz, M., Kasper, R., Seefeldt, B., Mukherjee, A., Tinnefeld, P., Sauer, M., 2008. Subdiffraction-Resolution Fluorescence Imaging with Conventional Fluorescent Probes. *Angew. Chem. Int. Ed.* 47, 6172–6176. doi:10.1002/anie.200802376
- Hell, S., Stelzer, E.H., 1992. Properties of a 4Pi confocal fluorescence microscope. *JOSA A* 9, 2159–2166.
- Hess, S.T., Girirajan, T.P.K., Mason, M.D., 2006. Ultra-High Resolution Imaging by Fluorescence Photoactivation Localization Microscopy. *Biophys. J.* 91, 4258–4272. doi:10.1529/biophysj.106.091116
- Hijikata, M., Mizushima, H., Akagi, T., Mori, S., Kakiuchi, N., Kato, N., Tanaka, T., Kimura, K., Shimotohno, K., 1993. Two distinct proteinase activities required for the processing of a putative nonstructural precursor protein of hepatitis C virus. *J. Virol.* 67, 4665–4675.
- Hirata, Y., Ikeda, K., Sudoh, M., Tokunaga, Y., Suzuki, A., Weng, L., Ohta, M., Tobita, Y., Okano, K., Ozeki, K., Kawasaki, K., Tsukuda, T., Katsume, A., Aoki, Y., Umehara, T., Sekiguchi, S., Toyoda, T., Shimotohno, K., Soga, T., Nishijima, M., Taguchi, R., Kohara, M., 2012. Self-enhancement of hepatitis C virus replication by promotion of specific sphingolipid biosynthesis. *PLoS Pathog.* 8, e1002860. doi:10.1371/journal.ppat.1002860
- Holthuis, J.C.M., Menon, A.K., 2014. Lipid landscapes and pipelines in membrane homeostasis. *Nature* 510, 48–57. doi:10.1038/nature13474
- Honda, M., Brown, E.A., Lemon, S.M., 1996. Stability of a stem-loop involving the initiator AUG controls the efficiency of internal initiation of translation on hepatitis C virus RNA. *RNA N. Y. N* 2, 955–968.
- Honda, M., Rijnbrand, R., Abell, G., Kim, D., Lemon, S.M., 1999. Natural variation in translational activities of the 5' nontranslated RNAs of hepatitis C virus genotypes 1a and 1b: evidence for a long-range RNA-RNA interaction outside of the internal ribosomal entry site. *J. Virol.* 73, 4941–4951.
- Hooke, R., 1667. *Micrographia: or some physiological descriptions of minute bodies made by magnifying glasses : with observations and inquiries thereupon.*
- Hopp, T.P., Prickett, K.S., Price, V.L., Libby, R.T., March, C.J., Pat Cerretti, D., Urdal, D.L., Conlon, P.J., 1988. A Short Polypeptide Marker Sequence Useful for Recombinant Protein Identification and Purification. *Nat. Biotechnol.* 6, 1204–1210. doi:10.1038/nbt1088-1204
- Horney, M.J., Evangelista, C.A., Rosenzweig, S.A., 2001. Synthesis and Characterization of Insulin-like Growth Factor (IGF)-1 Photoprobes Selective for the IGF-binding Proteins (IGFBPs) PHOTOAFFINITY LABELING OF THE IGF-BINDING DOMAIN ON IGFBP-2. *J. Biol. Chem.* 276, 2880–2889. doi:10.1074/jbc.M007526200

- Horton, R.M., Cai, Z.L., Ho, S.N., Pease, L.R., 1990. Gene splicing by overlap extension: tailor-made genes using the polymerase chain reaction. *BioTechniques* 8, 528–535.
- Hosokawa, N., Hara, T., Kaizuka, T., Kishi, C., Takamura, A., Miura, Y., Iemura, S., Natsume, T., Takehana, K., Yamada, N., Guan, J.-L., Oshiro, N., Mizushima, N., 2009. Nutrient-dependent mTORC1 Association with the ULK1–Atg13–FIP200 Complex Required for Autophagy. *Mol. Biol. Cell* 20, 1981–1991. doi:10.1091/mbc.E08-12-1248
- Huang, B., Babcock, H., Zhuang, X., 2010. Breaking the Diffraction Barrier: Super-Resolution Imaging of Cells. *Cell* 143, 1047–1058. doi:10.1016/j.cell.2010.12.002
- Huang, B., Jones, S.A., Brandenburg, B., Zhuang, X., 2008a. Whole cell 3D STORM reveals interactions between cellular structures with nanometer-scale resolution. *Nat. Methods* 5, 1047–1052. doi:10.1038/nmeth.1274
- Huang, B., Wang, W., Bates, M., Zhuang, X., 2008b. Three-dimensional Super-resolution Imaging by Stochastic Optical Reconstruction Microscopy. *Science* 319, 810–813. doi:10.1126/science.1153529
- Huang, L., Hwang, J., Sharma, S.D., Hargittai, M.R.S., Chen, Y., Arnold, J.J., Raney, K.D., Cameron, C.E., 2005. Hepatitis C Virus Nonstructural Protein 5A (NS5A) Is an RNA-binding Protein. *J. Biol. Chem.* 280, 36417–36428. doi:10.1074/jbc.M508175200
- Hughes, M., Griffin, S., Harris, M., 2009. Domain III of NS5A contributes to both RNA replication and assembly of hepatitis C virus particles. *J. Gen. Virol.* 90, 1329–1334. doi:10.1099/vir.0.009332-0
- Hüssy, P., Langen, H., Mous, J., Jacobsen, H., 1996. Hepatitis C virus core protein: carboxy-terminal boundaries of two processed species suggest cleavage by a signal peptide peptidase. *Virology* 224, 93–104. doi:10.1006/viro.1996.0510
- Huwart, L., van Beers, B.E., 2008. MR elastography. *Gastroentérologie Clin. Biol.* 32, 68–72. doi:10.1016/S0399-8320(08)73995-2
- Hwang, J., Huang, L., Cordek, D.G., Vaughan, R., Reynolds, S.L., Kihara, G., Raney, K.D., Kao, C.C., Cameron, C.E., 2010. Hepatitis C Virus Nonstructural Protein 5A: Biochemical Characterization of a Novel Structural Class of RNA-Binding Proteins. *J. Virol.* 84, 12480–12491. doi:10.1128/JVI.01319-10
- Igloi, Z., Kazlauskas, A., Saksela, K., Macdonald, A., Mankouri, J., Harris, M., 2015. Hepatitis C virus NS5A protein blocks epidermal growth factor receptor degradation via a proline motif-dependent interaction. *J. Gen. Virol.* 96, 2133–2144. doi:10.1099/vir.0.000145
- Isken, O., Baroth, M., Grassmann, C.W., Weinlich, S., Ostareck, D.H., Ostareck-Lederer, A., Behrens, S.-E., 2007. Nuclear factors are involved in hepatitis C virus RNA replication. *RNA* 13, 1675–1692. doi:10.1261/rna.594207
- Itano, M.S., Graus, M.S., Pehlke, C., Wester, M.J., Liu, P., Lidke, K.A., Thompson, N.L., Jacobson, K., Neumann, A.K., 2014. Super-resolution imaging of C-type lectin spatial rearrangement within the dendritic cell plasma membrane at fungal microbe contact sites. *Front. Phys.* 2. doi:10.3389/fphy.2014.00046
- Ivanyi-Nagy, R., Kanevsky, I., Gabus, C., Lavergne, J.-P., Ficheux, D., Penin, F., Fossé, P., Darlix, J.-L., 2006. Analysis of hepatitis C virus RNA dimerization and core–RNA interactions. *Nucleic Acids Res.* 34, 2618–2633. doi:10.1093/nar/gkl240
- Jackson, R.J., Hellen, C.U.T., Pestova, T.V., 2010. The mechanism of eukaryotic translation initiation and principles of its regulation. *Nat. Rev. Mol. Cell Biol.* 11, 113–127. doi:10.1038/nrm2838
- Jaeckel, E., Cornberg, M., Wedemeyer, H., Santantonio, T., Mayer, J., Zankel, M., Pastore, G., Dietrich, M., Trautwein, C., Manns, M.P., 2001. Treatment of

- Acute Hepatitis C with Interferon Alfa-2b. *N. Engl. J. Med.* 345, 1452–1457. doi:10.1056/NEJMoa011232
- Jäger, S., Bucci, C., Tanida, I., Ueno, T., Kominami, E., Saftig, P., Eskelinen, E.-L., 2004. Role for Rab7 in maturation of late autophagic vacuoles. *J. Cell Sci.* 117, 4837–4848. doi:10.1242/jcs.01370
- Jamur, M.C., Oliver, C., 2010. Permeabilization of cell membranes. *Methods Mol. Biol.* Clifton NJ 588, 63–66. doi:10.1007/978-1-59745-324-0_9
- Jao, C.Y., Salic, A., 2008. Exploring RNA transcription and turnover in vivo by using click chemistry. *Proc. Natl. Acad. Sci.* 105, 15779–15784. doi:10.1073/pnas.0808480105
- Jensen, M.A., Fukushima, M., Davis, R.W., 2010. DMSO and Betaine Greatly Improve Amplification of GC-Rich Constructs in De Novo Synthesis. *PLOS ONE* 5, e11024. doi:10.1371/journal.pone.0011024
- Ji, H., Fraser, C.S., Yu, Y., Leary, J., Doudna, J.A., 2004. Coordinated assembly of human translation initiation complexes by the hepatitis C virus internal ribosome entry site RNA. *Proc. Natl. Acad. Sci. U. S. A.* 101, 16990–16995. doi:10.1073/pnas.0407402101
- Jiang, J., Luo, G., 2009. Apolipoprotein E but not B is required for the formation of infectious hepatitis C virus particles. *J. Virol.* 83, 12680–12691. doi:10.1128/JVI.01476-09
- Jirasko, V., Montserret, R., Lee, J.Y., Gouttenoire, J., Moradpour, D., Penin, F., Bartenschlager, R., 2010. Structural and functional studies of nonstructural protein 2 of the hepatitis C virus reveal its key role as organizer of virion assembly. *PLoS Pathog.* 6, e1001233. doi:10.1371/journal.ppat.1001233
- Johnson, E., Seiradake, E., Jones, E.Y., Davis, I., Grünewald, K., Kaufmann, R., 2015. Correlative in-resin super-resolution and electron microscopy using standard fluorescent proteins. *Sci. Rep.* 5, 9583. doi:10.1038/srep09583
- Jones, C.T., Murray, C.L., Eastman, D.K., Tassello, J., Rice, C.M., 2007. Hepatitis C Virus p7 and NS2 Proteins Are Essential for Production of Infectious Virus. *J. Virol.* 81, 8374–8383. doi:10.1128/JVI.00690-07
- Jopling, C.L., Yi, M., Lancaster, A.M., Lemon, S.M., Sarnow, P., 2005. Modulation of hepatitis C virus RNA abundance by a liver-specific MicroRNA. *Science* 309, 1577–1581. doi:10.1126/science.1113329
- Juette, M.F., Gould, T.J., Lessard, M.D., Mlodzianoski, M.J., Nagpure, B.S., Bennett, B.T., Hess, S.T., Bewersdorf, J., 2008. Three-dimensional sub-100 nm resolution fluorescence microscopy of thick samples. *Nat. Methods* 5, 527–529. doi:10.1038/nmeth.1211
- Jung, C.H., Jun, C.B., Ro, S.-H., Kim, Y.-M., Otto, N.M., Cao, J., Kundu, M., Kim, D.-H., 2009. ULK-Atg13-FIP200 Complexes Mediate mTOR Signaling to the Autophagy Machinery. *Mol. Biol. Cell* 20, 1992–2003. doi:10.1091/mbc.E08-12-1249
- Kalveram, B., Lihoradova, O., Ikegami, T., 2011. NSs Protein of Rift Valley Fever Virus Promotes Posttranslational Downregulation of the TFIIF Subunit p62. *J. Virol.* 85, 6234–6243. doi:10.1128/JVI.02255-10
- Kanchanawong, P., Shtengel, G., Pasapera, A.M., Ramko, E.B., Davidson, M.W., Hess, H.F., Waterman, C.M., 2010. Nanoscale architecture of integrin-based cell adhesions. *Nature* 468, 580–584. doi:10.1038/nature09621
- Kapadia, S.B., Chisari, F.V., 2005. Hepatitis C virus RNA replication is regulated by host geranylgeranylation and fatty acids. *Proc. Natl. Acad. Sci. U. S. A.* 102, 2561–2566. doi:10.1073/pnas.0409834102
- Kapoor, A., Simmonds, P., Gerold, G., Qaisar, N., Jain, K., Henriquez, J.A., Firth, C., Hirschberg, D.L., Rice, C.M., Shields, S., Lipkin, W.I., 2011. Characterization of a canine homolog of hepatitis C virus. *Proc. Natl. Acad. Sci.* 108, 11608–11613. doi:10.1073/pnas.1101794108
- Kapoor, A., Simmonds, P., Scheel, T.K.H., Hjelle, B., Cullen, J.M., Burbelo, P.D., Chauhan, L.V., Duraisamy, R., Leon, M.S., Jain, K., Vandegriff, K.J.,

- Calisher, C.H., Rice, C.M., Lipkin, W.I., 2013. Identification of Rodent Homologs of Hepatitis C Virus and Pegiviruses. *mBio* 4, e00216-13. doi:10.1128/mBio.00216-13
- Karanasios, E., Stapleton, E., Manifava, M., Kaizuka, T., Mizushima, N., Walker, S.A., Ktistakis, N.T., 2013. Dynamic association of the ULK1 complex with omegasomes during autophagy induction. *J Cell Sci* 126, 5224–5238. doi:10.1242/jcs.132415
- Kati, W., Koev, G., Irvin, M., Beyer, J., Liu, Y., Krishnan, P., Reisch, T., Mondal, R., Wagner, R., Molla, A., Maring, C., Collins, C., 2015. In vitro activity and resistance profile of dasabuvir, a nonnucleoside hepatitis C virus polymerase inhibitor. *Antimicrob. Agents Chemother.* 59, 1505–1511. doi:10.1128/AAC.04619-14
- Kazmierski, W.M., Maynard, A., Duan, M., Baskaran, S., Botyanszki, J., Crosby, R., Dickerson, S., Tallant, M., Grimes, R., Hamatake, R., Leivers, M., Roberts, C.D., Walker, J., 2014. Novel spiroketal pyrrolidine GSK2336805 potently inhibits key hepatitis C virus genotype 1b mutants: from lead to clinical compound. *J. Med. Chem.* 57, 2058–2073. doi:10.1021/jm4013104
- Ke, P.-Y., Chen, S.S.-L., 2011. Activation of the unfolded protein response and autophagy after hepatitis C virus infection suppresses innate antiviral immunity in vitro. *J. Clin. Invest.* 121, 37–56. doi:10.1172/JCI41474
- Khan, A.G., Miller, M.T., Marcotrigiano, J., 2015. HCV Glycoprotein Structures: What to Expect from the Unexpected. *Curr. Opin. Virol.* 12, 53–58. doi:10.1016/j.coviro.2015.02.004
- Khan, I., Katikaneni, D.S., Han, Q., Sanchez-Felipe, L., Hanada, K., Ambrose, R.L., Mackenzie, J.M., Konan, K.V., 2014. Modulation of Hepatitis C Virus Genome Replication by Glycosphingolipids and Four-Phosphate Adaptor Protein 2. *J. Virol.* 88, 12276–12295. doi:10.1128/JVI.00970-14
- Khow, O., Suntrarachun, S., 2012. Strategies for production of active eukaryotic proteins in bacterial expression system. *Asian Pac. J. Trop. Biomed.* 2, 159–162. doi:10.1016/S2221-1691(11)60213-X
- Kieft, J.S., Zhou, K., Jubin, R., Doudna, J.A., 2001. Mechanism of ribosome recruitment by hepatitis C IRES RNA. *RNA N. Y. N* 7, 194–206.
- Kielian, M., 2006. Class II virus membrane fusion proteins. *Virology* 344, 38–47. doi:10.1016/j.virol.2005.09.036
- Kikuchi, K., Umehara, T., Fukuda, K., Hwang, J., Kuno, A., Hasegawa, T., Nishikawa, S., 2003. Structure-inhibition analysis of RNA aptamers that bind to HCV IRES. *Nucleic Acids Symp. Ser.* 3, 291–292. doi:10.1093/nass/3.1.291
- Kim, D.W., Gwack, Y., Han, J.H., Choe, J., 1995. C-Terminal Domain of the Hepatitis C Virus NS3 Protein Contains an RNA Helicase Activity. *Biochem. Biophys. Res. Commun.* 215, 160–166. doi:10.1006/bbrc.1995.2447
- Kim, S., Date, T., Yokokawa, H., Kono, T., Aizaki, H., Maurel, P., Gondeau, C., Wakita, T., 2014. Development of hepatitis C virus genotype 3a cell culture system. *Hepatology* 60, 1838–1850. doi:10.1002/hep.27197
- Kinge, C.N.W., Espiritu, C., Prabdial-Sing, N., Sithebe, N.P., Saeed, M., Rice, C.M., 2014. Hepatitis C Virus Genotype 5a Subgenomic Replicons for Evaluation of Direct-Acting Antiviral Agents. *Antimicrob. Agents Chemother.* 58, 5386–5394. doi:10.1128/AAC.03534-14
- Klar, T.A., Jakobs, S., Dyba, M., Egner, A., Hell, S.W., 2000. Fluorescence microscopy with diffraction resolution barrier broken by stimulated emission. *Proc. Natl. Acad. Sci.* 97, 8206–8210. doi:10.1073/pnas.97.15.8206
- Klinck, R., Westhof, E., Walker, S., Afshar, M., Collier, A., Aboul-Ela, F., 2000. A potential RNA drug target in the hepatitis C virus internal ribosomal entry site. *RNA N. Y. N* 6, 1423–1431.

- Koide, A., Bailey, C.W., Huang, X., Koide, S., 1998. The fibronectin type III domain as a scaffold for novel binding proteins. *J. Mol. Biol.* 284, 1141–1151. doi:10.1006/jmbi.1998.2238
- Kolupaeva, V.G., Pestova, T.V., Hellen, C.U.T., 2000. An Enzymatic Footprinting Analysis of the Interaction of 40S Ribosomal Subunits with the Internal Ribosomal Entry Site of Hepatitis C Virus. *J. Virol.* 74, 6242–6250.
- Kolykhalov, A.A., Feinstone, S.M., Rice, C.M., 1996. Identification of a highly conserved sequence element at the 3' terminus of hepatitis C virus genome RNA. *J. Virol.* 70, 3363–3371.
- Komar, A.A., Hatzoglou, M., 2011. Cellular IRES-mediated translation. *Cell Cycle* 10, 229–240. doi:10.4161/cc.10.2.14472
- Kondo, H., Abe, K., Emori, Y., Arai, S., 1991. Gene organization of oryzacystatin-II, a new cystatin superfamily member of plant origin, is closely related to that of oryzacystatin-I but different from those of animal cystatins. *FEBS Lett.* 278, 87–90.
- Kong, L., Giang, E., Nieusma, T., Kadam, R.U., Cogburn, K.E., Hua, Y., Dai, X., Stanfield, R.L., Burton, D.R., Ward, A.B., Wilson, I.A., Law, M., 2013. Hepatitis C virus E2 envelope glycoprotein core structure. *Science* 342, 1090–1094. doi:10.1126/science.1243876
- Kono, Y., Hayashida, K., Tanaka, H., Ishibashi, H., Harada, M., 2003. High-density lipoprotein binding rate differs greatly between genotypes 1b and 2a/2b of hepatitis C virus. *J. Med. Virol.* 70, 42–48. doi:10.1002/jmv.10372
- Kowdley, K.V., Gordon, S.C., Reddy, K.R., Rossaro, L., Bernstein, D.E., Lawitz, E., Shiffman, M.L., Schiff, E., Ghalib, R., Ryan, M., Rustgi, V., Chojkier, M., Herring, R., Di Bisceglie, A.M., Pockros, P.J., Subramanian, G.M., An, D., Svarovskaia, E., Hyland, R.H., Pang, P.S., Symonds, W.T., McHutchison, J.G., Muir, A.J., Pound, D., Fried, M.W., 2014. Ledipasvir and Sofosbuvir for 8 or 12 Weeks for Chronic HCV without Cirrhosis. *N. Engl. J. Med.* 370, 1879–1888. doi:10.1056/NEJMoa1402355
- Koyama-Honda, I., Itakura, E., Fujiwara, T.K., Mizushima, N., 2013. Temporal analysis of recruitment of mammalian ATG proteins to the autophagosome formation site. *Autophagy* 9, 1491–1499. doi:10.4161/auto.25529
- Kozlov, M.M., Campelo, F., Liska, N., Chernomordik, L.V., Marrink, S.J., McMahon, H.T., 2014. Mechanisms shaping cell membranes. *Curr. Opin. Cell Biol.* 29, 53–60. doi:10.1016/j.ceb.2014.03.006
- Krieger, N., Lohmann, V., Bartenschlager, R., 2001. Enhancement of Hepatitis C Virus RNA Replication by Cell Culture-Adaptive Mutations. *J. Virol.* 75, 4614–4624. doi:10.1128/JVI.75.10.4614-4624.2001
- Krishnan, P., Tripathi, R., Schnell, G., Reisch, T., Beyer, J., Irvin, M., Xie, W., Larsen, L., Cohen, D., Podsadecki, T., Pilot-Matias, T., Collins, C., 2015. Resistance Analysis of Baseline and Treatment-Emergent Variants in Hepatitis C Virus Genotype 1 in the AVIATOR Study with Paritaprevir-Ritonavir, Ombitasvir, and Dasabuvir. *Antimicrob. Agents Chemother.* 59, 5445–5454. doi:10.1128/AAC.00998-15
- Kuma, A., Matsui, M., Mizushima, N., 2007. LC3, an autophagosome marker, can be incorporated into protein aggregates independent of autophagy: caution in the interpretation of LC3 localization. *Autophagy* 3, 323–328.
- Kwong, A.D., Kauffman, R.S., Hurter, P., Mueller, P., 2011. Discovery and development of telaprevir: an NS3-4A protease inhibitor for treating genotype 1 chronic hepatitis C virus. *Nat. Biotechnol.* 29, 993–1003. doi:10.1038/nbt.2020
- Kyle, H.F., Wickson, K.F., Stott, J., Burslem, G.M., Breeze, A.L., Tiede, C., Tomlinson, D.C., Warriner, S.L., Nelson, A., Wilson, A.J., Edwards, T.A., 2015. Exploration of the HIF-1 α /p300 interface using peptide and Adhiron phage display technologies. *Mol. Biosyst.* 11, 2738–2749. doi:10.1039/C5MB00284B

- Lai, C.-K., Jeng, K.-S., Machida, K., Lai, M.M.C., 2008. Association of Hepatitis C Virus Replication Complexes with Microtubules and Actin Filaments Is Dependent on the Interaction of NS3 and NS5A. *J. Virol.* 82, 8838–8848. doi:10.1128/JVI.00398-08
- Lambacher, N.J., Bruel, A.-L., van Dam, T.J.P., Szymańska, K., Slaats, G.G., Kuhns, S., McManus, G.J., Kennedy, J.E., Gaff, K., Wu, K.M., van der Lee, R., Burglen, L., Doummar, D., Rivière, J.-B., Faivre, L., Attié-Bitach, T., Saunier, S., Curd, A., Peckham, M., Giles, R.H., Johnson, C.A., Huynen, M.A., Thauvin-Robinet, C., Blacque, O.E., 2016. TMEM107 recruits ciliopathy proteins to subdomains of the ciliary transition zone and causes Joubert syndrome. *Nat. Cell Biol.* 18, 122–131. doi:10.1038/ncb3273
- Lambert, S.M., Langley, D.R., Garnett, J.A., Angell, R., Hedgethorpe, K., Meanwell, N.A., Matthews, S.J., 2014. The crystal structure of NS5A domain 1 from genotype 1a reveals new clues to the mechanism of action for dimeric HCV inhibitors. *Protein Sci. Publ. Protein Soc.* 23, 723–734. doi:10.1002/pro.2456
- Lampe, A., Haucke, V., Sigrist, S.J., Heilemann, M., Schmoranzner, J., 2012. Multi-colour direct STORM with red emitting carbocyanines. *Biol. Cell Auspices Eur. Cell Biol. Organ.* 104, 229–237. doi:10.1111/boc.201100011
- Langer-Safer, P.R., Levine, M., Ward, D.C., 1982. Immunological method for mapping genes on *Drosophila* polytene chromosomes. *Proc. Natl. Acad. Sci. U. S. A.* 79, 4381–4385.
- Lapinsky, D.J., Johnson, D.S., 2015. Recent developments and applications of clickable photoprobes in medicinal chemistry and chemical biology. *Future Med. Chem.* 7, 2143–2171. doi:10.4155/fmc.15.136
- Lauck, M., Sibley, S.D., Lara, J., Purdy, M.A., Khudyakov, Y., Hyeroba, D., Tumukunde, A., Weny, G., Switzer, W.M., Chapman, C.A., Hughes, A.L., Friedrich, T.C., O'Connor, D.H., Goldberg, T.L., 2013. A Novel Hepacivirus with an Unusually Long and Intrinsically Disordered NS5A Protein in a Wild Old World Primate. *J. Virol.* 87, 8971–8981. doi:10.1128/JVI.00888-13
- Lavillette, D., Bartosch, B., Nourrisson, D., Verney, G., Cosset, F.-L., Penin, F., Pécheur, E.-I., 2006. Hepatitis C virus glycoproteins mediate low pH-dependent membrane fusion with liposomes. *J. Biol. Chem.* 281, 3909–3917. doi:10.1074/jbc.M509747200
- Lee, C., Ma, H., Hang, J.Q., Leveque, V., Sklan, E.H., Elazar, M., Klumpp, K., Glenn, J.S., 2011. The hepatitis C virus NS5A inhibitor (BMS-790052) alters the subcellular localization of the NS5A non-structural viral protein. *Virology* 414, 10–18. doi:10.1016/j.virol.2011.03.026
- Lee, C.H., Lee, Y.J., Kim, J.H., Lim, J.H., Kim, J.-H., Han, W., Lee, S.-H., Noh, G.-J., Lee, S.-W., 2013. Inhibition of Hepatitis C Virus (HCV) Replication by Specific RNA Aptamers against HCV NS5B RNA Replicase. *J. Virol.* 87, 7064–7074. doi:10.1128/JVI.00405-13
- Lee, K.J., Choi, J., Ou, J., Lai, M.M.C., 2004. The C-Terminal Transmembrane Domain of Hepatitis C Virus (HCV) RNA Polymerase Is Essential for HCV Replication In Vivo. *J. Virol.* 78, 3797–3802. doi:10.1128/JVI.78.7.3797-3802.2004
- Lee, N.P., Luk, J.M., 2010. Hepatic tight junctions: From viral entry to cancer metastasis. *World J. Gastroenterol. WJG* 16, 289–295. doi:10.3748/wjg.v16.i3.289
- Lee, S.-C., Park, K., Han, J., Lee, J., Kim, H.J., Hong, S., Heu, W., Kim, Y.J., Ha, J.-S., Lee, S.-G., Cheong, H.-K., Jeon, Y.H., Kim, D., Kim, H.-S., 2012. Design of a binding scaffold based on variable lymphocyte receptors of jawless vertebrates by module engineering. *Proc. Natl. Acad. Sci. U. S. A.* 109, 3299–3304. doi:10.1073/pnas.1113193109
- Lee, Y.-R., Lei, H.-Y., Liu, M.-T., Wang, J.-R., Chen, S.-H., Jiang-Shieh, Y.-F., Lin, Y.-S., Yeh, T.-M., Liu, C.-C., Liu, H.-S., 2008. Autophagic machinery

activated by dengue virus enhances virus replication. *Virology* 374, 240–248. doi:10.1016/j.virol.2008.02.016

- Leewenhoek, A. van, 1677. Observations, Communicated to the Publisher by Mr. Antony van Leewenhoek, in a Dutch Letter of the 9th of Octob. 1676. Here English'd: concerning Little Animals by Him Observed in Rain-Well-Sea. and Snow Water; as Also in Water Wherein Pepper Had Lain Infused. *Philos. Trans.* 12, 821–831. doi:10.1098/rstl.1677.0003
- Legant, W.R., Shao, L., Grimm, J.B., Brown, T.A., Milkie, D.E., Avants, B.B., Lavis, L.D., Betzig, E., 2016. High-density three-dimensional localization microscopy across large volumes. *Nat. Methods* 13, 359–365. doi:10.1038/nmeth.3797
- Lehmann, M., Meyer, M.F., Monazahian, M., Tillmann, H.L., Manns, M.P., Wedemeyer, H., 2004. High rate of spontaneous clearance of acute hepatitis C virus genotype 3 infection. *J. Med. Virol.* 73, 387–391. doi:10.1002/jmv.20103
- Lelek, M., Di Nunzio, F., Henriques, R., Charneau, P., Arhel, N., Zimmer, C., 2012. Superresolution imaging of HIV in infected cells with FIAsh-PALM. *Proc. Natl. Acad. Sci. U. S. A.* 109, 8564–8569. doi:10.1073/pnas.1013267109
- Lemay, K.L., Treadaway, J., Angulo, I., Tellinghuisen, T.L., 2013. A hepatitis C virus NS5A phosphorylation site that regulates RNA replication. *J. Virol.* 87, 1255–1260. doi:10.1128/JVI.02154-12
- Lemmer, P., Gunkel, M., Weiland, Y., Müller, P., Baddeley, D., Kaufmann, R., Urich, A., Eipel, H., Amberger, R., Hausmann, M., Cremer, C., 2009. Using conventional fluorescent markers for far-field fluorescence localization nanoscopy allows resolution in the 10-nm range. *J. Microsc.* 235, 163–171. doi:10.1111/j.1365-2818.2009.03196.x
- Levet, F., Hosy, E., Kechkar, A., Butler, C., Beghin, A., Choquet, D., Sibarita, J.-B., 2015. SR-Tesseler: a method to segment and quantify localization-based super-resolution microscopy data. *Nat. Methods* 12, 1065–1071. doi:10.1038/nmeth.3579
- Li, G., Li, K., Lea, A.S., Li, N.L., Abdulla, N.E., Eltorkey, M.A., Ferguson, M.R., 2013. In situ hybridization for the detection of hepatitis C virus RNA in human liver tissue. *J. Viral Hepat.* 20, 183–192. doi:10.1111/j.1365-2893.2012.01642.x
- Li, K., Foy, E., Ferreon, J.C., Nakamura, M., Ferreon, A.C.M., Ikeda, M., Ray, S.C., Gale, M., Lemon, S.M., 2005. Immune evasion by hepatitis C virus NS3/4A protease-mediated cleavage of the Toll-like receptor 3 adaptor protein TRIF. *Proc. Natl. Acad. Sci. U. S. A.* 102, 2992–2997. doi:10.1073/pnas.0408824102
- Li, Q., Brass, A.L., Ng, A., Hu, Z., Xavier, R.J., Liang, T.J., Elledge, S.J., 2009. A genome-wide genetic screen for host factors required for hepatitis C virus propagation. *Proc. Natl. Acad. Sci. U. S. A.* 106, 16410–16415. doi:10.1073/pnas.0907439106
- Li, Y.-P., Ramirez, S., Jensen, S.B., Purcell, R.H., Gottwein, J.M., Bukh, J., 2012. Highly efficient full-length hepatitis C virus genotype 1 (strain TN) infectious culture system. *Proc. Natl. Acad. Sci. U. S. A.* 109, 19757–19762. doi:10.1073/pnas.1218260109
- Liang, Y., Kang, C.B., Yoon, H.S., 2006. Molecular and structural characterization of the domain 2 of hepatitis C virus non-structural protein 5A. *Mol. Cells* 22, 13–20.
- Liang, Y., Ye, H., Kang, C.B., Yoon, H.S., 2007. Domain 2 of Nonstructural Protein 5A (NS5A) of Hepatitis C Virus Is Natively Unfolded. *Biochemistry (Mosc.)* 46, 11550–11558. doi:10.1021/bi700776e
- Lim, P.J., Chatterji, U., Cordek, D., Sharma, S.D., Garcia-Rivera, J.A., Cameron, C.E., Lin, K., Targett-Adams, P., Gallay, P.A., 2012. Correlation between NS5A Dimerization and Hepatitis C Virus Replication. *J. Biol. Chem.* 287, 30861–30873. doi:10.1074/jbc.M112.376822

- Lin, C., 2006. HCV NS3-4A Serine Protease, in: Tan, S.-L. (Ed.), *Hepatitis C Viruses: Genomes and Molecular Biology*. Horizon Bioscience, Norfolk (UK).
- Lin, C., Lindenbach, B.D., Prágai, B.M., McCourt, D.W., Rice, C.M., 1994. Processing in the hepatitis C virus E2-NS2 region: identification of p7 and two distinct E2-specific products with different C termini. *J. Virol.* 68, 5063–5073.
- Lindenbach, B.D., Evans, M.J., Syder, A.J., Wölk, B., Tellinghuisen, T.L., Liu, C.C., Maruyama, T., Hynes, R.O., Burton, D.R., McKeating, J.A., Rice, C.M., 2005. Complete Replication of Hepatitis C Virus in Cell Culture. *Science* 309, 623–626. doi:10.1126/science.1114016
- Lindenbach, B.D., Rice, C.M., 2013. The ins and outs of hepatitis C virus entry and assembly. *Nat. Rev. Microbiol.* 11, 688–700. doi:10.1038/nrmicro3098
- Liu, H.M., Aizaki, H., Machida, K., Ou, J.-H.J., Lai, M.M.C., 2012. Hepatitis C Virus Translation Preferentially Depends on Active RNA Replication. *PLOS ONE* 7, e43600. doi:10.1371/journal.pone.0043600
- Lloyd, S., 1982. Least squares quantization in PCM. *IEEE Trans. Inf. Theory* 28, 129–137. doi:10.1109/TIT.1982.1056489
- Lohmann, V., Körner, F., Koch, J.-O., Herian, U., Theilmann, L., Bartenschlager, R., 1999. Replication of Subgenomic Hepatitis C Virus RNAs in a Hepatoma Cell Line. *Science* 285, 110–113. doi:10.1126/science.285.5424.110
- Löschberger, A., Linde, S. van de, Dabauvalle, M.-C., Rieger, B., Heilemann, M., Krohne, G., Sauer, M., 2012. Super-resolution imaging visualizes the eightfold symmetry of gp210 proteins around the nuclear pore complex and resolves the central channel with nanometer resolution. *J Cell Sci* 125, 570–575. doi:10.1242/jcs.098822
- Love, R.A., Brodsky, O., Hickey, M.J., Wells, P.A., Cronin, C.N., 2009. Crystal Structure of a Novel Dimeric Form of NS5A Domain I Protein from Hepatitis C Virus. *J. Virol.* 83, 4395–4403. doi:10.1128/JVI.02352-08
- Lukavsky, P.J., Otto, G.A., Lancaster, A.M., Sarnow, P., Puglisi, J.D., 2000. Structures of two RNA domains essential for hepatitis C virus internal ribosome entry site function. *Nat. Struct. Biol.* 7, 1105–1110. doi:10.1038/81951
- Luo, G., Xin, S., Cai, Z., 2003. Role of the 5'-proximal stem-loop structure of the 5' untranslated region in replication and translation of hepatitis C virus RNA. *J. Virol.* 77, 3312–3318.
- Lupberger, J., Zeisel, M.B., Xiao, F., Thumann, C., Fofana, I., Zona, L., Davis, C., Mee, C.J., Turek, M., Gorke, S., Royer, C., Fischer, B., Zahid, M.N., Lavillette, D., Fresquet, J., Cosset, F.-L., Rothenberg, S.M., Pietschmann, T., Patel, A.H., Pessaux, P., Doffoël, M., Raffelsberger, W., Poch, O., McKeating, J.A., Brino, L., Baumert, T.F., 2011. EGFR and EphA2 are host factors for hepatitis C virus entry and possible targets for antiviral therapy. *Nat. Med.* 17, 589–595. doi:10.1038/nm.2341
- Lupold, S.E., Hicke, B.J., Lin, Y., Coffey, D.S., 2002. Identification and characterization of nuclease-stabilized RNA molecules that bind human prostate cancer cells via the prostate-specific membrane antigen. *Cancer Res.* 62, 4029–4033.
- Lyons, S., Kapoor, A., Sharp, C., Schneider, B.S., Wolfe, N.D., Culshaw, G., Corcoran, B., McGorum, B.C., Simmonds, P., 2012. Nonprimate hepaciviruses in domestic horses, United kingdom. *Emerg. Infect. Dis.* 18, 1976–1982. doi:10.3201/eid1812.120498
- Lytle, J.R., Wu, L., Robertson, H.D., 2002. Domains on the hepatitis C virus internal ribosome entry site for 40s subunit binding. *RNA* 8, 1045–1055.
- Lytle, J.R., Wu, L., Robertson, H.D., 2001. The Ribosome Binding Site of Hepatitis C Virus mRNA. *J. Virol.* 75, 7629–7636. doi:10.1128/JVI.75.16.7629-7636.2001

- Ma, Y., Yates, J., Liang, Y., Lemon, S.M., Yi, M., 2008. NS3 Helicase Domains Involved in Infectious Intracellular Hepatitis C Virus Particle Assembly. *J. Virol.* 82, 7624–7639. doi:10.1128/JVI.00724-08
- Macdonald, A., Crowder, K., Street, A., McCormick, C., Harris, M., 2004. The hepatitis C virus NS5A protein binds to members of the Src family of tyrosine kinases and regulates kinase activity. *J. Gen. Virol.* 85, 721–729. doi:10.1099/vir.0.19691-0
- Macdonald, A., Crowder, K., Street, A., McCormick, C., Saksela, K., Harris, M., 2003. The Hepatitis C Virus Non-structural NS5A Protein Inhibits Activating Protein-1 Function by Perturbing Ras-ERK Pathway Signaling. *J. Biol. Chem.* 278, 17775–17784. doi:10.1074/jbc.M210900200
- Majeau, N., Gagné, V., Boivin, A., Bolduc, M., Majeau, J.-A., Ouellet, D., Leclerc, D., 2004. The N-terminal half of the core protein of hepatitis C virus is sufficient for nucleocapsid formation. *J. Gen. Virol.* 85, 971–981. doi:10.1099/vir.0.79775-0
- Mankouri, J., Dallas, M.L., Hughes, M.E., Griffin, S.D.C., Macdonald, A., Peers, C., Harris, M., 2009. Suppression of a pro-apoptotic K⁺ channel as a mechanism for hepatitis C virus persistence. *Proc. Natl. Acad. Sci.* 106, 15903–15908. doi:10.1073/pnas.0906798106
- Mankouri, J., Griffin, S., Harris, M., 2008. The Hepatitis C Virus Non-Structural Protein NS5A Alters the Trafficking Profile of the Epidermal Growth Factor Receptor. *Traffic* 9, 1497–1509. doi:10.1111/j.1600-0854.2008.00779.x
- Mankouri, J., Walter, C., Stewart, H., Bentham, M., Park, W.S., Heo, W.D., Fukuda, M., Griffin, S., Harris, M., 2016. Release of Infectious Hepatitis C Virus from Huh7 Cells Occurs via a trans-Golgi Network-to-Endosome Pathway Independent of Very-Low-Density Lipoprotein Secretion. *J. Virol.* 90, 7159–7170. doi:10.1128/JVI.00826-16
- Manna, D., Aligo, J., Xu, C., Park, W.S., Koc, H., Heo, W.D., Konan, K.V., 2010. Endocytic Rab proteins are required for hepatitis C virus replication complex formation. *Virology* 398, 21–37. doi:10.1016/j.virol.2009.11.034
- Manns, M.P., McHutchison, J.G., Gordon, S.C., Rustgi, V.K., Shiffman, M., Reindollar, R., Goodman, Z.D., Koury, K., Ling, M., Albrecht, J.K., 2001. Peginterferon alfa-2b plus ribavirin compared with interferon alfa-2b plus ribavirin for initial treatment of chronic hepatitis C: a randomised trial. *Lancet Lond. Engl.* 358, 958–965.
- Manns, M.P., von Hahn, T., 2013. Novel therapies for hepatitis C - one pill fits all? *Nat. Rev. Drug Discov.* 12, 595–610. doi:10.1038/nrd4050
- Margolin, W., 2012. The Price of Tags in Protein Localization Studies. *J. Bacteriol.* 194, 6369–6371. doi:10.1128/JB.01640-12
- Martell, M., Esteban, J.I., Quer, J., Genescà, J., Weiner, A., Esteban, R., Guardia, J., Gómez, J., 1992. Hepatitis C virus (HCV) circulates as a population of different but closely related genomes: quasispecies nature of HCV genome distribution. *J. Virol.* 66, 3225–3229.
- Martin, B.R., Giepmans, B.N.G., Adams, S.R., Tsien, R.Y., 2005. Mammalian cell-based optimization of the biarsenical-binding tetracysteine motif for improved fluorescence and affinity. *Nat. Biotechnol.* 23, 1308–1314. doi:10.1038/nbt1136
- Masaki, T., Arend, K.C., Li, Y., Yamane, D., McGivern, D.R., Kato, T., Wakita, T., Moorman, N.J., Lemon, S.M., 2015. miR-122 Stimulates Hepatitis C Virus RNA Synthesis by Altering the Balance of Viral RNAs Engaged in Replication Versus Translation. *Cell Host Microbe* 17, 217–228. doi:10.1016/j.chom.2014.12.014
- Masaki, T., Matsunaga, S., Takahashi, H., Nakashima, K., Kimura, Y., Ito, M., Matsuda, M., Murayama, A., Kato, T., Hirano, H., Endo, Y., Lemon, S.M., Wakita, T., Sawasaki, T., Suzuki, T., 2014. Involvement of hepatitis C virus

- NS5A hyperphosphorylation mediated by casein kinase I- α in infectious virus production. *J. Virol.* 88, 7541–7555. doi:10.1128/JVI.03170-13
- Masaki, T., Suzuki, R., Murakami, K., Aizaki, H., Ishii, K., Murayama, A., Date, T., Matsuura, Y., Miyamura, T., Wakita, T., Suzuki, T., 2008. Interaction of Hepatitis C Virus Nonstructural Protein 5A with Core Protein Is Critical for the Production of Infectious Virus Particles. *J. Virol.* 82, 7964–7976. doi:10.1128/JVI.00826-08
- Mauger, D.M., Golden, M., Yamane, D., Williford, S., Lemon, S.M., Martin, D.P., Weeks, K.M., 2015. Functionally conserved architecture of hepatitis C virus RNA genomes. *Proc. Natl. Acad. Sci.* 112, 3692–3697. doi:10.1073/pnas.1416266112
- Maxfield, F.R., Wüstner, D., 2012. Analysis of cholesterol trafficking with fluorescent probes. *Methods Cell Biol.* 108, 367–393. doi:10.1016/B978-0-12-386487-1.00017-1
- Mayer, B.J., 2001. SH3 domains: complexity in moderation. *J. Cell Sci.* 114, 1253–1263.
- McCaughan, G.W., McGuinness, P.H., Bishop, G.A., Painter, D.M., Lien, A.S., Tulloch, R., Wylie, B.R., Archer, G.T., 1992. Clinical assessment and incidence of hepatitis C RNA in 50 consecutive RIBA-positive volunteer blood donors. *Med. J. Aust.* 157, 231–233.
- McCormick, C.J., Maucourant, S., Griffin, S., Rowlands, D.J., Harris, M., 2006. Tagging of NS5A expressed from a functional hepatitis C virus replicon. *J. Gen. Virol.* 87, 635–640. doi:10.1099/vir.0.81553-0
- McGivern, D.R., Masaki, T., Williford, S., Ingravallo, P., Feng, Z., Lahser, F., Asante-Appiah, E., Neddermann, P., Francesco, R.D., Howe, A.Y., Lemon, S.M., 2014. Kinetic Analyses Reveal Potent and Early Blockade of Hepatitis C Virus Assembly by NS5A Inhibitors. *Gastroenterology* 147, 453–462.e7. doi:10.1053/j.gastro.2014.04.021
- McKinney, S.A., Murphy, C.S., Hazelwood, K.L., Davidson, M.W., Looger, L.L., 2009. A bright and photostable photoconvertible fluorescent protein. *Nat. Methods* 6, 131–133. doi:10.1038/nmeth.1296
- McLauchlan, J., 2000. Properties of the hepatitis C virus core protein: a structural protein that modulates cellular processes. *J. Viral Hepat.* 7, 2–14.
- McLauchlan, J., Lemberg, M.K., Hope, G., Martoglio, B., 2002. Intramembrane proteolysis promotes trafficking of hepatitis C virus core protein to lipid droplets. *EMBO J.* 21, 3980–3988. doi:10.1093/emboj/cdf414
- McMahon, H.T., Gallop, J.L., 2005. Membrane curvature and mechanisms of dynamic cell membrane remodelling. *Nature* 438, 590–596. doi:10.1038/nature04396
- Merz, A., Long, G., Hiet, M.-S., Brügger, B., Chlanda, P., Andre, P., Wieland, F., Krijnse-Locker, J., Bartenschlager, R., 2011. Biochemical and morphological properties of hepatitis C virus particles and determination of their lipidome. *J. Biol. Chem.* 286, 3018–3032. doi:10.1074/jbc.M110.175018
- Messina, J.P., Humphreys, I., Flaxman, A., Brown, A., Cooke, G.S., Pybus, O.G., Barnes, E., 2015. Global distribution and prevalence of hepatitis C virus genotypes. *Hepatology* 61, 77–87. doi:10.1002/hep.27259
- Meunier, J.C., Fournillier, A., Choukhi, A., Cahour, A., Cocquerel, L., Dubuisson, J., Wychowski, C., 1999. Analysis of the glycosylation sites of hepatitis C virus (HCV) glycoprotein E1 and the influence of E1 glycans on the formation of the HCV glycoprotein complex. *J. Gen. Virol.* 80 (Pt 4), 887–896. doi:10.1099/0022-1317-80-4-887
- Milne, J.L.S., Borgnia, M.J., Bartesaghi, A., Tran, E.E.H., Earl, L.A., Schauder, D.M., Lengyel, J., Pierson, J., Patwardhan, A., Subramaniam, S., 2013. Cryo-electron microscopy--a primer for the non-microscopist. *FEBS J.* 280, 28–45. doi:10.1111/febs.12078

- Mitra, K., Ubarretxena-Belandia, I., Taguchi, T., Warren, G., Engelman, D.M., 2004. Modulation of the bilayer thickness of exocytic pathway membranes by membrane proteins rather than cholesterol. *Proc. Natl. Acad. Sci.* 101, 4083–4088. doi:10.1073/pnas.0307332101
- Miyanari, Y., Atsuzawa, K., Usuda, N., Watashi, K., Hishiki, T., Zayas, M., Bartenschlager, R., Wakita, T., Hijikata, M., Shimotohno, K., 2007. The lipid droplet is an important organelle for hepatitis C virus production. *Nat. Cell Biol.* 9, 1089–1097. doi:10.1038/ncb1631
- Miyanari, Y., Hijikata, M., Yamaji, M., Hosaka, M., Takahashi, H., Shimotohno, K., 2003. Hepatitis C Virus Non-structural Proteins in the Probable Membranous Compartment Function in Viral Genome Replication. *J. Biol. Chem.* 278, 50301–50308. doi:10.1074/jbc.M305684200
- Mizui, T., Yamashina, S., Tanida, I., Takei, Y., Ueno, T., Sakamoto, N., Ikejima, K., Kitamura, T., Enomoto, N., Sakai, T., Kominami, E., Watanabe, S., 2010. Inhibition of hepatitis C virus replication by chloroquine targeting virus-associated autophagy. *J. Gastroenterol.* 45, 195–203. doi:10.1007/s00535-009-0132-9
- Mizushima, N., 2010. The role of the Atg1/ULK1 complex in autophagy regulation. *Curr. Opin. Cell Biol., Cell regulation* 22, 132–139. doi:10.1016/j.ceb.2009.12.004
- Mohd Hanafiah, K., Groeger, J., Flaxman, A.D., Wiersma, S.T., 2013. Global epidemiology of hepatitis C virus infection: new estimates of age-specific antibody to HCV seroprevalence. *Hepatology* 57, 1333–1342. doi:10.1002/hep.26141
- Mohl, B.-P., Bartlett, C., Mankouri, J., Harris, M., 2016. Early events in the generation of autophagosomes are required for the formation of membrane structures involved in hepatitis C virus genome replication. *J. Gen. Virol.* 97, 680–693. doi:10.1099/jgv.0.000387
- Mohl, B.-P., Tedbury, P.R., Griffin, S., Harris, M., 2012. Hepatitis C Virus-Induced Autophagy Is Independent of the Unfolded Protein Response. *J. Virol.* 86, 10724–10732. doi:10.1128/JVI.01667-12
- Monazahian, M., Böhme, I., Bonk, S., Koch, A., Scholz, C., Grethe, S., Thomssen, R., 1999. Low density lipoprotein receptor as a candidate receptor for hepatitis C virus. *J. Med. Virol.* 57, 223–229.
- Moradpour, D., Evans, M.J., Gosert, R., Yuan, Z., Blum, H.E., Goff, S.P., Lindenbach, B.D., Rice, C.M., 2004. Insertion of Green Fluorescent Protein into Nonstructural Protein 5A Allows Direct Visualization of Functional Hepatitis C Virus Replication Complexes. *J. Virol.* 78, 7400–7409. doi:10.1128/JVI.78.14.7400-7409.2004
- Moradpour, D., Gosert, R., Egger, D., Penin, F., Blum, H.E., Bienz, K., 2003. Membrane association of hepatitis C virus nonstructural proteins and identification of the membrane alteration that harbors the viral replication complex. *Antiviral Res.* 60, 103–109.
- Mosley, R.T., Edwards, T.E., Murakami, E., Lam, A.M., Grice, R.L., Du, J., Sofia, M.J., Furman, P.A., Otto, M.J., 2012. Structure of Hepatitis C Virus Polymerase in Complex with Primer-Template RNA. *J. Virol.* 86, 6503–6511. doi:10.1128/JVI.00386-12
- Mottola, G., Cardinali, G., Ceccacci, A., Trozzi, C., Bartholomew, L., Torrisi, M.R., Pedrazzini, E., Bonatti, S., Migliaccio, G., 2002. Hepatitis C Virus Nonstructural Proteins Are Localized in a Modified Endoplasmic Reticulum of Cells Expressing Viral Subgenomic Replicons. *Virology* 293, 31–43. doi:10.1006/viro.2001.1229
- Murphy, D.B., 2002. *Fundamentals of Light Microscopy and Electronic Imaging.* John Wiley & Sons.
- Muyldermans, S., 2013. Nanobodies: Natural Single-Domain Antibodies. *Annu. Rev. Biochem.* 82, 775–797. doi:10.1146/annurev-biochem-063011-092449

- Nag, A., Robotham, J.M., Tang, H., 2012. Suppression of Viral RNA Binding and the Assembly of Infectious Hepatitis C Virus Particles In Vitro by Cyclophilin Inhibitors. *J. Virol.* 86, 12616–12624. doi:10.1128/JVI.01351-12
- Nakabayashi, H., Taketa, K., Miyano, K., Yamane, T., Sato, J., 1982. Growth of human hepatoma cell lines with differentiated functions in chemically defined medium. *Cancer Res.* 42, 3858–3863.
- Nakagawa, M., Sakamoto, N., Enomoto, N., Tanabe, Y., Kanazawa, N., Koyama, T., Kurosaki, M., Maekawa, S., Yamashiro, T., Chen, C.H., Itsui, Y., Kakinuma, S., Watanabe, M., 2004. Specific inhibition of hepatitis C virus replication by cyclosporin A. *Biochem. Biophys. Res. Commun.* 313, 42–47.
- Nakagawa, M., Sakamoto, N., Tanabe, Y., Koyama, T., Itsui, Y., Takeda, Y., Chen, C.-H., Kakinuma, S., Oooka, S., Maekawa, S., Enomoto, N., Watanabe, M., 2005. Suppression of Hepatitis C Virus Replication by Cyclosporin A Is Mediated by Blockade of Cyclophilins. *Gastroenterology* 129, 1031–1041. doi:10.1053/j.gastro.2005.06.031
- Nakamoto, S., Kanda, T., Wu, S., Shirasawa, H., Yokosuka, O., 2014. Hepatitis C virus NS5A inhibitors and drug resistance mutations. *World J. Gastroenterol.* WJG 20, 2902–2912. doi:10.3748/wjg.v20.i11.2902
- Nan, X., Collisson, E.A., Lewis, S., Huang, J., Tamgüney, T.M., Liphardt, J.T., McCormick, F., Gray, J.W., Chu, S., 2013. Single-molecule superresolution imaging allows quantitative analysis of RAF multimer formation and signaling. *Proc. Natl. Acad. Sci. U. S. A.* 110, 18519–18524. doi:10.1073/pnas.1318188110
- Nanda, S.K., Herion, D., Liang, T.J., 2006. Src Homology 3 Domain of Hepatitis C Virus NS5A Protein Interacts With Bin1 and Is Important for Apoptosis and Infectivity. *Gastroenterology* 130, 794–809. doi:10.1053/j.gastro.2005.12.030
- Neddermann, P., Clementi, A., De Francesco, R., 1999. Hyperphosphorylation of the Hepatitis C Virus NS5A Protein Requires an Active NS3 Protease, NS4A, NS4B, and NS5A Encoded on the Same Polyprotein. *J. Virol.* 73, 9984–9991.
- Nettles, J.H., Stanton, R.A., Broyde, J., Amblard, F., Zhang, H., Zhou, L., Shi, J., McBrayer, T.R., Whitaker, T., Coats, S.J., Kohler, J.J., Schinazi, R.F., 2014. Asymmetric Binding to NS5A by Daclatasvir (BMS-790052) and Analogs Suggests Two Novel Modes of HCV Inhibition. *J. Med. Chem.* 57, 10031–10043. doi:10.1021/jm501291c
- Nicovich, P.R., Owen, D.M., Gaus, K., 2017. Turning single-molecule localization microscopy into a quantitative bioanalytical tool. *Nat. Protoc.* 12, 453–460. doi:10.1038/nprot.2016.166
- Niepmann, M., 2013. Hepatitis C virus RNA translation. *Curr. Top. Microbiol. Immunol.* 369, 143–166. doi:10.1007/978-3-642-27340-7_6
- Nieuwenhuizen, R.P.J., Lidke, K.A., Bates, M., Puig, D.L., Grünwald, D., Stallinga, S., Rieger, B., 2013. Measuring image resolution in optical nanoscopy. *Nat. Methods* 10, 557–562. doi:10.1038/nmeth.2448
- Nikonov, A., Juronen, E., Ustav, M., 2008. Functional Characterization of Fingers Subdomain-specific Monoclonal Antibodies Inhibiting the Hepatitis C Virus RNA-dependent RNA Polymerase. *J. Biol. Chem.* 283, 24089–24102. doi:10.1074/jbc.M803422200
- Nixon, A.E., Wood, C.R., 2006. Engineered protein inhibitors of proteases. *Curr. Opin. Drug Discov. Devel.* 9, 261–268.
- Nord, K., Nilsson, J., Nilsson, B., Uhlén, M., Nygren, P.A., 1995. A combinatorial library of an alpha-helical bacterial receptor domain. *Protein Eng.* 8, 601–608.
- Núñez, M., Soriano, V., 2005. Hepatitis C Virus (HCV) Genotypes and Disease Progression in HIV/HCV-Coinfected Patients. *J. Infect. Dis.* 191, 1–1. doi:10.1086/426515

- Nuys, K.V., Brookmeyer, R., Chou, J.W., Dreyfus, D., Dieterich, D., Goldman, D.P., 2015. Broad Hepatitis C Treatment Scenarios Return Substantial Health Gains, But Capacity Is A Concern. *Health Aff. (Millwood)* 34, 1666–1674. doi:10.1377/hlthaff.2014.1193
- O'Boyle li, D.R., Sun, J.-H., Nower, P.T., Lemm, J.A., Fridell, R.A., Wang, C., Romine, J.L., Belema, M., Nguyen, V.N., Laurent, D.R.S., Serrano-Wu, M., Snyder, L.B., Meanwell, N.A., Langley, D.R., Gao, M., 2013. Characterizations of HCV NS5A replication complex inhibitors. *Virology* 444, 343–354. doi:10.1016/j.virol.2013.06.032
- Ogata, M., Hino, S. -i., Saito, A., Morikawa, K., Kondo, S., Kanemoto, S., Murakami, T., Taniguchi, M., Tanii, I., Yoshinaga, K., Shiosaka, S., Hammarback, J.A., Urano, F., Imaizumi, K., 2006. Autophagy Is Activated for Cell Survival after Endoplasmic Reticulum Stress. *Mol. Cell. Biol.* 26, 9220–9231. doi:10.1128/MCB.01453-06
- Ogawa, K., Hishiki, T., Shimizu, Y., Funami, K., Sugiyama, K., Miyanari, Y., Shimotohno, K., 2009. Hepatitis C virus utilizes lipid droplet for production of infectious virus. *Proc. Jpn. Acad. Ser. B Phys. Biol. Sci.* 85, 217–228.
- Okamoto, K., Mori, Y., Komoda, Y., Okamoto, T., Okochi, M., Takeda, M., Suzuki, T., Moriishi, K., Matsuura, Y., 2008. Intramembrane processing by signal peptide peptidase regulates the membrane localization of hepatitis C virus core protein and viral propagation. *J. Virol.* 82, 8349–8361. doi:10.1128/JVI.00306-08
- Oliphant, A.R., Brandl, C.J., Struhl, K., 1989. Defining the sequence specificity of DNA-binding proteins by selecting binding sites from random-sequence oligonucleotides: analysis of yeast GCN4 protein. *Mol. Cell. Biol.* 9, 2944–2949. doi:10.1128/MCB.9.7.2944
- Oliphant, T.E., 2007. Python for Scientific Computing. *Comput. Sci. Engg* 9, 10–20. doi:10.1109/MCSE.2007.58
- Opazo, F., Levy, M., Byrom, M., Schäfer, C., Geisler, C., Groemer, T.W., Ellington, A.D., Rizzoli, S.O., 2012. Aptamers as potential tools for super-resolution microscopy. *Nat. Methods* 9, 938–939. doi:10.1038/nmeth.2179
- Otto, G.A., Puglisi, J.D., 2004. The pathway of HCV IRES-mediated translation initiation. *Cell* 119, 369–380. doi:10.1016/j.cell.2004.09.038
- Owen, D.M., Rentero, C., Rossy, J., Magenau, A., Williamson, D., Rodriguez, M., Gaus, K., 2010. PALM imaging and cluster analysis of protein heterogeneity at the cell surface. *J. Biophotonics* 3, 446–454. doi:10.1002/jbio.200900089
- Owsianka, A., Tarr, A.W., Juttla, V.S., Lavillette, D., Bartosch, B., Cosset, F.-L., Ball, J.K., Patel, A.H., 2005. Monoclonal Antibody AP33 Defines a Broadly Neutralizing Epitope on the Hepatitis C Virus E2 Envelope Glycoprotein. *J. Virol.* 79, 11095–11104. doi:10.1128/JVI.79.17.11095-11104.2005
- Paige, J.S., Wu, K., Jaffrey, S.R., 2011. RNA mimics of green fluorescent protein. *Science* 333, 642–646. doi:10.1126/science.1207339
- Palomares-Jerez, F., Nemesio, H., Villalaín, J., 2012. The membrane spanning domains of protein NS4B from hepatitis C virus. *Biochim. Biophys. Acta* 1818, 2958–2966. doi:10.1016/j.bbamem.2012.07.022
- Palomares-Jerez, M.F., Guillén, J., Villalaín, J., 2010. Interaction of the N-terminal segment of HCV protein NS5A with model membranes. *Biochim. Biophys. Acta* 1798, 1212–1224. doi:10.1016/j.bbamem.2010.02.007
- Palomares-Jerez, M.F., Nemesio, H., Franquelim, H.G., Castanho, M.A.R.B., Villalaín, J., 2013. N-terminal AH2 segment of protein NS4B from hepatitis C virus. Binding to and interaction with model biomembranes. *Biochim. Biophys. Acta* 1828, 1938–1952. doi:10.1016/j.bbamem.2013.04.020
- Panyasrivanit, M., Khakpoor, A., Wikan, N., Smith, D.R., 2009. Co-localization of constituents of the dengue virus translation and replication machinery with amphisomes. *J. Gen. Virol.* 90, 448–456. doi:10.1099/vir.0.005355-0

- Papastergiou, V., Tsochatzis, E., Burroughs, A.K., 2012. Non-invasive assessment of liver fibrosis. *Ann. Gastroenterol.* 25, 218–231.
- Paredes, A.M., Blight, K.J., 2008. A Genetic Interaction between Hepatitis C Virus NS4B and NS3 Is Important for RNA Replication. *J. Virol.* 82, 10671–10683. doi:10.1128/JVI.00875-08
- Paul, D., Bartenschlager, R., 2015. Flaviviridae Replication Organelles: Oh, What a Tangled Web We Weave. *Annu. Rev. Virol.* 2, 289–310. doi:10.1146/annurev-virology-100114-055007
- Paul, D., Hoppe, S., Saher, G., Krijnse-Locker, J., Bartenschlager, R., 2013. Morphological and Biochemical Characterization of the Membranous Hepatitis C Virus Replication Compartment. *J. Virol.* 87, 10612–10627. doi:10.1128/JVI.01370-13
- Paul, D., Madan, V., Bartenschlager, R., 2014. Hepatitis C virus RNA replication and assembly: living on the fat of the land. *Cell Host Microbe* 16, 569–579. doi:10.1016/j.chom.2014.10.008
- Pawley, J., 2012. *Handbook of Biological Confocal Microscopy*. Springer Science & Business Media.
- Pawlotsky, J.-M., 2014. New Hepatitis C Therapies: The Toolbox, Strategies, and Challenges. *Gastroenterology* 146, 1176–1192. doi:10.1053/j.gastro.2014.03.003
- Pearlman, B.L., Traub, N., 2011. Sustained Virologic Response to Antiviral Therapy for Chronic Hepatitis C Virus Infection: A Cure and So Much More. *Clin. Infect. Dis.* 52, 889–900. doi:10.1093/cid/cir076
- Penin, F., Brass, V., Appel, N., Ramboarina, S., Montserret, R., Ficheux, D., Blum, H.E., Bartenschlager, R., Moradpour, D., 2004. Structure and Function of the Membrane Anchor Domain of Hepatitis C Virus Nonstructural Protein 5A. *J. Biol. Chem.* 279, 40835–40843. doi:10.1074/jbc.M404761200
- Pérez-Berná, A.J., Rodríguez, M.J., Chichón, F.J., Friesland, M.F., Sorrentino, A., Carrascosa, J.L., Pereiro, E., Gastaminza, P., 2016. Structural Changes In Cells Imaged by Soft X-ray Cryo-Tomography During Hepatitis C Virus Infection. *ACS Nano* 10, 6597–6611. doi:10.1021/acsnano.6b01374
- Perin, P.M., Haid, S., Brown, R.J.P., Doerrbecker, J., Schulze, K., Zeilinger, C., von Schaewen, M., Heller, B., Vercauteren, K., Luxenburger, E., Baktash, Y.M., Vondran, F.W.R., Speerstra, S., Awadh, A., Mukhtarov, F., Schang, L.M., Kirschning, A., Müller, R., Guzman, C.A., Kaderali, L., Randall, G., Meuleman, P., Ploss, A., Pietschmann, T., 2016. Flunarizine prevents hepatitis C virus membrane fusion in a genotype-dependent manner by targeting the potential fusion peptide within E1. *Hepatology* 63, 49–62. doi:10.1002/hep.28111
- Pertsinidis, A., Mukherjee, K., Sharma, M., Pang, Z.P., Park, S.R., Zhang, Y., Brunger, A.T., Südhof, T.C., Chu, S., 2013. Ultrahigh-resolution imaging reveals formation of neuronal SNARE/Munc18 complexes in situ. *Proc. Natl. Acad. Sci. U. S. A.* 110, E2812–2820. doi:10.1073/pnas.1310654110
- Pestova, T.V., Shatsky, I.N., Fletcher, S.P., Jackson, R.J., Hellen, C.U., 1998. A prokaryotic-like mode of cytoplasmic eukaryotic ribosome binding to the initiation codon during internal translation initiation of hepatitis C and classical swine fever virus RNAs. *Genes Dev.* 12, 67–83.
- Phan, T., Beran, R.K.F., Peters, C., Lorenz, I.C., Lindenbach, B.D., 2009. Hepatitis C Virus NS2 Protein Contributes to Virus Particle Assembly via Opposing Epistatic Interactions with the E1-E2 Glycoprotein and NS3-NS4A Enzyme Complexes. *J. Virol.* 83, 8379–8395. doi:10.1128/JVI.00891-09
- Pielak, R.M., Chou, J.J., 2011. Influenza M2 proton channels. *Biochim. Biophys. Acta* 1808, 522–529. doi:10.1016/j.bbamem.2010.04.015
- Platonova, E., Winterflood, C.M., Junemann, A., Albrecht, D., Faix, J., Ewers, H., 2015. Single-molecule microscopy of molecules tagged with GFP or RFP

- derivatives in mammalian cells using nanobody binders. *Methods, Super-resolution Light Microscopy* 88, 89–97. doi:10.1016/j.ymeth.2015.06.018
- Pleiner, T., Bates, M., Trakhanov, S., Lee, C.-T., Schliep, J.E., Chug, H., Böhning, M., Stark, H., Urlaub, H., Görlich, D., 2015. Nanobodies: site-specific labeling for super-resolution imaging, rapid epitope-mapping and native protein complex isolation. *eLife* 4, e11349. doi:10.7554/eLife.11349
- Ploss, A., Evans, M.J., Gaysinskaya, V.A., Panis, M., You, H., de Jong, Y.P., Rice, C.M., 2009. Human occludin is a hepatitis C virus entry factor required for infection of mouse cells. *Nature* 457, 882–886. doi:10.1038/nature07684
- Polson, H.E.J., Lartigue, J. de, Rigden, D.J., Reedijk, M., Urbé, S., Clague, M.J., Tooze, S.A., 2010. Mammalian Atg18 (WIPI2) localizes to omegasome-anchored phagophores and positively regulates LC3 lipidation. *Autophagy* 6, 506–522. doi:10.4161/auto.6.4.11863
- Popescu, C.-I., Riva, L., Vlaicu, O., Farhat, R., Rouillé, Y., Dubuisson, J., 2014. Hepatitis C Virus Life Cycle and Lipid Metabolism. *Biology* 3, 892–921. doi:10.3390/biology3040892
- Popescu, C.-I., Rouillé, Y., Dubuisson, J., 2011. Hepatitis C Virus Assembly Imaging. *Viruses* 3, 2238–2254. doi:10.3390/v3112238
- Popp, M.W., Antos, J.M., Grotenbreg, G.M., Spooner, E., Ploegh, H.L., 2007. Sortagging: a versatile method for protein labeling. *Nat. Chem. Biol.* 3, 707–708. doi:10.1038/nchembio.2007.31
- Premkumar, A., Wilson, L., Ewart, G.D., Gage, P.W., 2004. Cation-selective ion channels formed by p7 of hepatitis C virus are blocked by hexamethylene amiloride. *FEBS Lett.* 557, 99–103.
- Price, D.A., Bassendine, M.F., Norris, S.M., Golding, C., Toms, G.L., Schmid, M.L., Morris, C.M., Burt, A.D., Donaldson, P.T., 2006. Apolipoprotein ε3 allele is associated with persistent hepatitis C virus infection. *Gut* 55, 715–718. doi:10.1136/gut.2005.079905
- Qiu, D., Lemm, J.A., O’Boyle, D.R., Sun, J.-H., Nower, P.T., Nguyen, V., Hamann, L.G., Snyder, L.B., Deon, D.H., Ruediger, E., Meanwell, N.A., Belema, M., Gao, M., Fridell, R.A., 2011. The effects of NS5A inhibitors on NS5A phosphorylation, polyprotein processing and localization. *J. Gen. Virol.* 92, 2502–2511. doi:10.1099/vir.0.034801-0
- Qualmann, B., Koch, D., Kessels, M.M., 2011. Let’s go bananas: revisiting the endocytic BAR code. *EMBO J.* 30, 3501–3515. doi:10.1038/emboj.2011.266
- Quan, P.-L., Firth, C., Conte, J.M., Williams, S.H., Zambrana-Torrel, C.M., Anthony, S.J., Ellison, J.A., Gilbert, A.T., Kuzmin, I.V., Niezgod, M., Osinubi, M.O.V., Recuenco, S., Markotter, W., Breiman, R.F., Kalemba, L., Malekani, J., Lindblade, K.A., Rostal, M.K., Ojeda-Flores, R., Suzan, G., Davis, L.B., Blau, D.M., Ogunkoya, A.B., Alvarez Castillo, D.A., Moran, D., Ngam, S., Akaibe, D., Agwanda, B., Briese, T., Epstein, J.H., Daszak, P., Rupprecht, C.E., Holmes, E.C., Lipkin, W.I., 2013. Bats are a major natural reservoir for hepaciviruses and pegiviruses. *Proc. Natl. Acad. Sci. U. S. A.* 110, 8194–8199. doi:10.1073/pnas.1303037110
- Quinkert, D., Bartenschlager, R., Lohmann, V., 2005. Quantitative analysis of the hepatitis C virus replication complex. *J. Virol.* 79, 13594–13605. doi:10.1128/JVI.79.21.13594-13605.2005
- Quintavalle, M., Sambucini, S., Summa, V., Orsatti, L., Talamo, F., De Francesco, R., Neddermann, P., 2007. Hepatitis C virus NS5A is a direct substrate of casein kinase I-alpha, a cellular kinase identified by inhibitor affinity chromatography using specific NS5A hyperphosphorylation inhibitors. *J. Biol. Chem.* 282, 5536–5544. doi:10.1074/jbc.M610486200
- R Core Team, 2013. R: A Language and Environment for statistical computing. R Foundation for Statistical Computing.

- Ranjith-Kumar, C.T., Kao, C.C., 2006. Biochemical Activities of the HCV NS5B RNA-Dependent RNA Polymerase, in: Tan, S.-L. (Ed.), *Hepatitis C Viruses: Genomes and Molecular Biology*. Horizon Bioscience, Norfolk (UK).
- Rao, Y., Haucke, V., 2011. Membrane shaping by the Bin/amphiphysin/Rvs (BAR) domain protein superfamily. *Cell. Mol. Life Sci. CMLS* 68, 3983–3993. doi:10.1007/s00018-011-0768-5
- Rau, M., Baur, K., Geier, A., 2012. Host genetic variants in the pathogenesis of hepatitis C. *Viruses* 4, 3281–3302.
- Rautou, P.-E., Cazals-Hatem, D., Feldmann, G., Mansouri, A., Grodet, A., Barge, S., Martinot-Peignoux, M., Duces, A., Bièche, I., Lebrech, D., Bedossa, P., Paradis, V., Marcellin, P., Valla, D., Asselah, T., Moreau, R., 2011. Changes in Autophagic Response in Patients with Chronic Hepatitis C Virus Infection. *Am. J. Pathol.* 178, 2708–2715. doi:10.1016/j.ajpath.2011.02.021
- Rawlings, A.E., Bramble, J.P., Tang, A.A.S., Somner, L.A., Monnington, A.E., Cooke, D.J., McPherson, M.J., Tomlinson, D.C., Staniland, S.S., 2015. Phage display selected magnetite interacting Adhirons for shape controlled nanoparticle synthesis. *Chem. Sci.* 6, 5586–5594. doi:10.1039/C5SC01472G
- Rayleigh, Lord, 1896. XV. On the theory of optical images, with special reference to the microscope. *Philos. Mag. Ser. 5* 42, 167–195. doi:10.1080/14786449608620902
- Reghellin, V., Donnici, L., Fenu, S., Berno, V., Calabrese, V., Pagani, M., Abrignani, S., Peri, F., Francesco, R.D., Neddermann, P., 2014. NS5A Inhibitors Impair NS5A–Phosphatidylinositol 4-Kinase III α Complex Formation and Cause a Decrease of Phosphatidylinositol 4-Phosphate and Cholesterol Levels in Hepatitis C Virus-Associated Membranes. *Antimicrob. Agents Chemother.* 58, 7128–7140. doi:10.1128/AAC.03293-14
- Reid, D.W., Nicchitta, C.V., 2015. Diversity and selectivity in mRNA translation on the endoplasmic reticulum. *Nat. Rev. Mol. Cell Biol.* 16, 221–231. doi:10.1038/nrm3958
- Reid, S.P., Tritsch, S.R., Kota, K., Chiang, C.-Y., Dong, L., Kenny, T., Brueggemann, E.E., Ward, M.D., Cazares, L.H., Bavari, S., 2015. Sphingosine kinase 2 is a chikungunya virus host factor co-localized with the viral replication complex. *Emerg. Microbes Infect.* 4, e61. doi:10.1038/emi.2015.61
- Reiss, S., Rebhan, I., Backes, P., Romero-Brey, I., Erfle, H., Matula, P., Kaderali, L., Poenisch, M., Blankenburg, H., Hiet, M.-S., Longerich, T., Diehl, S., Ramirez, F., Balla, T., Rohr, K., Kaul, A., Bühler, S., Pepperkok, R., Lengauer, T., Albrecht, M., Eils, R., Schirmacher, P., Lohmann, V., Bartenschlager, R., 2011. Recruitment and activation of a lipid kinase by hepatitis C virus NS5A is essential for integrity of the membranous replication compartment. *Cell Host Microbe* 9, 32–45. doi:10.1016/j.chom.2010.12.002
- Remenyi, R., Qi, H., Su, S.-Y., Chen, Z., Wu, N.C., Arumugaswami, V., Truong, S., Chu, V., Stokelman, T., Lo, H.-H., Olson, C.A., Wu, T.-T., Chen, S.-H., Lin, C.-Y., Sun, R., 2014. A Comprehensive Functional Map of the Hepatitis C Virus Genome Provides a Resource for Probing Viral Proteins. *mBio* 5, e01469-14. doi:10.1128/mBio.01469-14
- Reynolds, J.E., Kaminski, A., Carroll, A.R., Clarke, B.E., Rowlands, D.J., Jackson, R.J., 1996. Internal initiation of translation of hepatitis C virus RNA: the ribosome entry site is at the authentic initiation codon. *RNA* 2, 867–878.
- Reynolds, J.E., Kaminski, A., Kettinen, H.J., Grace, K., Clarke, B.E., Carroll, A.R., Rowlands, D.J., Jackson, R.J., 1995. Unique features of internal initiation of hepatitis C virus RNA translation. *EMBO J.* 14, 6010–6020.
- Ribeiro, R.M., Li, H., Wang, S., Stoddard, M.B., Learn, G.H., Korber, B.T., Bhattacharya, T., Guedj, J., Parrish, E.H., Hahn, B.H., Shaw, G.M.,

- Perelson, A.S., 2012. Quantifying the diversification of hepatitis C virus (HCV) during primary infection: estimates of the in vivo mutation rate. *PLoS Pathog.* 8, e1002881. doi:10.1371/journal.ppat.1002881
- Ridley, S.H., Ktistakis, N., Davidson, K., Anderson, K.E., Manifava, M., Ellson, C.D., Lipp, P., Bootman, M., Coadwell, J., Nazarian, A., Erdjument-Bromage, H., Tempst, P., Cooper, M.A., Thuring, J.W.J.F., Lim, Z.-Y., Holmes, A.B., Stephens, L.R., Hawkins, P.T., 2001. FENS-1 and DFCP1 are FYVE domain-containing proteins with distinct functions in the endosomal and Golgi compartments. *J. Cell Sci.* 114, 3991–4000.
- Ries, J., Kaplan, C., Platonova, E., Eghlidi, H., Ewers, H., 2012. A simple, versatile method for GFP-based super-resolution microscopy via nanobodies. *Nat. Methods* 9, 582–584. doi:10.1038/nmeth.1991
- Rigat, K.L., Lu, H., Wang, Y.-K., Argyrou, A., Fanslau, C., Beno, B., Wang, Y., Marcinkeviciene, J., Ding, M., Gentles, R.G., Gao, M., Abell, L.M., Roberts, S.B., 2014. Mechanism of inhibition for BMS-791325, a novel non-nucleoside inhibitor of hepatitis C virus NS5B polymerase. *J. Biol. Chem.* 289, 33456–33468. doi:10.1074/jbc.M114.613653
- Rijnbrand, R., Bredenbeek, P., van der Straaten, T., Whetter, L., Inchauspé, G., Lemon, S., Spaan, W., 1995. Almost the entire 5' non-translated region of hepatitis C virus is required for cap-independent translation. *FEBS Lett.* 365, 115–119. doi:10.1016/0014-5793(95)00458-L
- Rijnbrand, R.C.A., Lemon, S.M., 2000. Internal ribosome entry site-mediated translation in hepatitis C virus replication. *Curr. Top. Microbiol. Immunol.* 242, 85–116.
- Ripley, B.D., 1977. Modelling spatial patterns. *J. R. Stat. Soc.* 39, 172–212. doi:10.2307/2984796
- Romano, K.P., Ali, A., Aydin, C., Soumana, D., Ozen, A., Deveau, L.M., Silver, C., Cao, H., Newton, A., Petropoulos, C.J., Huang, W., Schiffer, C.A., 2012. The molecular basis of drug resistance against hepatitis C virus NS3/4A protease inhibitors. *PLoS Pathog.* 8, e1002832. doi:10.1371/journal.ppat.1002832
- Romano, K.P., Ali, A., Royer, W.E., Schiffer, C.A., 2010. Drug resistance against HCV NS3/4A inhibitors is defined by the balance of substrate recognition versus inhibitor binding. *Proc. Natl. Acad. Sci. U. S. A.* 107, 20986–20991. doi:10.1073/pnas.1006370107
- Romero-Brey, I., Bartenschlager, R., 2014. Membranous Replication Factories Induced by Plus-Strand RNA Viruses. *Viruses* 6, 2826–2857. doi:10.3390/v6072826
- Romero-Brey, I., Berger, C., Kallis, S., Kolovou, A., Paul, D., Lohmann, V., Bartenschlager, R., 2015. NS5A Domain 1 and Polyprotein Cleavage Kinetics Are Critical for Induction of Double-Membrane Vesicles Associated with Hepatitis C Virus Replication. *mBio* 6, e00759-15. doi:10.1128/mBio.00759-15
- Romero-Brey, I., Merz, A., Chiramel, A., Lee, J.-Y., Chlanda, P., Haselman, U., Santarella-Mellwig, R., Habermann, A., Hoppe, S., Kallis, S., Walther, P., Antony, C., Krijnse-Locker, J., Bartenschlager, R., 2012. Three-Dimensional Architecture and Biogenesis of Membrane Structures Associated with Hepatitis C Virus Replication. *PLOS Pathog* 8, e1003056. doi:10.1371/journal.ppat.1003056
- Romero-López, C., Barroso-Deljesus, A., García-Sacristán, A., Briones, C., Berzal-Herranz, A., 2014. End-to-end crosstalk within the hepatitis C virus genome mediates the conformational switch of the 3'X-tail region. *Nucleic Acids Res.* 42, 567–582. doi:10.1093/nar/gkt841
- Romero-López, C., Barroso-Deljesus, A., García-Sacristán, A., Briones, C., Berzal-Herranz, A., 2012. The folding of the hepatitis C virus internal ribosome

- entry site depends on the 3'-end of the viral genome. *Nucleic Acids Res.* 40, 11697–11713. doi:10.1093/nar/gks927
- Romero-López, C., Berzal-Herranz, A., 2009. A long-range RNA-RNA interaction between the 5' and 3' ends of the HCV genome. *RNA N. Y. N* 15, 1740–1752. doi:10.1261/rna.1680809
- Ron, D., Walter, P., 2007. Signal integration in the endoplasmic reticulum unfolded protein response. *Nat. Rev. Mol. Cell Biol.* 8, 519–529. doi:10.1038/nrm2199
- Rosenthal, E.S., Graham, C.S., 2016. Price and affordability of direct-acting antiviral regimens for hepatitis C virus in the United States. *Infect. Agent. Cancer* 11. doi:10.1186/s13027-016-0071-z
- Rosnoblet, C., Fritzingier, B., Legrand, D., Launay, H., Wieruszeski, J.-M., Lippens, G., Hanouille, X., 2012. Hepatitis C virus NS5B and host cyclophilin A share a common binding site on NS5A. *J. Biol. Chem.* 287, 44249–44260. doi:10.1074/jbc.M112.392209
- Ross-Thriepland, D., Amako, Y., Harris, M., 2013. The C terminus of NS5A domain II is a key determinant of hepatitis C virus genome replication, but is not required for virion assembly and release. *J. Gen. Virol.* 94, 1009–1018. doi:10.1099/vir.0.050633-0
- Ross-Thriepland, D., Harris, M., 2015. Hepatitis C virus NS5A: enigmatic but still promiscuous 10 years on! *J. Gen. Virol.* 96, 727–738. doi:10.1099/jgv.0.000009
- Ross-Thriepland, D., Harris, M., 2014. Insights into the Complexity and Functionality of Hepatitis C Virus NS5A Phosphorylation. *J. Virol.* 88, 1421–1432. doi:10.1128/JVI.03017-13
- Ross-Thriepland, D., Mankouri, J., Harris, M., 2015. Serine Phosphorylation of the Hepatitis C Virus NS5A Protein Controls the Establishment of Replication Complexes. *J. Virol.* 89, 3123–3135. doi:10.1128/JVI.02995-14
- Rouillé, Y., Helle, F., Delgrange, D., Roingeard, P., Voisset, C., Blanchard, E., Belouzard, S., McKeating, J., Patel, A.H., Maertens, G., Wakita, T., Wychowski, C., Dubuisson, J., 2006. Subcellular localization of hepatitis C virus structural proteins in a cell culture system that efficiently replicates the virus. *J. Virol.* 80, 2832–2841. doi:10.1128/JVI.80.6.2832-2841.2006
- Rubín, A., Aguilera, V., Berenguer, M., 2011. Liver transplantation and hepatitis C. *Clin. Res. Hepatol. Gastroenterol.* 35, 805–812. doi:10.1016/j.clinre.2011.04.009
- Rubin-Delanchy, P., Burn, G.L., Griffié, J., Williamson, D.J., Heard, N.A., Cope, A.P., Owen, D.M., 2015. Bayesian cluster identification in single-molecule localization microscopy data. *Nat. Methods* 12, 1072–1076. doi:10.1038/nmeth.3612
- Rust, M.J., Bates, M., Zhuang, X., 2006. Stochastic optical reconstruction microscopy (STORM) provides sub-diffraction-limit image resolution. *Nat. Methods* 3, 793–795. doi:10.1038/nmeth929
- Saeed, M., Scheel, T.K.H., Gottwein, J.M., Marukian, S., Dustin, L.B., Bukh, J., Rice, C.M., 2012. Efficient Replication of Genotype 3a and 4a Hepatitis C Virus Replicons in Human Hepatoma Cells. *Antimicrob. Agents Chemother.* 56, 5365–5373. doi:10.1128/AAC.01256-12
- Sainz, B., Barretto, N., Martin, D.N., Hiraga, N., Imamura, M., Hussain, S., Marsh, K.A., Yu, X., Chayama, K., Alrefai, W.A., Uprichard, S.L., 2012. Identification of the Niemann-Pick C1-like 1 cholesterol absorption receptor as a new hepatitis C virus entry factor. *Nat. Med.* 18, 281–285. doi:10.1038/nm.2581
- Sakdinawat, A., Attwood, D., 2010. Nanoscale X-ray imaging. *Nat. Photonics* 4, 840–848. doi:10.1038/nphoton.2010.267
- Santantonio, T., Fasano, M., Sinisi, E., Guastadisegni, A., Casalino, C., Mazzola, M., Francavilla, R., Pastore, G., 2005. Efficacy of a 24-week course of PEG-interferon alpha-2b monotherapy in patients with acute hepatitis C after

- failure of spontaneous clearance. *J. Hepatol.* 42, 329–333. doi:10.1016/j.jhep.2004.11.021
- Santolini, E., Migliaccio, G., La Monica, N., 1994. Biosynthesis and biochemical properties of the hepatitis C virus core protein. *J. Virol.* 68, 3631–3641.
- Saxton, W.O., Baumeister, W., 1982. The correlation averaging of a regularly arranged bacterial cell envelope protein. *J. Microsc.* 127, 127–138. doi:10.1111/j.1365-2818.1982.tb00405.x
- Scarselli, E., Ansuini, H., Cerino, R., Roccasecca, R.M., Acali, S., Filocamo, G., Traboni, C., Nicosia, A., Cortese, R., Vitelli, A., 2002. The human scavenger receptor class B type I is a novel candidate receptor for the hepatitis C virus. *EMBO J.* 21, 5017–5025.
- Schaller, T., Appel, N., Koutsoudakis, G., Kallis, S., Lohmann, V., Pietschmann, T., Bartenschlager, R., 2007. Analysis of Hepatitis C Virus Superinfection Exclusion by Using Novel Fluorochrome Gene-Tagged Viral Genomes. *J. Virol.* 81, 4591–4603. doi:10.1128/JVI.02144-06
- Scheel, T.K.H., Prentoe, J., Carlsen, T.H.R., Mikkelsen, L.S., Gottwein, J.M., Bukh, J., 2012. Analysis of Functional Differences between Hepatitis C Virus NS5A of Genotypes 1–7 in Infectious Cell Culture Systems. *PLOS Pathog.* 8, e1002696. doi:10.1371/journal.ppat.1002696
- Schermelleh, L., Heintzmann, R., Leonhardt, H., 2010. A guide to super-resolution fluorescence microscopy. *J. Cell Biol.* 190, 165–175. doi:10.1083/jcb.201002018
- Schindelin, J., Rueden, C.T., Hiner, M.C., Eliceiri, K.W., 2015. The ImageJ ecosystem: An open platform for biomedical image analysis. *Mol. Reprod. Dev.* 82, 518–529. doi:10.1002/mrd.22489
- Schlehuber, S., Skerra, A., 2005. Anticalins as an alternative to antibody technology. *Expert Opin. Biol. Ther.* 5, 1453–1462. doi:10.1517/14712598.5.11.1453
- Schmidt-Mende, J., Bieck, E., Hügler, T., Penin, F., Rice, C.M., Blum, H.E., Moradpour, D., 2001. Determinants for Membrane Association of the Hepatitis C Virus RNA-dependent RNA Polymerase. *J. Biol. Chem.* 276, 44052–44063. doi:10.1074/jbc.M103358200
- Schneider, C.A., Rasband, W.S., Eliceiri, K.W., 2012. NIH Image to ImageJ: 25 years of image analysis. *Nat. Methods* 9, 671–675.
- Schreiber, G.B., Busch, M.P., Kleinman, S.H., Korelitz, J.J., 1996. The risk of transfusion-transmitted viral infections. The Retrovirus Epidemiology Donor Study. *N. Engl. J. Med.* 334, 1685–1690. doi:10.1056/NEJM199606273342601
- Scrima, N., Caillet-Saguy, C., Ventura, M., Harrus, D., Astier-Gin, T., Bressanelli, S., 2012. Two crucial early steps in RNA synthesis by the hepatitis C virus polymerase involve a dual role of residue 405. *J. Virol.* 86, 7107–7117. doi:10.1128/JVI.00459-12
- Sengupta, P., Jovanovic-Taliman, T., Skoko, D., Renz, M., Veatch, S.L., Lippincott-Schwartz, J., 2011. Probing protein heterogeneity in the plasma membrane using PALM and pair correlation analysis. *Nat. Methods* 8, 969–975. doi:10.1038/nmeth.1704
- Sengupta, P., Lippincott-Schwartz, J., 2012. Quantitative analysis of photoactivated localization microscopy (PALM) datasets using pair-correlation analysis. *BioEssays* 34, 396–405. doi:10.1002/bies.201200022
- Shannon, C.E., 1949. Communication in the Presence of Noise. *Proc. IRE* 37, 10–21. doi:10.1109/JRPROC.1949.232969
- Shao, L., Isaac, B., Uzawa, S., Agard, D.A., Sedat, J.W., Gustafsson, M.G.L., 2008. I5S: wide-field light microscopy with 100-nm-scale resolution in three dimensions. *Biophys. J.* 94, 4971–4983. doi:10.1529/biophysj.107.120352
- Sheppard, C.J.R., 1988. Super-resolution in confocal imaging. *Optik* 80, 53–54.

- Shi, G., Ando, T., Suzuki, R., Matsuda, M., Nakashima, K., Ito, M., Omatsu, T., Oba, M., Ochiai, H., Kato, T., Mizutani, T., Sawasaki, T., Wakita, T., Suzuki, T., 2016. Involvement of the 3' Untranslated Region in Encapsidation of the Hepatitis C Virus. *PLOS Pathog.* 12, e1005441. doi:10.1371/journal.ppat.1005441
- Shi, S., Yu, X., Gao, Y., Xue, B., Wu, X., Wang, X., Yang, D., Zhu, H., 2014. Inhibition of Hepatitis C Virus Production by Aptamers against the Core Protein. *J. Virol.* 88, 1990–1999. doi:10.1128/JVI.03312-13
- Shi, S.T., Lee, K.-J., Aizaki, H., Hwang, S.B., Lai, M.M.C., 2003. Hepatitis C Virus RNA Replication Occurs on a Detergent-Resistant Membrane That Cofractionates with Caveolin-2. *J. Virol.* 77, 4160–4168. doi:10.1128/JVI.77.7.4160-4168.2003
- Shimakami, T., Hijikata, M., Luo, H., Ma, Y.Y., Kaneko, S., Shimotohno, K., Murakami, S., 2004. Effect of interaction between hepatitis C virus NS5A and NS5B on hepatitis C virus RNA replication with the hepatitis C virus replicon. *J. Virol.* 78, 2738–2748.
- Shinohara, Y., Imajo, K., Yoneda, M., Tomeno, W., Ogawa, Y., Kirikoshi, H., Funakoshi, K., Ikeda, M., Kato, N., Nakajima, A., Saito, S., 2013. Unfolded protein response pathways regulate Hepatitis C virus replication via modulation of autophagy. *Biochem. Biophys. Res. Commun.* 432, 326–332. doi:10.1016/j.bbrc.2013.01.103
- Shiogama, K., Inada, K., Kohara, M., Teramoto, H., Mizutani, Y., Onouchi, T., Tsutsumi, Y., 2013. Demonstration of Hepatitis C Virus RNA with In Situ Hybridization Employing a Locked Nucleic Acid Probe in Humanized Liver of Infected Chimeric Mice and in Needle-Biopsied Human Liver. *Int. J. Hepatol.* 2013, e249535. doi:10.1155/2013/249535
- Shirota, Y., Luo, H., Qin, W., Kaneko, S., Yamashita, T., Kobayashi, K., Murakami, S., 2002. Hepatitis C Virus (HCV) NS5A Binds RNA-dependent RNA Polymerase (RdRP) NS5B and Modulates RNA-dependent RNA Polymerase Activity. *J. Biol. Chem.* 277, 11149–11155. doi:10.1074/jbc.M111392200
- Shrivastava, S., Chowdhury, J.B., Steele, R., Ray, R., Ray, R.B., 2012. Hepatitis C Virus Upregulates Beclin1 for Induction of Autophagy and Activates mTOR Signaling. *J. Virol.* 86, 8705–8712. doi:10.1128/JVI.00616-12
- Shroff, H., White, H., Betzig, E., 2013. Photoactivated Localization Microscopy (PALM) of adhesion complexes. *Curr. Protoc. Cell Biol.* Editor. Board Juan Bonifacino AI Chapter 4, Unit4.21. doi:10.1002/0471143030.cb0421s58
- Shulla, A., Randall, G., 2015. Spatiotemporal Analysis of Hepatitis C Virus Infection. *PLOS Pathog* 11, e1004758. doi:10.1371/journal.ppat.1004758
- Simister, P., Schmitt, M., Geitmann, M., Wicht, O., Danielson, U.H., Klein, R., Bressanelli, S., Lohmann, V., 2009. Structural and Functional Analysis of Hepatitis C Virus Strain JFH1 Polymerase. *J. Virol.* 83, 11926–11939. doi:10.1128/JVI.01008-09
- Simmonds, P., Bukh, J., Combet, C., Deléage, G., Enomoto, N., Feinstone, S., Halfon, P., Inchauspé, G., Kuiken, C., Maertens, G., Mizokami, M., Murphy, D.G., Okamoto, H., Pawlotsky, J.-M., Penin, F., Sablon, E., Shin-I, T., Stuyver, L.J., Thiel, H.-J., Viazov, S., Weiner, A.J., Widell, A., 2005. Consensus proposals for a unified system of nomenclature of hepatitis C virus genotypes. *Hepatol. Baltim. Md* 42, 962–973. doi:10.1002/hep.20819
- Sir, D., Chen, W., Choi, J., Wakita, T., Yen, T.S.B., Ou, J.J., 2008. Induction of incomplete autophagic response by hepatitis C virus via the unfolded protein response. *Hepatology* 48, 1054–1061. doi:10.1002/hep.22464
- Sir, D., Kuo, C., Tian, Y., Liu, H.M., Huang, E.J., Jung, J.U., Machida, K., Ou, J.-H.J., 2012. Replication of hepatitis C virus RNA on autophagosomal membranes. *J. Biol. Chem.* jbc.M111.320085. doi:10.1074/jbc.M111.320085

- Sletten, E.M., Bertozzi, C.R., 2009. Bioorthogonal Chemistry: Fishing for Selectivity in a Sea of Functionality. *Angew. Chem. Int. Ed Engl.* 48, 6974–6998. doi:10.1002/anie.200900942
- Smith, D.B., Bukh, J., Kuiken, C., Muerhoff, A.S., Rice, C.M., Stapleton, J.T., Simmonds, P., 2014. Expanded classification of hepatitis C virus into 7 genotypes and 67 subtypes: updated criteria and genotype assignment web resource. *Hepatology* 59, 318–327. doi:10.1002/hep.26744
- Snapp, E., 2005. Design and Use of Fluorescent Fusion Proteins in Cell Biology. *Curr. Protoc. Cell Biol.* Editor. Board Juan Bonifacino AI CHAPTER, Unit-21.4. doi:10.1002/0471143030.cb2104s27
- Sobell, H.M., 1985. Actinomycin and DNA transcription. *Proc. Natl. Acad. Sci. U. S. A.* 82, 5328–5331.
- Sofia, M.J., Chang, W., Furman, P.A., Mosley, R.T., Ross, B.S., 2012. Nucleoside, nucleotide, and non-nucleoside inhibitors of hepatitis C virus NS5B RNA-dependent RNA-polymerase. *J. Med. Chem.* 55, 2481–2531. doi:10.1021/jm201384j
- Sonenberg, N., Hinnebusch, A.G., 2009. Regulation of translation initiation in eukaryotes: mechanisms and biological targets. *Cell* 136, 731–745. doi:10.1016/j.cell.2009.01.042
- Song, Y., Friebe, P., Tzima, E., Jünemann, C., Bartenschlager, R., Niepmann, M., 2006. The Hepatitis C Virus RNA 3'-Untranslated Region Strongly Enhances Translation Directed by the Internal Ribosome Entry Site. *J. Virol.* 80, 11579–11588. doi:10.1128/JVI.00675-06
- Sourisseau, M., Michta, M.L., Zony, C., Israelow, B., Hopcraft, S.E., Narbus, C.M., Parra Martín, A., Evans, M.J., 2013. Temporal analysis of hepatitis C virus cell entry with occludin directed blocking antibodies. *PLoS Pathog.* 9, e1003244. doi:10.1371/journal.ppat.1003244
- Spahn, C.M., Kieft, J.S., Grassucci, R.A., Penczek, P.A., Zhou, K., Doudna, J.A., Frank, J., 2001. Hepatitis C virus IRES RNA-induced changes in the conformation of the 40s ribosomal subunit. *Science* 291, 1959–1962. doi:10.1126/science.1058409
- Stadler, C., Rexhepaj, E., Singan, V.R., Murphy, R.F., Pepperkok, R., Uhlén, M., Simpson, J.C., Lundberg, E., 2013. Immunofluorescence and fluorescent-protein tagging show high correlation for protein localization in mammalian cells. *Nat. Methods* 10, 315–323. doi:10.1038/nmeth.2377
- Stagge, F., Mitronova, G.Y., Belov, V.N., Wurm, C.A., Jakobs, S., 2013. Snap-, CLIP- and Halo-Tag Labelling of Budding Yeast Cells. *PLOS ONE* 8, e78745. doi:10.1371/journal.pone.0078745
- Stallinga, S., Rieger, B., 2010. Accuracy of the gaussian point spread function model in 2D localization microscopy. *Opt. Express* 18, 24461–24476.
- Stapleford, K.A., Lindenbach, B.D., 2011. Hepatitis C Virus NS2 Coordinates Virus Particle Assembly through Physical Interactions with the E1-E2 Glycoprotein and NS3-NS4A Enzyme Complexes. *J. Virol.* 85, 1706–1717. doi:10.1128/JVI.02268-10
- Stapleton, J.T., Fong, S., Muerhoff, A.S., Bukh, J., Simmonds, P., 2011. The GB viruses: a review and proposed classification of GBV-A, GBV-C (HGV), and GBV-D in genus Pegivirus within the family Flaviviridae. *J. Gen. Virol.* 92, 233–246. doi:10.1099/vir.0.027490-0
- Steinmann, E., Penin, F., Kallis, S., Patel, A.H., Bartenschlager, R., Pietschmann, T., 2007. Hepatitis C Virus p7 Protein Is Crucial for Assembly and Release of Infectious Virions. *PLOS Pathog* 3, e103. doi:10.1371/journal.ppat.0030103
- Stewart, H., Bingham, R.J., White, S.J., Dykeman, E.C., Zothner, C., Tuplin, A.K., Stockley, P.G., Twarock, R., Harris, M., 2016. Identification of novel RNA secondary structures within the hepatitis C virus genome reveals a

- cooperative involvement in genome packaging. *Sci. Rep.* 6. doi:10.1038/srep22952
- Stone, M., Jia, S., Heo, W.D., Meyer, T., Konan, K.V., 2007. Participation of rab5, an early endosome protein, in hepatitis C virus RNA replication machinery. *J. Virol.* 81, 4551–4563. doi:10.1128/JVI.01366-06
- Street, A., Macdonald, A., Crowder, K., Harris, M., 2004. The Hepatitis C Virus NS5A Protein Activates a Phosphoinositide 3-Kinase-dependent Survival Signaling Cascade. *J. Biol. Chem.* 279, 12232–12241. doi:10.1074/jbc.M312245200
- Su, W.-C., Chao, T.-C., Huang, Y.-L., Weng, S.-C., Jeng, K.-S., Lai, M.M.C., 2011. Rab5 and Class III Phosphoinositide 3-Kinase Vps34 Are Involved in Hepatitis C Virus NS4B-Induced Autophagy. *J. Virol.* 85, 10561–10571. doi:10.1128/JVI.00173-11
- Subach, F.V., Patterson, G.H., Manley, S., Gillette, J.M., Lippincott-Schwartz, J., Verkhusha, V.V., 2009. Photoactivatable mCherry for high-resolution two-color fluorescence microscopy. *Nat. Methods* 6, 153–159. doi:10.1038/nmeth.1298
- Summa, V., Ludmerer, S.W., McCauley, J.A., Fandozzi, C., Burlein, C., Claudio, G., Coleman, P.J., Dimuzio, J.M., Ferrara, M., Di Filippo, M., Gates, A.T., Graham, D.J., Harper, S., Hazuda, D.J., Huang, Q., McHale, C., Monteagudo, E., Pucci, V., Rowley, M., Rudd, M.T., Soriano, A., Stahlhut, M.W., Vacca, J.P., Olsen, D.B., Liverton, N.J., Carroll, S.S., 2012. MK-5172, a selective inhibitor of hepatitis C virus NS3/4a protease with broad activity across genotypes and resistant variants. *Antimicrob. Agents Chemother.* 56, 4161–4167. doi:10.1128/AAC.00324-12
- Suzich, J.A., Tamura, J.K., Palmer-Hill, F., Warrenner, P., Grakoui, A., Rice, C.M., Feinstone, S.M., Collett, M.S., 1993. Hepatitis C virus NS3 protein polynucleotide-stimulated nucleoside triphosphatase and comparison with the related pestivirus and flavivirus enzymes. *J. Virol.* 67, 6152–6158.
- Svarovskaia, E.S., Dvory-Sobol, H., Parkin, N., Hebner, C., Gontcharova, V., Martin, R., Ouyang, W., Han, B., Xu, S., Ku, K., Chiu, S., Gane, E., Jacobson, I.M., Nelson, D.R., Lawitz, E., Wyles, D.L., Bekele, N., Brainard, D., Symonds, W.T., McHutchison, J.G., Miller, M.D., Mo, H., 2014. Infrequent development of resistance in genotype 1-6 hepatitis C virus-infected subjects treated with sofosbuvir in phase 2 and 3 clinical trials. *Clin. Infect. Dis. Off. Publ. Infect. Dis. Soc. Am.* 59, 1666–1674. doi:10.1093/cid/ciu697
- Sy, T., Jamal, M.M., 2006. Epidemiology of hepatitis C virus (HCV) infection. *Int. J. Med. Sci.* 3, 41–46.
- Szymborska, A., Marco, A. de, Daigle, N., Cordes, V.C., Briggs, J.A.G., Ellenberg, J., 2013. Nuclear Pore Scaffold Structure Analyzed by Super-Resolution Microscopy and Particle Averaging. *Science* 341, 655–658. doi:10.1126/science.1240672
- Tai, A.W., Benita, Y., Peng, L.F., Kim, S.-S., Sakamoto, N., Xavier, R.J., Chung, R.T., 2009. A functional genomic screen identifies cellular cofactors of hepatitis C virus replication. *Cell Host Microbe* 5, 298–307. doi:10.1016/j.chom.2009.02.001
- Tai, C.L., Chi, W.K., Chen, D.S., Hwang, L.H., 1996. The helicase activity associated with hepatitis C virus nonstructural protein 3 (NS3). *J. Virol.* 70, 8477–8484.
- Tamai, K., Shiina, M., Tanaka, N., Nakano, T., Yamamoto, A., Kondo, Y., Kakazu, E., Inoue, J., Fukushima, K., Sano, K., Ueno, Y., Shimosegawa, T., Sugamura, K., 2012. Regulation of hepatitis C virus secretion by the Hrs-dependent exosomal pathway. *Virology* 422, 377–385. doi:10.1016/j.virol.2011.11.009

- Tan, S.-L., Nakao, H., He, Y., Vijaysri, S., Neddermann, P., Jacobs, B.L., Mayer, B.J., Katze, M.G., 1999. NS5A, a nonstructural protein of hepatitis C virus, binds growth factor receptor-bound protein 2 adaptor protein in a Src homology 3 domain/ligand-dependent manner and perturbs mitogenic signaling. *Proc. Natl. Acad. Sci.* 96, 5533–5538. doi:10.1073/pnas.96.10.5533
- Tanaka, T., Kato, N., Cho, M.J., Shimotohno, K., 1995. A novel sequence found at the 3' terminus of hepatitis C virus genome. *Biochem. Biophys. Res. Commun.* 215, 744–749. doi:10.1006/bbrc.1995.2526
- Tanaka, T., Kato, N., Cho, M.J., Sugiyama, K., Shimotohno, K., 1996. Structure of the 3' terminus of the hepatitis C virus genome. *J. Virol.* 70, 3307–3312.
- Tanida, I., 2011. Autophagy basics. *Microbiol. Immunol.* 55, 1–11. doi:10.1111/j.1348-0421.2010.00271.x
- Targett-Adams, P., Hope, G., Boulant, S., McLauchlan, J., 2008. Maturation of Hepatitis C Virus Core Protein by Signal Peptide Peptidase Is Required for Virus Production. *J. Biol. Chem.* 283, 16850–16859. doi:10.1074/jbc.M802273200
- Taylor, M.P., Kirkegaard, K., 2007. Modification of Cellular Autophagy Protein LC3 by Poliovirus. *J. Virol.* 81, 12543–12553. doi:10.1128/JVI.00755-07
- Tellinghuisen, T.L., Foss, K.L., Treadaway, J., 2008a. Regulation of Hepatitis C Virion Production via Phosphorylation of the NS5A Protein. *PLOS Pathog* 4, e1000032. doi:10.1371/journal.ppat.1000032
- Tellinghuisen, T.L., Foss, K.L., Treadaway, J.C., Rice, C.M., 2008b. Identification of Residues Required for RNA Replication in Domains II and III of the Hepatitis C Virus NS5A Protein. *J. Virol.* 82, 1073–1083. doi:10.1128/JVI.00328-07
- Tellinghuisen, T.L., Marcotrigiano, J., Gorbalenya, A.E., Rice, C.M., 2004. The NS5A Protein of Hepatitis C Virus Is a Zinc Metalloprotein. *J. Biol. Chem.* 279, 48576–48587. doi:10.1074/jbc.M407787200
- Tellinghuisen, T.L., Marcotrigiano, J., Rice, C.M., 2005. Structure of the zinc-binding domain of an essential component of the hepatitis C virus replicase. *Nature* 435, 374–379. doi:10.1038/nature03580
- Theise, N.D., 2007. Liver biopsy assessment in chronic viral hepatitis: a personal, practical approach. *Mod. Pathol. Off. J. U. S. Can. Acad. Pathol. Inc* 20 Suppl 1, S3-14. doi:10.1038/modpathol.3800693
- Thimme, R., Oldach, D., Chang, K.-M., Steiger, C., Ray, S.C., Chisari, F.V., 2001. Determinants of Viral Clearance and Persistence during Acute Hepatitis C Virus Infection. *J. Exp. Med.* 194, 1395–1406. doi:10.1084/jem.194.10.1395
- Thompson, R.E., Larson, D.R., Webb, W.W., 2002. Precise nanometer localization analysis for individual fluorescent probes. *Biophys. J.* 82, 2775–2783.
- Thomssen, R., Bonk, S., Propfe, C., Heermann, K.H., Köchel, H.G., Uy, A., 1992. Association of hepatitis C virus in human sera with beta-lipoprotein. *Med. Microbiol. Immunol. (Berl.)* 181, 293–300.
- Tiede, C., Tang, A.A.S., Deacon, S.E., Mandal, U., Nettleship, J.E., Owen, R.L., George, S.E., Harrison, D.J., Owens, R.J., Tomlinson, D.C., McPherson, M.J., 2014. Adhiron: a stable and versatile peptide display scaffold for molecular recognition applications. *Protein Eng. Des. Sel.* 27, 145–155. doi:10.1093/protein/gzu007
- Timpe, J.M., Stamataki, Z., Jennings, A., Hu, K., Farquhar, M.J., Harris, H.J., Schwarz, A., Desombere, I., Roels, G.L., Balfe, P., McKeating, J.A., 2008. Hepatitis C virus cell-cell transmission in hepatoma cells in the presence of neutralizing antibodies. *Hepatology* 47, 17–24. doi:10.1002/hep.21959
- Tollervey, D., Lehtonen, H., Carmo-Fonseca, M., Hurt, E.C., 1991. The small nucleolar RNP protein NOP1 (fibrillarin) is required for pre-rRNA processing in yeast. *EMBO J.* 10, 573–583.
- Tong, X., Le Pogam, S., Li, L., Haines, K., Piso, K., Baronas, V., Yan, J.-M., So, S.-S., Klumpp, K., Nájera, I., 2014. In vivo emergence of a novel mutant

- L159F/L320F in the NS5B polymerase confers low-level resistance to the HCV polymerase inhibitors mericitabine and sofosbuvir. *J. Infect. Dis.* 209, 668–675. doi:10.1093/infdis/jit562
- Tripathi, L.P., Kambara, H., Chen, Y.-A., Nishimura, Y., Moriishi, K., Okamoto, T., Morita, E., Abe, T., Mori, Y., Matsuura, Y., Mizuguchi, K., 2013. Understanding the biological context of NS5A-host interactions in HCV infection: a network-based approach. *J. Proteome Res.* 12, 2537–2551. doi:10.1021/pr3011217
- Trooskin, S.B., Poceta, J., Towey, C.M., Yolken, A., Rose, J.S., Luqman, N.L., Preston, T.-W.L., Chan, P.A., Beckwith, C., Feller, S.C., Lee, H., Nunn, A.S., 2015. Results from a Geographically Focused, Community-Based HCV Screening, Linkage-to-Care and Patient Navigation Program. *J. Gen. Intern. Med.* 30, 950–957. doi:10.1007/s11606-015-3209-6
- Trotard, M., Lepère-Douard, C., Régeard, M., Piquet-Pellorce, C., Lavillette, D., Cosset, F.-L., Gripon, P., Le Seyec, J., 2009. Kinases required in hepatitis C virus entry and replication highlighted by small interference RNA screening. *FASEB J. Off. Publ. Fed. Am. Soc. Exp. Biol.* 23, 3780–3789. doi:10.1096/fj.09-131920
- Tscherne, D.M., Jones, C.T., Evans, M.J., Lindenbach, B.D., McKeating, J.A., Rice, C.M., 2006. Time- and temperature-dependent activation of hepatitis C virus for low-pH-triggered entry. *J. Virol.* 80, 1734–1741. doi:10.1128/JVI.80.4.1734-1741.2006
- Tu, H., Gao, L., Shi, S.T., Taylor, D.R., Yang, T., Mircheff, A.K., Wen, Y., Gorbalenya, A.E., Hwang, S.B., Lai, M.M., 1999. Hepatitis C virus RNA polymerase and NS5A complex with a SNARE-like protein. *Virology* 263, 30–41. doi:10.1006/viro.1999.9893
- Tuerk, C., Gold, L., 1990. Systematic evolution of ligands by exponential enrichment: RNA ligands to bacteriophage T4 DNA polymerase. *Science* 249, 505–510. doi:10.1126/science.2200121
- Tuplin, A., Evans, D.J., Simmonds, P., 2004. Detailed mapping of RNA secondary structures in core and NS5B-encoding region sequences of hepatitis C virus by RNase cleavage and novel bioinformatic prediction methods. *J. Gen. Virol.* 85, 3037–3047. doi:10.1099/vir.0.80141-0
- Unser, M., Trus, B.L., Steven, A.C., 1987. A new resolution criterion based on spectral signal-to-noise ratios. *Ultramicroscopy* 23, 39–51.
- van de Linde, S., Endesfelder, U., Mukherjee, A., Schüttpelz, M., Wiebusch, G., Wolter, S., Heilemann, M., Sauer, M., 2009. Multicolor photoswitching microscopy for subdiffraction-resolution fluorescence imaging. *Photochem. Photobiol. Sci. Off. J. Eur. Photochem. Assoc. Eur. Soc. Photobiol.* 8, 465–469. doi:10.1039/b822533h
- van den Dries, K., Schwartz, S.L., Byars, J., Meddens, M.B.M., Bolomini-Vittori, M., Lidke, D.S., Figdor, C.G., Lidke, K.A., Cambi, A., 2013. Dual-color superresolution microscopy reveals nanoscale organization of mechanosensory podosomes. *Mol. Biol. Cell* 24, 2112–2123. doi:10.1091/mbc.E12-12-0856
- van Meer, G., Voelker, D.R., Feigenson, G.W., 2008. Membrane lipids: where they are and how they behave. *Nat. Rev. Mol. Cell Biol.* 9, 112–124. doi:10.1038/nrm2330
- Verdegem, D., Badillo, A., Wieruszkeski, J.-M., Landrieu, I., Leroy, A., Bartenschlager, R., Penin, F., Lippens, G., Hanouille, X., 2011. Domain 3 of NS5A Protein from the Hepatitis C Virus Has Intrinsic α -Helical Propensity and Is a Substrate of Cyclophilin A. *J. Biol. Chem.* 286, 20441–20454. doi:10.1074/jbc.M110.182436
- Vieyres, G., Brohm, C., Friesland, M., Gentzsch, J., Wölk, B., Roingeard, P., Steinmann, E., Pietschmann, T., 2013. Subcellular Localization and

- Function of an Epitope-Tagged p7 Viroporin in Hepatitis C Virus-Producing Cells. *J. Virol.* 87, 1664–1678. doi:10.1128/JVI.02782-12
- Vieyres, G., Thomas, X., Descamps, V., Duverlie, G., Patel, A.H., Dubuisson, J., 2010. Characterization of the Envelope Glycoproteins Associated with Infectious Hepatitis C Virus. *J. Virol.* 84, 10159–10168. doi:10.1128/JVI.01180-10
- von dem Bussche, A., Machida, R., Li, K., Loevinsohn, G., Khander, A., Wang, J., Wakita, T., Wands, J.R., Li, J., 2010. Hepatitis C virus NS2 protein triggers endoplasmic reticulum stress and suppresses its own viral replication. *J. Hepatol.* 53, 797–804. doi:10.1016/j.jhep.2010.05.022
- Wakita, T., Pietschmann, T., Kato, T., Date, T., Miyamoto, M., Zhao, Z., Murthy, K., Habermann, A., Kräusslich, H.-G., Mizokami, M., Bartenschlager, R., Liang, T.J., 2005. Production of infectious hepatitis C virus in tissue culture from a cloned viral genome. *Nat. Med.* 11, 791–796. doi:10.1038/nm1268
- Wang, C., Le, S.Y., Ali, N., Siddiqui, A., 1995. An RNA pseudoknot is an essential structural element of the internal ribosome entry site located within the hepatitis C virus 5' noncoding region. *RNA N. Y. N* 1, 526–537.
- Wang, H., Perry, J.W., Lauring, A.S., Neddermann, P., De Francesco, R., Tai, A.W., 2014. Oxysterol-binding protein is a phosphatidylinositol 4-kinase effector required for HCV replication membrane integrity and cholesterol trafficking. *Gastroenterology* 146, 1373-1385–11. doi:10.1053/j.gastro.2014.02.002
- Wansink, D.G., Schul, W., Kraan, I. van der, Steensel, B. van, Driel, R. van, Jong, L. de, 1993. Fluorescent labeling of nascent RNA reveals transcription by RNA polymerase II in domains scattered throughout the nucleus. *J. Cell Biol.* 122, 283–293. doi:10.1083/jcb.122.2.283
- Watanabe, S., Punge, A., Hollopeter, G., Willig, K.I., Hobson, R.J., Davis, M.W., Hell, S.W., Jorgensen, E.M., 2011. Protein localization in electron micrographs using fluorescence nanoscopy. *Nat. Methods* 8, 80–84. doi:10.1038/nmeth.1537
- Watashi, K., Hijikata, M., Hosaka, M., Yamaji, M., Shimotohno, K., 2003. Cyclosporin A suppresses replication of hepatitis C virus genome in cultured hepatocytes. *Hepatol. Baltim. Md* 38, 1282–1288. doi:10.1053/jhep.2003.50449
- Wei, X., Somanathan, S., Samarabandu, J., Berezney, R., 1999. Three-Dimensional Visualization of Transcription Sites and Their Association with Splicing Factor–Rich Nuclear Speckles. *J. Cell Biol.* 146, 543–558. doi:10.1083/jcb.146.3.543
- Welbourn, S., Pause, A., 2006. HCV NS2/3 Protease, in: Tan, S.-L. (Ed.), *Hepatitis C Viruses: Genomes and Molecular Biology*. Horizon Bioscience, Norfolk (UK).
- Welsch, S., Miller, S., Romero-Brey, I., Merz, A., Bleck, C.K.E., Walther, P., Fuller, S.D., Antony, C., Krijnse-Locker, J., Bartenschlager, R., 2009. Composition and Three-Dimensional Architecture of the Dengue Virus Replication and Assembly Sites. *Cell Host Microbe* 5, 365–375. doi:10.1016/j.chom.2009.03.007
- Weng, L., Hirata, Y., Arai, M., Kohara, M., Wakita, T., Watashi, K., Shimotohno, K., He, Y., Zhong, J., Toyoda, T., 2010. Sphingomyelin activates hepatitis C virus RNA polymerase in a genotype-specific manner. *J. Virol.* 84, 11761–11770. doi:10.1128/JVI.00638-10
- Wiegand, J., Buggisch, P., Boecher, W., Zeuzem, S., Gelbmann, C.M., Berg, T., Kauffmann, W., Kallinowski, B., Cornberg, M., Jaeckel, E., Wedemeyer, H., Manns, M.P., German HEP-NET Acute HCV Study Group, 2006. Early monotherapy with pegylated interferon alpha-2b for acute hepatitis C infection: the HEP-NET acute-HCV-II study. *Hepatol. Baltim. Md* 43, 250–256. doi:10.1002/hep.21043

- Wilner, S.E., Wengerter, B., Maier, K., de Lourdes Borba Magalhães, M., Del Amo, D.S., Pai, S., Opazo, F., Rizzoli, S.O., Yan, A., Levy, M., 2012. An RNA Alternative to Human Transferrin: A New Tool for Targeting Human Cells. *Mol. Ther. — Nucleic Acids* 1, e21. doi:10.1038/mtna.2012.14
- Wirth, M., Joachim, J., Tooze, S.A., 2013. Autophagosome formation--the role of ULK1 and Beclin1-PI3KC3 complexes in setting the stage. *Semin. Cancer Biol.* 23, 301–309. doi:10.1016/j.semcancer.2013.05.007
- Witteveldt, J., Evans, M.J., Bitzegeio, J., Koutsoudakis, G., Owsianka, A.M., Angus, A.G.N., Keck, Z.-Y., Fong, S.K.H., Pietschmann, T., Rice, C.M., Patel, A.H., 2009. CD81 is dispensable for hepatitis C virus cell-to-cell transmission in hepatoma cells. *J. Gen. Virol.* 90, 48–58. doi:10.1099/vir.0.006700-0
- Wolff, G., Hagen, C., Grünwald, K., Kaufmann, R., 2016. Towards correlative super-resolution fluorescence and electron cryo-microscopy. *Biol. Cell Auspices Eur. Cell Biol. Organ.* 108, 245–258. doi:10.1111/boc.201600008
- Wölk, B., Büchele, B., Moradpour, D., Rice, C.M., 2008. A Dynamic View of Hepatitis C Virus Replication Complexes. *J. Virol.* 82, 10519–10531. doi:10.1128/JVI.00640-08
- Wood, J., Frederickson, R.M., Fields, S., Patel, A.H., 2001. Hepatitis C virus 3'X region interacts with human ribosomal proteins. *J. Virol.* 75, 1348–1358. doi:10.1128/JVI.75.3.1348-1358.2001
- Wozniak, A.L., Griffin, S., Rowlands, D., Harris, M., Yi, M., Lemon, S.M., Weinman, S.A., 2010. Intracellular proton conductance of the hepatitis C virus p7 protein and its contribution to infectious virus production. *PLoS Pathog.* 6, e1001087. doi:10.1371/journal.ppat.1001087
- Wu, X., Zhou, Y., Zhang, K., Liu, Q., Guo, D., 2008. Isoform-specific interaction of pyruvate kinase with hepatitis C virus NS5B. *FEBS Lett.* 582, 2155–2160. doi:10.1016/j.febslet.2008.05.033
- Wyles, D.L., Kaihara, K.A., Korba, B.E., Schooley, R.T., Beadle, J.R., Hostetler, K.Y., 2009. The Octadecyloxyethyl Ester of (S)-9-[3-Hydroxy-2-(Phosphonomethoxy) Propyl]Adenine Is a Potent and Selective Inhibitor of Hepatitis C Virus Replication in Genotype 1A, 1B, and 2A Replicons. *Antimicrob. Agents Chemother.* 53, 2660–2662. doi:10.1128/AAC.01546-08
- Yakovlev, A.A., 2009. Crosslinkers and their utilization for studies of intermolecular interactions. *Neurochem. J.* 3, 139–144. doi:10.1134/S181971240902010X
- Yamada, N., Tanihara, K., Takada, A., Yorihuzi, T., Tsutsumi, M., Shimomura, H., Tsuji, T., Date, T., 1996. Genetic organization and diversity of the 3' noncoding region of the hepatitis C virus genome. *Virology* 223, 255–261. doi:10.1006/viro.1996.0476
- Yanagi, M., St Claire, M., Shapiro, M., Emerson, S.U., Purcell, R.H., Bukh, J., 1998. Transcripts of a chimeric cDNA clone of hepatitis C virus genotype 1b are infectious in vivo. *Virology* 244, 161–172. doi:10.1006/viro.1998.9092
- Yang, D., Meng, X., Yu, Q., Xu, L., Long, Y., Liu, B., Fang, X., Zhu, H., 2013. Inhibition of Hepatitis C Virus Infection by DNA Aptamer against Envelope Protein. *Antimicrob. Agents Chemother.* 57, 4937–4944. doi:10.1128/AAC.00897-13
- Yang, L., Tang, X., Weisbrod, C., Munske, G., Eng, J., von Haller, P., Kaiser, N., Bruce, J.E., 2010. pcPIR, a photocleavable and mass spectrometry identifiable cross-linker for protein interaction studies. *Anal. Chem.* 82, 3556–3566. doi:10.1021/ac902615g
- Yen, C.-L.E., Stone, S.J., Koliwad, S., Harris, C., Farese, R.V., 2008. Thematic Review Series: Glycerolipids. DGAT enzymes and triacylglycerol biosynthesis. *J. Lipid Res.* 49, 2283–2301. doi:10.1194/jlr.R800018-JLR200
- Yi, M., Lemon, S.M., 2003. 3' nontranslated RNA signals required for replication of hepatitis C virus RNA. *J. Virol.* 77, 3557–3568.

- Yi, M., Ma, Y., Yates, J., Lemon, S.M., 2007. Compensatory Mutations in E1, p7, NS2, and NS3 Enhance Yields of Cell Culture-Infectious Intergenotypic Chimeric Hepatitis C Virus. *J. Virol.* 81, 629–638. doi:10.1128/JVI.01890-06
- Yi, M., Villanueva, R.A., Thomas, D.L., Wakita, T., Lemon, S.M., 2006. Production of infectious genotype 1a hepatitis C virus (Hutchinson strain) in cultured human hepatoma cells. *Proc. Natl. Acad. Sci. U. S. A.* 103, 2310–2315. doi:10.1073/pnas.0510727103
- York, A.G., Chandris, P., Nogare, D.D., Head, J., Wawrzusin, P., Fischer, R.S., Chitnis, A., Shroff, H., 2013. Instant super-resolution imaging in live cells and embryos via analog image processing. *Nat. Methods* 10, 1122–1126. doi:10.1038/nmeth.2687
- York, A.G., Parekh, S.H., Dalle Nogare, D., Fischer, R.S., Temprine, K., Mione, M., Chitnis, A.B., Combs, C.A., Shroff, H., 2012. Resolution doubling in live, multicellular organisms via multifocal structured illumination microscopy. *Nat. Methods* 9, 749–754. doi:10.1038/nmeth.2025
- You, S., Stump, D.D., Branch, A.D., Rice, C.M., 2004. A cis-acting replication element in the sequence encoding the NS5B RNA-dependent RNA polymerase is required for hepatitis C virus RNA replication. *J. Virol.* 78, 1352–1366.
- Younis, B.B., Arshad, R., Khurhsid, S., Masood, J., Nazir, F., Tahira, M., 2015. Fulminant hepatic failure (FHF) due to acute hepatitis C. *Pak. J. Med. Sci.* 31, 1009–1011. doi:10.12669/pjms.314.7618
- Yu, M., Peng, B., Chan, K., Gong, R., Yang, H., Delaney, W., Cheng, G., 2014. Robust and Persistent Replication of the Genotype 6a Hepatitis C Virus Replicon in Cell Culture. *Antimicrob. Agents Chemother.* 58, 2638–2646. doi:10.1128/AAC.01780-13
- Yu, M.-L., Hou, N.-J., Dai, C.-Y., Chang, W.-Y., Chuang, W.-L., 2005. Successful Treatment of Fulminant Hepatitis C by Therapy with Alpha Interferon and Ribavirin. *Antimicrob. Agents Chemother.* 49, 3986–3987. doi:10.1128/AAC.49.9.3986-3987.2005
- Yu, X., Gao, Y., Xue, B., Wang, X., Yang, D., Qin, Y., Yu, R., Liu, N., Xu, L., Fang, X., Zhu, H., 2014. Inhibition of hepatitis C virus infection by NS5A-specific aptamer. *Antiviral Res.* 106, 116–124. doi:10.1016/j.antiviral.2014.03.020
- Zahid, M.N., Turek, M., Xiao, F., Thi, V.L.D., Guérin, M., Fofana, I., Bachellier, P., Thompson, J., Delang, L., Neyts, J., Bankwitz, D., Pietschmann, T., Dreux, M., Cosset, F.-L., Grunert, F., Baumert, T.F., Zeisel, M.B., 2013. The postbinding activity of scavenger receptor class B type I mediates initiation of hepatitis C virus infection and viral dissemination. *Hepatology* 57, 492–504. doi:10.1002/hep.26097
- Zayas, M., Long, G., Madan, V., Bartenschlager, R., 2016. Coordination of Hepatitis C Virus Assembly by Distinct Regulatory Regions in Nonstructural Protein 5A. *PLOS Pathog* 12, e1005376. doi:10.1371/journal.ppat.1005376
- Zech, B., Kurtenbach, A., Krieger, N., Strand, D., Blencke, S., Morbitzer, M., Salassidis, K., Cotten, M., Wissing, J., Obert, S., Bartenschlager, R., Herget, T., Daub, H., 2003. Identification and characterization of amphiphysin II as a novel cellular interaction partner of the hepatitis C virus NS5A protein. *J. Gen. Virol.* 84, 555–560. doi:10.1099/vir.0.18801-0
- Zeuzem, S., Berg, T., Gane, E., Ferenci, P., Foster, G.R., Fried, M.W., Hezode, C., Hirschfield, G.M., Jacobson, I., Nikitin, I., Pockros, P.J., Poordad, F., Scott, J., Lenz, O., Peeters, M., Sekar, V., De Smedt, G., Sinha, R., Beumont-Mauviel, M., 2014. Simeprevir increases rate of sustained virologic response among treatment-experienced patients with HCV genotype-1 infection: a phase IIb trial. *Gastroenterology* 146, 430–441.e6. doi:10.1053/j.gastro.2013.10.058
- Zhang, C., Cai, Z., Kim, Y.-C., Kumar, R., Yuan, F., Shi, P.-Y., Kao, C., Luo, G., 2005. Stimulation of hepatitis C virus (HCV) nonstructural protein 3 (NS3)

- helicase activity by the NS3 protease domain and by HCV RNA-dependent RNA polymerase. *J. Virol.* 79, 8687–8697. doi:10.1128/JVI.79.14.8687-8697.2005
- Zhang, M., Chang, H., Zhang, Y., Yu, J., Wu, L., Ji, W., Chen, J., Liu, B., Lu, J., Liu, Y., Zhang, J., Xu, P., Xu, T., 2012. Rational design of true monomeric and bright photoactivatable fluorescent proteins. *Nat. Methods* 9, 727–729. doi:10.1038/nmeth.2021
- Zhao, T., Wang, Y., Zhai, Y., Qu, X., Cheng, A., Du, S., Loy, M.M.T., 2015. A user-friendly two-color super-resolution localization microscope. *Opt. Express* 23, 1879. doi:10.1364/OE.23.001879
- Zipfel, W.R., Williams, R.M., Webb, W.W., 2003. Nonlinear magic: multiphoton microscopy in the biosciences. *Nat. Biotechnol.* 21, 1369–1377. doi:10.1038/nbt899
- Zordan, R.E., Beliveau, B.J., Trow, J.A., Craig, N.L., Cormack, B.P., 2015. Avoiding the Ends: Internal Epitope Tagging of Proteins Using Transposon Tn7. *Genetics* 200, 47–58. doi:10.1534/genetics.114.169482

Chapter 9 - Appendix

Name	T_m (°C)	%GC	Sequence (5' – 3')
NS5A mEos3.2 FW	70.3	52.6	CTGTCACGTGATCACGGAAGTAGCGGGTCATCGATGAGTGCGATTAAGCCAGACAT G
NS5A mEos3.2 RV	69.7	50.0	CTGTCACGTGATCAGATGAAGAACCTGAAGATCCTCGTCTGGCATTGTCAGGCAAT CC
NS3 TC FW	72.4	51.5	CTGTCATACCATGGGATCCTCCTTTCTCAACTGTTGTCCAGGGTGTTGTATGGAACC TG GTAGCTCTGCTCCCATCACTGCTTATGCCAGCAAACACG
NS3 TC RV	64.7	55.1	GACCTCAAGGTCAGCTTGCATGCATGTGG
NS5B <i>Nrul</i> FW	73.6	75.8	CACAGCGTGTGCGGAGCCCGACCCCGCTC
NS5B <i>Nrul</i> RV	73.6	75.8	GAGCGGGTCTGGGCTCGCGACACGCTGTG
NS5B TC FW	72.6	54.1	CTGTCATATCGCGAGGATCCTCTTTTCTCAACTGTTGTCCAGGGTGTTGTATGGAAC CT GGTAGCTCTGCCCGACCCCGCTCATTACTCTTCGGCC
NS5B TC RV	58.6	50.0	GTACCAGAGCTCACCTAGGTATCTAGAC
Adhiron P1	69.3	50.0	ATGGCTAGCAACTCCCTGGAAATCGAAG
Adhiron P2	78.2	39.5	CAACACGAACGAATTCCAGACAAGCGTTTTCTTTTTTGTGTG
Adhiron P3	78.2	39.5	CACAACAAAAAAGAAAACGCTTGTCTGGAATTCGTTTCGTGTTG
Adhiron P4	83.1	55.3	TACTAATGCGGCCGCACAAGCGTCACCAACCGTTTG

Appendix 1: List of cloning primers

Name	Tm (°C)	%GC	Sequence (5' – 3')
Luciferase Start FW	71.3	73.7	GCAGTTGCGCCCGCGAACG
Luciferase Mid FW	65.7	52.4	GCTCACTGAGACTACATCAGC
Neomycin Start FW	73.5	75.0	CGGCTGCTCTGATGCCGCCG
NS3 Mid FW	62.7	52.6	ACTGGCAGTGGAAAGAGCA
NS3 End	63.0	61.1	CTGGACCCACCTTCACT
NS4 FW	60.2	47.4	TAAGGAGGTCCTGTATGAG
NS5A Start FW	75.5	65.0	GGATGCGTCGCAGCGTGTGA
NS5A Mid FW	73.4	79.0	CACGGCGGAGACTGCGGCG
NS5A End FW	71.3	73.7	GGGTAGCTCCCGGTTCCGGG
NS5A End RV	63.0	50.0	GTTATGGTATCGCAACAGCG
NS5B Mid FW	60.2	47.4	AACGGGTGGAGTATCTCTT
NS5B End FW	62.7	52.6	TGGGTTCGCATGGTCCTAA
mEos3.2 FW	55.1	47.6	ATGAGTGCGATTAAGCCAGAC
mEos3.2 RV	59.8	52.1	TCGTCTGGCATTGTCAGGCAATC
DFCP1 Start FW	51.0	60.0	ATGAGTGCCCAGACTTCCCC
DFCP1 Mid FW	54.0	54.2	GGGGATGCCTCAGAAGCTTATCTG
DFCP1 End FW	50.0	63.2	GCTTAGCCTTGGACCCACC
mCherry Start FW	50.0	63.1	ATGGTGAGCAAGGGCGAGG
mCherry End RV	51.0	57.1	CTTGTACAGCTCGTCCATGCC

Appendix 2: List of sequencing primers

```

## getpalm3ddata.R
library(rPython)
# Extract data from palm3d generated files
# A pickle (.pkl) contains the drift information for each image
# A .py in the image data folder contains the localisations from one acquisition
getpalm3ddata <- function() {
cat("Where is the pickle?\n\n")
flush.console()
pkfile <- file.choose()
cat("Where is the localisations file?\n\n")
flush.console()
locfile <- file.choose()
pyfile <- "getpalm3ddata.py"
# Load my Python function(s) with rPython package
python.load(pyfile)
# Run my Python function with rPython
# This returns a lists of x, y, z, correl, with one item for each localisation
# correl is lists of correlations: one member-list for each image
palmdata <- python.call("getpalm3ddata", pkfile, locfile)
# Convert to data frame
palmdata <- data.frame(palmdata)
# Add region column to work with nearest neighbour calculations from tiled
histograms
palmdata <- cbind(region = 1, palmdata)
palmdata      }
ConvertNm <- function(xyzdata) {
  # Add x,y,z columns in nm to pixel data
  # User input of pixel to distance conversion
nm.ppx.x <- as.numeric(readline("nm per pixel (if unbinned) or bin (if via histogram)
in x? "))
nm.ppx.y <- as.numeric(readline("nm per pixel (if unbinned) or bin (if via histogram)
in y? "))
nm.ppx.z <- as.numeric(readline("nm per pixel (if unbinned) or bin (if via histogram)
in z? "))
  # Append coordinates in nm
xyzdata$x.nm <- xyzdata$x * nm.ppx.x
xyzdata$y.nm <- xyzdata$y * nm.ppx.y
xyzdata$z.nm <- xyzdata$z * nm.ppx.z
  # Return
xyzdata      }

```

Appendix 3

R processing script to load localisation coordinates from software into R. Script written by Alistair Curd at the University of Leeds.

```

# For 3D density calculation and interactive 3D plots
library(misc3d)
library(rgl)
working.dir.script <- getwd()
# Use functions in get3dpalmdata.r
source("getpalm3ddata.r")
palmdata <- getpalm3ddata()
palmdata <- ConvertNm(palmdata)
cat("\nGot data.\n")
cat("Plotting data.\n")
flush.console()
# Subset data with correlation value above 0.4 and plot to screen
gooddata <- subset(palmdata, correl > 0.4)
plot(y~x, data = gooddata)
# Choose directory to save density files in
cat("Choose a directory to save the density files in. \n")
flush.console()
direc <- choose.dir()
# Define sub-region to analyse (x0-50 y0-50)
flush.console()
subgooddata <- subset(gooddata, x.nm < 5000 & y.nm < 5000 & z.nm > 1800 &
z.nm < 3300)
# Calculate density of subregion with bandwidth of localisation precision
# h = bandwidth of kernel density estimation in X, Y and Z
# n = number of grid points in X, Y and Z
dens <- with(subgooddata, { kde3d(x.nm,y.nm,z.nm, h=c(8.49, 8.49, 12.74),
n=c(501, 501, 51)) } )
# Save file
flush.console()
filename <- "kde3d_x0-50_y0-50_z20-36_h8-8-12_n501-501-51"
flush.console()
path <- paste(direc, "\\", filename, ".dat", sep="")
f <- file(path, "wb")
writeBin(dens$d[1:length(dens$d)], f)
close(f)
# Calculate density of subregion with bandwith of ~125 nm
# Create "oversmoothed" file for cluster processing script in ImageJ
dens <- with(subgooddata, { kde3d(x.nm,y.nm,z.nm, h=50, n=c(501, 501, 51)) } )
# Save file
flush.console()
filename <- "kde3d_x0-50_y0-50_z20-36_h50_n501-501-51"
flush.console()
path <- paste(direc, "\\", filename, ".dat", sep="")
f <- file(path, "wb")
writeBin(dens$d[1:length(dens$d)], f)
close(f)

```

Appendix 4

R processing script to apply kernel density estimation to localisations and save output as binary file. Density estimation code repeated on each sub-region under investigation. Two density files for each sub-region are created, first with smoothing defined by localisation precision. Second with ~125 nm smoothing to create “oversmoothed”. Code originally written by Alistair Curd and modified by Chris Bartlett at the University of Leeds.


```

""" Originally written by Alistair Curd
zdiscneighbours.py
Find vectors from each localisation to all localisations
within a chosen distance from it.
Modified by Chris Bartlett
"""

import cPickle, shelve
from Tkinter import Tk
from tkFileDialog import askopenfilename
from tkFileDialog import askdirectory
import numpy as np
from scipy.ndimage.filters import gaussian_filter
import time
from collections import Counter
import math
import random
from sklearn.neighbors import NearestNeighbors as nn
def getcorrecteddata(pkldata, locsfile, offset,
                    qualmin,
                    x_to_nm, y_to_nm, z_to_nm):
    """Get co-ordinates for selected data.

    Minimum correlation specified,
    z extremes truncated to avoid these gluts of poor data.
    Co-ordinates corrected for drift and converted to nm
    (user inputs conversion factors).
    Returns:
        This data as a numpy array with shape (N, 3),
        where N is the number of localisations.
    """

    # Separate out offset components for use when corrected x, y and z, below.
    (xoffset, yoffset, zoffset) = offset
    # Get raw localisations (not drift-corrected).
    # locsimages is a shelve, or uber-list of images, called '0' '1', '2', etc.
    # Each image - locsimages['0'] or locsimages[repr(0)] -
    # is a list of localisations within that image
    # Each localisation - e.g. locsimages[repr(1)][1] -
    # is a dictionary of properties
    # Each localisation contains position, e.g. 'x', and other information
    locsimages = shelve.open(locsfile, protocol=2)
    # Initialise co-ordinates and data quality/correlation arrays
    # Over all of the images, find drift-corrected coordinates and 'qual'
    xs = []
    ys = []
    zs = []
    qual = []
    for imagecount in range(len(pkldata.images)):
        for loc in locsimages[repr(imagecount)]:
            # Exclude poor correlations with calibration stack
            if(loc['qual'] > qualmin):
                # Exclude the extremes in z
                # (where incorrect localisations in z end up)
                if(loc['z'] > 5 and loc['z'] < 75):
                    xs.append(loc['x'] - pkldata.drift['x'][imagecount] - xoffset)
                    ys.append(loc['y'] - pkldata.drift['y'][imagecount] - yoffset)
                    zs.append(loc['z'] - pkldata.drift['z'][imagecount] - zoffset)

```

```

        qual.append(loc['qual']) # May use it later
locsimages.close()
# Numpy array of coordinates...with each (x,y,z) along one row
xyz = np.array([xs,ys,zs])
xyz = np.transpose(xyz)
# Convert pixels to nm
conv_to_nm = np.array([x_to_nm, y_to_nm, z_to_nm])
xyz = np.multiply(xyz, conv_to_nm)
# Save a little memory/time
# We could usually get away with 16-bit
# (350 pixels * 167 nm = 58450 nm < 65536)
# But do want to keep 1 or decimal places as well.
xyz = xyz.astype(np.float32)
print ('\n%i localisations found before subsetting.' % len(xyz))
return xyz
def combineacquisitions(savefolder):
    """Combine data from multiple acquisitions for analysis.
    User input required to find acquisition data.
    Args:
        Folder in which to save data
    Returns:
        Numpy array as in getcorrected data().
    """
    Tk().withdraw()
    # Get localisations either from palm3d data files
    # or from a previous run of this program
    print('Do you already have an AllCorrectedLocalizations.npy')
    ans = raw_input('for your FOV/minimum correlation/linking setting? y/n: ')
    if ans == 'n':
        print '\nPlease find me the first pickle (pkl)!'
        pkldata = askopenfilename()
        print '%s\n' % pkldata
        print 'Please find me the first localizations file.'
        print '(Usually in raw data folder, e.g. z=...)'
        print 'Use _palm_localizations for unlinked localisations'
        print 'or _palm_particles for localisations after linking.'
        locsfile = askopenfilename()
        print '%s' % locsfile
        # Get acquisition information, including drift.
        with open(pkldata, 'rb') as f:
            pkldata = cPickle.load(f)
        # Initial fiducial position, from which subsequent offsets are calculated
        veryfirstfidpos = pkldata.drift['initial_xyz']
        # Get pixel to distance conversion factors
        # and minimum correlation with calibration stack
        x_to_nm = raw_input('\nHow many nm per pixel in x? ')
        x_to_nm = float(x_to_nm)
        y_to_nm = raw_input('How many nm per pixel in y? ')
        y_to_nm = float(y_to_nm)
        z_to_nm = raw_input('How many nm per pixel in z? ')
        z_to_nm = float(z_to_nm)
        qualmin = float(raw_input('\nChoose minimum correlation for the data: '))
        print '\nReading these localisations. Please wait...'
        xyz = getcorrecteddata(pkldata=pkldata, locsfile=locsfile,
                               offset=np.array([0., 0., 0.]),
                               qualmin=qualmin,

```

```

        x_to_nm=x_to_nm, y_to_nm=y_to_nm, z_to_nm=z_to_nm)
while(raw_input(
    '\nDo you want to include another acquisition run from this FOV? [y]/n: '
) != 'n'):
    # Find the data, as before
    print '\nPlease find me that pickle then (pkl).'
    pkldata = askopenfilename()
    print '%s\n' % pkldata
    print 'Please find me relevant localizations file too.'
    print 'Use _palm_localizations for unlinked localisations'
    print 'or _palm_particles for localisations after linking.'
    locsfile = askopenfilename()
    print '%s' % locsfile
    with open(pkldata, 'rb') as f:
        pkldata = cPickle.load(f)
    print '\nReading these localisations. Please wait...'
    # Get the offset relative to the first run
    firstfidpos = np.array(pkldata.drift['initial_xyz'])
    offset = firstfidpos - veryfirstfidpos
    xyz_next = getcorrecteddata(pkldata, locsfile, offset,
                                qualmin,
                                x_to_nm, y_to_nm, z_to_nm)
    xyz = np.append(xyz, xyz_next, axis=0)
    np.save('%s\\AllCorrectedLocalizations' % savefolder, xyz)
elif ans == 'y':
    print("\nCan I have it then please?")
    xyzfile = askopenfilename()
    xyz = np.load(xyzfile)
    print(xyzfile)
    x_to_nm = raw_input('\nHow many nm per pixel in x? ')
    x_to_nm = float(x_to_nm)
    y_to_nm = raw_input('How many nm per pixel in y? ')
    y_to_nm = float(y_to_nm)
    z_to_nm = raw_input('How many nm per pixel in z? ')
    z_to_nm = float(z_to_nm)
else:
    print('Oops - try again with \'y\' or \'n\'.')
    print('Bye! (Hit enter.)')
    raw_input()
    return(ouch)
# Subset FOV to the chosen area if desired
# Uses 4000 for maximum z in nm
print('\nTo subset an area for analysis,')
print('use pixel values from a square-bin reconstruction')
print('(e.g. from a histogram with 100 nm bins, with 100 nm ppx in x and y).')
    # user input to subset a region
    # TO DO: Save number of locs in each subregion into an excel file (.csv)
    # Run in infinite loop to crop region
    # Files saved with cropped region size in filename
while True:
    ans = raw_input('\nDo you want to crop a region? y/n: ')
    if ans == 'y':
        ymin = float(raw_input('\nMinimum horizontal pixel (0 for full FOV): '))
        ymax = float(raw_input('Maximum horizontal pixel (350 for full FOV): '))
        xmin = float(raw_input('Minimum vertical pixel (0 for full FOV): '))
        xmax = float(raw_input('Maximum vertical pixel (350 for full FOV): '))

```

```

xyzmin = np.array([xmin * x_to_nm, ymin * y_to_nm, 0])
xyzmax = np.array([xmax * x_to_nm, ymax * y_to_nm, 4000])
subsetfilter = np.logical_and(xyz >= xyzmin, xyz <= xyzmax)
chosenlocs = np.all(subsetfilter, axis = 1)
subxyz = xyz[chosenlocs]
title = ('RegionX' + str(xmin) + '-' + str(xmax) + 'Y' + str(ymin) + '-' +
str(ymax))
np.save(title, subxyz)
np.savetxt((title+'.csv'), subxyz, delimiter = ',', header = 'X, Y, Z')
print('\nSubset contains %i localisations.' % len(subxyz))
elif ans == 'n':
    subxyz = []
    xmin = 0
    xmax = 0
    ymin = 0
    ymax = 0
    break
else:
    print('Try again with \'y\' or \'n\'.')
    pass
return(xyz, subxyz, xmin, xmax, ymin, ymax, x_to_nm, y_to_nm, z_to_nm)
def main():
    Tk().withdraw()
    print 'Where do you want to save the results?'
    savefolder = askdirectory()
    print '%s\n' % savefolder
    # Call getcorrecteddata for each acqn. run
    # xyz = combineacquisitions() # This calls getcorrecteddata for each acqn. run
    (xyz, subxyz, xmin, xmax, ymin, ymax,
    x_to_nm, y_to_nm, z_to_nm) = combineacquisitions(savefolder)
    return
if __name__ == '__main__':
    main()
    print '\nHit Enter to exit'
    raw_input()

```

Appendix 5

Python processing script to extract super-resolution microscopy coordinates from palm3d into NumPy array. User input to select .pkl file and corresponding localisations file for coordinate extraction of a processed image series. User input the specify x and y pixel corrections factors and correlation strength. Additional files can be appended if more than one acquisition run required. User input to define region for sub-setting.

```

"""
Compute DBSCAN at set min_cluster_size
Plot graph with clusters coloured according to cluster identity
Calculate cluster size parameters using pairwise distances
Input
User input to select min_cluster_size
Output
Will save files in directory that script runs from
.csv file of coordinates with cluster identity with and without "noise"
Graph of clusters coloured according to identity
.csv file of size parameters for each cluster
"""

import os
import numpy as np
from sklearn.cluster import DBSCAN
import time
from tkinter import Tk
from tkinter.filedialog import askopenfilename
from tkinter.filedialog import askdirectory
import matplotlib.pyplot as plt
import scipy.spatial.distance as distance
from sklearn.neighbors import NearestNeighbors
def removefiducial(savefolder, data):
    """
    Remove fiducial localisations
    Search filter applied to localisations
    If localisation has >500 locs within 30 nm cube then consider it fiducial
    Save all localisations other than fiducial for DBSCAN analysis
    Returns
    Array of localisations without fiducial
    """
    print("\nRemoving fiducial localisations...')
    # Distance to search for localisations
    # 30 nm is ~localisation precision in Z
    filter = 30
    filterarray = np.array([filter, filter, filter])
    x = []
    y = []
    z = []
    loc = 0
    while loc < len(data):
        # Reference localisation
        locA = data[loc]
        # A filter to search for localisation coordinate within filter distance
        # Returns an np array of True / False
        testfilter = np.logical_and(data > locA - filterarray, data < locA +
filterarray)

        # Find pos of all localisations within filter distance of reference loc
        chosenlocs = np.all(testfilter, axis = 1)
        subxyz = data[chosenlocs]
        # Check how many neighbours reference localisation has
        # If less than 500 save reference localisation coordinates
        if len(subxyz) < 500:
            x = np.append(x, locA[0])
            y = np.append(y, locA[1])
            z = np.append(z, locA[2])

```

```

        loc = loc + 1
    # Save data without fiducial for DBSCAN analysis
    xyz = np.array([x, y, z])
    xyz = np.transpose(xyz)
    print('Original total: %i' % len(data))
    print('After total: %i' % len(xyz))
    return (xyz)
def runDBSCAN(savefolder, data, neighbourhood, nlocs):
    """ Run DBSCAN """
    t = time.time()
    print('\nRunning DBSCAN...')
    clusterer = DBSCAN(eps = neighbourhood, min_samples = nlocs).fit(data)
    cluster_labels = clusterer.labels_
    # combine XYZ coordinates with cluster identity from DBSCAN
    dataDBSCANnoise = np.c_[ data, cluster_labels ]
    np.savetxt('%s\coordinatesDBSCANnoise.csv'
% savefolder, dataDBSCANnoise, delimiter = ',', header = 'DBSCAN Clustered
Data')
    # Remove coordinates classified as noise by DBSCAN
    # Value of -1 from DBSCAN assigned as noise
    row = 0
    x = []
    y = []
    z = []
    c = []
    while row < len(dataDBSCANnoise):
        if dataDBSCANnoise[row, 3] != -1 :
            x = np.append(x, dataDBSCANnoise[row,0])
            y = np.append(y, dataDBSCANnoise[row,1])
            z = np.append(z, dataDBSCANnoise[row,2])
            c = np.append(c, dataDBSCANnoise[row,3])
        row = row + 1
    dataDBSCAN = np.array([x, y, z, c])
    dataDBSCAN = np.transpose(dataDBSCAN)
    np.savetxt('%s\coordinatesDBSCAN.csv' % savefolder, dataDBSCAN,
delimiter = ',')
    """ Plot DBSCAN results """
    print('\nSaving plots...')
    # Plot of clusters including noise localisations in black and white
    # Get X and Y coordinates
    xdata = dataDBSCANnoise[:,0]
    ydata = dataDBSCANnoise[:,1]
    fig = plt.figure()
    plt.title('Original', fontsize = 20, y = 1.04)
    noisepts = plt.scatter(xdata, ydata, marker='.', lw = 0, c = 'black')
    # Set axis limits
    xmin = np.min(xdata)
    xmax = np.max(xdata)
    ymin = np.min(ydata)
    ymax = np.max(ydata)
    ax = plt.gca()
    ax.set_xlim(xmin-500, xmax+500)
    ax.set_ylim(ymin-500, ymax+500)
    # Control axis; values and ticks
    #ax.xaxis.set_ticklabels([])
    #ax.yaxis.set_ticklabels([])

```

```

ax.set_xlabel('X (nm)', labelpad = 10)
ax.set_ylabel('Y (nm)', labelpad = 10)
ax.tick_params(axis = u'both', which = u'both', length = 0, pad = 10)
# Set figure aspect ratio
xsize = ((xmax-xmin)/1000)+1
ysize = ((ymax-ymin)/1000)+1
size = plt.gcf()
size.set_size_inches(xsize, ysize)
# Add scale bar to image
scalebar = plt.plot([xmin, xmin+500], [ymin-350, ymin-350], color = 'k',
linestyle = '-', linewidth = '5')
scalelabel = ax.text(xmin-50, ymin-250, '500 nm', fontsize = 10, name =
'Arial')
plt.savefig('%s\\DBSCANnoise.png' % savefolder)
# Get X and Y coordinates of DBSCAN clusters
# Colour clusters according to cluster identity
xdata = dataDBSCAN[:,0]
ydata = dataDBSCAN[:,1]
colour = dataDBSCAN[:,3]
# Plot DBSCAN clusters according to cluster identity on top of original locs
pts = plt.scatter(xdata, ydata, marker='.', lw = 0, c = colour)
plt.title('Cluster ID', fontsize = 20)
plt.savefig('%s\\DBSCANcolouridentity.png' % savefolder)
# Plot DBSCAN clusters only
noisepts.remove()
pts = plt.scatter(xdata, ydata, marker='.', lw = 0, c = colour)
plt.title('DBSCAN', fontsize = 20)
plt.savefig('%s\\DBSCAN.png' % savefolder)
plt.close()
""" Calculate cluster parameters """
# Save individual clusters and average cluster as binary files
# Calculate size parameters of clusters using pairwise distances
print('\nSaving clusters...')
id = []
num = []
xymin = []
xymax = []
xymin = []
xymax = []
xymean = []
zmax = []
zmin = []
zmean = []
xcentroid = []
ycentroid = []
zcentroid = []
# Array for distance to centroid position
distcentroid = []
# Array for saving average cluster
xavgcentroidnorm = []
yavgcentroidnorm = []
zavgcentroidnorm = []
# iterate through each cluster
clusterid = 0
while clusterid < cluster_labels.max()+1:
    row = 0
    xc = []
    yc = []

```

```

zc = []
# move coords for each cluster into array for distance measurement
while row < len(dataDBSCAN):
    if dataDBSCAN[row, 3] == clusterid:
        xc = np.append(xc, dataDBSCAN[row, 0])
        yc = np.append(yc, dataDBSCAN[row, 1])
        zc = np.append(zc, dataDBSCAN[row, 2])
    row = row + 1
# Full cluster coordinates for saving image files
xyzclust = np.array([xc, yc, zc])
xyzclust = np.transpose(xyzclust)

# get centroid position
xavg = np.mean(xyzclust[:,0])
yavg = np.mean(xyzclust[:,1])
zavg = np.mean(xyzclust[:,2])
# calculate distance of localisation to centroid position
centroid = np.array([xavg, yavg, zavg])
locA = 0
while locA < len(xyzclust):
    locB = xyzclust[locA]
    cdist = distance.euclidean(locB, centroid)
    distcentroid = np.append(distcentroid, cdist)
    locA = locA + 1
# XY coordinates for distance measurements
xyclust = np.array([xc, yc])
xyclust = np.transpose(xyclust)
# Z coordinates for distance measurements in Z axis only
# Append column of zeros to array
zclust = np.c_[np.zeros(len(zc)), zc]
# calculate pairwise distances in clusters for XY, and Z axis
xydist = distance.pdist(xyclust, 'euclidean')
zdist = distance.pdist(zclust, 'euclidean')
# save cluster parameters to array
id = np.append(id, clusterid)
num = np.append(num, len(xyzclust))
xymin = np.append(xymin, xydist.min())
xymax = np.append(xymax, xydist.max())
xymean = np.append(xymean, xydist.mean())
zmin = np.append(zmin, zdist.min())
zmax = np.append(zmax, zdist.max())
zmean = np.append(zmean, zdist.mean())
xcentroid = np.append(xcentroid, xavg)
ycentroid = np.append(ycentroid, yavg)
zcentroid = np.append(zcentroid, zavg)
# save cluster parameters
parameters = np.array([id, num, xymax, xymin, xymean, zmax, zmin,
zmean, xcentroid, ycentroid, zcentroid])
parameters = np.transpose(parameters)
# save distances to centroid
# distance of each loc within a cluster to its cluster centroid
np.savetxt('%s\\DistancetoCentroid.csv' % savefolder, distcentroid, delimiter
= ',')
# calculate distances between cluster centroids
all_centroids = np.array([xcentroid, ycentroid, zcentroid])
all_centroids = np.transpose(all_centroids)

```

```

    pdist_all_centroids = distance.pdist(all_centroids, 'euclidean')
    np.savetxt('%s\PDistCentroids.csv' % savefolder, pdist_all_centroids,
delimiter = ',')
    percentclust = ((len(dataDBSCAN) / len(dataDBSCANnoise) * float(100)))
    np.savetxt('%s\DBSCANClusterParameters.csv' % savefolder, parameters,
delimiter = ',')
    header = 'ID, Locs/Cluster, XY Max Dist, XY Min Dist, XY Mean Dist,
Z Max Dist, Z min Dist, Z Mean Dist, X Centroid, Y Centroid, Z
Centroid',
    footer = 'Total: %s\nClustered: %s\nPercentage : %s' %
(len(dataDBSCANnoise), len(dataDBSCAN), percentclust))
    print('Clusters: %s' % len(parameters))
    # Message completion
    print('\n%.2f sec to run DBSCAN analysis' % (time.time() - t) )
    return
def main():
    Tk().withdraw()
    print('\nWhat region would you like to analyse')
    xyzfile = askopenfilename()
    print(xyzfile)
    search_radius = int(input('\nWhat is the search radius? '))
    min_cluster_size = int(input('What is the minimum number of locs per
cluster? '))
    directory = str(xyzfile) + '-DBSCAN-Analysis_eps-' + str(search_radius) +
'_nlocs-' + str(min_cluster_size)
    os.mkdir(directory)
    xyz = np.load(xyzfile)

    ansfid = input('\nDo you want to remove fiducial locs? [y]/n: ')
    if ansfid != 'n':
        xyz = removefiducial(savefolder = directory, data = xyz)
    runDBSCAN(savefolder = directory, data = xyz, neighbourhood =
search_radius, nlocs = min_cluster_size)
    while True:
        ans = input('\nDo you want to run another analysis? [y]/n: ')
        if ans != 'n':
            # Import data set
            print('\nWhat region would you like to analyse?')
            xyzfile = askopenfilename()
            print(xyzfile)
            directory = str(xyzfile) + '-DBSCAN-Analysis_eps-' +
str(search_radius) + '_nlocs-' + str(min_cluster_size)
            # Check if analysis has already been run
            if os.path.exists(directory) == False:
                os.mkdir(directory)
                xyz = np.load(xyzfile)
                if ansfid != 'n':
                    xyz = removefiducial(savefolder = directory,
data = xyz)

            # run DBSCAN
            runDBSCAN(savefolder = directory, data = xyz,
neighbourhood = search_radius, nlocs = min_cluster_size)
            else:
                print('\nYou have already analysed this data!')
                print('Please try again')
        if ans == 'n':

```

```
                print('\nFinished DBSCAN analysis - Hit Enter to Exit')
                break
if __name__ == '__main__':
    main()
    input()
```

Appendix 6

Python processing script to run DBSCAN analysis on super-resolution microscopy data. User input to select save folder, file for analysis and DBSCAN parameters of minimum points and search radius (nm). User input to remove fiducial localisations. Fiducial localisations determined from filtering the data set for localisations with 500th neighbour within 30 nm Euclidean distance. DBSCAN analysis calculates cluster size, number of localisations per cluster and distance to centroid. Cluster size is defined as mean Euclidean distance (nm) in *x-y*. Distance to centroid is calculated for each localisation in a cluster to its cluster centroid. Distance between different cluster centroids are also calculated. Parameters are saved to .csv files in directory. Plots of localisations and clusters coloured according to cluster identity are plotted using matplotlib.pyplot.